THE SOLUBILITY AND SECONDARY STRUCTURE OF ZEIN IN IMIDAZOLIUM-
BASED IONIC LIQUIDS

by

SEAN R. TOMLINSON

B.S., Kansas State University, 2005

AN ABSTRACT OF A DISSERTATION

Submitted in partial fulfillment of the requirements for the degree

DOCTOR OF PHILOSOPHY

Department of Chemical Engineering
College of Engineering

KANSAS STATE UNIVERSITY
Manhattan, Kansas

2013

Abstract

Ionic liquids are low melting salts composed of an organic cation and an inorganic or organic anion. Ionic liquids are of interest for their wide range of applications and unique properties, such as the negligible vapor pressure of some types of ionic liquids, and the ability to modify ionic liquid properties by selection of the cation or anion. It has been hypothesized that over one million binary ionic liquids (meaning a single cation/anion pair) are possible. Due to the vast number of potential combinations, it should be possible to design ionic liquids specifically for an application of interest. One potential application is their use as protein solvents. However there is little understanding of how ionic liquids affect proteins.

This research examined the solubility and secondary structure of the hydrophobic corn protein zein in seven ionic liquids and three conventional solvents as a function of temperature and solvent properties. Zein's solubility in the solvents was measured gravimetrically from 30 to 60 degrees Celsius. Solubility was then related to solvent properties to gain an understanding of what solvent properties are important, and how to design an ionic liquid to dissolve zein. It was found that a good solvent for zein has a small molecular volume, a low polarity, and is a weak hydrogen bond acceptor.

Infrared spectroscopy with curve fitting was used to examine the secondary structure of zein as a function of both solvent and temperature from 25 to 95 degrees Celsius. It was found that most of the ionic liquids change zein's secondary structure, but those secondary structure changes were not affected by temperature. Aprotic ionic liquids increase the amount of β-turn secondary structure through non-polar interactions between the mixed aromatic-alkyl imidazolium cations and the non-polar portions of the zein. Strong hydrogen bond accepting molecules were found to increase the amount of β-turn secondary structure.

It is hypothesized from this research that suitable solvents for zein will have a small molar volume, low polarity, and be poor hydrogen bond acceptors. This combination of properties will enhance zein's solubility and limit secondary structure changes that can harm protein properties.

THE SOLUBILITY AND SECONDARY STRUCTURE OF ZEIN IN IMIDAZOLIUM-
BASED IONIC LIQUIDS

by

SEAN R. TOMLINSON

B.S., Kansas State University, 2005

A DISSERTATION

Submitted in partial fulfillment of the requirements for the degree

DOCTOR OF PHILOSOPHY

Department of Chemical Engineering
College of Engineering

KANSAS STATE UNIVERSITY
Manhattan, Kansas

2013

Approved by:

Major Professor
Jennifer L. Anthony

Copyright

SEAN TOMLINSON

2013

Abstract

Ionic liquids are low melting salts composed of an organic cation and an inorganic or organic anion. Ionic liquids are of interest for their wide range of applications and unique properties, such as the negligible vapor pressure of some types of ionic liquids, and the ability to modify ionic liquid properties by selection of the cation or anion. It has been hypothesized that over one million binary ionic liquids (meaning a single cation/anion pair) are possible. Due to the vast number of potential combinations, it should be possible to design ionic liquids specifically for an application of interest. One potential application is their use as protein solvents. However there is little understanding of how ionic liquids affect proteins.

This research examined the solubility and secondary structure of the hydrophobic corn protein zein in seven ionic liquids and three conventional solvents as a function of temperature and solvent properties. Zein's solubility in the solvents was measured gravimetrically from 30 to 60 degrees Celsius. Solubility was then related to solvent properties to gain an understanding of what solvent properties are important, and how to design an ionic liquid to dissolve zein. It was found that a good solvent for zein has a small molecular volume, a low polarity, and is a weak hydrogen bond acceptor.

Infrared spectroscopy with curve fitting was used to examine the secondary structure of zein as a function of both solvent and temperature from 25 to 95 degrees Celsius. It was found that most of the ionic liquids change zein's secondary structure, but those secondary structure changes were not affected by temperature. Aprotic ionic liquids increase the amount of β-turn secondary structure through non-polar interactions between the mixed aromatic-alkyl imidazolium cations and the non-polar portions of the zein. Strong hydrogen bond accepting molecules were found to increase the amount of β-turn secondary structure.

It is hypothesized from this research that suitable solvents for zein will have a small molar volume, low polarity, and be poor hydrogen bond acceptors. This combination of properties will enhance zein's solubility and limit secondary structure changes that can harm protein properties.

Table of Contents

List of Figures

List of Tables

Acknowledgements

Dedication

I dedicate this thesis to my mother, Paula L. Tomlinson, and the memory of my father, G. Richard Tomlinson Lt. Col. C.A.P. (Ret.)

Chapter 1 - Introduction

Ionic liquids are salts composed of an organic cation (such as imidazolium, pyrrolidinium, or tetraalkylphosphonium) and an organic or inorganic anion (such as ethoxide, acetate, or bromide).[1] Ionic liquids are generally defined as having a melting point less than 100°C, and many have a melting point lower than room temperature (room temperature ionic liquids – RTILs) which makes them useful as solvents.[2-4] Ionic liquids have received much interest in the last decade for a variety of tasks due to their unique properties. One unique advantage over molecular solvents is that aprotic ionic liquids (such as the 1-ethyl-3-methyimidazolium bromide used in inorganic syntheses) have negligible vapor pressure until decomposition.[5] Another advantage over conventional solvents is the huge number of potential ionic liquids. Over one million different binary ionic liquids (meaning a single cation/anion pair) are possible by altering the cation and anion compared to the approximately 600 molecular solvents currently in use.[1] Therefore it should be feasible to create designer ionic liquids for particular applications.[1]

Ionic liquids have been used as solvents for many materials-based applications, from novel zeolite syntheses to cellulose dissolution.[6-14] One application is using ionic liquids as solvents for proteins or enzymes.[15-17] Previous research has found that ionic liquids are capable of stabilizing proteins and that some enzymes are still capable of catalysis when dissolved in ionic liquids.[16] However, there has been no systematic research into what properties control the solubility or the structure of proteins in the ionic liquid. This research systematically examines the solubility and secondary structure as functions of temperature of an industrially useful corn protein (zein) with the goal of understanding solvent property importance to enable the design of solvents for zein and other hydrophobic proteins. A model is developed to predict solubility and the relative energy of interaction using common solvent parameters.

Hypothesis

It is hypothesized that ionic liquid properties control the solubility and structure of solutes, including proteins. Because it is possible to design ionic liquids to possess certain properties, an understanding of how solvent properties affect the solute is useful for designing ionic liquids for a particular task. In particular, as protein properties are affected by protein

structures which are in turn affected by solvent properties, an understanding of how solvent properties affect the secondary structure is necessary to optimize ionic liquid design.

Objective

While it has been found that ionic liquids are capable of dissolving proteins and can even serve as media for enzymatic catalysis, there has been no systematic research into how ionic liquids affect protein structure in solution. An understanding of how the protein's structure is changed in solution is important as the properties of many proteins are related to its structure. Understanding what solvent properties are important for protein solubility is also important for designing ionic liquids, but there is currently only a little research into this important field. How does temperature affect protein structure and solubility in ionic liquids? What ionic liquid can dissolve zein most efficiently close to room temperature and pressure, without affecting the protein's structure? The purpose of this research is to address these questions about ionic liquids for a particular protein, zein, which is a useful industrial resource, produced in corn.

This research will answer the above questions through an investigation of the corn protein zein's solubility and structure in ionic liquids. Because imidazolium-based ionic liquids are well characterized, the imidazolium cation will serve as a basis for the ionic liquids investigated here. The solubility of zein will be investigated gravimetrically, repeated at least in triplicate, from 30°C to 60°C. The structure of zein will be investigated from 25°C to 95°C using infrared spectroscopy, a widely used experimental technique for the characterization of protein's secondary structure (the arrangement of local protein segments in three dimensions).[18-21]

Following this introduction, Chapter 2 reviews the background on ionic liquids, protein structure and its importance, infrared spectroscopy applied to protein structure, the corn protein zein itself, and finally solvent properties of interest in this research. Chapter 3 details the experimental methods used in this research. Chapters 4 and 5 present the experimental results for the solubility and secondary structure of zein, respectively. Chapter 6 examines the importance of various solvent properties in the interactions with zein. Chapter 7 draws conclusions from this work and gives recommendations for future investigations.

The appendices detail other work performed as part of my research into material synthesis. Appendices A and B show how infrared spectroscopy can be used to analyze structural changes of zeolites. Appendix C examines the impact of ionothermal versus hydrothermal

synthesis methods and sublimated versus unsublimated aluminum isopropoxide on the particle size of aluminophosphate molecular sieves. Appendix D is a tutorial for the peak fitting performed using the GRAMS/AI software from Thermo Fisher Scientific. Appendix E is a tutorial for 2-D correlation using the freeware 2Dshige©, and presents the data obtained using 2-D correlation in the course of this research. Appendix F is a derivation of the van't Hoff equation used to find the change in standard Gibbs free energy, enthalpy, and entropy of dissolution of zein in the solvents examined. Finally, Appendix G is a table of nomenclature for the ionic liquids and other potentially unfamiliar terms used in this text. Appendix G also includes the molecular structures of the ionic liquids used.

References

1. Rogers, R. D.; Seddon, K. R. Ionic Liquids-Solvents of the Future? *Science* **2003**, 792.

2. Welton, T. Room-temperature ionic liquids. Solvents for synthesis and catalysis, *Chem. Rev.* **1999***, 8,* 2071-2084.

3. Wilkes, J. S. Properties of ionic liquid solvents for catalysis, *J. Mol. Catal. A: Chem.* **2004***, 1,* 11-17.

4. Wasserscheid, P., Welton,T. Ionic Liquids in Synthesis, **2003**, 9-12.

5. Earle, M. J.; Esperança, J. M. S. S.; Gilea, M. A.; Lopes, J. N. C.; Rebelo, L. P. N.; Magee, J. W.; Seddon, K. R.; Widegren, J. A. The distillation and volatility of ionic liquids, *Nature* **2006***, 7078,* 831-834.

6. Freemantle, M. *An introduction to ionic liquids;* Royal Society of Chemistry: Cambridge, U.K., 2009; , pp 281.

7. Sun, X.; King, J.; Anthony, J. L. Molecular sieve synthesis in the presence of tetraalkylammonium and dialkylimidazolium molten salts, *Chem. Eng. J.* **2009***, 1,* 2-5.

8. Parnham, E. R.; Morris, R. E. Ionothermal Synthesis of Zeolites, Metal–Organic Frameworks, and Inorganic–Organic Hybrids, *Acc. Chem. Res.* **2007**, 1005.

9. Gericke, M.; Liebert, T.; Seoud, O. A. E.; Heinze, T. Tailored Media for Homogeneous Cellulose Chemistry: Ionic Liquid/Co-Solvent Mixtures, *Macromolecular Materials and Engineering* **2011***, 6,* 483-493.

10. Doherty, T. V.; Mora-Pale, M.; Foley, S. E.; Linhardt, R. J.; Dordick, J. S. Ionic liquid solvent properties as predictors of lignocellulose pretreatment efficacy, *Green Chem.* **2010***, 11,* 1967-1975.

11. Kahlen, J.; Masuch, K.; Leonhard, K. Modelling cellulose solubilities in ionic liquids using COSMO-RS, *Green Chem.* **2010***, 12,* 2172-2181.

12. Ohno, H.; Fukaya, Y. Task specific ionic liquids for cellulose technology, *Chem. Lett.* **2009***, 1,* 2-7.

13. Vitz, J.; Erdmenger, T.; Haensch, C.; Schubert, U. S. Extended dissolution studies of cellulose in imidazolium based ionic liquids, *Green Chem.* **2009***, 3,* 417-424.

14. Swatloski, R. P.; Spear, S. K.; Holbrey, J. D.; Rogers, R. D. Dissolution of cellulose with ionic liquids, *J. Am. Chem. Soc.* **2002***, 18,* 4974-4975.

15. Weingärtner, H.; Cabrele, C.; Herrmann, C. How ionic liquids can help to stabilize native proteins, *Phys. Chem. Chem. Phys.* **2012***, 2,* 415-426.

16. Naushad, M.; ALOthman, Z. A.; Khan, A. B.; Ali, M. Effect of ionic liquid on activity, stability, and structure of enzymes: A review, *Int. J. Biol. Macromol.* **2012**, 555-560.

17. Ha, S. H.; Koo, Y. M. Enzyme performance in ionic liquids, *Korean J. Chem. Eng.* **2011**, 1-7.

18. D'antonio, J.; Murphy, B. M.; Manning, M. C.; Al-azzam, W. A. Comparability of protein therapeutics: Quantitative comparison of second-derivative amide I infrared spectra, *J. Pharm. Sci.* **2012**.

19. Carbonaro, M.; Maselli, P.; Nucara, A. Relationship between digestibility and secondary structure of raw and thermally treated legume proteins: a Fourier transform infrared (FT-IR) spectroscopic study, *Amino Acids* **2011**, 1-11.

20. Barth, A. Infrared spectroscopy of proteins, *Biochim Biophys Acta* **2007***, 9,* 1073-1101.

21. Sachdeva, A.; Cai, S. Structural Differences of Proteins Between Solution State and Solid State Probed by Attenuated Total Reflection Fourier Transform Infrared Spectroscopy, *Appl. Spectrosc.* **2009***, 4,* 458-464.

Chapter 2 - Background

Ionic liquid introduction

Ionic liquids are ionic compounds composed of an organic cation (such as imidazolium, pyrrolidinium, or tetraalkylphosphonium) and an anion that can be organic or inorganic (such as ethoxide, acetate, or bromide).[1] By current convention ionic liquids have a melting point less than 100°C, and many have a melting point lower than room temperature (so-called room temperature ionic liquids – RTILs) making them useful as solvents.[4-6] The first credited ionic liquid dates from Gabriel and Weiner's 1888 discovery of what is now known as ethanolammonium nitrate.[2, 3] With a melting point of 52°C to 55°C, ethanolammonium nitrate was the first recorded organic salt with a melting point less than 100°C.[2, 3] The first RTIL, ethylammonium nitrate, was prepared by Walden and reported in 1914.[7] However, development of ionic liquids languished until 1992 when air-stable ionic liquids were first published, facilitating examination of their unique properties.[3] In 1997 Seddon published an article identifying ionic liquids as promising tools for clean technology.[8] The *Chemical & Engineering News* article in 1998, "Designer solvents-Ionic liquids may boost clean technology development", has been cited as the cause of the subsequent eruption in ionic liquid research because of interest in more environmentally friendly chemical processes.[9, 10] Abbreviations are often used for ionic liquids as their names can become onerous. Therefore, the ionic liquid 1-ethyl-3-methylimidazolium bromide, shown in Figure 2.1 (frequently used to in inorganic syntheses) is abbreviated from 1-**E**thyl-3-**m**ethyl**im**idazolium **Br**omide to [Emim][Br].[3]
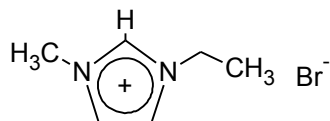
Figure 2.1 Structure of 1-ethyl-3-methylimidazolium bromide

A full description of the ionic liquid names used for this research is provided in Appendix G, along with the ionic liquid structures.

Because ionic liquids consist of cations and anions, ionic liquids have dual functionality and the ability, through careful selection and design of each ion, to dissolve disparate materials in a single solvent.[3] It has been calculated that over one million different binary ionic liquids, each with a particular pairing of cation and anion, are possible. Therefore it should be feasible to

create designer ionic liquid solutions for particular applications by independent selection of the cation and anion.[1] By contrast, there are approximately 600 molecular solvents in use.[1, 3] The variety of ionic liquids has led to a wide range of applications taking advantage of their useful properties.

One unique and important property is that aprotic ionic liquids (such as [Emim][Br] shown above) have negligible vapor pressure until decomposition, which facilities their handling and means that aprotic ionic liquids cannot evaporate.[3, 11] Ionic liquids have also received attention as "green" solvents because they are generally non-flammable and because it is possible to recycle them.[3, 12-14] However ionic liquids are often made from toxic compounds, so their "greenness" is always discussed with respect to their role and what solvent they may replace.[13-15] That being said, much work has been performed to prepare ionic liquids from environmentally benign compounds such as choline (an ingredient in energy drinks) and amino acids, which opens the door to non-toxic and potentially truly green ionic liquids.[16-21]

Ionic liquid applications

Ionic liquids have been used in a variety of research areas. For example, research into ionic liquid applications include carbon dioxide capture,[22] organometallic catalysis,[23] unique roles in electrochemistry,[24] nanoparticle synthesis,[25-27] gas chromatography,[28, 29] and even as solutions for enzyme catalysis.[30] The solution thermodynamics of ionic liquids with water and alcohols,[31-33] and gases[34, 35] have also been investigated. BASF performed the first commercial-scale application of an ionic liquid, using 1-methylimidazole to scavenge unwanted hydrochloric acid from a reaction stream.[36, 37] Another area of research uses ionic liquids as solvents for aluminophosphate molecular sieve synthesis.[38-46] Researchers have successfully prepared both already known and novel crystal structures in ionic liquids.[38-51] The ability of the ionic liquid to both dissolve reagents and direct the structure of the resulting molecular sieve has proven to be an important benefit of the ionothermal method.

In the course of the ionothermal molecular sieve research it was recognized that water plays less of a role in the synthesis of molecular sieves than expected by water's behavior in other solvents.[42, 52] The "water deactivating" effect is the lack of chemical activity of water to the degree expected by its concentration.[52] The "water deactivating" effect has been described as the molecular dispersion of the water because of water's strong nucleophilic attraction to the ionic

liquid's anion.[42] This dispersion reduces the hydrolysis activity of the water, effectively deactivating its ability to participate in reactions.[42] This phenomenon has been used to prepare compounds in ionic liquids that would otherwise be unstable in the presence of catalytic amounts of water, such as phosphorus trichloride.[53, 54]

Research into using ionic liquids for the dissolution and conversion of cellulose for new materials won the United States' Environmental Protection Agency's 2005 Green Chemistry Challenge's Academic Award.[3, 13, 55, 56] Dr. Robin Rogers' group showed that it is possible to dissolve cellulose and lignocellulosic material (wood) with ionic liquids, leading to further research into using ionic liquids as a key step on the path towards cellulosic biofuels and other bio-based materials.[21, 57-63]

The successful use of ionic liquids with cellulose led to further research using ionic liquids and other biopolymers. This work has led to research into how ionic liquids dissolve and stabilize biopolymers.[64, 65] For example, starch and a water insoluble yet biodegradable protein, zein, were found to dissolve in 1-butyl-3-methylimidazolium chloride ([Bmim][Cl]).[66] The [Bmim][Cl] solution was also used as a reaction media for the successful acylation of starch and protein.[66] The more environmentally benign ionic liquids N-(2-hydroxyethyl) ammonium formate and N-(2-hydroxyethyl) ammonium acetate were also found to dissolve zein.[67] Research into using ionic liquids as solvents for enzymes showed that enzymes retain at least some of their activity in ionic liquid solution.[68, 69] In 2012 Lozano et al. published research where an immobilized enzyme was dissolved in an ionic liquid for catalysis to prepare expensive flavor esters used in commercial products.[70] It is the ability to design biocompatibility into the ionic liquids that has made them of such interest in biochemical applications.[64] The search for solvents other than water for biological applications is important because aqueous solutions can be hampered by side reactions, hydrolysis, or poor substrate solubility.[64] The flexibility of ionic liquids because of their wide range of cations and anions is important to their versatility.

Ionic liquid syntheses

There are two classes of ionic liquids, aprotic and protic. The synthesis of aprotic ionic liquids (AIL), the most widely examined type, is based on the reaction of a nucleophile with a halogen substituted organic compound, shown in Figure 2.2 for the synthesis of 1-butyl-3-methylimidazolium chloride ([Bmim][Cl]).[3]
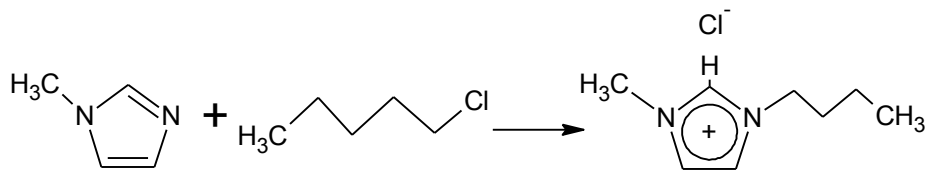
Figure 2.2 Synthesis of [Bmim][Cl]

The reaction of a nucleophile (1-methylimidazole) with a halogen substituted organic compound (such as bromobutane) yields 1-butyl-3-methylimidazolium bromide. The bromide or other anion associates with the mildly acidic hydrogen at the C-2 position on the imidazolium ring.[3, 64] The anion is changed via salt metathesis reaction.[3] The synthesis procedure in Figure 2.2 can be performed for many other types of nucleophilic compounds, such as pyridine, pyrrolidine, trialkylammonia, and trialkylphosphate.[3] The reaction is effectively irreversible because of the covalent bond formed between the substituted nitrogen and the organic compound and the anion is not a strong enough nucleophile to remove the acidic proton at the C_2 position.[71]

By contrast, protic ionic liquids (PIL) are produced through the reversible combination of a Brønsted acid and Brønsted base, shown in Figure 2.3 for the synthesis of 1-methylimidazolium acetate ([mim][OAc]).[72]
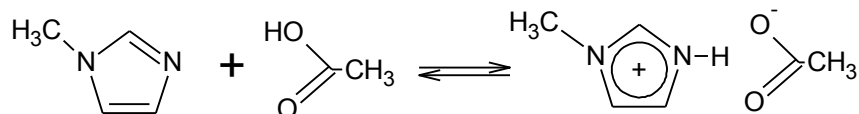
Figure 2.3 Reaction of a Brønsted base (1-methylimidazole) with a Brønsted acid (acetic acid) to form a protic ionic liquid ([mim][OAc])

The difference in the pK_a of the acid and base is used to quantify the strength of the proton transfer (the larger the difference, the stronger the proton transfer and the fewer reactants in solution), and hence the stability of the ionic liquid formed.[72] However, because PIL reactions are reversible, PIL solutions have a vapor pressure from the reactants in the solution (unlike AILs). Because the reactants have a vapor pressure, this may limit their appeal in "green" chemistry applications, despite their easier synthesis than AILs.[72, 73]

Introduction to protein structure analysis

As discussed above, research has been conducted into using ionic liquids as solvents and media for proteins and other biopolymers. It has already been found that ionic liquids have some

uniquely beneficial properties, but what has been missing is an understanding of what ionic liquid properties are important, particularly in respect to understanding how solvent properties affect protein structure. The Gibbs energy of unfolding (denaturing) from a protein's native state to an unfolded state is typically less than 60 kJ/mol. The low stability of proteins reflects the balance in stabilizing forces (primarily intra-protein hydrogen bonding) and destabilizing forces (entropically driven protein unfolding). Therefore only moderate changes to a protein's environment, such as temperature, pressure, or solvent (of particular interest here), can upset the balance and significantly alter protein structure.[64] As many protein properties are related to protein structure, such as gas permeability, tensile strength, enzymatic activity, and digestibility, an understanding of how the protein structure changes in solution is needed when selecting or designing a solvent.[68, 74-79] On the other hand, an understanding of how ionic liquids can stabilize protein structure and what ionic liquid properties are important in that stabilization will be of significant benefit to industries such as pharmaceuticals.[64]

There are three types of individual protein structure, primary (the sequence of amino acids that make up the protein), secondary (the arrangement of those amino acids into the characteristic three dimensional structures of a protein) and tertiary (the three-dimensional location of its atoms).[80-82] The protein primary structure contains all the information necessary for the protein to adopt its secondary, and therefore tertiary, configuration, but is of limited interest in solution because the only way to change the primary structure is through destroying the original protein.[80] The secondary structure, however, is of immense interest because changes in the secondary structure affect the protein properties listed above.[68, 74-79] The four different protein secondary structures are shown in Figure 2.4 for an example protein.[83]
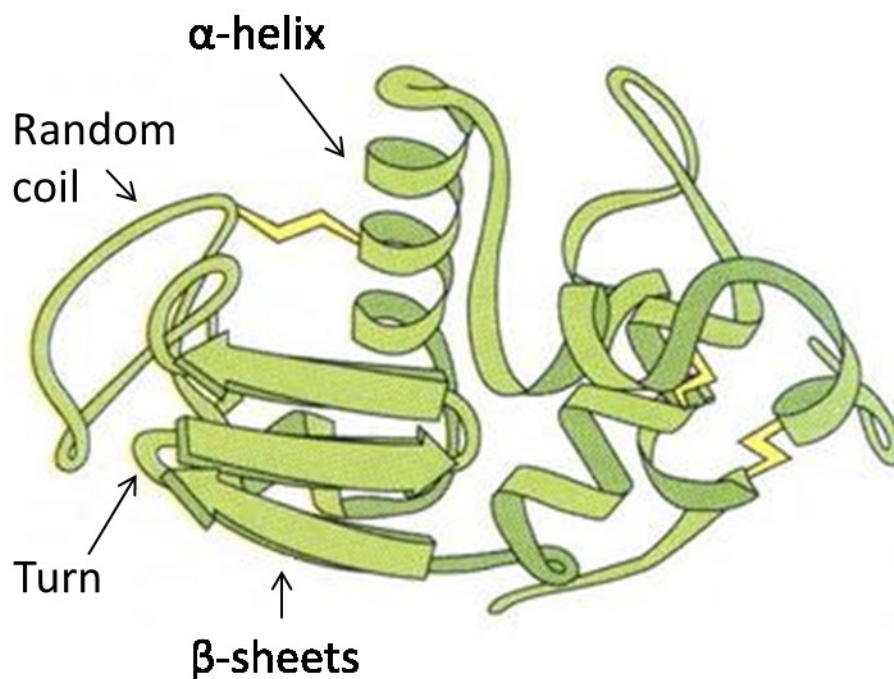
Figure 2.4. Examples of protein secondary structure

All proteins are composed of the secondary structures shown in Figure 2.4, the β-turn, α-helix, random coil, and β-sheet structures; and the amount of each secondary structure varies for the same protein depending on such factors as temperature, solvent, pH, or physical stresses.[80]

Alteration of a protein's secondary structure is known as denaturing, which can be reversible or irreversible depending on the extent of denaturing.[80] Temperature is a primary means of denaturing proteins.[80] The cooking of an egg leads to the irreversible denaturing of the enzyme lysozyme.[80] It has been found that protein solvents affect protein structure, with some, such as aqueous urea or guanidinium solutions, capable of denaturing proteins without thermal changes, and others, such as aqueous sodium chloride, capable of stabilizing proteins to higher denaturing temperatures.[80] The stabilizing or destabilizing effect of ions was first observed by Franz Hofmeister and reported in 1888.[84]

Protein stabilizing anions are known as kosmotropes (such as acetate or chloride) for their ability organize water near the protein, and protein destabilizing anions are known as chaotropes (such as chlorate, thiocyanate, and dicyanamide) for their ability to disrupt water organization near the protein.[85, 86] Kosmotropic anions have stronger interactions with water than water does with itself, thus kosmotropic anions (the stabilizers) disrupt water-water hydrogen-

bond networks but stabilize hydrogen-bond networks overall by hydrogen-bonding with water in solution.[85] Chaotropic anions have weaker interactions with water than water does with itself, so water hydrogen-bond networks are more disrupted by the presence of the chaotropic anion.[85] This disruption of the water hydrogen-bond network gives proteins more structural freedom for entropy-driven denaturing (as the proteins are no longer constrained by a hydrogen-bonded water network), exposing more of their usually buried non-polar portions for interaction with non-polar portions of the solvent.[85, 87-89] This phenomenon is shown and discussed in Chapter 5.

Protein secondary structure can be examined with many tools. A popular method in biochemistry is dichroism, which uses the difference in absorption of polarized light by chiral molecules to identify changes in secondary structure (albeit circular dichroism requires curve fitting to obtain quantitative results).[90] Nuclear magnetic resonance spectroscopy exploits differences in the magnetic properties of atoms in a molecule depending on their environment to develop a structure, and is capable of identifying secondary structures without curve fitting.[90] Raman spectroscopy examines the vibrational modes of amino acids and can also be used to examine protein secondary structure.[91] A commonly used tool for examining protein secondary structure is infrared spectroscopy, which examines the intra-protein hydrogen bonding through bending and stretching modes, and has been used for decades.[90, 92-96]

An introduction to infrared spectroscopy

The principles of infrared (IR) spectroscopy are readily available so only a brief introduction is provided here.[97-99] Infrared spectroscopy is the study and characterization of the vibrational modes of bonds between two atoms in a molecule using electromagnetic radiation between 10 and 14000 cm^{-1} (700 nm to 1 mm wavelength). The infrared region is subdivided into three regions, the near (14000 to 4000 cm^{-1} or 750 nm to 2.5 μm), the mid (4000 to 400 cm^{-1} or 2.5 to 25 μm), and the far (400 to 10 cm^{-1} 25 μm to 1 mm).[97-99] Bonds have particular vibrational frequencies that correspond to certain energy levels. These energy levels depend on the atoms in the molecule, not just on each end of the bond, but from neighboring atoms as well, and thus detailed information can be gathered about molecular structure from the functional groups identified.[97-99]

The near-infrared is the region of molecular overtones and combination bands. These low molar absorptivity bands arise even though they are forbidden by the selection rules of quantum

mechanics, resulting in weak absorptions.[100, 101] The far-infrared region examines molecular rotations among other vibrations and is generally associated with larger elements that vibrate more slowly than carbon or oxygen.[102] The most commonly used region is the mid-infrared, which is the region of the absorptions of the bonds between atoms such as carbon, oxygen, and nitrogen, and thus is the primary region to see many organic and inorganic functional groups.[97-99]

Infrared spectroscopy analyzes the absorption of infrared radiation over a range of wavelengths (700 nm to 1 mm).[97-99] Fourier Transform IR (FTIR) is the most widely used experimental type because of its ability to examine the entire radiation range of interest simultaneously.[97-99] The data collected is used to prepare a plot of absorbance or transmittance versus wavelength (shown as wavenumber cm^{-1}) to show where the molecule absorbed the infrared radiation. The locations of the absorptions correspond to the bonds between atoms, which correspond to particular functional groups. This information is then used to determine what bonds are present to give some understanding of the molecular configuration. A wide range of IR experimental methods exist including transmission (passing the IR radiation through the sample); diffuse or specular reflectance, for solid samples; and attenuated total reflectance which is particularly suitable for liquids.[97-99] Appendices A and B of this dissertation show applications of IR for molecular sieve structure analysis, as do selected references.[103-108]

Attenuated total reflectance IR spectroscopy

First pioneered by N. J. Harrick, Attenuated Total Reflectance (ATR) infrared spectroscopy uses reflections within high refractive index media in intimate contact to examine the sample, in contrast to the typical IR method, transmission, which passes the IR radiation directly through a sample.[109] Light striking an interface between two transparent media of different refractive indexes (a dimensionless quantification of how radiation propagates through that material) will be partially reflected and partially transmitted. The transmitted beam is refracted according to Snell's law:

$$n_i \sin\theta_i = n_r \sin\theta_r \hspace{6cm} 2.1$$

In equation 2.1 n_i and n_r are the refractive indexes of the incident and refractive material respectively, and θ_i and θ_r are angles of incidence and refraction, respectively. Total internal

reflectance occurs when a beam strikes the boundary between two media with different refractive indexes (where the index of refraction of the refractive media is lower than that of the incident media) at an angle greater than the critical angle. The critical angle (θ_c) is obtained from the refractive indexes of the two media using equation 2.2:

$$\theta_c = arcsin\left(\frac{n_r}{n_i}\right) \hspace{4cm} 2.2$$

So long as n_r is less than n_i and the angle of incidence is greater than θ_c the beam will reflect inside the incident media. Figure 2.5 shows total internal reflectance within a piece of acrylic plastic.[110]
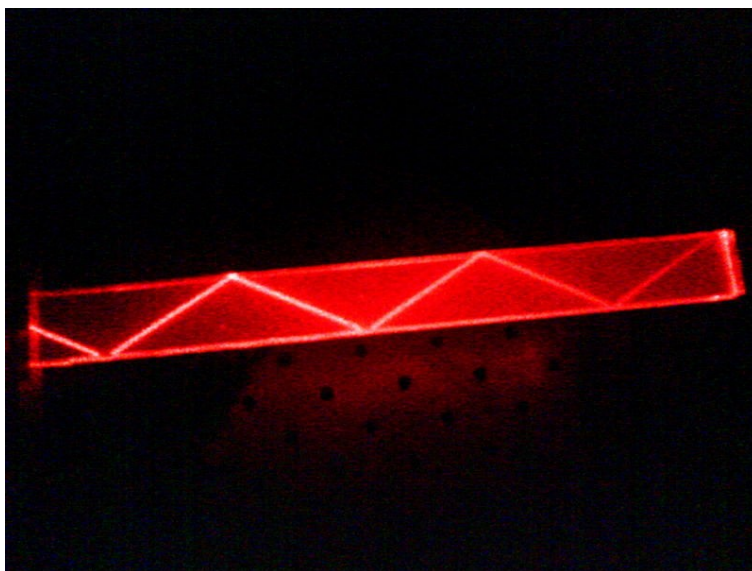
Figure 2.5 Total internal reflectance in a block of acrylic plastic

Figure 2.5 shows there is no refracted radiation visible leaving the sample. However, an evanescent wave is formed on the surface where the beam reflects within the acrylic plastic.[109] An evanescent wave is a standing wave with an intensity that decays exponentially with distance from the surface, penetrating into the external media. The penetration depth is typically between 0.5 and 2.0 μm, depending on the angles and indexes of refraction of the media.[109] The end effect is that the evanescent wave obtains absorption information about the external media, which is then transmitted through the crystal to the detector, as with any IR spectroscopic method. There are single and multiple reflection methods available (this research uses a thirteen reflection method, seven of those on the sample side). Figure 2.6 shows the interactions between the

14

incident radiation and the evanescent wave and a sample mounted on a nine reflection ATR crystal.[111]
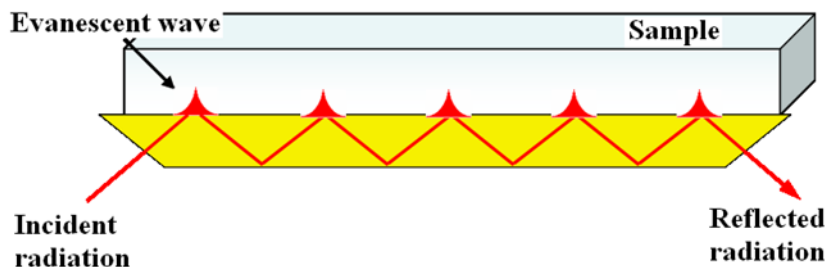
Figure 2.6 Illustration of attenuated total reflectance spectroscopy

One of the keys of ATR is that the reflection media (the crystal) has to be of a higher index of refraction than the material being studied. Therefore high index of refection materials such as diamond, germanium, thallium bromide, or zinc selenide (used in this research) are used.[109, 112]

One of the benefits of ATR is the consistent, short, path length of the radiation. The consistent path length is important for Beer's law, which is used to find the concentration of a substance in solution (in this case, water). Beer's law state's that the absorption of radiation by the samples is a function of concentration, path length, and molar absorptivity (equation 3).

$$A = \varepsilon P c \qquad\qquad 2.3$$

In Beer's law, equation 2.3, A is absorbance, ε is molar absorptivity (how strongly the chemical species of interest absorbs the radiation at that wavelength, units of L/mol/cm), P is path length of the light through the sample, and c is the concentration of the chemical species of interest. As one can see from equation 2.3, the path length of the radiation is important to maintain for quantitative investigations, and ATR gives consistent, short, path lengths. Short path length is valuable when examining samples high water concentration because it is possible that the water will totally absorb the radiation, masking all other absorptions and preventing solvent subtraction. In this research a thirteen reflection crystal is used, and as seven of those reflections were on the sample side, and each reflection's evanescent wave penetrates from 0.5 to 2 μm into the sample, the path length used in this research is from 6.5 to 26 μm. Most importantly, the path length was the same for all samples examined, facilitating the quantitative research reported in

Chapters 5 and 6. See Chapter 3, Experimental Methods, for details of the IR spectroscopic equipment used in this research.

Application of IR spectroscopy to protein secondary structure

As mentioned above, IR spectroscopy has been used for decades to examine proteins and it is still used extensively today.[95, 96] Infrared spectroscopy is able to view nine different characteristic "Amide" bands of the protein, including the important "Amide I" C=O band between 1690 and 1600 cm^{-1}.[92, 113-115] Table 2.1 gives a list of the characteristic infrared bands of proteins.[92, 95, 96]

Table 2.1 List of Amide bands in mid-infrared region

Designation	Approximate frequency (cm^{-1})	Description
Amide A	3300	N-H stretching
Amide B	3100	N-H stretching
Amide I	1690 – 1600	C=O stretching
Amide II	1575 – 1480	C-N stretching, N-H bending
Amide III	1300 – 1230	C-N stretching, N-H bending
Amide IV	770 – 625	O-C-N bending
Amide V	800 – 400	Out-of-plane N-H bending
Amide VI	610 – 530	Out-of-plane C=O bending
Amide VII	200	Skeletal torsion

The Amide I band is of particular importance because of its sensitivity to changes in the protein's secondary structure. The oxygen of the Amide I band is hydrogen bonded to nearby amide hydrogens; changes in the secondary structure alter the length of the hydrogen bond, thus altering the frequency of the absorption.[92-96, 116] These absorptions fall into characteristic regions for each type of secondary structure, see Table 2.2.[93-96, 116, 117]

Table 2.2 Infrared spectroscopy Amide I locations of secondary structure of proteins

Secondary structure element	Band position (cm^{-1})
β-turn	1690-1665
α-helix	1665-1655
Random coil	1655-1645
β-sheet	1645-1610

Each secondary structure has a different, unique, peak location.[93-96, 116, 117] For example, α-helix bonds are visible between 1665 and 1655 cm^{-1}, while β-sheet bonds are visible between 1645 and 1610 cm^{-1}.[92] The β-sheet region is interesting from a quantitative perspective because often more than one peak is found from 1645 to 1610 cm^{-1}, indicating the presence of more than one type of β-sheet structure.[92, 96] Due to the narrow range of characteristic locations for these bonds, it is possible to perform detailed analysis of changes in the secondary structure due to solvent, chemical, or thermal effects.[92, 93, 113, 114, 116-118] For example, in 2004 Lau et al. showed the loss of enzymatic activity for proteins dissolved in ionic liquids through changes in the enzyme's secondary structure using infrared spectroscopy, but without quantification of the secondary structure changes.[79]

However, the absorptions overlap in the Amide I region, requiring further analysis before qualification or quantification can be performed.[92-96, 116] The first step is to find the location of the bands in the Amide I region. Often the second derivative of the Amide I absorption is used, which gives the location of each of the bands present and is useful for locating peaks (indicating the presence and then decline or increase of a particular secondary structure).[79, 94, 113, 116, 119, 120] Figure 2.7 is an example of curve fitting analysis applied to a spectrum obtained in the course of this research, including the original data, the second derivative of the original data, with the curve fit peaks and the combined peak fit.
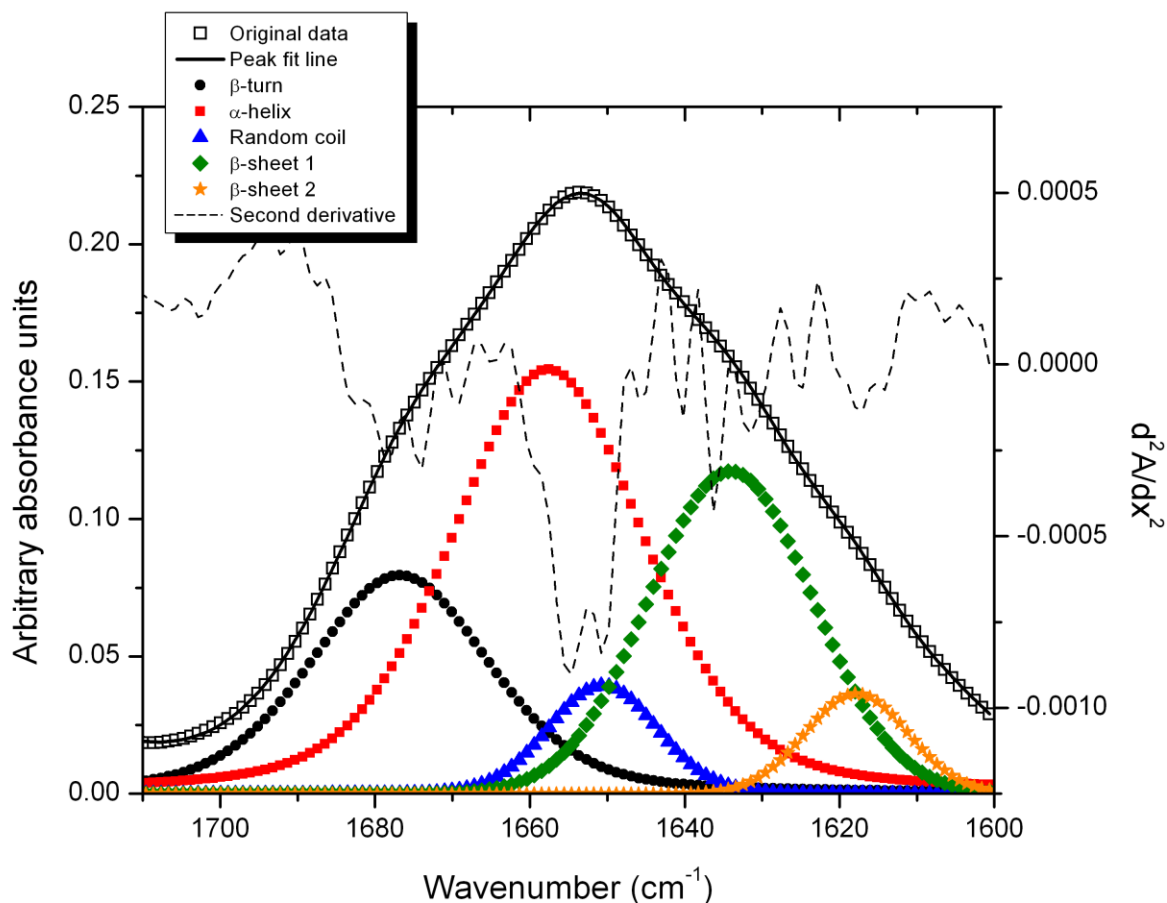
Figure 2.7 Example of peak fitting analysis of Amide I band for zein in 70 vol.% aqueous ethanol

After finding the second derivative (the dotted line in Figure 2.7) of the Amide I band, curve fitting is applied (the solid dots within the original data) using the peak locations obtained from the second derivative (see Chapter 3).[94-96, 113, 116, 119, 120] However, each secondary structure has its own molar absorptivity, how much radiation each type of secondary structure absorbs, and thus the molar absorptivity must be taken into account.[121] The relative molar absorptivities used in this research are given in Table 2.3.[121]

18

Table 2.3 Relative molar absorptivities for secondary structures used in this research

Secondary structure	Relative secondary structure molar absorptivity (L/mol/cm)[121]
β-turn	1.42 ± 0.83
α-helix	2.96 ± 0.20
Random coil	1.61 ± 0.07
β-sheet	4.27 ± 0.28

The values in Table 2.3 were obtained by by de Jongh et al. by comparing the infrared radiation absorbed by 15 globular proteins.[121] These absorptions were then examined with nonlinear least-square regression to identify each secondary structures' relative molar absorptivity.[121] Given that the path length is consistent, the relative molar absorptivities are known, and a consistent internal standard is used, it is possible to use Beer's Law (equation 2.3) to find the concentration of that secondary structure in the protein. Dividing the concentration of each secondary structure by the sum of all secondary structure concentrations yields the percent of each secondary structure.

Infrared spectroscopy is still widely applied to protein secondary structure analysis. For example, in 2008, 2010, and 2011 Carbonaro et al. used infrared spectroscopy with curve fitting to analyze the secondary structure of legume seed flour for differences in secondary structure and how those differences affect the flour's digestibility.[122-124] The solvent accessibility of proteins in heart valves was studied in 2012.[125] Interactions of the anti-inflammatory and antioxidant curcumin were studied for its interactions with human serum albumin in 2009.[126] Denaturation of β-lactoglobulin caused by urea was studied in 2009.[127]

Infrared spectroscopy also has a long history with the protein zein, examining how its structure varies according different samples and with temperature.[128, 129] Using IR spectroscopy to analyze ionic liquid solutions is not a novel idea, IR has been applied to questions of the state of water in ionic liquid for years.[130-134] However, IR has not been used to quantitatively examine proteins dissolved in ionic liquids.

Introduction to zein

An interesting biopolymer is zein, a prolamin (energy storage) mixture of proteins found in corn. Zein was first described in 1821, and its solubility in low molecular weight aqueous

alcohols was first explored in 1897.[135, 136] Zein is tough, insoluble in water and grease, and biodegradable, and clear when cast as a film. Zein can be used as a coating for food products (it was Generally Recognized As Safe by the United States Food and Drug Administration in 1985) and in cosmetics, fibers, ceramics, inks, adhesives, and biodegradable plastics.[137-139] Zein is a mixture of different proteins, differentiated by solubilities in mixtures of ethanol and isopropanol.[138-140] The most common type of zein is α-zein, which is >80% of the zein in corn, while β makes up ~10% and δ and γ make up the remainder.[137] The fractions of each type vary depending on species of corn.[138] The most common type, α-zein, is the only type of zein used commercially, and all further discussion of zein is focused solely on α-zein. Commercial production of zein began in the 1930s and peaked in the 1950s at 15 million pounds per year in the United States. However, the increasing availability and decreasing costs of petroleum-based polymers diminished the market for zein. Zein has languished commercially since then, despite the large amount of research invested in zein's applications and methods to extract zein.[137-139, 141]

Interest in zein is increasing today because of its properties and the desirability of biologically-based chemicals.[138, 139, 141] The solubility of zein has been examined in a variety of solvents including aqueous ethanol and acetic acid.[137-139, 141-148] Zein's structure, properties, and applications have been examined in solid form,[129, 137-139, 149] in acetic acid,[76, 150, 151] and in aqueous ethanol.[151-153] Figure 2.8 shows an image of α-zein prepared computationally using data graciously provided by Bugs et al.[154]
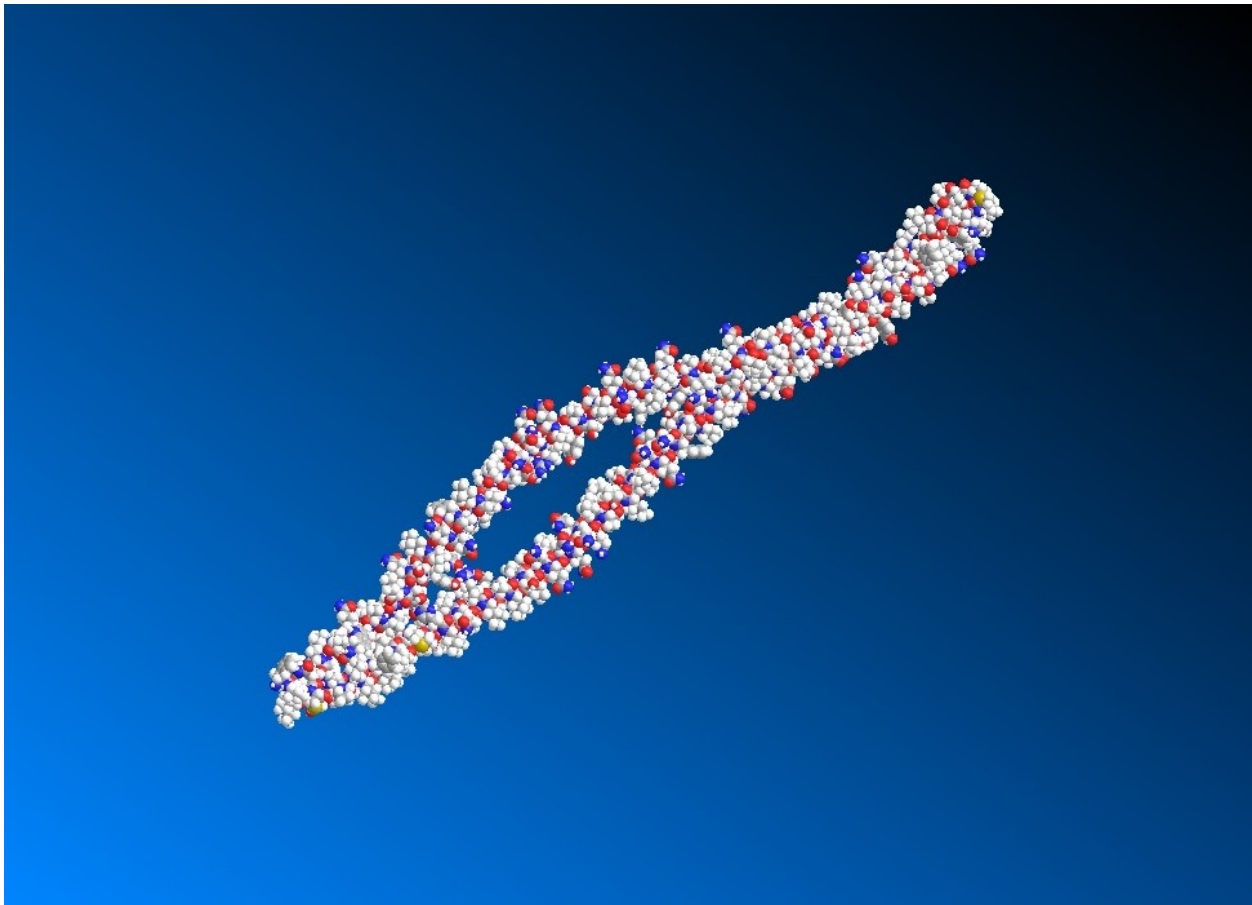
Figure 2.8 Image of α-zein prepared computationally using data provided by Bugs et al.

The primary commercial difficulty with zein is its cost of production and extraction.[138,] [139, 141] Corn contains approximately 9-12% protein and approximately half of that is zein.[137, 139] Zein extraction is still expensive because of the limitations of the current methods of zein production which uses large amounts of aqueous alcohols. The most common current industrial method uses excesses of either ethanol or isopropanol to extract zein from DDGS or other corn products. Zein is currently sold for $10 – 40/kg, depending on the purity, compared to petroleum-based polymers which are sold for less than $2/kg.[138, 139, 143] Other processes have been examined for zein production including acetic acid extraction,[76] using 100% ethanol at 120°C,[140] and chromatography for ultra-high purity zein.[155] Zein's properties of water and grease insolubility, its biodegradability, and its industrial usefulness in coatings, cosmetics, fibers, ceramics and other applications warrant increasing its production. However, increasing its production depends on decreasing its production costs.[137-139] It is hoped that this research into the

21

interactions of zein and ionic liquids will facilitate the design of new solvents and processes for zein production to make zein more economically competitive with petroleum-based polymers.

Solvent properties

The purpose of this research is to investigate how ionic liquid properties affect zein solubility and secondary structure. This information will then be used to develop a model for zein solubility and secondary structure as a function of solvent properties that are either known or can be estimated. It has been found that a particularly solvent property, hydrogen bond accepting ability, is important in the cellulose and lignocellulose applications discussed above.[55, 56, 63] Therefore a discussion of relevant solvent properties is in order.

The first solvent properties investigated are the solvent hydrogen bond donating (Lewis acidity) and hydrogen bond accepting (Lewis basicity) abilities. The hydrogen bond donating and accepting ability are related to the structure of the solvent and impact the solute by hydrogen bonding with it as well. The most common method of measuring solvent hydrogen bond accepting or donating ability is the use of solvatochromic dyes, dyes that alter their UV/vis/near-IR absorption through hydrogen bonding interactions with a solvent of interest.[156] These interactions occur through changes in the solvation of the ground- and first- excited state of a light-absorbing molecule.[156] Kamlet and Taft pioneered the use of these changes in light absorption to quantify, on an empirical scale, the ability of a solvent to donate or accept hydrogen bonds, relative to the reference molecule cyclohexane.[157, 158] The better the hydrogen bond donator, the higher the solvent's α parameter; the better the acceptor, the higher the solvent's β-parameter.[157, 158] In the cases referred to above of ionic liquids successfully dissolving cellulose, it was found that the hydrogen bond accepting ability (or Lewis basicity) was the most important factor.[55, 56, 63] Thus in this research the hydrogen bonding ability of the solvents has been of prime interest. The effects of hydrogen bonding ability on the solubility and structure of zein are described in Chapter 6.

In addition to the hydrogen bond donating or accepting ability, the dipolarity or polarizability of the solvent is also of interest. Dipolarity is the separation of a positive portion of a molecule from the negative portion of a molecule.[159] Polarizability is the ease with which a molecule's electron cloud can be displaced from its ordinary position due to an external electric field.[159] For example, argon has no permanent dipole moment, but it can develop a momentary

one when an external electric field moves the argon's electrons from their ordinary position.[159] It is possible to measure the combined dipolarity and polarizability of a molecule using the same techniques pioneered by Kamlet and Taft as the examination of hydrogen bond donating or accepting ability described above.[156] The dipolarity/polarizability of a molecule is noted by the π^* parameter.[156]

The $E_T(30)$ scale has gained wide acceptance as a solvatochromic measure of solvent polarity, the difference in electron density between one part of a molecule and another.[160-162] The $E_T(30)$ values are an empiricism based on the electron energy level molar transition energies (the change in energy of an electron from an excited to ground state, in kcal/mol) of the standard betaine dye number 30, measured at room temperature and normal pressure.[160, 161] Standard betaine dye number 30 is not soluble in nonpolar solvents, but it has been widely studied for ionic liquid solutions and is thus used in this research.[161] The $E_T(30)$ scale ranges from 63.1 kcal/mol for water (the most polar conventional solvent) to 30.7 kcal/mol for tetramethylsilane (the least polar solvent for which $E_T(30)$ data is available), with many ionic liquids between 48 and 56 kcal/mol.[156, 161]

The final solvent property to be examined in this research is molecular size. It is expected that the size of the solvent will affect how it interacts with the solute. While it is easy to find the size of individual atoms, the peculiar packing and association characteristics of ionic liquids means that the pure solvent size (expressed as milliliters per mole of solvent) needs to be identified. The pycnometer method used to find the pure solvent molar volume is described in Chapter 3.

Linear solvation energy relationship

The effects of solvent parameters can be examined statistically using regression analysis. Kamlet et al. systematized the use of hydrogen bonding ability and dipolarity/polarizability to model solvent behavior in 1983.[157] The research by Kamlet et al.'s enables the researcher to use solvent properties to model a measureable reaction parameter, such as solubility at a temperature, as a function of the chosen solvent properties.[157] Equation 8 gives the generalized form first proposed by Kamlet et al.[157]

$$XYZ = XYZ_0 + a\alpha + b\beta + s(\pi^* + d\delta) + h\delta_h + e\varepsilon \qquad\qquad 2.4$$

In equation 6.4 XYZ is the measureable reaction property of interest, π* is the solvent dipolarity/polarizability, δ is the solvent "polarizability correction term", α is the solvent hydrogen bond donating ability, β is the solvent hydrogen bond accepting ability, δ_h is the Hildebrand solubility parameter, and ε is the solvent coordinate covalency. The parameter XYZ_0 is the regression intercept. The coefficients s, a, b, h, and e are empirical regression parameters that measure the relative susceptibilities of XYZ to the indicated solvent property scales.[157, 163] That is, the coefficients quantify the importance of each solvent parameter's contribution to XYZ. The larger the magnitude of the coefficient, the more important that solvent property is in modeling the behavior of the solute. The method to find the coefficients is simple, requiring multivariate statistical regression of the measureable reaction property as a function of the solvent parameters of interest. It is important to note that not all six solvent parameters in equation 2.4 need to be known for this empirical analysis to be performed.[157] In this research δ, δ_h, and ε were not available for the solvents of interest and thus were not used, resulting in equation 2.5.

$$XYZ = XYZ_0 + a\alpha + b\beta + s\pi^*$$
2.5

The LSER method is used in Chapter 6 to quantify the importance of the Kamlet-Taft parameters in modeling the solubility, and Mz (related to the enthalpy of dissolution of zein found with the van't Hoff equation, see below).

Temperature effects on solubility

The effect of temperature on solubility can be quantified by finding the enthalpy of dissolution. The enthalpy of dissolution of a solute quantifies the energetic favorability of the dissolution of a solute into a solvent. The enthalpy of dissolution depends on how the solute interacts with the solvent and is thus a function of the chemical properties of the solute and solvent. The enthalpy of dissolution can be obtained from temperature dependent solubility data. The enthalpy of dissolution is the sum of the energy required to break the intra-solute and intra-solvent bonds (endothermic processes) and the energy released by the formation of solute-solvent bonds (an exothermic process).[159, 164] Thus negative values for the enthalpy of dissolution

are enthalpically favorable as exothermic processes, but positive values are enthalpically unfavorable as endothermic processes. The greater the value of the enthalpy of dissolution, the more energy required to dissolve the solute in the solvent, resulting in lower solubility.

The van't Hoff equation can be used to find the enthalpy of dissolution, through the following derivation beginning with the standard state (298 K, 1 atmosphere pressure in biochemistry) Gibbs free energy (the thermodynamic potential) of a pure system, equation 2.5.[81, 159, 165, 166]

$$dG^o = dH^o - TdS^o \qquad\qquad 2.6$$

In equation 2.5 dG° is the standard Gibbs free energy of reaction, dH° is the standard reaction enthalpy, T is absolute temperature, and dS° is standard reaction entropy. The Gibbs free energy of a different composition, one that is not pure, is written as equation 2.6.

$$dG = dG^o + RTlnQ \qquad\qquad 2.7$$

In equation 2.6 dG is the Gibbs free energy at temperature T with reaction quotient Q (a dimensionless quantity that describes the extent of chemical transformation). At equilibrium, dG = 0 and Q becomes K, the equilibrium coefficient, a dimensionless quantity that is usually the mole ratio of products versus reactants but can also be the equilibrium mass fraction solubility, equation 2.7.[164, 167, 168]

$$0 = dG^o + RTlnK \qquad\qquad 2.8$$

Substituting equation 2.7 into equation 2.5 and then solving for lnK results in equation 4, also known as the van't Hoff equation.

$$lnK = \frac{-dH^o}{R}\left(\frac{1}{T}\right) + \frac{dS^o}{R} \qquad\qquad 2.9$$

However, this derivation assumes that the heat capacity (C_p) of the solute is not a function of temperature, which is the case for most solutes. Unfortunately that is not the case when the solute is a protein. The C_p of a protein is a function of its structure.[81] As the structure of proteins change with temperature (see Chapter 5) the C_p is thus a function of temperature.[81] Therefore, in a plot of the natural log of solubility versus the inverse of temperature, the slope represents a combination of the enthalpy of dissolution and the enthalpy of denaturing.[81] It is impossible calculate the enthalpy and entropy of dissolution for proteins without detailed knowledge of the changes of C_p of the protein, which is not available for zein. However, since the solute of interest (zein) is always the same, it is a reasonable assumption that the temperature influence on zein denaturing is the same for each of the solute-solvent systems studied. Therefore the relative changes of slope (defined as Mz) are due solely to the solvent effects on the protein in the form of dissolution or denaturing. Equation 2.9 shows the equation used for this work, and equation 2.10 shows that Mz is a function of solute-solvent interactions and temperature.

$$lnK = Mz\left(\frac{1}{T}\right) + constant \qquad\qquad 2.10$$

$$Mz \cong \Delta H_{dissolution}(solute, solvent) + \Delta H_{dentaturing}(T) + \Delta H_{denaturing}(solute, solvent) \, 2.11$$

Although the slope (Mz) cannot provide a quantitative enthalpy as it would if the van't Hoff assumptions applied, the relative values still provide a useful comparison of the different solvents.

References

1. Rogers, R. D.; Seddon, K. R. Ionic Liquids-Solvents of the Future? *Science* **2003**, 792.

2. Gabriel, S.; Weiner, J. On some Derivatives of Propylamine, *Ber. Dtsch. Chem. Ges.* **1888**, 2669-2679.

3. Freemantle, M. *An introduction to ionic liquids;* Royal Society of Chemistry: Cambridge, U.K., 2009; , pp 281.

4. Welton, T. Room-temperature ionic liquids. Solvents for synthesis and catalysis, *Chem. Rev.* **1999**, *8,* 2071-2084.

5. Wilkes, J. S. Properties of ionic liquid solvents for catalysis, *J. Mol. Catal. A: Chem.* **2004**, *1,* 11-17.

6. Wasserscheid, P., Welton,T. Ionic Liquids in Synthesis, **2003**, 9-12.

7. Walden, P. Molecular weights and electrical conductivity of several fused salts, *Bull. Acad. Imper. Sci. (St. Petersburg)* **1914**, 405-422.

8. Seddon, K. R. Ionic liquids for clean technology, *J. Chem. Tech. and Biotech.* **1997**, *4,* 351-356.

9. Freemantle, M. Designer solvents-Ionic liquids may boost clean technology development, *C&E News* **1998**, *13,* 32-37.

10. Rogers, R.; Voth, G. Guest editorial–ionic liquids, *Acc. Chem. Res.* **2007**, 1077-1078.

11. Earle, M. J.; Esperança, J. M. S. S.; Gilea, M. A.; Lopes, J. N. C.; Rebelo, L. P. N.; Magee, J. W.; Seddon, K. R.; Widegren, J. A. The distillation and volatility of ionic liquids, *Nature* **2006**, *7078,* 831-834.

12. Jessop, P. G. Searching for green solvents, *Green Chem.* **2011**, *6,* 1391-1398.

13. Holbrey, J. D.; Turner, M. B.; Rogers, R. D. In *In Selection of ionic liquids for green chemical applications;* ACS Symposium Series; ACS Publications: 2003; Vol. 856, pp 2-13.

14. Swatloski, R. P.; Holbrey, J. D.; Rogers, R. D. Ionic liquids are not always green: hydrolysis of 1-butyl-3-methylimidazolium hexafluorophosphate, *Green Chem.* **2003**, *4,* 361-363.

15. Uerdingen, M.; Treber, C.; Balser, M.; Schmitt, G.; Werner, C. Corrosion behaviour of ionic liquids, *Green Chem.* **2005**, *5,* 321-325.

16. Abbott, A. P.; Capper, G.; Davies, D. L.; Rasheed, R. K.; Shikotra, P. Selective extraction of metals from mixed oxide matrixes using choline-based ionic liquids, *Inorg. Chem.* **2005**, *19,* 6497-6499.

17. Nockemann, P.; Thijs, B.; Driesen, K.; Janssen, C. R.; Van Hecke, K.; Van Meervelt, L.; Kossmann, S.; Kirchner, B.; Binnemans, K. Choline saccharinate and choline acesulfamate: Ionic liquids with low toxicities, *J. Phys. Chem. B* **2007***, 19,* 5254-5263.

18. Ohno, H.; Fukumoto, K. Amino acid ionic liquids, *Acc. Chem. Res.* **2007***, 11,* 1122-1129.

19. Fujita, K.; MacFarlane, D. R.; Forsyth, M.; Yoshizawa-Fujita, M.; Murata, K.; Nakamura, N.; Ohno, H. Solubility and stability of cytochrome c in hydrated ionic liquids: effect of oxo acid residues and kosmotropicity, *Biomacromolecules* **2007***, 7,* 2080-2086.

20. Fukaya, Y.; Hayashi, K.; Wada, M.; Ohno, H. Cellulose dissolution with polar ionic liquids under mild conditions: required factors for anions, *Green Chem.* **2008***, 1,* 44-46.

21. Ohno, H.; Fukaya, Y. Task specific ionic liquids for cellulose technology, *Chem. Lett.* **2009***, 1,* 2-7.

22. Bates, E. D.; Mayton, R. D.; Ntai, I.; Davis Jr, J. H. CO2 capture by a task-specific ionic liquid, *J. Am. Chem. Soc.* **2002***, 6,* 926-927.

23. Dupont, J.; de Souza, R. F.; Suarez, P. A. Z. Ionic liquid (molten salt) phase organometallic catalysis, *Chem. Rev.* **2002***, 10,* 3667-3692.

24. Armand, M.; Endres, F.; MacFarlane, D. R.; Ohno, H.; Scrosati, B. Ionic-liquid materials for the electrochemical challenges of the future, *Nature materials* **2009***, 8,* 621-629.

25. Mudring, A. V.; Alammar, T.; Bäcker, T.; Richter, K. Nanoparticle Synthesis in Ionic Liquids, **2009**.

26. Lee, C. M.; Jeong, H. J.; Lim, S. T.; Sohn, M. H.; Kim, D. W. Synthesis of Iron Oxide Nanoparticles with Control over Shape Using Imidazolium-Based Ionic Liquids, *ACS Appl. Mater. Interfaces* **2010***, 3,* 756-759.

27. Dupont, J.; Scholten, J. D. On the structural and surface properties of transition-metal nanoparticles in ionic liquids, *Chem. Soc. Rev.* **2010***, 5,* 1780-1804.

28. Anderson, J. L.; Armstrong, D. W. High-stability ionic liquids. A new class of stationary phases for gas chromatography, *Anal. Chem.* **2003***, 18,* 4851-4858.

29. Ding, J.; Welton, T.; Armstrong, D. W. Chiral ionic liquids as stationary phases in gas chromatography, *Anal. Chem.* **2004***, 22,* 6819-6822.

30. Kragl, U.; Eckstein, M.; Kaftzik, N. Enzyme catalysis in ionic liquids, *Curr. Opin. Biotechnol.* **2002***, 6,* 565-571.

31. Anthony, J. L.; Maginn, E. J.; Brennecke, J. F. Solution thermodynamics of imidazolium-based ionic liquids and water, *J Phys Chem B* **2001***, 44,* 10942-10949.

32. Crosthwaite, J. M.; Aki, S. N. V. K.; Maginn, E. J.; Brennecke, J. F. Liquid phase behavior of imidazolium-based ionic liquids with alcohols, *The Journal of Physical Chemistry B* **2004***, 16,* 5113-5119.

33. Menjoge, A.; Dixon, J. N.; Brennecke, J. F.; Maginn, E. J.; Vasenkov, S. Influence of Water on Diffusion in Imidazolium-Based Ionic Liquids: A Pulsed Field Gradient NMR study, *The Journal of Physical Chemistry B* **2009***, 18,* 6353-6359.

34. Anthony, J. L.; Maginn, E. J.; Brennecke, J. F. Solubilities and thermodynamic properties of gases in the ionic liquid 1-n-butyl-3-methylimidazolium hexafluorophosphate, *The Journal of Physical Chemistry B* **2002***, 29,* 7315-7320.

35. Anthony, J. L.; Anderson, J. L.; Maginn, E. J.; Brennecke, J. F. Anion effects on gas solubility in ionic liquids, *J. Phys. Chem. B* **2005***, 13,* 6366-6374.

36. Maase, M.; Massonne, K. Biphasic acid scavenging utilizing ionic liquids: The first commercial process with ionic liquids. In *Ionic Liquids IIIB: Fundamentals, Progress, Challenges, and Opportunities. Transformations and Processes, ACS Symposium Series;* Rogers, R. D., Seddon, K. R., Eds.; ACS Publications: 2005; Vol. 902, pp 126-132.

37. Maase, M.; Massonne, K.; Vagt, U. BASIL-BASF's Process Based on Ionic Liquids. *http://www.sigmaaldrich.com/technical-documents/articles/chemfiles/basil-basf-s-processes.html* (accessed February/4, 2013).

38. Parnham, E. R.; Morris, R. E. 1-Alkyl-3-methyl Imidazolium Bromide Ionic Liquids in the Ionothermal Synthesis of Aluminum Phosphate Molecular Sieves, *Chem. Mater.* **2006**, 4882.

39. Parnham, E. R.; Morris, R. E. The Ionothermal Synthesis of Cobalt Aluminophosphate Zeolite Frameworks, *J. Amer. Chem. Soc.* **2006**, 2204.

40. Parnham, E. R.; Morris, R. E. Ionothermal synthesis using a hydrophobic ionic liquid as solvent in the preparation of a novel aluminophosphate chain structure, *J. Mater. Chem.* **2006**, 3682-3684.

41. Parnham, E. R.; Wheatley, P. S.; Morris, R. E. The ionothermal synthesis of SIZ-6—a layered aluminophosphate, *Chem. Comm.* **2006***, 4,* 380-382.

42. Parnham, E. R.; Morris, R. E. Ionothermal Synthesis of Zeolites, Metal–Organic Frameworks, and Inorganic–Organic Hybrids, *Acc. Chem. Res.* **2007**, 1005.

43. Morris, R. E. Concepts in the ionothermal synthesis of zeolites and metal organic frameworks. In *Proceedings of the 4th International FEZA Conference;* 2008; pp 33.

44. Morris, R. E. Ionothermal synthesis-ionic liquids as functional solvents in the preparation of crystalline materials, *Chem. Comm.* **2009**, 2990-2998.

45. Byrne, P. J.; Wragg, D. S.; Warren, J. E.; Morris, R. E. Ionothermal synthesis of two novel metal organophosphonates, *Dalton Trans.* **2009**, 795.

46. Wheatley, P. S.; Allan, P. K.; Teat, S. J.; Ashbrook, S. E.; Morris, R. E. Task specific ionic liquids for the ionothermal synthesis of siliceous zeolites, *Chemical Science* **2010**, *4,* 483-487.

47. Cooper, E. R.; Andrews, C. D.; Wheatley, P. S.; Webb, P. B.; Wormald, P.; Morris, R. E. Ionic Liquids and Eutectic Mixtures as Solvent and Template in Synthesis of Zeolite Analogues, *Nature* **2004**, 1012-1016.

48. Wragg, D. S.; Slawin, A. M. Z.; Morris, R. E. The role of added water in the ionothermal synthesis of microporous aluminum phosphates, *Solid State Sciences* **2009**, 411.

49. Wragg, D. S.; Byrne, P. J.; Giriat, G.; Ouay, B. L.; Gyepes, R.; Harrison, A.; Whittaker, A. G.; Morris, R. E. In Situ Comparison of Ionothermal Kinetics Under Microwave And Conventional Heating, *J. Phys. Chem. C* **2009**, *48,* 296-319.

50. Liu, L.; Wragg, D. S.; Zhang, H.; Kong, Y.; Byrne, P. J.; Prior, T. J.; Warren, J. E.; Lin, Z.; Dong, J.; Morris, R. E. Ionothermal synthesis, structure and characterization of three-dimensional zinc phosphates, *Dalton Trans.* **2009**, *34,* 6715-6718.

51. Martins, G. A. V.; Byrne, P. J.; Allan, P.; Teat, S. J.; Slawin, A. M. Z.; Li, Y.; Morris, R. E. The use of ionic liquids in the synthesis of zinc imidazolate frameworks, *Dalton Transactions* **2010**, *7,* 1758-1762.

52. Yasaka, Y.; Wakai, C.; Matubayasi, N.; Nakahara, M. Slowdown of H/D exchange reaction rate and water dynamics in ionic liquids: Deactivation of solitary water solvated by small anions in 1-butyl-3-methyl-imidazolium chloride, *J. Phys. Chem. A* **2007**, *4,* 541-543.

53. Amigues, E.; Hardacre, C.; Keane, G.; Migaud, M.; O'Neill, M. Ionic liquids—media for unique phosphorus chemistry, *Chemical Communications* **2006**, *1,* 72-74.

54. Hardacre, C.; Holbrey, J. D.; McMath, S. E. J.; Bowron, D. T.; Soper, A. K. Structure of molten 1, 3-dimethylimidazolium chloride using neutron diffraction, *J. Chem. Phys.* **2003**, 273.

55. Swatloski, R. P.; Spear, S. K.; Holbrey, J. D.; Rogers, R. D. Dissolution of cellulose with ionic liquids, *J. Am. Chem. Soc.* **2002**, *18,* 4974-4975.

56. Turner, M. B.; Spear, S. K.; Holbrey, J. D.; Rogers, R. D. Production of bioactive cellulose films reconstituted from ionic liquids, *Biomacromolecules* **2004**, *4,* 1379-1384.

57. Zhang, H.; Wu, J.; Zhang, J.; He, J. 1-Allyl-3-methylimidazolium chloride room temperature ionic liquid: A new and powerful nonderivatizing solvent for cellulose, *Macromolecules* **2005**, *20,* 8272-8277.

58. Hermanutz, F.; Gähr, F.; Uerdingen, E.; Meister, F.; Kosan, B. In *In New developments in dissolving and processing of cellulose in ionic liquids;* Macromolecular Symposia; Wiley Online Library: 2008; Vol. 262, pp 23-27.

59. Wu, R. L.; Wang, X. L.; Wang, Y. Z.; Bian, X. C.; Li, F. Cellulose/soy protein isolate blend films prepared via room-temperature ionic liquid, *Ind Eng Chem Res* **2009**, *15,* 7132-7136.

60. Vitz, J.; Erdmenger, T.; Haensch, C.; Schubert, U. S. Extended dissolution studies of cellulose in imidazolium based ionic liquids, *Green Chem.* **2009**, *3,* 417-424.

61. Liebner, F.; Patel, I.; Ebner, G.; Becker, E.; Horix, M.; Potthast, A.; Rosenau, T. Thermal aging of 1-alkyl-3-methylimidazolium ionic liquids and its effect on dissolved cellulose, *Holzforschung* **2010**, *2,* 161-166.

62. Hesse-Ertelt, S.; Heinze, T.; Kosan, B.; Schwikal, K.; Meister, F. In *In Solvent Effects on the NMR Chemical Shifts of Imidazolium-Based Ionic Liquids and Cellulose Therein;* Macromolecular Symposia; Wiley Online Library: 2010; Vol. 294, pp 75-89.

63. Kahlen, J.; Masuch, K.; Leonhard, K. Modelling cellulose solubilities in ionic liquids using COSMO-RS, *Green Chem.* **2010**, *12,* 2172-2181.

64. Weingärtner, H.; Cabrele, C.; Herrmann, C. How ionic liquids can help to stabilize native proteins, *Phys. Chem. Chem. Phys.* **2012**, *2,* 415-426.

65. Naushad, M.; ALOthman, Z. A.; Khan, A. B.; Ali, M. Effect of ionic liquid on activity, stability, and structure of enzymes: A review, *Int. J. Biol. Macromol.* **2012**, 555-560.

66. Biswas, A.; Shogren, R. L.; Stevenson, D. G.; Willett, J. L.; Bhowmik, P. K. Ionic liquids as solvents for biopolymers: Acylation of starch and zein protein, *Carbohydr. Polym.* **2006**, *4,* 546-550.

67. Choi, H. M.; Kwon, I. Dissolution of Zein Using Protic Ionic Liquids: N-(2-Hydroxyethyl) Ammonium Formate and N-(2-Hydroxyethyl) Ammonium Acetate, *Ind Eng Chem Res* **2011**, 2452-2454.

68. Ha, S. H.; Koo, Y. M. Enzyme performance in ionic liquids, *Korean J. Chem. Eng.* **2011**, 1-7.

69. Naushad, M.; AL-Othman, Z. A.; Khan, A. B.; Ali, M. Effect of Ionic Liquid on Activity, Stability, and Structure of Enzymes: A Short Review, *Int. J. Biol. Macromol.* **2012**.

70. Lozano, P.; Bernal, J. M.; Navarro, A. Clean enzymatic process for producing flavour esters by direct esterification in switchable ionic liquid/solid phases, *Green Chem.* **2012**, 3026-3033.

71. Tsuzuki, S.; Tokuda, H.; Mikami, M. Theoretical analysis of the hydrogen bond of imidazolium C2–H with anions, *Phys. Chem. Chem. Phys.* **2007**, *34,* 4780-4784.

72. Greaves, T. L.; Drummond, C. J. Protic ionic liquids: properties and applications, *Chem. Rev.* **2008***, 1,* 206-237.

73. Angell, C. A.; Byrne, N.; Belieres, J. P. Parallel developments in aprotic and protic ionic liquids: Physical chemistry and applications, *Acc. Chem. Res.* **2007***, 11,* 1228-1236.

74. Gennadios, A.; Weller, C. L.; Testin, R. Temperature Effect on Oxygen Permeability of Edible Protein-based Films, *J. Food Sci.* **2006***, 1,* 212-214.

75. Nack, T. J.; Ludescher, R. D. Molecular mobility and oxygen permeability in amorphous bovine serum albumin films, *Food Biophysics* **2006***, 3,* 151-162.

76. Selling, G. W.; Woods, K. K. Improved isolation of zein from corn gluten meal using acetic acid and isolate characterization as solvent, *Cereal Chem.* **2008***, 2,* 202-206.

77. Duodu, K. G.; Tang, H.; Grant, A.; Wellner, N.; Belton, P. S.; Taylor, J. R. N. FTIR and Solid State 13C NMR Spectroscopy of Proteins of Wet Cooked and Popped Sorghum and Maize, *J. Cereal Sci.* **2001***, 3,* 261-269.

78. Duodu, K. G.; Taylor, J. R. N.; Belton, P. S.; Hamaker, B. R. Factors affecting sorghum protein digestibility, *J. Cereal Sci.* **2003***, 2,* 117-131.

79. Lau, R. M.; Sorgedrager, M. J.; Carrea, G.; van Rantwijk, F.; Secundo, F.; Sheldon, R. A. Dissolution of Candida antarctica lipase B in ionic liquids: effects on structure and activity, *Green Chem.* **2004***, 9,* 483-487.

80. Horton, H. R.; Moran, L. A.; Ochs, R. S.; Rawn, J. D.; Scrimgeour, K. G. *Principles of Biochemistry;* Prentice Hall: Upper Saddle River, NJ, 1996; , pp 862.

81. Haynie, D. T. *Biological thermodynamics;* Cambridge University Press: University Press, Cambridge, 2008; , pp 422.

82. Schellman, J. A. Fifty years of solvent denaturation, *Biophys. Chem.* **2002***, 2,* 91-101.

83. Patnaik, S. Alignment And Prediction Of Secondary Structures Of Proteins. *http://stanxterm.aecom.yu.edu/wiki/index.php?page=Protein_secondary_structures* (accessed January/25, 2013).

84. Hofmeister, F. Zur Lehre von der Wirkung der Salze, *Arch. Exp. Pathol. Pharmakol.* **1888**, 247-260.

85. Zhao, H.; Olubajo, O.; Song, Z.; Sims, A. L.; Person, T. E.; Lawal, R. A.; Holley, L. D. A. Effect of kosmotropicity of ionic liquids on the enzyme stability in aqueous solutions, *Bioorg. Chem.* **2006***, 1,* 15-25.

86. Zhao, H.; Campbell, S. M.; Jackson, L.; Song, Z.; Olubajo, O. Hofmeister series of ionic liquids: kosmotropic effect of ionic liquids on the enzymatic hydrolysis of enantiomeric phenylalanine methyl ester, *Tetrahedron: Asymmetry* **2006***, 3,* 377-383.

87. Burley, S.; Petsko, G. Aromatic-aromatic interaction: a mechanism of protein structure stabilization, *Science* **1985**, *4708,* 23-28.

88. Pace, C. N.; Treviño, S.; Prabhakaran, E.; Scholtz, J. M. Protein structure, stability and solubility in water and other solvents, *Phil. Trans. R. Soc. Lond. B* **2004**, *1448,* 1225-1235.

89. Sachdeva, A.; Cai, S. Structural Differences of Proteins Between Solution State and Solid State Probed by Attenuated Total Reflection Fourier Transform Infrared Spectroscopy, *Appl. Spectrosc.* **2009**, *4,* 458-464.

90. Pelton, J. T.; McLean, L. R. Spectroscopic methods for analysis of protein secondary structure, *Anal. Biochem.* **2000**, *2,* 167-176.

91. Benevides, J. M.; Overman, S. A.; Thomas, G. J. Raman spectroscopy of proteins, *Current protocols in protein science* **2004**, 17.8. 1-17.8. 35.

92. Kong, J.; Yu, S. Fourier transform infrared spectroscopic analysis of protein secondary structures, *Acta biochimica et biophysica Sinica* **2007**, *8,* 549-559.

93. Surewicz, W. K.; Mantsch, H. H.; Chapman, D. Determination of protein secondary structure by Fourier transform infrared spectroscopy: a critical assessment, *Biochemistry (N. Y.)* **1993**, *2,* 389-394.

94. Jackson, M.; Mantsch, H. H. The use and misuse of FTIR spectroscopy in the determination of protein structure, *Crit. Rev. Biochem. Mol. Biol.* **1995**, *2,* 95-120.

95. Barth, A.; Zscherp, C. What vibrations tell us about proteins, *Q. Rev. Biophys.* **2002**, *4,* 369-430.

96. Barth, A. Infrared spectroscopy of proteins, *Biochim Biophys Acta* **2007**, *9,* 1073-1101.

97. Stuart, B. H. *Infrared spectroscopy: fundamentals and applications;* Wiley: 2004; .

98. Stuart, B. *Infrared spectroscopy;* Wiley Online Library: 2005; .

99. Smith, B. C. *Fundamentals of FourierTransform Infrared Spectroscopy;* CRC: Boca Raton, FL, 2009; , pp 194.

100. Ciurczak, E. W. Principles of near-infrared spectroscopy. In *Handbook of Near-Infrared Analysis;* Burns, D. A., Ciurczak, E. W., Eds.; Marcel Dekker: New York, 2001; Vol. 27, pp 7-18.

101. Siesler, H. W.; Ozaki, Y.; Kawata, S.; Heise, H. M. *Near-infrared spectroscopy: Principles, instruments, applications;* Wiley-Vch: Weinheim, 2008; , pp 348.

102. Moller, K. D. a. W. G. R. *Far-Infrared Spectroscopy;* Wiley-Interscience: New York, 1971; .

103. Hajjar, R.; Millot, Y.; Man, P. P.; Che, M.; Dzwigaj, S. Two Kinds of Framework Al Sites Studied in BEA Zeolite by X-ray Diffraction, Fourier Transform Infrared Spectroscopy, NMR Techniques, and V Probe, *J. Phys. Chem. C* **2008***, 51,* 20167-20175.

104. Lercher, J. A.; Jentys, A. Infrared and Raman spectroscopy for characterizing zeolites, *Stud. Surf. Sci. Catal.* **2007**, 435-476.

105. Marques, J. P.; Gener, I.; Ayrault, P.; Bordado, J. C.; Lopes, J. M.; Ramoa Ribeiro, F.; Guisnet, M. Infrared spectroscopic study of the acid properties of dealuminated BEA zeolites, *Micro. Meso. Mater.* **2003**, 251.

106. Arean, C. O. Zeolites and Intrazeolite Chemistry: Insights from Infrared Spectroscopy, **2000***, 3&4,* 243-273.

107. Flanigen, E. M.; Khatami, H.; Szymanski, H. A. Infrared structural studies of zeolite frameworks, *Adv. Chem. Ser.* **1971**, 201-229.

108. Flanigen, E. M. Structural analysis by infrared spectroscopy, *ACS Monograph* **1976**, 80-117.

109. Harrick, N. J. *Internal Reflection Spectroscopy;* John Wiley & Sons: New York, 1967; , pp 327.

110. Anonymous. TIR in PMMA. *http://en.wikipedia.org/wiki/File:TIR_in_PMMA.jpg* (accessed February/6, 2013).

111. Mosely ATR.png. (accessed March/8, 2013).

112. Mirabella, F. M. *Internal reflection spectroscopy: Theory and applications;* CRC: 1992; Vol. 15.

113. Dong, A.; Huang, P.; Caughey, W. S. Protein secondary structures in water from second-derivative amide I infrared spectra, *Biochemistry (N. Y.)* **1990***, 13,* 3303-3308.

114. Gallagher, W. FTIR Analysis of Protein Structure. *http://www.chem.uwec.edu/Chem455_S05/Pages/Manuals/FTIR_of_proteins.pdf* (accessed January/4, 2012).

115. Kalnin, N. N.; Baikalov, I. A.; Venyaminov, S. Y. Quantitative IR spectrophotometry of peptide compounds in water (H2O) solutions. III. Estimation of the protein secondary structure, *Biopolymers* **1990***, 13-14,* 1273-1280.

116. Susi, H.; Michael Byler, D. Protein structure by Fourier transform infrared spectroscopy: second derivative spectra, *Biochem. Biophys. Res. Commun.* **1983***, 1,* 391-397.

117. Byler, D. M.; Susi, H. Examination of the secondary structure of proteins by deconvolved FTIR spectra, *Biopolymers* **1986***, 3,* 469-487.

118. Anderle, G.; Mendelsohn, R. Thermal denaturation of globular proteins. Fourier transform-infrared studies of the amide III spectral region, *Biophys. J.* **1987**, *1,* 69-74.

119. Zhang, J.; Yan, Y. B. Probing conformational changes of proteins by quantitative second-derivative infrared spectroscopy, *Anal. Biochem.* **2005**, *1,* 89-98.

120. D'antonio, J.; Murphy, B. M.; Manning, M. C.; Al-azzam, W. A. Comparability of protein therapeutics: Quantitative comparison of second-derivative amide I infrared spectra, *J. Pharm. Sci.* **2012**.

121. de Jongh, H. H. J.; Goormaghtigh, E.; Ruysschaert, J. M. The different molar absorptivities of the secondary structure types in the amide I region: an attenuated total reflection infrared study on globular proteins, *Anal. Biochem.* **1996**, *1,* 95-103.

122. Carbonaro, M.; Maselli, P.; Dore, P.; Nucara, A. Application of Fourier transform infrared spectroscopy to legume seed flour analysis, *Food Chem.* **2008**, *1,* 361-368.

123. Carbonaro, M.; Nucara, A. Secondary structure of food proteins by Fourier transform spectroscopy in the mid-infrared region, *Amino Acids* **2010**, *3,* 679-690.

124. Carbonaro, M.; Maselli, P.; Nucara, A. Relationship between digestibility and secondary structure of raw and thermally treated legume proteins: a Fourier transform infrared (FT-IR) spectroscopic study, *Amino Acids* **2011**, 1-11.

125. Wang, S.; Oldenhof, H.; Hilfiker, A.; Harder, M.; Wolkers, W. F. Protein secondary structure and solvent accessibility of proteins in decellularized heart valve scaffolds, *Biomed. Spect. Imag.* **2012**, *1,* 79-87.

126. Mandeville, J. S.; Froehlich, E.; Tajmir-Riahi, H. Study of curcumin and genistein interactions with human serum albumin, *J. Pharm. Biomed. Anal.* **2009**, *2,* 468-474.

127. Czarnik-Matusewicz, B.; Kim, S. B.; Jung, Y. M. A Study of Urea-dependent Denaturation of β-Lactoglobulin by Principal Component Analysis and Two-dimensional Correlation Spectroscopy, *J. Phys. Chem. B* **2009**, *2,* 559-566.

128. Kretschmer, C. B. Infrared spectroscopy and optical rotatory dispersion of zein, wheat gluten and gliadin, *J. Phys. Chem.* **1957**, *12,* 1627-1631.

129. Forato, L. A.; Bicudo, T. D. C.; Colnago, L. A. Conformation of α zeins in solid state by Fourier transform IR, *Biopolymers* **2003**, *6,* 421-426.

130. Umebayashi, Y.; Jiang, J.; Shan, Y.; Lin, K.; Fujii, K.; Seki, S.; Ishiguro, S.; Lin, S. H.; Chang, H. Structural change of ionic association in ionic liquid/water mixtures: A high-pressure infrared spectroscopic study, *The Journal of Chemical Physics* **2009**, 124503.

131. Wu, B.; Liu, Y.; Zhang, Y.; Wang, H. Probing Interomolecular Interactions in Ionic Liquid-Water Mixtures by Near-Infrared Spectroscopy, *Chemistry - A European Journal* **2009**, 6889.

132. Dominguez-Vidal, A.; Kaun, N.; Lendl, B. Probing intermolecular interactions in water/ionic liquid mixtures by far-infrared spectroscopy, *J Phys Chem B* **2007**, *17,* 4446-4452.

133. Ficke, L. E.; Brennecke, J. F. Interactions of Ionic Liquids and Water, *J. Phys. Chem. B* **2010**, 10496-10501.

134. Zhang, Q. G.; Wang, N. N.; Yu, Z. W. The Hydrogen Bonding Interactions between the Ionic Liquid 1-Ethyl-3-Methylimidazolium Ethyl Sulfate and Water, *The Journal of Physical Chemistry B* **2010**, *14,* 4747-4754.

135. Gorham, J. Analysis of Indian Corn, *Quart. J. Sci. Lit. Arts II* **1821**, 206-208.

136. Osborne, T. B. The amount and properties of the proteids of the maize kernel, *J. Am. Chem. Soc.* **1897**, 525-532.

137. Anderson, T. J.; Lamsal, B. P. REVIEW: Zein Extraction from Corn, Corn Products, and Coproducts and Modifications for Various Applications: A Review, *Cereal Chem.* **2011**, *2,* 159-173.

138. Lawton, J. W. Zein: A history of processing and use, *Cereal Chem.* **2002**, *1,* 1-18.

139. Shukla, R.; Cheryan, M. Zein: the industrial protein from corn, *Industrial Crops and Products* **2001**, *3,* 171-192.

140. Lawton, J. W. Isolation of zein using 100% ethanol, *Cereal Chem.* **2006**, *5,* 565-568.

141. Momany, F. A.; Sessa, D. J.; Lawton, J. W.; Gordon, W.; Hamaker, S. A. H.; Willett, J. L. Structural characterization of α-zein, *J. Agric. Food Chem.* **2006**, *2,* 543-547.

142. Xu, W.; Reddy, N.; Yang, Y. An acidic method of zein extraction from DDGS, *J. Agric. Food Chem.* **2007**, *15,* 6279-6284.

143. Parris, N.; Dickey, L. C. Extraction and solubility characteristics of zein proteins from dry-milled corn, *J. Agric. Food Chem.* **2001**, *8,* 3757-3760.

144. Mossé, J. Monographie sur une protéine du mais: La zéine, *Ann. Physiol. Veg* **1961**, 105-139.

145. Evans, C. D.; Manley, R. H. Solvents for Zein. Primary Solvents, *Ind. Eng. Chem. Res.* **1941**, *11,* 1416-1417.

146. Manley, R. H.; Evans, C. D. Binary solvents for zein, *Ind. Eng. Chem. Res.* **1943**, *6,* 661-665.

147. Evans, C. D.; Manley, R. H. Stabilizing zein dispersions against gelation, *Ind. Eng. Chem. Res.* **1943**, *2,* 230-232.

148. Tomlinson, S. R.; Anthony, J. L.; Schlup, J. R. Temperature effects on the secondary structure of the corn protein zein, as a film, in aqueous ethanol, and in acetic acid, *Submitted for publication* **2013**.

149. Forato, L. A.; Doriguetto, A. C.; Fischer, H.; Mascarenhas, Y. P.; Craievich, A. F.; Colnago, L. A. Conformation of the Z19 prolamin by FTIR, NMR, and SAXS, *J. Agric. Food Chem.* **2004**, *8,* 2382-2385.

150. Huang, H.; Xie, J.; Chen, H. Adsorption behavior of human serum albumin on ATR crystal studied by in situ ATR/FTIR spectroscopy and two-dimensional correlation analysis, *Analyst* **2011**, *8,* 1747-1752.

151. Li, Y.; Li, J.; Xia, Q.; Zhang, B.; Wang, Q.; Huang, Q. Understanding the Dissolution of α-Zein in Aqueous Ethanol and Acetic Acid Solutions, *J. Phys. Chem. B* **2012**, 12057-12064.

152. Cabra, V.; Arreguin, R.; Vazquez-Duhalt, R.; Farres, A. Effect of temperature and pH on the secondary structure and processes of oligomerization of 19 kDa alpha-zein, *Biochim Biophys Acta* **2006**, *6,* 1110-1118.

153. Selling, G. W.; Hamaker, S. A. H.; Sessa, D. J. Effect of Solvent and Temperature on Secondary and Tertiary Structure of Zein by Circular Dichroism. *Cereal Chem.* **2007**, 265-270.

154. Bugs, M. R.; Forato, L. A.; Bortoleto-Bugs, R. K.; Fischer, H.; Mascarenhas, Y. P.; Ward, R. J.; Colnago, L. A. Spectroscopic characterization and structural modeling of prolamin from maize and pearl millet, *European Biophysics Journal* **2004**, *4,* 335-343.

155. Kale, A.; Zhu, F.; Cheryan, M. Separation of high-value products from ethanol extracts of corn by chromatography, *Industrial Crops and Products* **2007**, *1,* 44-53.

156. Reichardt, C. Solvatochromic dyes as solvent polarity indicators, *Chem. Rev.* **1994**, *8,* 2319-2358.

157. Kamlet, M. J.; Abboud, J. L. M.; Abraham, M. H.; Taft, R. Linear solvation energy relationships. 23. A comprehensive collection of the solvatochromic parameters,. pi.*,. alpha., and. beta., and some methods for simplifying the generalized solvatochromic equation, *J. Org. Chem.* **1983**, *17,* 2877-2887.

158. Kamlet, M.; Abboud, J.; Taft, R. An examination of linear solvation energy relationships, *Progress in Physical Organic Chemistry, Volume 13* **2007**, 485-630.

159. Prausnitz, J. M.; Lichtenthaler, R. N.; de Azevedo, E. G. *Molecular Thermodynamics of Fluid-Phase Equilibria;* Prentice-Hall PTR: Upper Saddle River, New Jersey, 1998; , pp 860.

160. Reichardt, C. Solvatochromism, thermochromism, piezochromism, halochromism, and chiro-solvatochromism of pyridinium N-phenoxide betaine dyes, *Chem. Soc. Rev.* **1992**, *3,* 147-153.

161. Reichardt, C. Polarity of ionic liquids determined empirically by means of solvatochromic pyridinium N-phenolate betaine dyes, *Green Chem.* **2005**, *5,* 339-351.

162. Matyushov, D. V.; Schmid, R.; Ladanyi, B. M. A Thermodynamic Analysis of the π^* and ET (30) Polarity Scales, *J. Phys. Chem. B* **1997**, *6,* 1035-1050.

163. Kolling, O. W. A Note on Dipolarity-Polarizability Effects for Aromatic Solvents, *Trans. Kans. Aca. Sci.* **1995**, *3/4,* 113-117.

164. Suzuki, Y.; Konda, E.; Hondoh, H.; Tamura, K. Effects of temperature, pressure, and pH on the solubility of triclinic lysozyme crystals, *J. Cryst. Growth* **2011**, *1,* 1085-1088.

165. Krug, R.; Hunter, W.; Grieger, R. Enthalpy-entropy compensation. 1. Some fundamental statistical problems associated with the analysis of van't Hoff and Arrhenius data, *J. Phys. Chem.* **1976**, *21,* 2335-2341.

166. Krug, R.; Hunter, W.; Grieger, R. Enthalpy-entropy compensation. 2. Separation of the chemical from the statistical effect, *J. Phys. Chem.* **1976**, *21,* 2341-2351.

167. Delgado, D. R.; Vargas, E. F.; Martínez, F. Thermodynamic Study of the Solubility of Procaine HCl in Some Ethanol Water Cosolvent Mixtures, *J. Chem. Eng. Data* **2010**, *8,* 2900-2904.

168. Eghrary, S. H.; Zarghami, R.; Martinez, F.; Jouyban, A. Solubility of 2-Butyl-3-benzofuranyl 4-(2-(Diethylamino) ethoxy)-3, 5-diiodophenyl Ketone Hydrochloride (Amiodarone HCl) in Ethanol Water and N-Methyl-2-pyrrolidone Water Mixtures at Various Temperatures, *J. Chem. Eng. Data* **2012**, 1544-1550.

Chapter 3 - Experimental Methods

Ionic liquid synthesis

Full names and chemical structures of all the ionic liquids used are given in Appendix G. The ionic liquids [Bmim][OAc], [Emim][OAc], and [Emim][DCA] were obtained from IoLiTec Inc. and used without further purification. Their ^{1}H NMR spectra were obtained to confirm product identity.

The ionic liquid [Bmim][Cl] was prepared by combining 0.5 mol 1-methylimidazole (99+%, Aldrich) with 0.51 mol 1-chlorobutane (99+% Fisher) in 50 g methanol. The mixture was heated and stirred for 48 hours at 50°C. The solution was dried under vacuum at 50°C for 48 hours and then for 6 hours at 75°C to remove the solvent and excess reagents. Proton NMR was performed to confirm the product synthesis.

The protic ionic liquids [mim][OAc], [mim][HSO$_4$], and 1-methylimidazolium formate [mim][Fr], were prepared by slowly adding an equimolar amount of the acid (acetic, sulfuric, or formic) to 1-methylimidazole in an ice water bath. The ionic liquids were subsequently stirred overnight at room temperature. The ionic liquids were dried under vacuum for 48 hours at 50°C, then for another 6 hours at 75°C to remove solvent and unreacted reagent. The water content of each solvent was tested in triplicate with a calibrated coulometric Karl-Fischer titrator and the results are given in Table 3.1.

Table 3.1 Karl-Fischer titration water concentration results with one standard deviation of results

Solvent	Mean wt.% water	mol% water
Karl-Fischer titration standard (0.10 wt.%)	0.097 ± 0.007	
Acetic Acid	0.422 ± 0.002	1.407 ± 0.007
1-Methylimidazole	0.242 ± 0.014	1.102 ± 0.062
[mim][OAc]	0.283 ± 0.003	2.232 ± 0.024
[mim][Fr]	0.211 ± 0.018	1.502 ± 0.129
[mim][HSO$_4$]	0.703 ± 0.048	7.034 ± 0.476
[Emim][OAc] - 4.0 mol% water	0.423 ± 0.068	4.000 ± 0.070
[Emim][OAc] - 11.1 mol% water	1.172 ± 0.054	11.079 ± 0.507
[Bmim][OAc]	0.620 ± 0.036	6.833 ± 0.393
[Bmim][Cl]	0.494 ± 0.012	4.791 ± 0.119
[Emim][DCA]	0.279 ± 0.040	2.741 ± 0.390

Solvent density and molar volume

Each solvent's density was measured using a 25 mL pycnometer by my undergraduate researcher Mayra Lopez. The pycnometer was calibrated with deionized water. Measurements were taken at least three times for each liquid. The densities were averaged for each solvent, and the molar volume was calculated by dividing the molecular weight of each solvent by the average density measured. All data were obtained at 25°C, using a temperature controlled water bath. The water content of each solvent was tested in triplicate with a calibrated coulometric Karl-Fischer titrator. The density of the solvent was used to find the pure solvent molar volume given below (Table 3.2). The values obtained for acetic acid, 1-methylimidazole, and [Bmim][Cl] match those from the literature.[1-3]

Table 3.2 Solvent density and molar volume with one standard deviation of results

Solvent	Density (g/cm^3)	Molar Volume (mL/mol)
Acetic acid	1.045 ± 0.0003	57.47 ± 0.02
1-Methylimidazole	1.032 ± 0.0004	79.57 ± 0.03
[mim][OAc]	1.070 ± 0.0001	132.81 ± 0.01
[mim][Fr]	1.133 ± 0.0003	113.13 ± 0.03
[mim][HSO$_4$]	1.480 ± 0.0004	121.73 ± 0.07
[Emim][OAc]	1.098 ± 0.0002	154.98 ± 0.03
[Bmim][OAc]	1.059 ± 0.0007	187.28 ± 0.13
[Emim][DCA]	1.101 ± 0.0002	160.93 ± 0.04
[Bmim][Cl]	1.052 ± 0.0009	165.98 ± 0.15

Zein solubility

Commercial food-grade zein (F4000), consisting primarily α-zein, was obtained from Flo Chemical Corporation, formerly Freeman Industries, of Ashburnham, Massachusetts. Glacial acetic acid from Fischer Scientific and 1-methylimidazole (99+%) from Aldrich Chemicals were obtained and used without further purification. Zein solubility in the solvents was measured using the gravimetric method at 30°C, 40°C, 50°C, and 60°C by my undergraduate research Christian Kehr for most of the samples.[4, 5] A maximum temperature of 60°C was used because of decomposition concerns with the imidazolium-based ionic liquids held for extended periods of time above 60°C.[6] Two grams of solvent were measured into a vial and a small amount of zein was added. The vial was stirred and held at constant temperature in a water or silicone oil bath. The solution was monitored until the zein dissolved, whereupon more zein was added. When the zein no longer dissolved at that temperature within 16 hours, the temperature was increased and held constant until the zein dissolved. At that point more zein was added. The mass of zein dissolved before the previous addition, which did not dissolve in 16 hours, was calculated to be the solubility at that temperature. The gravimetric solubility of zein in each solvent was reproduced at least three times.

The effect of water concentration on the solubility of zein as a function of temperature was examined. Water (0.053 g) was added to six grams of [Emim][OAc] to increase the water concentration from 4.0 mol% to 11.1 mol%. The six grams of [Emim][OAc] with 11.1 mol% water was divided into three vials of two grams each. The gravimetric solubility of zein was obtained from 30°C to 60°C in all three samples and compared to the solubility of zein in [Emim][OAc] with 4.0 mol% water.

Infrared analysis

Infrared (IR) spectroscopy was performed with a Mattson Cygnus IR spectrometer, using a Harrick Scientific Horizon attenuated total reflectance (ATR) accessory with a zinc selenide crystal and a temperature-controlled top plate. A DTGS (deuterated triglycine sulfate) detector and germanium coated potassium bromide beam splitter were used. The iris was set to 50% open. Each sample and background spectrum was collected with 256 co-added scans at 2 cm^{-1} resolution. The moving mirror velocity was 10 kHz, both forward and reverse. The spectral

window examined was from 4000 to 900 cm^{-1}. The IR spectrometer control software is WinFIRST, version 3.61, from Mattson Instruments of Madison, Wisconsin.

Spectra were obtained from 25°C to 95°C at 10°C intervals. While the solubility work stopped at 60°C as a precaution to avoid even minimal decomposition of the imidazolium-based ionic liquids, the structure studies continued higher because no notable decomposition in the shorter period of time of 4 total hours for the structure studies, compared to up to 16 hours at a temperature for solubility measurements. The zein solutions prepared are shown in Table 3.3. As zein was more soluble in 70 vol% aqueous ethanol, acetic acid, 1-methylimidazole, [mim][OAc] and [Emim][DCA] at 25°C than in the other solvents, 10 wt.% solutions of zein were prepared, compared to the other solvents 5 wt.% solutions.

Table 3.3 Weight percent zein solutions prepared for analysis with IR spectroscopy

Solvent	Weight percent zein solution prepared
70 vol% (41.6 mol%) aqueous ethanol	10
Acetic acid	10
1-Methylimidazole	10
[mim][OAc]	10
[mim][Fr]	5
[Emim][OAc]	5
[Emim][DCA]	10
[Bmim][Cl]	5
[Bmim][OAc]	5

The solutions from Table 3.3 were prepared and sufficient time was given to allow the zein to dissolve. First a spectrum of the pure solvent was obtained. The ATR trough plate was then cleaned, allowed to dry, and then the dissolved zein mixture from Table 3.3 was poured into the trough. Spectra were obtained from 25°C to 95°C at 10°C intervals, with each temperature being held for 20 minutes prior to obtaining the spectra. No infrared analysis of zein in [mim][HSO$_4$] was performed because so little zein dissolved that it was impossible to detect the protein in solution.

The pure solvent spectra were subtracted from the mixture spectra in GRAMS/AI software (Graphic Relational Array Management System Spectroscopy Software Suite, Thermo Fisher Scientific Inc.) at each temperature to obtain a difference spectrum used for subsequent analysis.

Curve fitting was performed on the Amide I (1700 to 1600 cm^{-1}) region of the difference spectrum with GRAMS/AI software, using the second derivative of the difference spectra to determine each peak location, which varied less than 2 cm^{-1} between samples. The Levenberg-Marquadt algorithm was used with mixed Gaussian-Lorentzian peaks.[7-13] Appendix D describes the curve fitting process in detail. Figure 3.1 shows an example of the curve fitting performed, including the second derivative used to identify peak locations and each secondary structure peak.
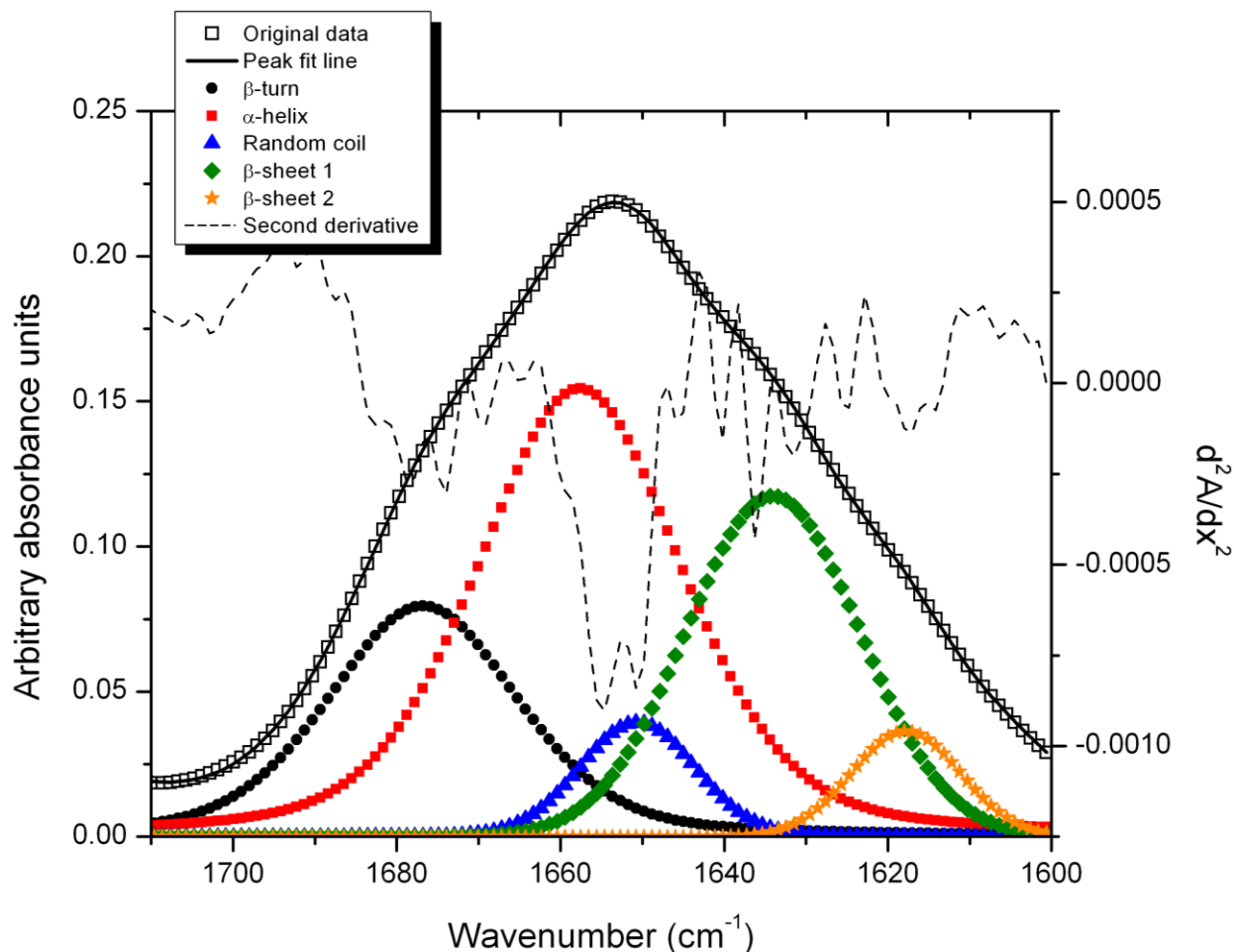
Figure 3.1 Curve fitting example of the Amide I band for zein dissolved in 25°C aqueous ethanol

Appendix D details how to perform curve fitting in GRAMS/AI. The fraction of each secondary structure was obtained by dividing the area of each peak by the molar absorptivity of that secondary structure (discussed in Chapter 2).[14] The total Amide I concentration is the sum of the partial concentrations for each secondary structure. The fraction of each structure was obtained by dividing its partial concentration by the total concentration of the Amide I band. Three samples were prepared and examined for each solvent mixture.

To compare the effects of water content in the ionic liquid on the secondary structure of zein, three new samples of 10 wt.% zein in [Emim][DCA] (water content 2.74 mol%) were prepared and then the zein secondary structure was analyzed. First [Emim][DCA] was dried under vacuum at 50°C for two days. This resulted in a water content of 2.1 mol%, as measured with a columetric Karl-Fischer titrator, repeated in triplicate. Then water was added to two

44

different samples of the dried [Emim][DCA], to attain 12.3 mol% and 25.0 mol% water. Ten weight percent zein was added to these samples and allowed to dissolve overnight before IR analysis.

For comparison with the secondary structure changes of dissolved zein in each of the solvents, a solid zein film was prepared and analyzed. A 10 wt.% solution of zein in the 70 vol.% aqueous ethanol solution was prepared and poured into the ATR trough plate. The solvent evaporated overnight leaving a film of zein on the ATR crystal. The film was then analyzed using the IR method described above. This process was repeated in triplicate. The spectrum of the zein films obtained were found to be identical to zein IR spectra previously reported in the literature.[15-17]

Linear solvation energy relationship

The linear solvation energy relationship (LSER) coefficients were calculated using multivariate least squares linear regression.

References

1. Sigma Product Information 1-Methylimidazole, Product number M 8878. *http://www.sigmaaldrich.com/etc/medialib/docs/Sigma/Product_Information_Sheet/1/m8878pis.Par.0001.File.tmp/m8878pis.pdf* (accessed November 29, 2012).

2. Makhatadze, G.; Privalov, P. Heat capacity of proteins: I. Partial molar heat capacity of individual amino acid residues in aqueous solution: hydration effect, J. Mol. Biol. **1990**, 2, 375-384.

3. Sun, X.; Anthony, J. L. Effect of structure of ionic liquids and phosphoric acid on the structure of aluminium isopropoxide, **2012**, Manuscript in preparation.

4. Fuchs, D.; Fischer, J.; Tumakaka, F.; Sadowski, G. Solubility of amino acids: Influence of the pH value and the addition of alcoholic cosolvents on aqueous solubility, Ind. Eng. Chem. Res. **2006**, 19, 6578-6584.

5. Ferreira, L. A.; Macedo, E. A.; Pinho, S. P. Solubility of amino acids and diglycine in aqueous–alkanol solutions, Chem. Eng. Sci. **2004**, 15, 3117-3124.

6. Ngo, H. L.; LeCompte, K.; Hargens, L.; McEwen, A. B. Thermal properties of imidazolium ionic liquids, Themo. Acta. **2000**, 97-102.

7. Susi, H.; Michael Byler, D. Protein structure by Fourier transform infrared spectroscopy: second derivative spectra, Biochem. Biophys. Res. Commun. **1983**, 1, 391-397.

8. Dong, A.; Huang, P.; Caughey, W. S. Protein secondary structures in water from second-derivative amide I infrared spectra, Biochemistry (N. Y.) **1990**, 13, 3303-3308.

9. Zhang, J.; Yan, Y. B. Probing conformational changes of proteins by quantitative second-derivative infrared spectroscopy, Anal. Biochem. **2005**, 1, 89-98.

10. D'antonio, J.; Murphy, B. M.; Manning, M. C.; Al-azzam, W. A. Comparability of protein therapeutics: Quantitative comparison of second-derivative amide I infrared spectra, J. Pharm. Sci. **2012**.

11. Jackson, M.; Mantsch, H. H. The use and misuse of FTIR spectroscopy in the determination of protein structure, Crit. Rev. Biochem. Mol. Biol. **1995**, 2, 95-120.

12. Barth, A.; Zscherp, C. What vibrations tell us about proteins, Q. Rev. Biophys. **2002**, 4, 369-430.

13. Barth, A. Infrared spectroscopy of proteins, Biochim Biophys Acta **2007**, 9, 1073-1101.

14. de Jongh, H. H. J.; Goormaghtigh, E.; Ruysschaert, J. M. The different molar absorptivities of the secondary structure types in the amide I region: an attenuated total reflection infrared study on globular proteins, Anal. Biochem. **1996**, 1, 95-103.

15. Forato, L. A.; Bicudo, T. D. C.; Colnago, L. A. Conformation of α zeins in solid state by Fourier transform IR, Biopolymers **2003**, 6, 421-426.

16. Kretschmer, C. B. Infrared spectroscopy and optical rotatory dispersion of zein, wheat gluten and gliadin, J. Phys. Chem. **1957**, 12, 1627-1631.

17. Xu, W.; Reddy, N.; Yang, Y. An acidic method of zein extraction from DDGS, J. Agric. Food Chem. **2007**, 15, 6279-6284.

Chapter 4 - Solubility of Zein

Introduction

The solubility and gelation behavior of zein in various solvents has been studied extensively to facilitate zein's commercial use.[1-12] Zein is insoluble in water and poorly soluble in pure alcohols such as ethanol or isopropanol, but zein is soluble in aqueous alcohols.[1-4, 9, 13] However, it has been found that gelation occurs irreversibly for zein dissolved in aqueous alcohols.[1-4, 9, 14] Indeed, gelation problems for zein used as a shellac replacement during World War II were so severe that consumers preferred the more expensive shellac ($0.52/lb.) over much cheaper zein ($0.30/lb.).[2] To avoid the gelation issue other solvents have been examined, such as acetic acid.[8, 12] While zein is soluble in acetic acid, it has been found that the properties, such as tensile strength, of zein precipitated from acetic acid are inferior.[12, 13, 15] Therefore, acetic acid has not been used as a solvent in industry.[12, 13, 15]

Limited research has been conducted into using ionic liquids as solvents for zein. In 2006 Biswas et al. used the ionic liquids 1-butyl-3-methylimidazolium chloride ([Bmim][Cl]) and 1-butyl-3-methylimidazolium dicyanamide ([Bmim][DCA]) to dissolve zein and corn starch at 80°C and to acylate them in the presence of pyridine.[16] In 2011 Choi and Kwon found that two protic quaternary ammonium-based ionic liquids are capable of dissolving zein at 95°C.[17] However there has been no systematic examination of zein's solubility in ionic liquids and, in particular, no examination of the effects of temperature on solubility in ionic liquids. The solubility of zein in a family of imidazolium-based ionic liquids from 25°C to 95°C is reported in this chapter. The solubility of zein in the conventional solvents 1-methylimdiazole (the precursor to all the ionic liquid cations), and acetic acid (acetate is a common anion for three of the ionic liquids) is also examined. For comparison, results for zein solubility in aqueous ethanol are also reported.[11] The full names and structures of all the ionic liquids are given in Appendix G.

Results and Discussion

Table 4.1 gives the mean solubility (in wt.%) and standard deviation for zein dissolved in all the solvents, using the gravimetric method described in Chapter 3, along with previously reported solubilities in aqueous ethanol.[11]

Table 4.1 Weight percent solubility of zein in solvents at 30°C, 40°C, 50°C, and 60°C with one standard deviation of results

Solvent	Solubility at 30°C (wt.%)	Solubility at 40°C (wt.%)	Solubility at 50°C (wt.%)	Solubility at 60°C (wt.%)
Acetic Acid	23.7 ± 2.9	31.4 ± 1.5	39.1 ± 4.5	41.4 ± 4.6
1-Methylimidazole	15.0 ± 4.0	19.0 ± 3.8	21.9 ± 2.6	24.6 ± 2.2
[mim][OAc]	18.0 ± 0.9	21.6 ± 1.7	24.5 ± 1.8	26.2 ± 4.0
[mim][Fr]	4.8 ± 1.1	7.9 ± 0.7	10.3 ± 0.2	12.3 ± 1.3
[mim][HSO$_4$]	<0.2	<0.2	<0.2	<1.0
[Emim][OAc] - 11.1 mol% water	3.5 ± 0.6	6.2 ± 0.3	8.9 ± 0.7	12.9 ± 0.3
[Emim][OAc] - 4.0 mol% water	4.3 ± 0.3	6.7 ± 0.6	9.0 ± 0.4	11.4 ± 1.3
[Bmim][OAc]	7.6 ± 0.9	12.4 ± 3.1	17.8 ± 2.8	22.2 ± 2.2
[Bmim][Cl]	6.8 ± 2.3	13.1 ± 1.1	16.8 ± 1.1	21.1 ± 0.8
[Emim][DCA]	15.5 ± 0.4	20.7 ± 2.0	24.7 ± 2.2	25.3 ± 2.2
70 vol.% (41.6 mol%) aqueous ethanol[11]	8.7	9.1	9.4	9.7
75 mol% aqueous ethanol[11]	4.6	5.7	7.1	8.6
100% ethanol[11]	0.5	1.1	2.5	5.3

As one can see, zein dissolves readily in many of the ionic liquids examined here (with the exception of [mim][HSO$_4$], discussed below). These results contrast previous studies that found the solubility of proteins in ionic liquid was less than 1 wt.%.[16, 18-21] However, the previous studies examined water-soluble proteins (such as hen egg lysozyme and cytochrome c) rather than a water-insoluble protein such as zein.[16, 18-21]

The solubility of zein in acetate ionic liquids

Figure 4.1 shows the solubility of zein in acetic acid, 1-methylimidazole, [mim][OAc], [Emim][OAc] with two different water concentrations, and [Bmim][OAc] (full chemical names are given in Appendix G), with error bars representing one standard deviation of each result (as is the case for all figures in this chapter). Previously reported data for the solubility of zein in aqueous ethanol mixtures are plotted as lines for comparison.[11]
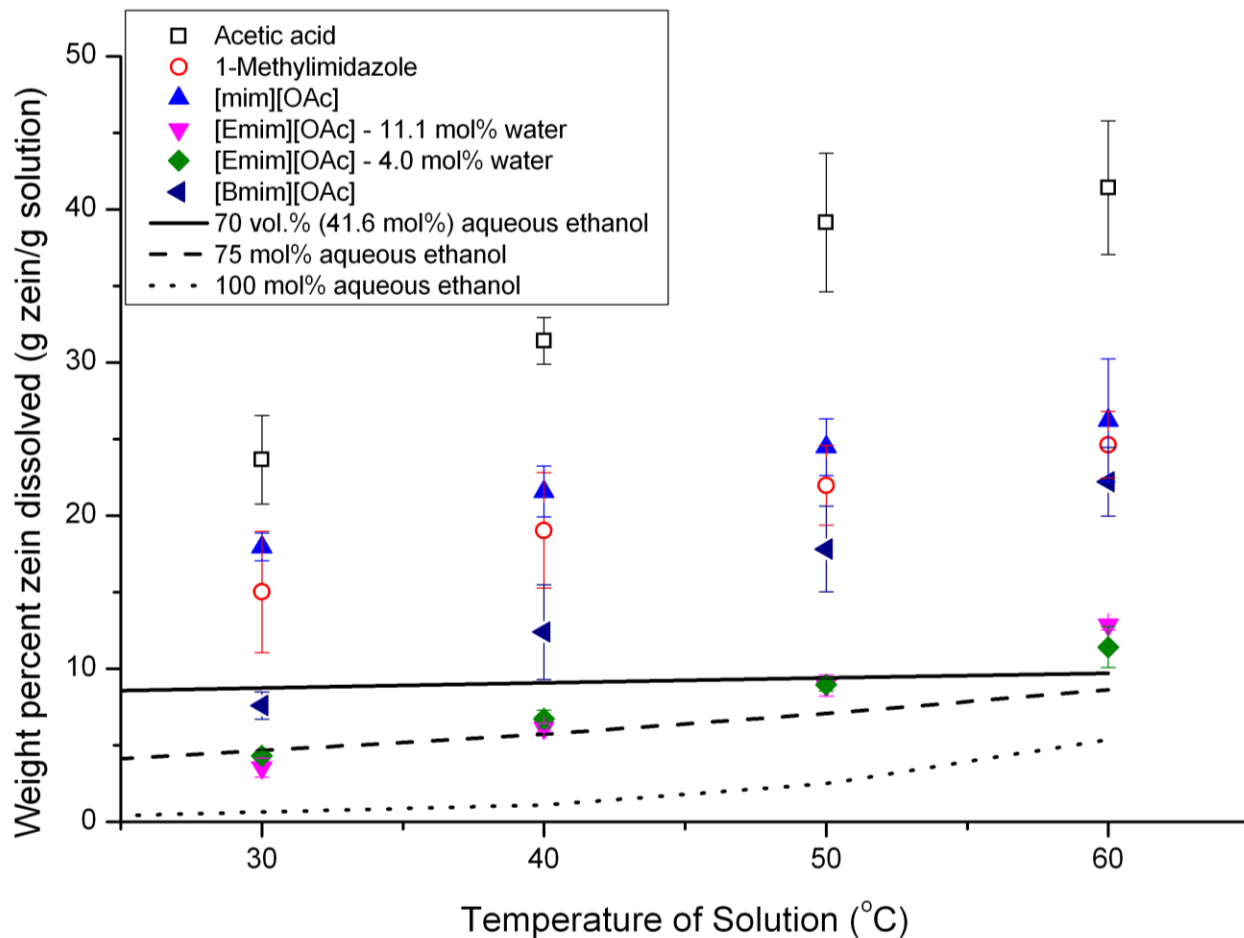
Figure 4.1 The solubility of zein in the acetate family of solvents, error bars represent one standard deviation

The differences in solubility for the acetate family of ionic liquids, [mim][OAc], [Emim][OAc], and [Bmim][OAc], shows the effect of cation size (particularly alkyl chain length) on solubility. The solubility of zein in [mim][OAc] was the second highest recorded among all solvents. The solubility of zein in [Bmim][OAc] increased strongly from 30°C to 60°C. The solubility remained relatively low in [Emim][OAc]. The superior solubility of zein in [mim][OAc]'s compared to [Emim][OAc] and [Bmim][OAc] is likely due to [mim][OAc]'s lower viscosity, 5.6 cP at 80°C, compared to [Emim][OAc]'s 10 cP at 80°C, and presumably higher (but undetermined) viscosity for the larger [Bmim][OAc].[22, 23] The smaller molecular size and lower viscosity facilitate conformational changes of the protein, which disrupt the protein's intramolecular hydrogen bonding and thus facilitate the dissolution of the protein.[24-26] In contrast to the viscosity effects for the solubility of zein in [mim][OAc], the difference in solubility for

50

zein in [Bmim][OAc] compared to [Emim][OAc] is due to stronger intermolecular interactions between the ionic liquid and the protein, such as van der Waals interactions, between the non-polar parts of the protein's amino acids and the larger cation of the ionic liquid.[27] It has been seen that, in addition to van der Waals interactions, aromatic-aromatic interactions between the solvent and the protein can improve the solubility of the protein.[28] Approximately 80% of non-polar side-chains are buried inside a protein. As the protein warms, the non-polar side-chains become more accessible for interactions with the solvent because of the increased molecular motion from higher temperatures, which facilitates the increase in solubility.[29] As zein contains approximately 13% amino acids with aromatic side chains (plus approximately 10% of the lactam-containing amino acid proline),[4, 7] the aromatic-aromatic interactions help to explain the large increase in solubility with temperature.[28]

The more rapid increase in the solubility of zein in [Bmim][OAc] compared to zein in [mim][OAc] also indicates the importance of the interactions between the non-polar parts of the protein. While the solubility of zein in [mim][OAc] is three times that of zein in [Bmim][OAc] at 30°C because of the lower viscosity of [mim][OAc], zein's solubility increases 190% by 60°C (to 22.2 wt.%) in [Bmim][OAc], compared to an increase of only 44% for zein in [mim][OAc] (to 24.6 wt.%). This change is because of the increase in solvent-solute interactions due to the higher temperature facilitating dissolution of the zein. From Figure 4.1 it appears possible that the solubility of zein in [Bmim][OAc] will intersect with the solubility in [mim][OAc] at approximately 80°C. The increase in temperature reduces solvent viscosity, so the lower viscosity of [mim][OAc] is less of an advantage, and the stronger interactions between the larger [Bmim][OAc] cation and zein is able to improve zein's solubility.

The effect of added water in the ionic liquid solvent is shown as well. The comparison of zein solubility in [Emim][OAc] with 11.1 mol% and 4.0 mol% water in the ionic liquid shows no statistically significant difference despite zein's insolubility in water. Previous research showed that small increases in water fraction in aqueous alcohols could exponentially increase the upper critical solution temperature (the temperature above which the compounds in the mixture are miscible in all proportions), indicating that even small increases in the amount of water would hamper zein solubility.[9] This research, in contrast, shows an insensitivity to water concentration, likely due to the "water deactivating" effect described in Chapter 2.[30-33] This result is particularly

useful because it shows that concentrations as high as 11 mol% have no apparent effect, facilitating ionic liquid use.

Comparing the conventional molecular solvents, these results show that acetic acid dissolves the most zein of the solvents examined. However acetic acid has been found to harm zein's physical properties because of changes in zein's secondary structure (see Chapter 5).[12, 15] Therefore acetic acid is not used as a solvent for commercial zein production.[12, 15] The molecular solvent 1-methylimidazole is only slightly inferior to [mim][OAc]. It has been found that other substituted amines such as pyridine and diethylenetriamine have low (less than -40°C) upper critical solution temperatures wherein the zein and solvent are fully miscible.[8] The low upper critical solution temperature indicates that the substituted amines are well suited to dissolve zein, so this result for 1-methylimidazole fits in well with what has been described previously.[8]

The 70 vol.% aqueous ethanol (41.6 mol% aqueous ethanol) is the solvent mixture used for commercial zein production.[2, 4, 6] However, the solubility of zein in 70 vol.% aqueous ethanol is much inferior to the solubility in [mim][OAc], 1-methylimidazole, and in [Bmim][OAc] above 40°C. It is also clear from Figure 4.1 that 100% ethanol is a poor solvent for zein.[3]

The solubility of zein in other ionic liquids

The solubility of zein in the other ionic liquids examined, [mim][HSO$_4$], [mim][Fr], [Emim][DCA], [Bmim][Cl] are shown in Figure 4.2. The ionic liquid [mim][OAc] is shown to directly compare the three protic ionic liquids, and [Bmim][OAc] is shown with [Bmim][Cl] to compare the effects of different anions. Again the lines showing the solubility of zein in solutions of aqueous ethanol at three different concentrations of ethanol are provided as well.[11]
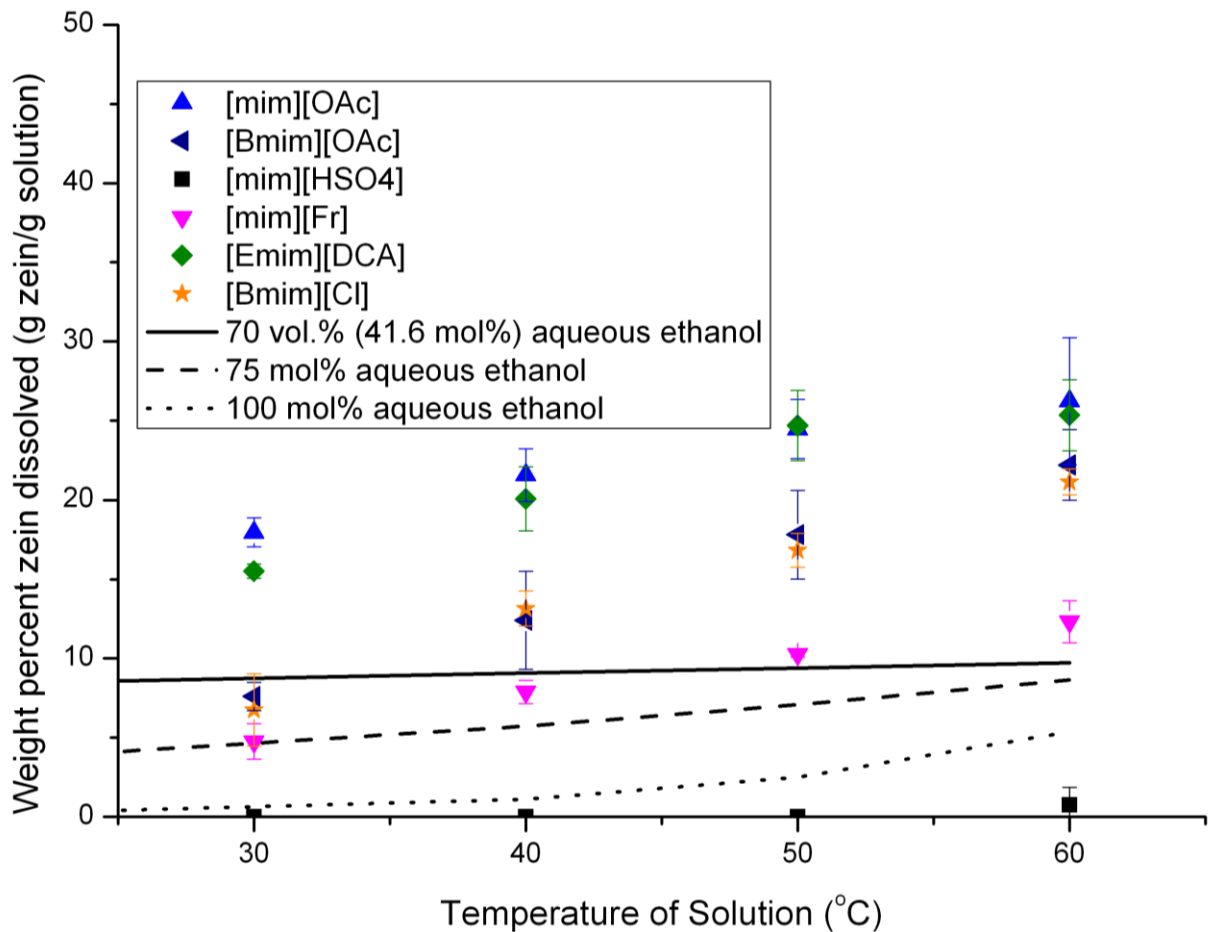
Figure 4.2 The solubility of zein in other solvents

The solubility of zein in [Emim][DCA] is quite high, nearly matching [mim][OAc]. This result is surprising because it has not been shown previously that the dicyanamide anion is particularly useful in aqueous solutions for improving the solubility of proteins. However, it is well known in aqueous protein chemistry that dicyanamide is a very strong protein-denaturing anion as discussed in Chapter 2.[34-36] This strong denaturing is also related to the "salting-out" behavior dicyanamide exhibits, where addition of dicyanamide to aqueous solutions causes the precipitation of the protein.[34] This precipitation is caused by protein denaturing causing the exposure of the non-polar side chains to water, an energetically unfavorable interaction, which causes the protein to precipitate. However, in ionic liquids that same denaturing exposure of the non-polar side chain may improve solubility, because denaturing the protein exposes more of the non-polar side chains for interactions with the non-polar cation of the ionic liquid.

53

The zein has statistically similar solubility in the aprotic ionic liquids [Bmim][Cl] and [Bmim][OAc]. Even though chloride is an inferior anion for cellulose dissolution (and also a mild protein destabilizer), here the similarity in solubility shows the importance of the [Bmim] cation over the different anions.[24, 37]

The contrast in solubility of zein in the three protic ionic liquids is of interest because it shows the effect of the anion on the solvent property and thus solubility. Figure 4.3 shows the chemical structures of the protic ionic liquids and their $E_T(30)$ scale polarity (discussed in Chapter 2).[38]

[mim][HSO$_4$]   [mim][Fr]   [mim][OAc]

$E_T(30)$ = 63.6 kcal/mol $E_T(30)$ = 56.0 kcal/mol $E_T(30)$ = 50.5 kcal/mol
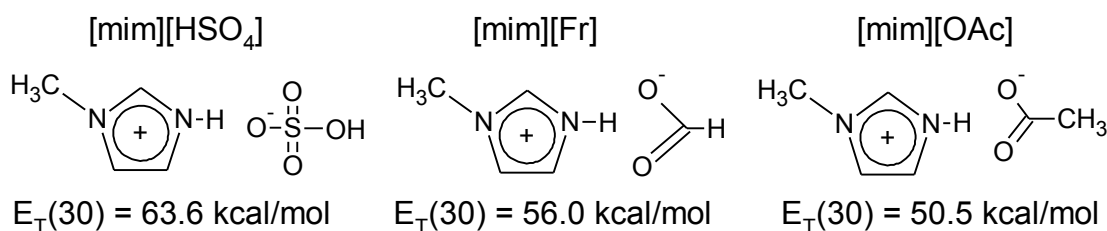
Figure 4.3 Structure and polarity comparison of [mim][HSO$_4$], [mim][Fr], and [mim][OAc] Each protic ionic liquid has the same 1-methylimidazolium cation, and yet the zein solubilities are very different. At 60°C zein solubility is <1.0 wt.% in [mim][HSO$_4$] versus 12.3 wt.% in [mim][Fr] versus 26.2% wt.% in [mim][OAc]. This difference is due to the different anions, and, more particularly, the different solvent polarities due to the anions. As discussed above, zein is insoluble in highly polar water ($E_T(30)$ = 63.1 kcal/mol) and yet is soluble in less polar 70 vol% ethanol ($E_T(30)$ = 54.4 kcal/mol).[39, 40] As one can see from the $E_T(30)$ polarity values given in Figure 4.3, the solubility is a function of the solvent polarity when comparing these protic ionic liquids. The more polar ionic liquids are poor solvents because they interact poorly with the mostly non-polar zein. This also relates to the previously discussed poor solubility of water-soluble proteins in ionic liquids. As most ionic liquids are less polar than water (see Chapter 6), it should not be expected that ionic liquids can dissolve polar proteins effectively. Further examination of the effect of solvent polarity on zein solubility is provided in Chapter 6.

Temperature effects on solubility

As discussed in Chapter 2 the van't Hoff equation assumes that the C_p of the solute is not a function of temperature. Unfortunately, that is not the case for proteins. The C_p of a protein is a function of its structure.[41] As the structure of proteins changes with temperature and solvent (see

Chapter 5), C_p is thus a function of temperature and solvent.[41] Therefore, it is impossible to calculate the enthalpy and entropy of dissolution without detailed knowledge of the changes of C_p of the protein, which is not available for zein in ionic liquids. However, the slope from the plot of the natural log of solubility versus inverse absolute temperature (denoted herein as Mz) is related to the enthalpy of dissolution (as discussed in Chapter 2) and can be used in the analysis to give a sense of the relative enthalpies of dissolution as a function of solvents.[41] Because the same source of zein is used for all samples, the temperature dependence of the unfolding process on zein is expected to be the same for all samples. Therefore, changes in Mz are due solely to solvent effects, comparison of Mz shows the relative solvent effects on solubility. The lower the value of Mz, the more energy is required to dissolve the solute in the solvent, resulting in lower solubility. Figure 4.4 shows the plot for the data reported here.
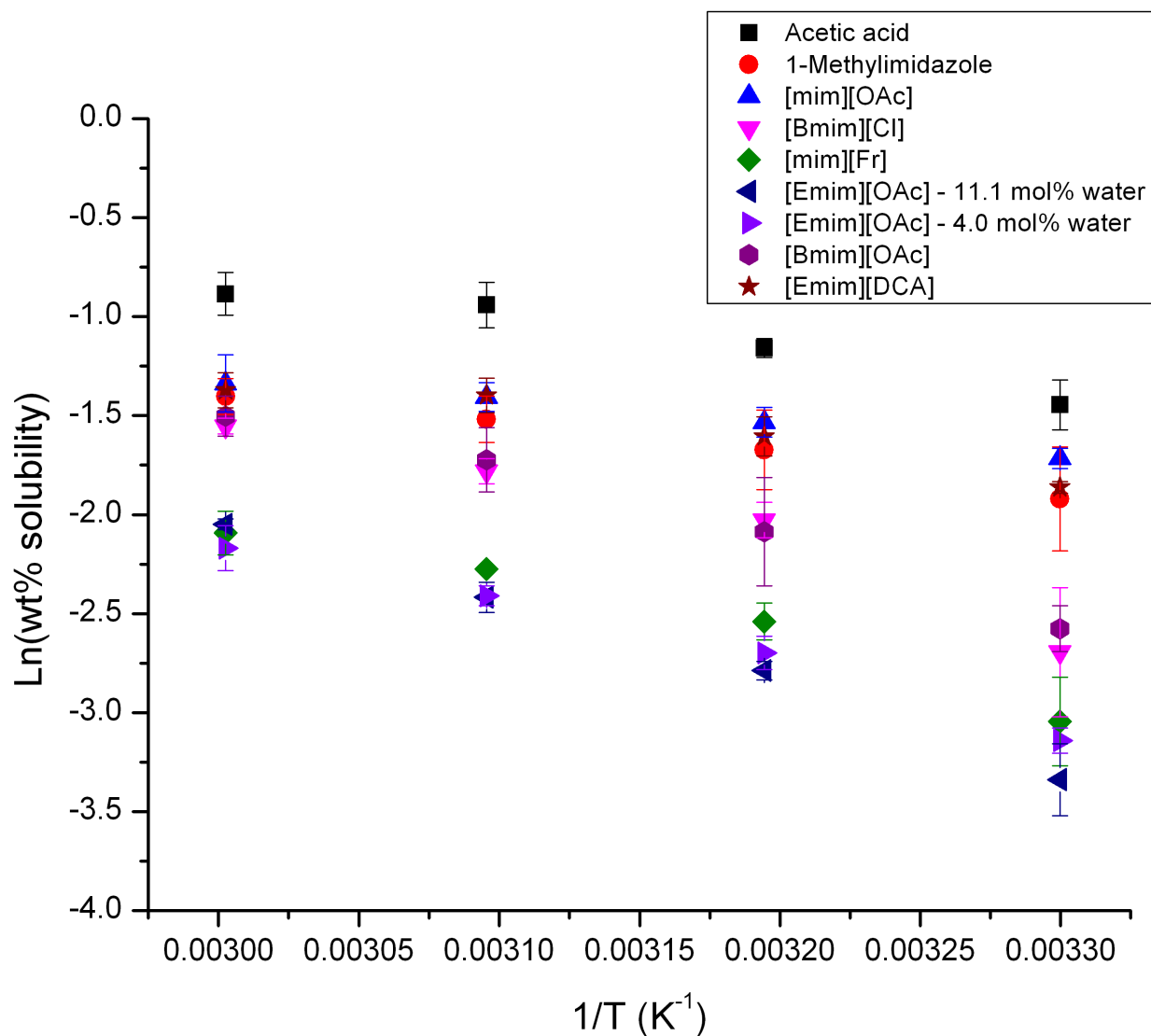
Figure 4.4 Plot of the natural log of solubility versus 1/T(K)

Table 4.2 gives the values of Mz (the slope) and the standard deviation for the dissolution of zein in all the solvents examined in Figure 4.4. The solubility of zein in [mim][HSO$_4$] was so low that finding Mz was not possible.

Table 4.2 The slope from the natural log of zein solubility versus 1/T (K), Mz, for solvents examined with standard deviation

Solvent	Mz (dimensionless)
Acetic Acid	-1900 ± 700
1-Methylimidazole	-1700 ± 700
[mim][OAc]	-1300 ± 400
[mim][Fr]	-3200 ± 800
[Emim][OAc] - 11.1 mol% water	-4300 ± 600
[Emim][OAc] - 4.0 mol% water	-4700 ± 200
[Bmim][OAc]	-3800 ± 50
[Bmim][Cl]	-3800 ± 900
[Emim][DCA]	-1700 ± 300

The lower the Mz, the more energy is required to dissolve the zein. This explains why the highest solubility is found for those solvents with the high Mz. The Mz for [Emim][OAc] with different water concentrations is statistically similar, show again that water has a negligible effect between 4 and 11 mol%. The temperature dependence of solubility is also important. It can be seen that the greater the increase in solubility with temperature, the lower the Mz, and the lower the zein solubility. Figure 4.5 compares Mz as a function of zein solubility at 60°C.
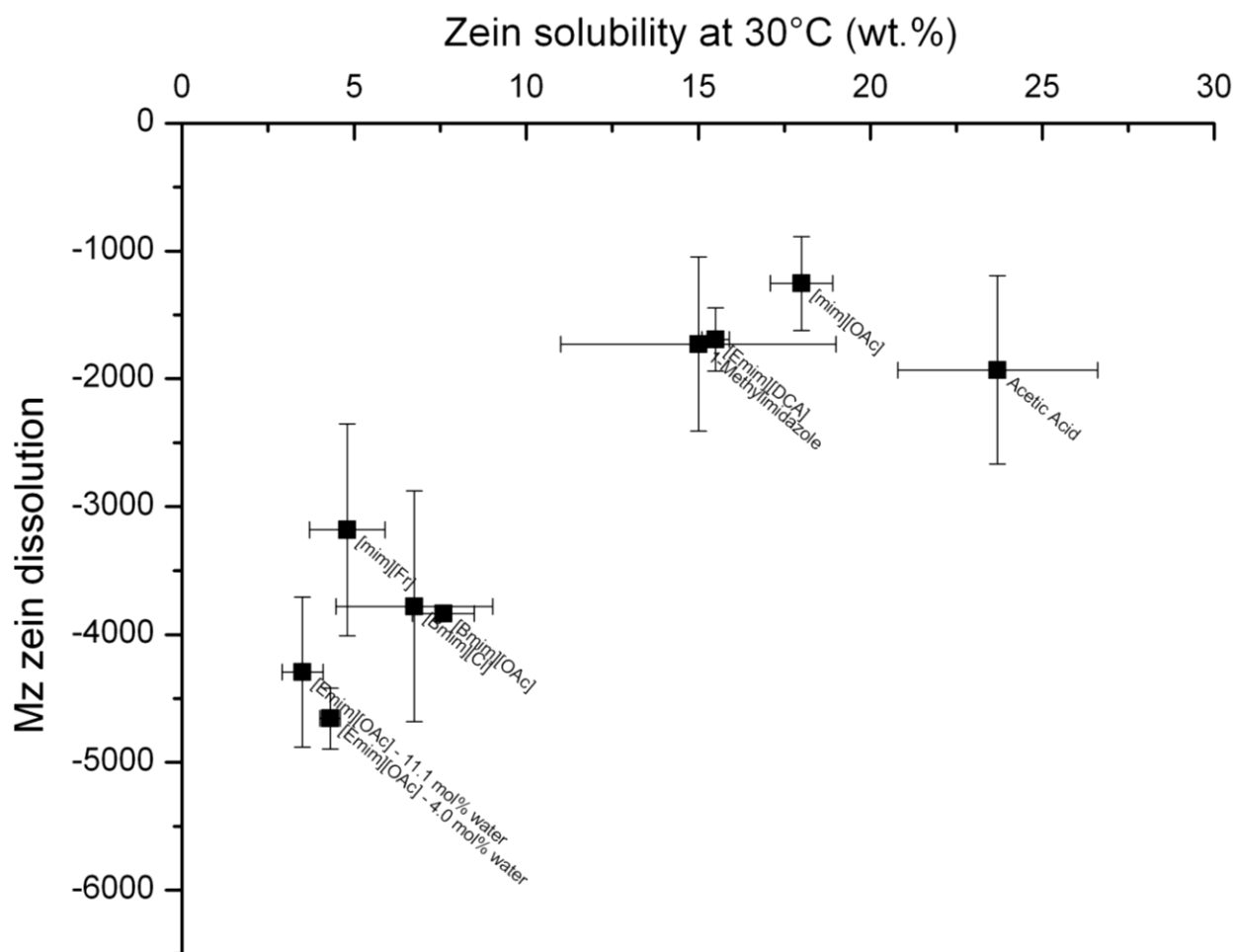
Figure 4.5 Mz versus zein solubility at 30°C

Figure 4.5 also explains differences in solubility examined above as well. For example it was shown that [mim][Fr] has a smaller Mz, which is related to the enthalpy of dissolution for the zein as discussed above, than [mim][OAc], and thus [mim][Fr] cannot dissolve as much zein as [mim][OAc]. The difference in zein solubility between acetate ionic liquids is also shown, because for both solubility and Mz [mim][OAc] > [Bmim][OAc] > [Emim][OAc].

Zein gelation observed

As mentioned above, gelation has long been recognized as an issue for zein dissolved in aqueous alcohols.[2, 4, 10, 13, 14] Gelation is known to be a result of the unfolding and aggregation of proteins.[42-44] Li et al. identified an "aging effect" wherein the rheological profiles of zein dissolved in aqueous ethanol changed from Newtonian to a non-Newtonian shear thinning behavior after 24 hours, and the shear thinning behavior became more pronounced at higher zein

concentrations.[13] During this research it was observed that some of the room temperature samples of zein dissolved in ionic liquid (used for the IR analysis of the secondary structure of the protein) never gelled, remaining apparently Newtonian (meaning that there was no apparent Bingham plastic behavior), albeit viscous, for months after the initial preparation of the samples. The samples used for IR analysis of zein's secondary structure had either 5 wt.% zein ([mim][Fr], [Bmim][OAc], [Bmim][Cl] and [Emim][OAc]) or 10 wt.% zein (70 vol.% aqueous ethanol, acetic acid, 1-methylimidazole, [mim][OAc], and [Emim][DCA]). The notable exceptions to this behavior were the 5 wt.% zein in [mim][Fr] and 10 wt.% zein in [mim][OAc]. All of the 5 wt.% zein in [mim][Fr] and 10 wt.% zein in [mim][OAc] samples gelled after some time (approximately 1 month for [mim][Fr] and 2 to 4 weeks for [mim][OAc]). In contrast a sample of 5 wt.% zein in [mim][OAc] did not gel even after 7 months. Additionally, all of the 10 wt.% zein dissolved in 70 vol.% aqueous ethanol samples gelled within 7 days of preparation, confirming the previous research about the change from Newtonian to non-Newtonian behavior.[13] What is curious about this behavior is that the IR analysis of zein in both 70 vol.% aqueous ethanol and [mim][OAc] do not show substantial changes in the secondary structure as zein in [mim][Fr] or any of the aprotic ionic liquids (see Chapter 5). Changes in the secondary structure of zein in acetic acid and 1-methylimidazole (prepared with the same 10 wt.% zein) are similar to the changes seen for zein in [mim][OAc] (see Chapter 5). Yet zein in acetic acid or 1-methylimidzole never gelled. Protein concentration is an important factor in gelation (the higher the concentration, the faster the gelation); yet both 5 wt.% zein in [mim][Fr] and 10 wt.% zein in [mim][OAc] and 70 vol.% aqueous ethanol gelled.[42-44] By contrast 5 wt.% zein in [mim][OAc], [Bmim][OAc], [Bmim][Cl], and [Emim][OAc], and 10 wt.% zein in acetic acid, 1-methylimidazole, and [Emim][DCA] did not gel. Because of the difference in behavior in concentration between the 5 wt.% (which did not gel) and 10 wt.% (which did gel) zein in [mim][OAc], the concentration of zein in solution clearly has an effect, as expected.[42-44] More interesting is the role solvent chemistry plays in the gelation behavior. Zein in aqueous alcohols have been known to gel for decades.

However, explaining why zein in [mim][Fr] and [mim][OAc] gelled and zein in acetic acid, 1-methylimidazole and the aprotic ionic liquids did not gel is difficult. Referring to previous research on solvents for zein it has been found that while pyridine has a low (-40°C) turbidity temperature, indicating it is a good solvent for zein, aromatic solvents with amines

(such as aniline) are poor solvents.[8] As both [mim][Fr] and [mim][OAc] are 1-methylimidazolium-based ionic liquids with acidic hydrogens on the 3-position nitrogen, they exhibit similar amine character to aniline. By contrast acetic acid, 1-methylimidazole, and the aprotic ionic liquids do not have an amine, and zein does not gel in any of them. Thus the difference in gelation behavior may be related to the presence or absence of amine-hydrogens.

Conclusions

This research is the first to examine how temperature and solvent affects zein solubility in ionic liquids. The solubility and gelation behavior of zein in industrial solvents such as aqueous ethanol has hampered zein's commercial use. As stated above zein dissolves readily in many of the ionic liquids examined, in contrast with previous studies that found the solubility of proteins in ionic liquid was less than 1 wt.%.[16, 18-21] This research found that zein is more soluble in ionic liquids such as [mim][OAc] and [Emim][DCA] than in commercially used aqueous ethanol, but [mim][HSO$_4$] is a very poor solvent for zein because of its high polarity. Water concentration in the ionic liquid was not found to be an important contributor to zein solubility, at least between 11.1 mol% and 4.0 mol% water in the ionic liquid, likely due to the water deactivating effects of ionic liquids described above.

Gelation has proven to be less of an issue than in aqueous alcohols, even if the protic ionic liquid solvents, [mim][OAc] and [mim][Fr], were found to gel after weeks of solubility. However zein never gelled in any of the aprotic ionic liquids after months, indicating that these aprotic solvents are superior long term solvents for zein.

References

1. Anderson, T. J.; Lamsal, B. P. REVIEW: Zein Extraction from Corn, Corn Products, and Coproducts and Modifications for Various Applications: A Review, *Cereal Chem.* **2011**, *2,* 159-173.

2. Lawton, J. W. Zein: A history of processing and use, *Cereal Chem.* **2002**, *1,* 1-18.

3. Lawton, J. W. Isolation of zein using 100% ethanol, *Cereal Chem.* **2006**, *5,* 565-568.

4. Shukla, R.; Cheryan, M. Zein: the industrial protein from corn, *Industrial Crops and Products* **2001**, *3,* 171-192.

5. Parris, N.; Dickey, L. C. Extraction and solubility characteristics of zein proteins from dry-milled corn, *J. Agric. Food Chem.* **2001**, *8,* 3757-3760.

6. Shukla, R.; Cheryan, M.; DeVor, R. E. Solvent extraction of zein from dry-milled corn, *Cereal Chem.* **2000**, *6,* 724-730.

7. Mossé, J. Monographie sur une protéine du mais: La zéine, *Ann. Physiol. Veg* **1961**, 105-139.

8. Evans, C. D.; Manley, R. H. Solvents for Zein. Primary Solvents, *Ind. Eng. Chem. Res.* **1941**, *11,* 1416-1417.

9. Manley, R. H.; Evans, C. D. Binary solvents for zein, *Ind. Eng. Chem. Res.* **1943**, *6,* 661-665.

10. Evans, C. D.; Manley, R. H. Stabilizing zein dispersions against gelation, *Ind. Eng. Chem. Res.* **1943**, *2,* 230-232.

11. Fu, D. Zein Properties and Alternative Recovery Methods, University of Nebraska - Lincoln, University of Nebraska, 2000.

12. Xu, W.; Reddy, N.; Yang, Y. An acidic method of zein extraction from DDGS, *J. Agric. Food Chem.* **2007**, *15,* 6279-6284.

13. Li, Y.; Li, J.; Xia, Q.; Zhang, B.; Wang, Q.; Huang, Q. Understanding the Dissolution of α-Zein in Aqueous Ethanol and Acetic Acid Solutions, *J. Phys. Chem. B* **2012**, 12057-12064.

14. Swallen, L. Zein. A new industrial protein, *Ind. Eng. Chem. Res.* **1941**, *3,* 394-398.

15. Selling, G. W.; Woods, K. K. Improved isolation of zein from corn gluten meal using acetic acid and isolate characterization as solvent, *Cereal Chem.* **2008**, *2,* 202-206.

16. Biswas, A.; Shogren, R. L.; Stevenson, D. G.; Willett, J. L.; Bhowmik, P. K. Ionic liquids as solvents for biopolymers: Acylation of starch and zein protein, *Carbohydr. Polym.* **2006**, *4,* 546-550.

17. Choi, H. M.; Kwon, I. Dissolution of Zein Using Protic Ionic Liquids: N-(2-Hydroxyethyl) Ammonium Formate and N-(2-Hydroxyethyl) Ammonium Acetate, *Ind Eng Chem Res* **2011**, 2452-2454.

18. Weingärtner, H.; Cabrele, C.; Herrmann, C. How ionic liquids can help to stabilize native proteins, *Phys. Chem. Chem. Phys.* **2012***, 2,* 415-426.

19. Kohno, Y.; Saita, S.; Murata, K.; Nakamura, N.; Ohno, H. Extraction of proteins with temperature sensitive and reversible phase change of ionic liquid/water mixture, *Polym.Chem.* **2011**.

20. Constantinescu, D.; Herrmann, C.; Weingärtner, H. In *In Protein Denaturation by Ionic Liquids and the Hofmeister Series;* ACS symposium series; ACS Publications: 2009; Vol. 1030, pp 107-117.

21. Fujita, K.; MacFarlane, D. R.; Forsyth, M. Protein solubilising and stabilising ionic liquids, *Chem. Comm.* **2005***, 38,* 4804-4806.

22. Greaves, T. L.; Drummond, C. J. Protic ionic liquids: properties and applications, *Chem. Rev.* **2008***, 1,* 206-237.

23. Sun, N.; Rahman, M.; Qin, Y.; Maxim, M. L.; Rodríguez, H.; Rogers, R. D. Complete dissolution and partial delignification of wood in the ionic liquid 1-ethyl-3-methylimidazolium acetate, *Green Chem.* **2009***, 5,* 646-655.

24. Kahlen, J.; Masuch, K.; Leonhard, K. Modelling cellulose solubilities in ionic liquids using COSMO-RS, *Green Chem.* **2010***, 12,* 2172-2181.

25. Chin, J. T.; Wheeler, S. L.; Klibanov, A. M. On Protein Solubility in Organic Solvents, *Biotechnol. Bioeng.* **1994**, 140-145.

26. Griebenow, K.; Klibanov, A. M. On protein denaturation in aqueous-organic mixtures but not in pure organic solvents, *J. Am. Chem. Soc.* **1996***, 47,* 11695-11700.

27. Horton, H. R.; Moran, L. A.; Ochs, R. S.; Rawn, J. D.; Scrimgeour, K. G. *Principles of Biochemistry;* Prentice Hall: Upper Saddle River, NJ, 1996; , pp 862.

28. Burley, S.; Petsko, G. Aromatic-aromatic interaction: a mechanism of protein structure stabilization, *Science* **1985***, 4708,* 23-28.

29. Wang, W. Instability, stabilization, and formulation of liquid protein pharmaceuticals, *Int. J. Pharm.* **1999***, 2,* 129-188.

30. Parnham, E. R.; Morris, R. E. Ionothermal Synthesis of Zeolites, Metal–Organic Frameworks, and Inorganic–Organic Hybrids, *Acc. Chem. Res.* **2007**, 1005.

31. Cammarata, L.; Kazarian, S. G.; Salter, P. A.; Welton, T. Molecular states of water in room temperature ionic liquids, *Physical Chemistry Chemical Physics* **2001**, 5192.

32. Hanke, C. G.; Lynden-Bell, R. M. A Simulation Study of Water− Dialkylimidazolium Ionic Liquid Mixtures, *J Phys Chem B* **2003**, *39,* 10873-10878.

33. Amigues, E.; Hardacre, C.; Keane, G.; Migaud, M.; O'Neill, M. Ionic liquids—media for unique phosphorus chemistry, *Chemical Communications* **2006**, *1,* 72-74.

34. Zhao, H.; Campbell, S. M.; Jackson, L.; Song, Z.; Olubajo, O. Hofmeister series of ionic liquids: kosmotropic effect of ionic liquids on the enzymatic hydrolysis of enantiomeric phenylalanine methyl ester, *Tetrahedron: Asymmetry* **2006**, *3,* 377-383.

35. Constantinescu, D.; Weingärtner, H.; Herrmann, C. Protein denaturation by ionic liquids and the Hofmeister series: a case study of aqueous solutions of ribonuclease A, *Angew. Chem. , Int. Ed.* **2007**, *46,* 8887-8889.

36. Yang, Z. Hofmeister effects: an explanation for the impact of ionic liquids on biocatalysis, *J. Biotechnol.* **2009**, *1,* 12-22.

37. Sun, N.; Rodríguez, H.; Rahman, M.; Rogers, R. D. Where are ionic liquid strategies most suited in the pursuit of chemicals and energy from lignocellulosic biomass? *Chem. Commun.* **2010**, 1405.

38. Shukla, S. K.; Khupse, N. D.; Kumar, A. Do anions influence the polarity of protic ionic liquids? *Phys.Chem.Chem.Phys.* **2011**, 2761.

39. Reichardt, C. Solvatochromic dyes as solvent polarity indicators, *Chem. Rev.* **1994**, *8,* 2319-2358.

40. Altun, Y. Study of Solvent Composition Effects on the Protonation Equilibria of Various Anilines by Multiple Linear Regression and Factor Analysis Applied to the Correlation Between Protonation Constants and Solvatochromic Parameters in Ethanol−Water Mixed Solvents, *J. Sol. Chem.* **2004**, *5,* 479-497.

41. Haynie, D. T. *Biological thermodynamics;* Cambridge University Press: University Press, Cambridge, 2008; , pp 422.

42. Ziegler, G. R.; Foegeding, E. A. The gelation of proteins, *Adv. Food Nutr. Res.* **1990**, 203-298.

43. Morris, A. M.; Watzky, M. A.; Finke, R. G. Protein aggregation kinetics, mechanism, and curve-fitting: a review of the literature, *Biochim Biophys Acta* **2009**, *3,* 375-397.

44. Roberts, C. J. Kinetics of irreversible protein aggregation: analysis of extended Lumry-Eyring models and implications for predicting protein shelf life, *J. Phys. Chem. B* **2003**, *5,* 1194-1207.

Chapter 5 - Zein Secondary Structure as a Function of Solvent

Introduction

Protein secondary structure is the arrangement of local segments of amino acids into the characteristic three dimensional portions of a protein as discussed in Chapter 2. The secondary structure is of interest to researchers because it has been found that protein and enzyme properties, such as gas permeability, tensile strength, or enzymatic activity, are related to protein secondary structure.[1-3, 4] The secondary structure of zein has been examined with both infrared and far-ultraviolet circular dichroism spectroscopy.[5-8] Cabra et al. showed, for zein dissolved in 70 vol% aqueous ethanol using far-UV circular dichroism, that α-helix decreases while the other secondary structures all increase with increasing temperature.[6] In their analysis of the secondary structure of zein from six different sources, Forato et al. showed, using transmission IR spectroscopy and singular value decomposition, that the secondary structure of solid zein and zein dissolved in aqueous ethanol are the same.[5] This demonstration of the secondary structure similarity between solid and dissolved states means that the secondary structure of solid zein can be compared to zein dissolved in other solvents using IR spectroscopy thus enabling the *in situ* examination of solvent and temperature effects on protein secondary structure. The results obtained by Forato et al. for their zein samples show that the secondary structure of zein depends on source and method of production. Figure 5.1 compares the six secondary structures obtained by Forato for solid zein produced from various methods, and the secondary structure of the solid zein examined here with an error bar representing one standard deviation of the result (as is the case for all figures in this chapter).[5]

64
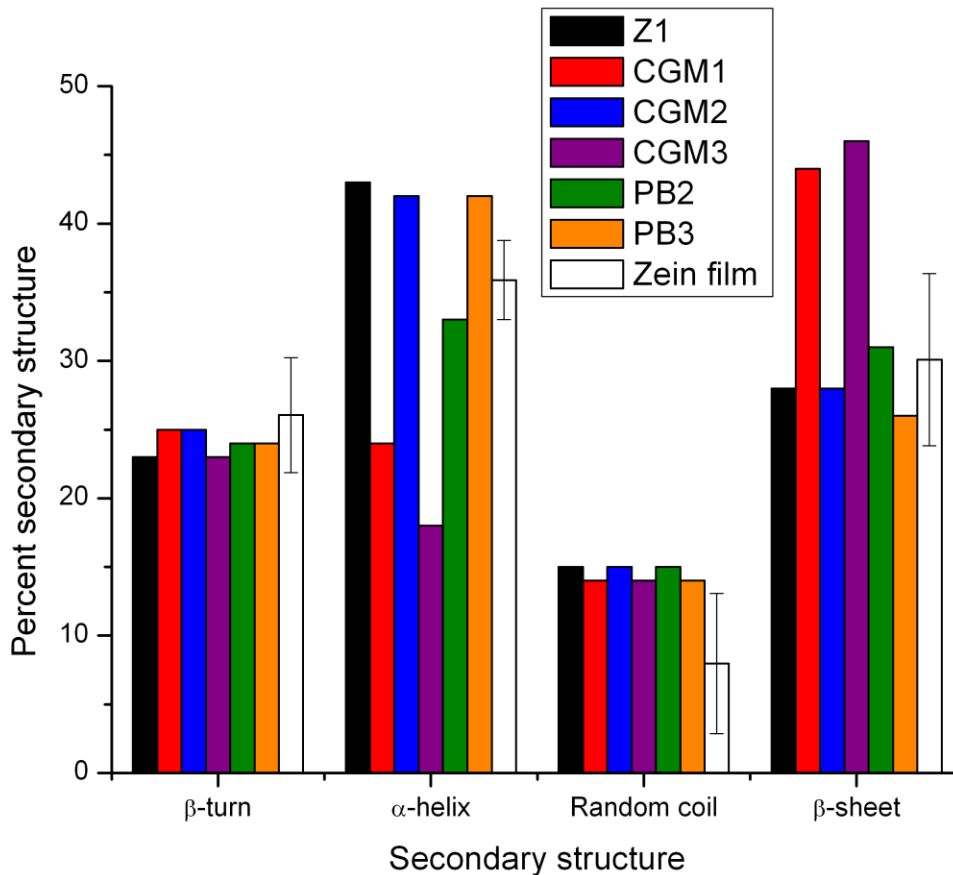
Figure 5.1 Comparison of zein secondary structures obtained from different zein sources, with the 25°C secondary structure obtained for this research

In Figure 5.1 the α-helix and β-sheet secondary structures were the most affected by zein's source and preparation method.[5] The variation between samples means that one should be cautious when quantitatively comparing protein secondary structure from different sources and references. In this research the same source of zein was used for all samples, relieving concerns about sample variability.

While it has been found that ionic liquids can dissolve zein, no research has been performed examining the secondary structure of zein in ionic liquids.[9, 10] Because it has been shown that some solvents, such as acetic acid, can dissolve zein but alter its secondary structure, it is important to know how ionic liquids affect the secondary structure of the protein.[3, 11] This chapter will examine the secondary structure of zein as a solid film, dissolved in the industrial zein solvent 70 vol% aqueous ethanol, a family of imidazolium-based ionic liquids, and in the

related molecular solvents acetic acid and 1-methylimidazole. The secondary structure of zein dissolved in [mim][HSO$_4$] was not examined because insufficient zein dissolved to be visible with IR spectroscopy. The full names and structures of all the ionic liquids are given in Appendix G.

Results and Discussion

Zein as a film

To compare solvent effects on the temperature behavior of the secondary structure of zein, a zein film was prepared (see Chapter 3). The change in secondary structure as a function of temperature was examined, see Figure 5.2, including selected representative error bars (each showing the standard deviation of that value) for ease of viewing.
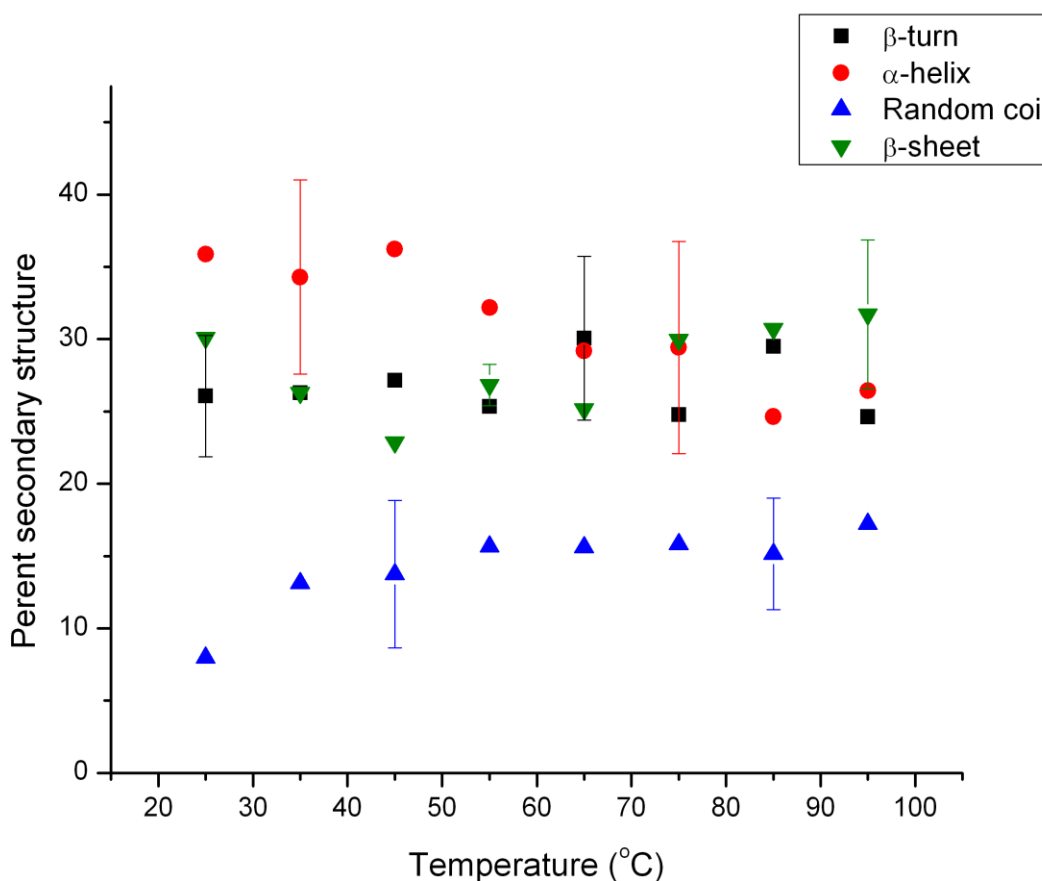
Figure 5.2 Secondary structures of solid zein versus temperature. Representative error bars shown for ease of viewing.

Statistically significant temperature dependence was found for α-helix (decrease), random coil (increase), and β-sheet (increase) secondary structures using single variable least squares regression, with a 95% confidence interval. Approximately 0.2% α-helix secondary structure is lost per degree Celsius, and approximately 0.2% β-sheet and random coil secondary structure is gained per degree Celsius. No statistically significant temperature dependence was found for β-turn secondary structure. The changes of the α-helix and β-sheet secondary structures are similar to previously reported literature for zein in aqueous ethanol solution and as a solid, which shows that as zein is heated, the secondary structure changes from α-helix to β-sheet.[12-14] This behavior has been explained that as the temperature increases, the hydrogen bonds that maintain the stability of the α-helix are destroyed. Then the β-sheet, which is more stable at higher temperatures in solid zein and zein dissolved in aqueous ethanol, is formed from the destroyed α-helix.[14, 15] A similar decrease in α-helix and increase in β-sheet as functions of temperature have been reported for other globular proteins.[6, 12, 13]

Zein in 70 vol% aqueous ethanol

The secondary structure changes with temperature for zein in 70 vol% aqueous ethanol are shown in Figure 5.3.
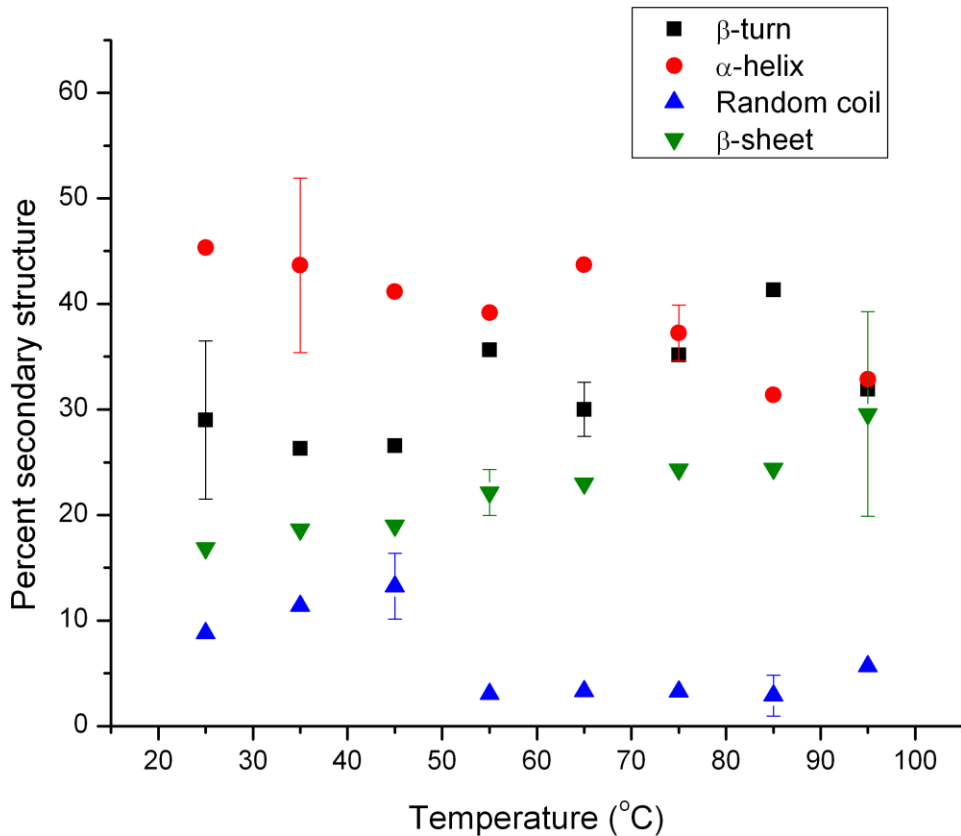
Figure 5.3 Secondary structures of zein dissolved in 70 vol% aqueous ethanol versus temperature. Representative error bars shown for ease of viewing.

Similar to the behavior seen in Figure 5.2 for the solid zein, as the temperature increases the α-helix declines at 0.2% per degree Celsius and β-sheet increases at 0.2% per degree Celsius. As discussed above, this behavior has been seen before by Cabra et al. using deconvolution of far-ultraviolet circular dichroism data.[6] However, unlike the zein film presented in Figure 5.2, no temperature dependence is seen for random coil from 25°C to 95°C. Comparing the secondary structures present at each temperature between Figures 5.2 and 5.3, one can see similarities in the fraction of α-helix, β-turn, and β-sheet, indicating, as Forato et al. reported, the secondary structure of zein in aqueous ethanol and solid zein is similar.[5]

Zein in acetic acid

Acetic acid, although a good solvent for zein (see Chapter 4), is not used for commercial zein production because it has been found to harm protein properties such as tensile strength,

compared to zein produced from aqueous alcohol.[3, 7, 16] Figure 5.4 shows that the secondary structure of zein in acetic acid changes with increasing temperature, showing greater deviation from the structure of pure zein film (see Figure 5.2) than zein dissolved in aqueous ethanol (Figure 5.3).

Figure 5.4 Secondary structures of zein in acetic acid versus temperature. Representative error bars shown for ease of viewing.

Comparing Figures 5.2 and 5.3 to Figure 5.4, one can see more β-sheet and less β-turn is present in acetic acid with increasing temperature, and approximately equal amounts of α-helix and random coil compared to the zein film or zein in aqueous ethanol. The differences in the percent of each secondary structure between zein in 70 vol% aqueous ethanol (Figure 5.3) and zein in acetic acid (Figure 5.4) may help to explain previous research that showed zein extracted with acetic acid has less tensile strength than zein extracted with aqueous ethanol.[3] The research presented here shows that while zein has similar fractions of α-helix and β-turn secondary

structures in aqueous ethanol and acetic acid, the fraction β-sheet and random coil in aqueous ethanol and acetic acid are different. Zein in acetic acid has significantly more random coil above 55°C, indicating zein is more denatured in acetic acid than in aqueous ethanol. In 2008 Selling and Woods found that films made from zein extracted with acetic acid have approximately 60% less tensile strength than films made from zein extracted with aqueous ethanol.[3] The decrease in zein's tensile strength relates to differences in the protein's secondary structure in solution.

Analysis of covariance for zein as a film and dissolved in aqueous ethanol and acetic acid shows that the functional dependence of the behavior of α-helix and β-sheet on temperature is statistically similar in all cases. Despite differences in the state of the zein (solid or dissolved) or solvent (aqueous ethanol or acetic acid), the decline of the α-helix (0.2% per degree Celsius) and increase of the β-sheet (0.2% per degree Celsius) are statistically similar. This means that temperature affects the secondary structure of solid zein similarly to dissolved zein in aqueous ethanol or acetic acid.

Zein in 1-methylimidzole

The secondary structure of zein in 1-methylimidazole is of interest because the ionic liquids examined are based on the 1-methylimidazole ring. Of note is that there is more α-helix and less random coil secondary structures than is seen in the previous figures. No significant temperature dependence of any secondary structure is seen in Figure 5.5.

Figure 5.5 Secondary structures of zein in 1-methylimidzole versus temperature. Representative error bars shown for ease of viewing.

The lack of statistically significant secondary structure change with increasing temperature, compared to previous figures, indicates that 1-methylimidazole thermally stabilizes zein's secondary structure, even if zein's structure is different at 25°C from what is shown in the previous figures.[17, 18]

Zein in [mim][OAc]

At 25°C zein in [mim][OAc] has a similar secondary structure to zein in 70 vol% aqueous ethanol and solid zein. Similar to zein in 70 vol% aqueous ethanol, Figure 5.6 shows some secondary structure change with temperature for zein in [mim][OAc].

Figure 5.6 Secondary structure of zein in [mim][OAc] versus temperature. Representative error bars shown for ease of viewing.

Figure 5.6 does not show a statistically significant dependence of changes in β-turn, α-helix, or β-sheet on temperature from 25°C to 95°C. However, random coil is a function of temperature, increasing approximately 0.2% per degree Celsius. This change in protein secondary structure, demonstrated by the increase in random coil, indicates that the protein is denaturing with increasing temperature, unlike zein dissolved in 1-methylimidazole, which has no significant secondary structure dependence on temperature. This shows that despite the similar structure between the cation with 1-methylimidazole, the anion plays a role and the ionic liquid does not thermally stabilize the zein.

Zein in [mim][Fr]

Figure 5.7 shows the changes in the secondary structure of zein in [mim][Fr] as a function of temperature, showing a different secondary structure from solid zein or zein in [mim][OAc].
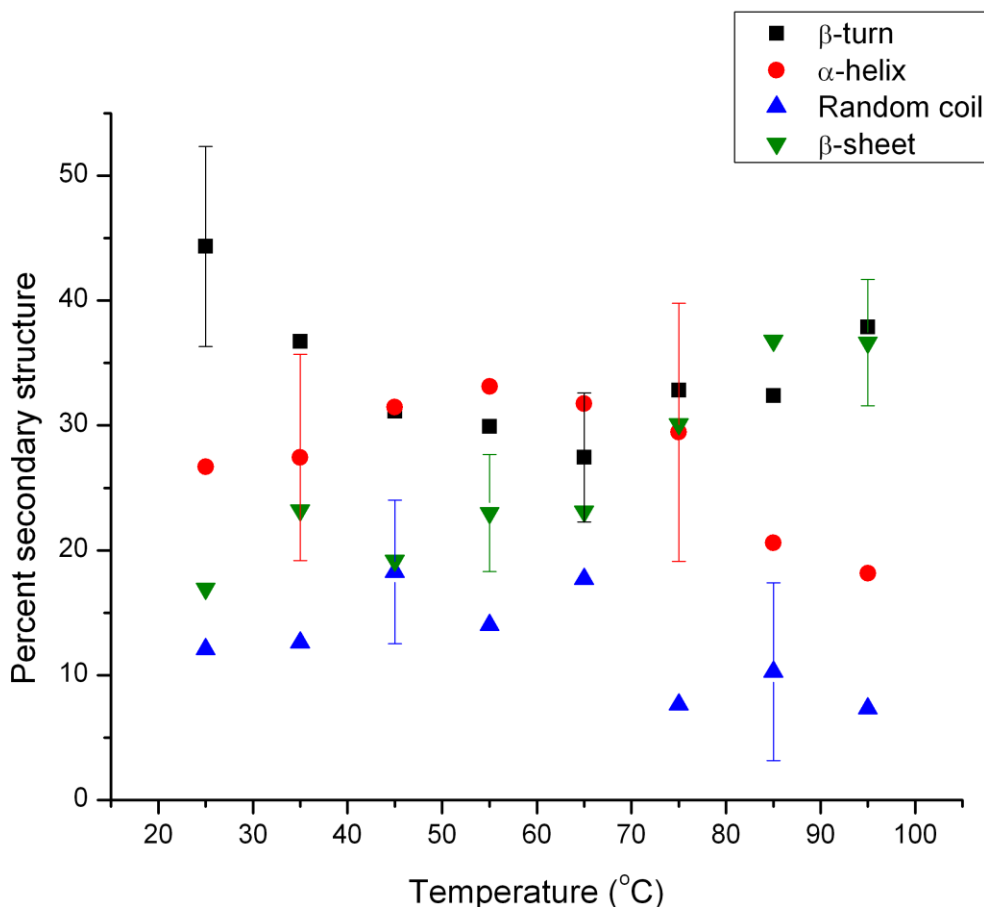
Figure 5.7 Secondary structure of zein in [mim][Fr] versus temperature. Representative error bars shown for ease of viewing.

The β-turn, α-helix, and random coil of zein in [mim][Fr] have no statistically significant dependence on temperature, but β-sheet does, with an increase of approximately 0.3% per degree Celsius. This increase in β-sheet, similar to zein in [mim][OAc]'s increase in random coil, indicates that the protein is denaturing with increasing temperature, as seen for solid zein and zein dissolved in 70 vol% aqueous ethanol and acetic acid. As discussed in Chapter 4, the differences in the zein's behavior in protic ionic liquids are likely related to the different

polarizabilities of the solvents. The more polar [mim][Fr] causes greater structural disruption than the less polar [mim][OAc].

Zein in [Emim][OAc]

Zein in [Emim][OAc] can be seen in Figure 5.8 to have a much different secondary structure than solid zein, with more β-turn and less β-sheet secondary structure similar to zein in [mim][Fr]. The dependence of the secondary structure of zein in [Emim][OAc] on temperature is shown in Figure 5.8.
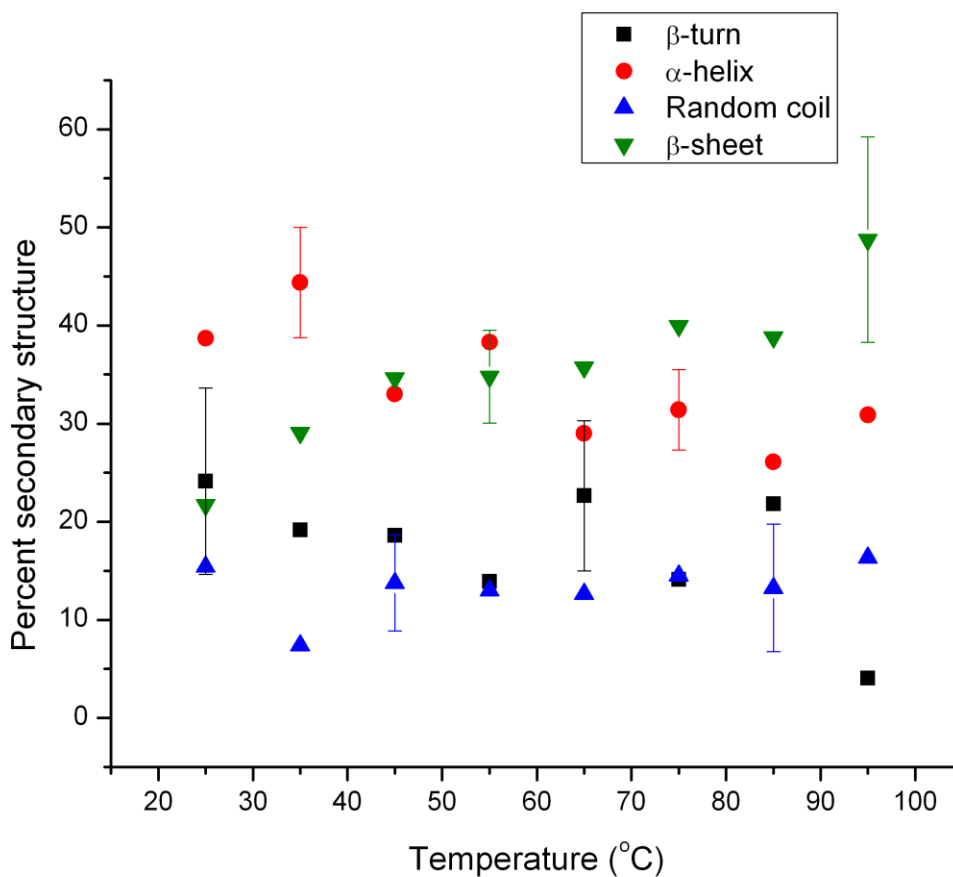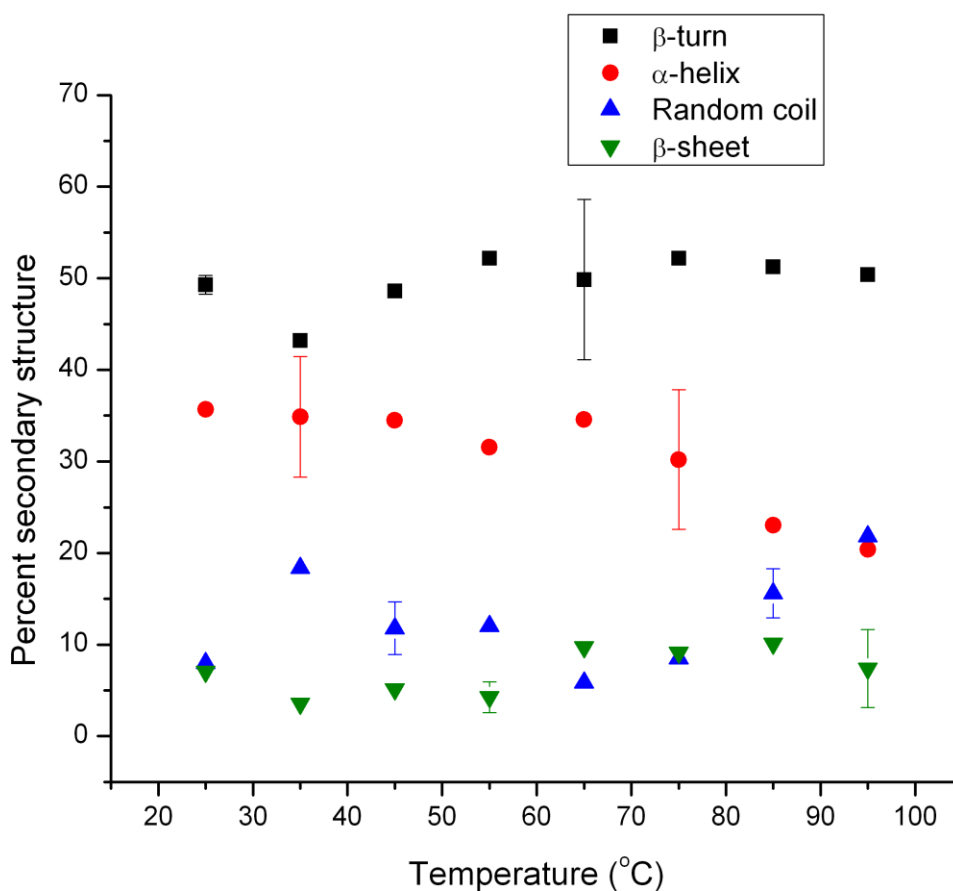

Figure 5.8 Secondary structures of zein in [Emim][OAc] versus temperature. Representative error bars shown for ease of viewing.

The higher β-turn and lower β-sheet compared to solid zein or zein in aqueous ethanol or acetic acid is maintained throughout the temperature range. The decrease in α-helix is a statistically significant function of temperature over the whole temperature range from 25°C to 95°C. There

is also, beginning at 65°C, a statistically significant increase in random coil. The decreasing amount of α-helix and increasing amount of random coil recalls the behavior of zein with temperature shown in Figures 5.3 for zein as a film or for zein dissolved in either aqueous ethanol or acetic acid (Figures 5.4 and 5.5). The previous examples of secondary structure change have been credited to the change from α-helix to the more thermally stable β-sheet by a disruption of the hydrogen bonds that maintain the protein's secondary structure.[12-15] In Figure 5.8 however, the increase does not occur in the β-sheet but rather in the random coil. In comparison to zein in the protic [mim][OAc], zein in [Emim][OAc] has a substantially denatured structure. Larger cations are known to destabilize proteins through their non-hydrogen bonding interactions with the non-polar parts of the protein, explaining why [Emim][OAc] denatures zein more than [mim][OAc].[19-22]

Zein in [Bmim][OAc]

Zein in [Bmim][OAc] has substantially different secondary structure changes compared to solid zein, shown in Figure 5.2, including more β-turn and less α-helix secondary structure. Unlike zein in [Emim][OAc] (Figure 5.8) with the decrease in α-helix observed, zein in [Bmim][OAc] shows no temperature dependence of any secondary structure between 25°C and 95°C, see Figure 5.9.
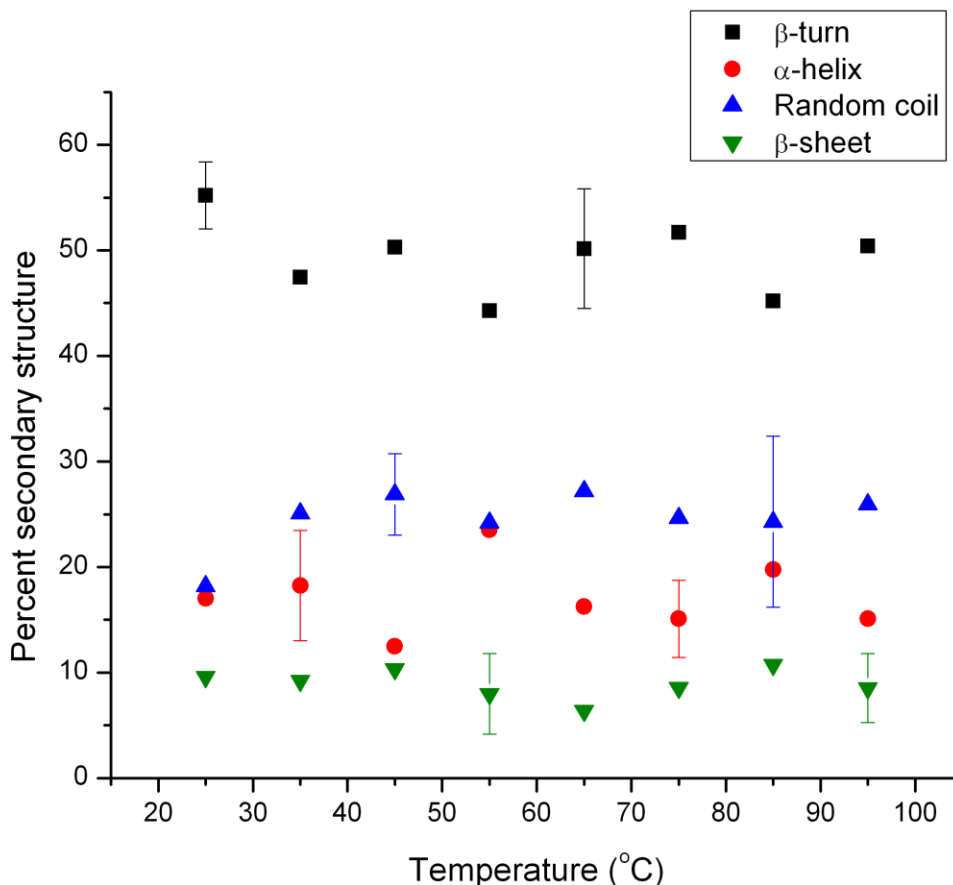
Figure 5.9 Secondary structure of zein in [Bmim][OAc] versus temperature. Representative error bars shown for ease of viewing.

However, there is more random coil and less α-helix secondary structure than has heretofore been seen. This indicates more changes to zein's secondary structure by [Bmim][OAc] than were seen for zein in [Emim][OAc]. As mentioned above, larger cations are known to destabilize native protein structure; this result fits with what has been previously discussed in the literature.[20-22]

Zein in [Bmim][Cl]

By comparing zein in [Bmim][Cl] in Figure 5.10 to zein in [Bmim][OAc] in Figure 5.9 it can be seen that zein has more α-helix and less random coil in [Bmim][Cl] than in [Bmim][OAc]. Figure 5.10 also shows that the secondary structure of zein in [Bmim][Cl] is not a function of temperature.
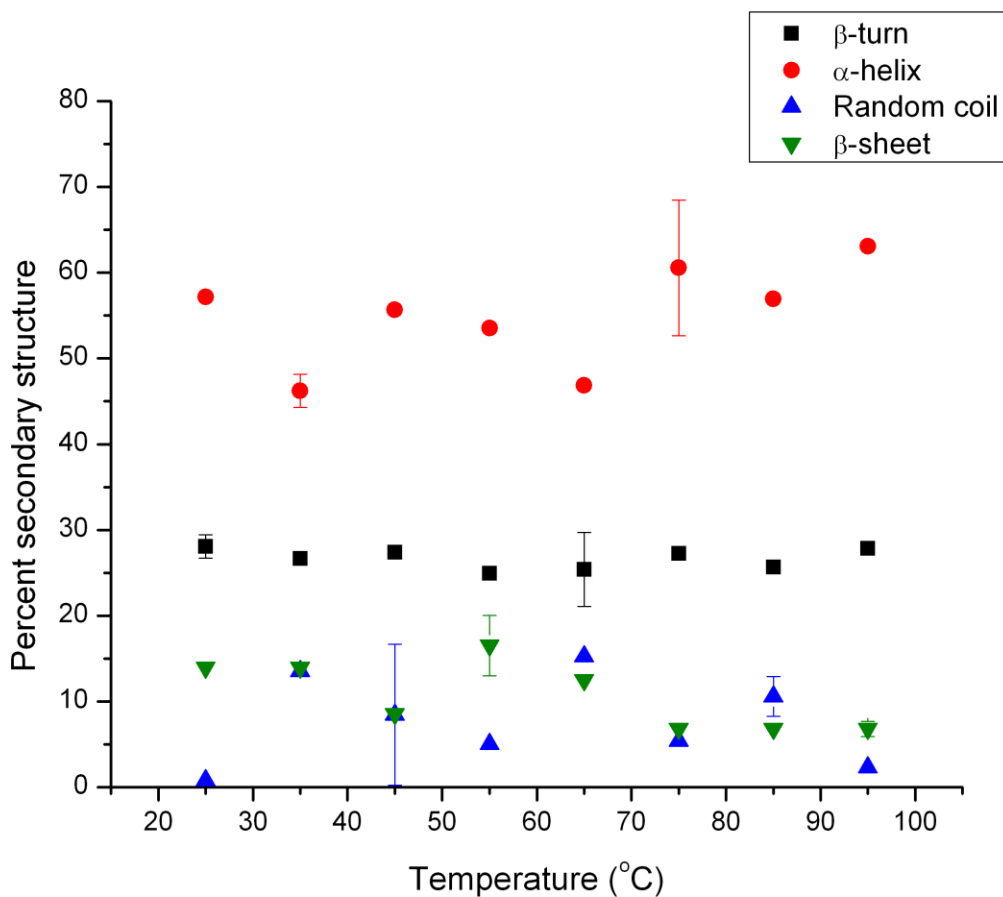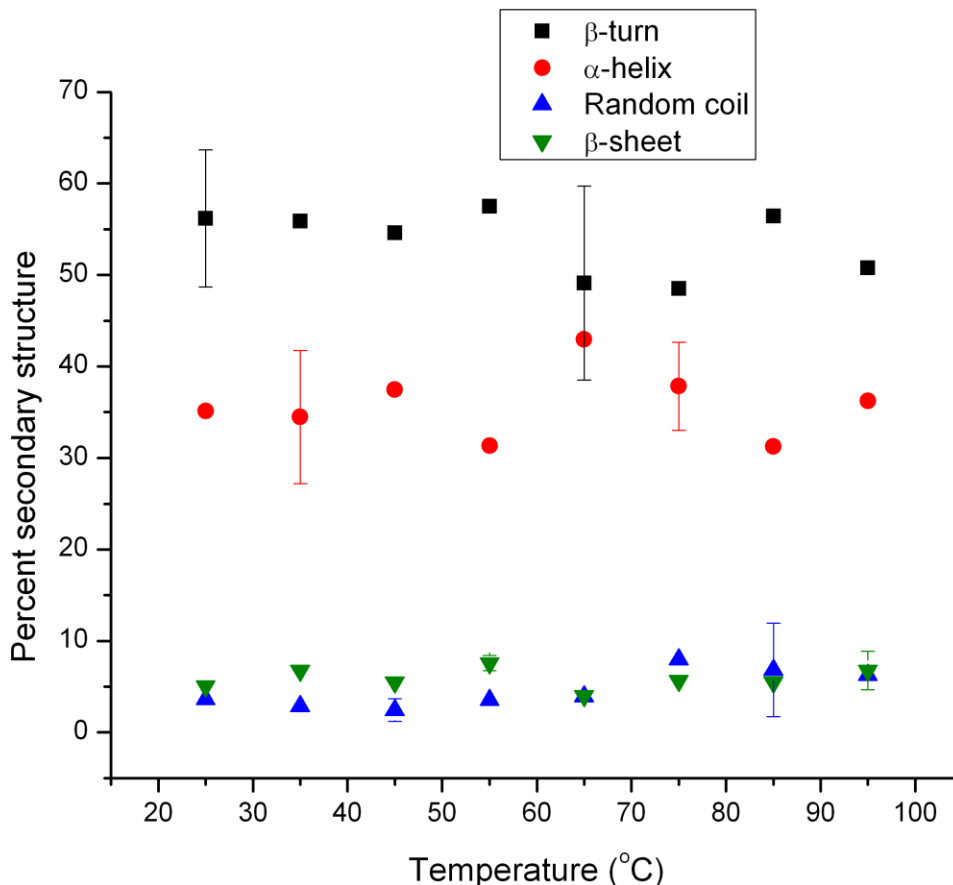
Figure 5.10 Secondary structures of zein in [Bmim][Cl] versus temperature. Representative error bars shown for ease of viewing.

The dissimilarity compared to [Bmim][OAc] shows the importance of the anion in controlling the secondary structure of zein. Significantly more α-helix and less random coil secondary structure is observed for zein dissolved in [Bmim][Cl] than for zein dissolved in [Bmim][OAc]. As it is usually thought that the acetate anion is more stabilizing for proteins (a kosmotropic anion, see Chapter 2) than the chloride anion, this difference is unexpected.

Zein in [Emim][DCA]

As discussed in Chapter 4 [Emim][DCA] exhibits unusual behavior due to its protein destabilizing dicyanamide anion. In Figure 5.11 zein in [Emim][DCA] is seen to have the most β-turn and the least α-helix secondary structure of zein in any solvent. As seen for zein in the other aprotic ionic liquids, there is no secondary structure change with temperature.
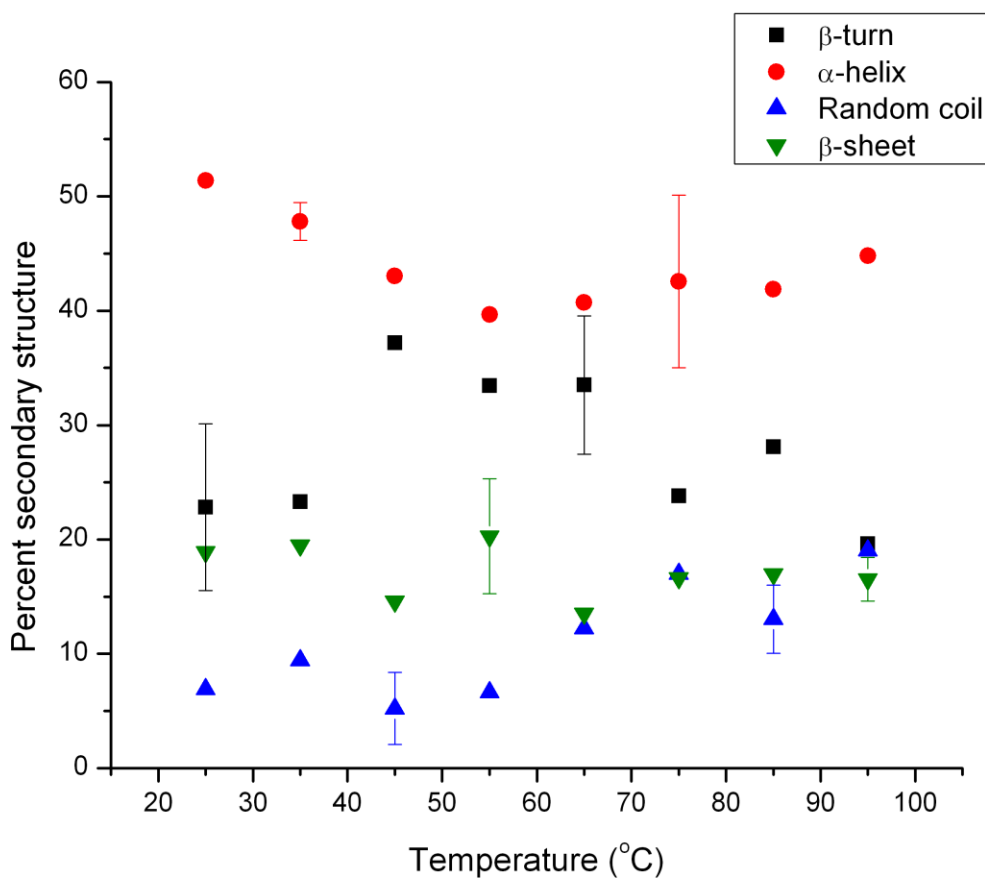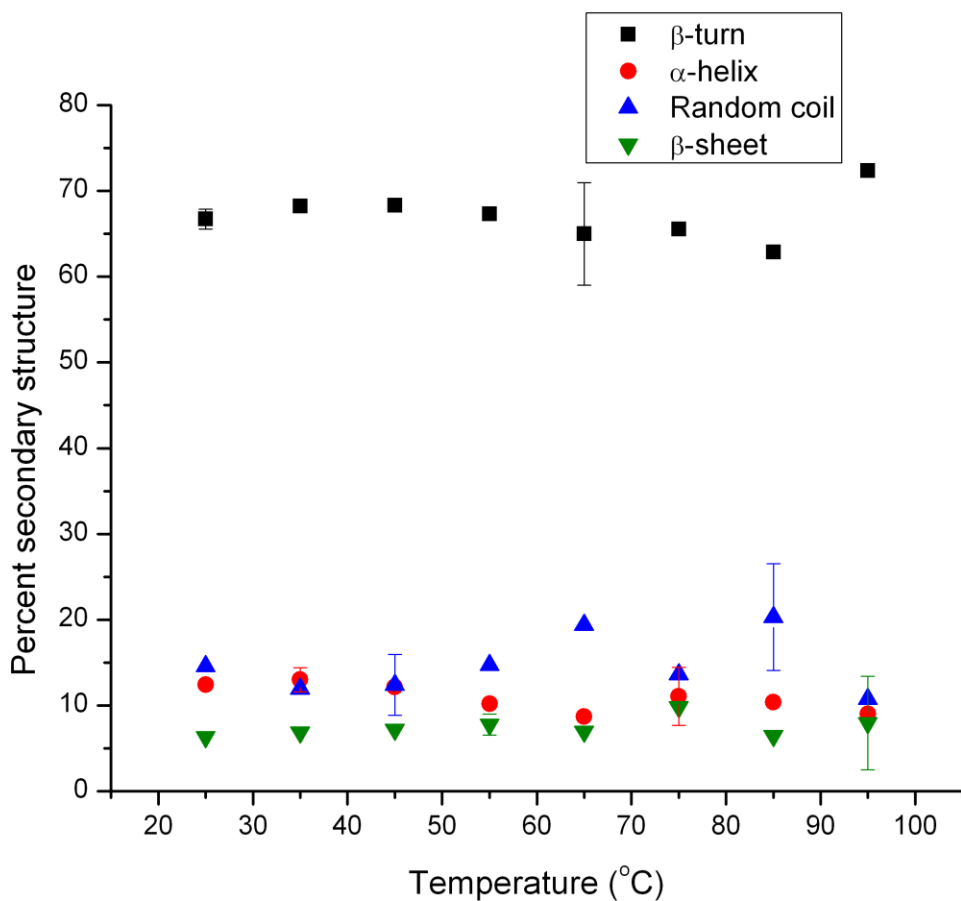
Figure 5.11 Secondary structures of zein in [Emim][DCA] versus temperature. Representative error bars shown for ease of viewing.

This indicates that, while the protein is strongly denatured by the ionic liquid, more so than is seen for any other solvent, there are no statistically significant apparent thermal effects on the secondary structure from 25°C to 95°C.

Comparison of zein secondary structures at 25°C

Comparing the secondary structure of zein in the solvents at 25°C and as a film shows how the solvent affects the secondary structure irrespective of temperature effects, shown in Figure 5.12. For comparison purposes Figure 5.12 also includes previous literature values for zein secondary structure found for solid zein and in aqueous ethanol.[5, 6]
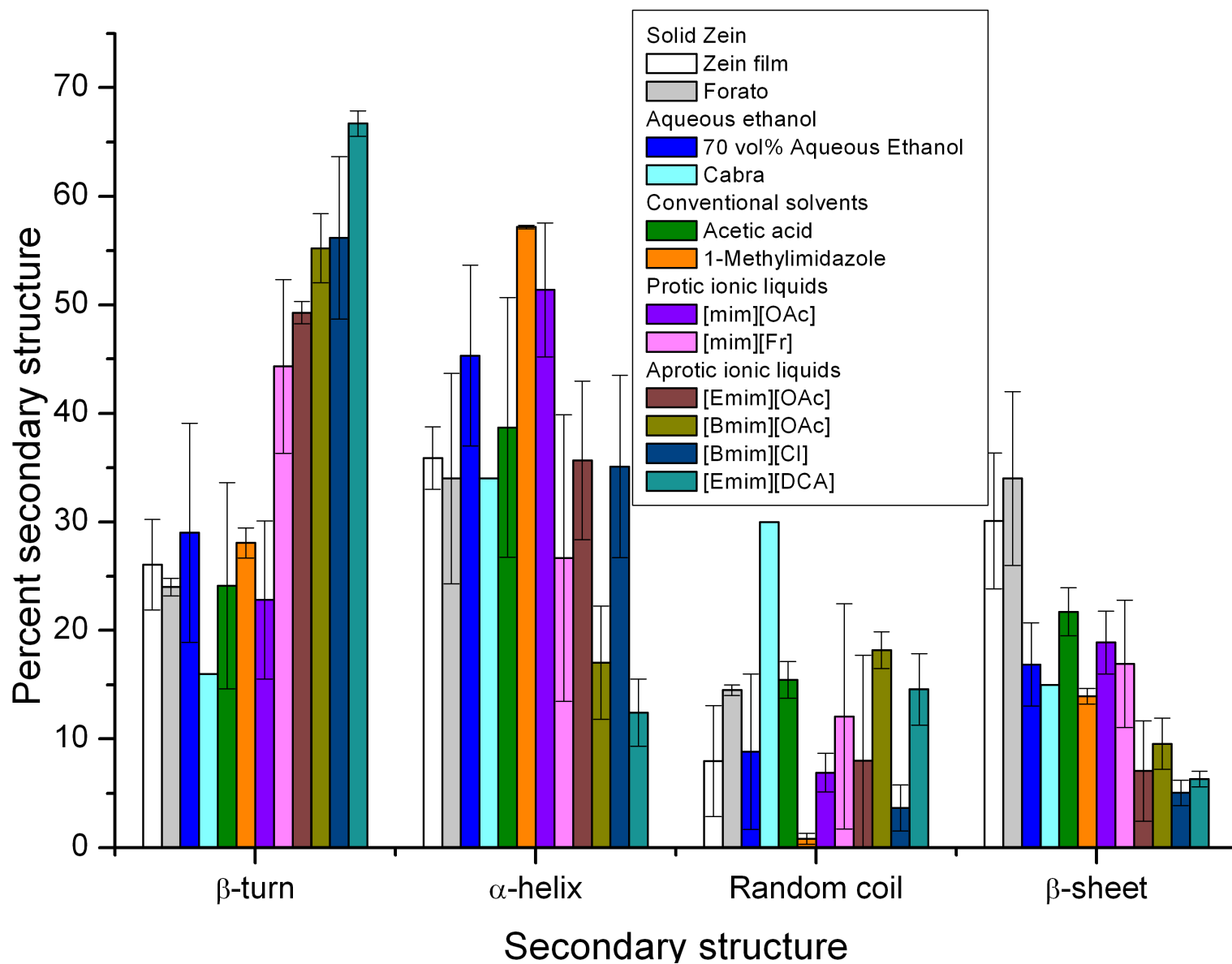
Figure 5.12 Comparison of secondary structure at 25°C in different solvents.

For example, Figure 5.12 shows that the solid zein film has 26.1 ± 4.2% β-turn, 35.9 ± 2.8% α-helix, 8.0 ± 5.1% random coil, and 30.0 ± 6.3% β-sheet secondary structure at 25°C. Figure 5.12 shows that the secondary structure obtained for the solid zein film and the aqueous ethanol are similar to the literature work from Forato et al.[5] and Cabra et al.,[6] respectively.

As one can see from Figure 5.12, the secondary structure at 25°C varies widely between the solvents. It can be seen that zein in 1-methylimidazole and [mim][OAc] show similar secondary structures, which have more α-helix than solid zein. In contrast, the aprotic ionic liquids and [mim][Fr] show more β-turn and less β-sheet secondary structure than pure zein. The changes in zein's secondary structure show that the protein is denaturing in solution but resulting in different denatured conformations. These results are in contrast to previous research which found that denaturing zein with aqueous urea showed a decrease β-turn and increases α-helix and random coil secondary structures, in direct contrast to what is seen in Figure 5.12 for the aprotic ionic liquids.[23] Other research has shown that thermal denaturing of zein results in more β-sheet at the expense of α-helix, so the denaturing of zein caused by the aprotic ionic liquids results in an unusual new conformation.[14, 15] As even the small changes caused by acetic acid change zein's physical properties, these 25°C results show that, while some ionic liquids may be suitable to dissolve zein, careful examination of the solvent effects on secondary structure is necessary to ensure the zein maintains the secondary structure desired.

Effect of water concentration on zein secondary structure in [Emim][DCA]

To compare the effects of the amount of water in ionic liquid on the secondary structure of dissolve zein, three samples of zein in [Emim][DCA] were prepared (see Chapter 3) and examined. The results are given in Figure 5.13.
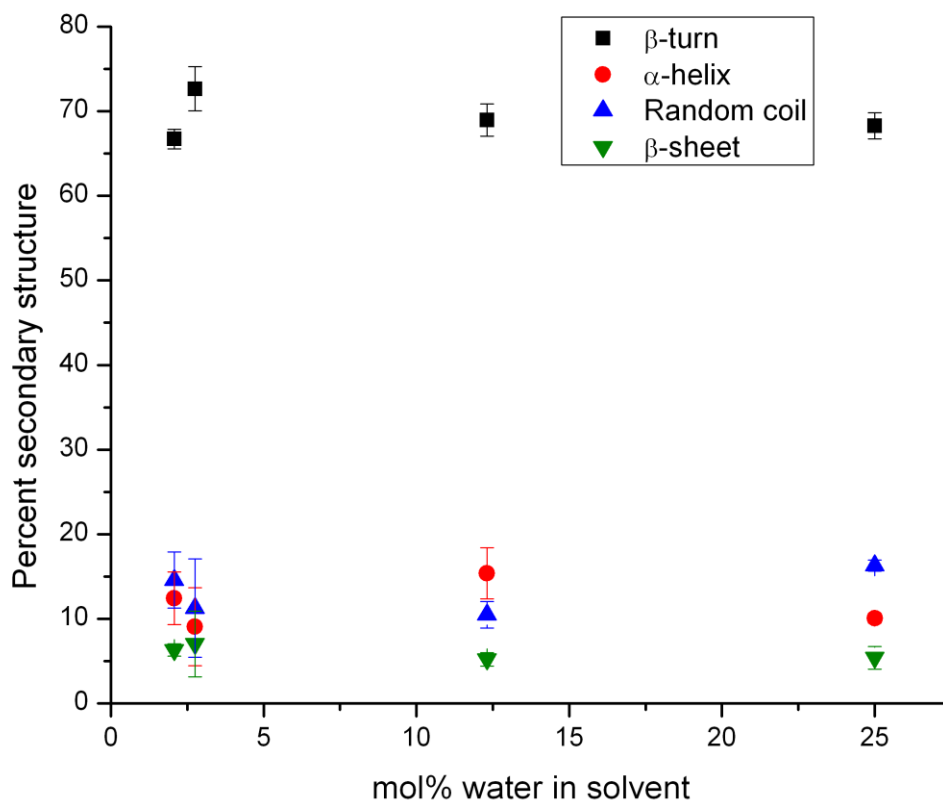
Figure 5.13 Comparison of the effects of water content on the secondary structures of zein dissolved in [Emim][DCA].

Figure 5.13 shows that there is no secondary structure dependence on the fraction of water in the ionic liquid solvent from 2.0 mol% to 25.0 mol%. In addition, the apparent solubility of zein in [Emim][DCA] did not vary with the different water fractions. In all cases zein was dissolved the following morning. Sample viscosities were apparently similar as well. It is surprising that 25 mol% water has so little effect on the secondary structure of zein, and no apparent effect on the solubility and viscosity of the solutions, compared to 2.7 mol% water [Emim][DCA].

Previous research using ionic liquids for inorganic materials synthesis has discovered a so-called "water deactivating" effect (see Chapter 2).[24-27] The "water deactivating" effect is the lack of chemical activity of water to the degree expected by its concentration. The "water deactivating" effect has been described as molecular dispersion of the water in solution, so water is not present in many-molecule micelles. This dispersion is due to water's strong nucleophilic attraction to the ionic liquid's anion, even the chaotropic bromide anion which interacts poorly

with water.[24] This dispersion thus reduces the hydrolysis activity of water, effectively deactivating its ability to participate in reactions.[24]

Temperature effects on solution

Table 5.1 is a reproduction of Table 4.2, giving the Mz from the solubility of zein in each of the solvents examined.[28] As discussed in Chapter 2 and applied in Chapter 4, the value of Mz is related to solvent effects on the zein. The lower the value of Mz, the more energy required to dissolve the solute in the solvent, resulting in lower solubility.

Table 5.1 The slope from the natural log of zein solubility versus 1/T (K), Mz, for solvents examined.

Solvent	Mz (dimensionless)
Acetic Acid	-1900 ± 700
1-Methylimidazole	-1700 ± 700
[mim][OAc]	-1300 ± 400
[mim][Fr]	-3200 ± 800
[Emim][OAc] - 11.1 mol% water	-4300 ± 600
[Emim][OAc] - 4.0 mol% water	-4700 ± 200
[Bmim][OAc]	-3800 ± 50
[Bmim][Cl]	-3800 ± 900
[Emim][DCA]	-1700 ± 300

The Mz from solubility is related to the change in secondary structure of zein (compared to solid zein) in most solvents. Figure 5.14 shows the percent change in the percent β-turn secondary structure versus Mz.
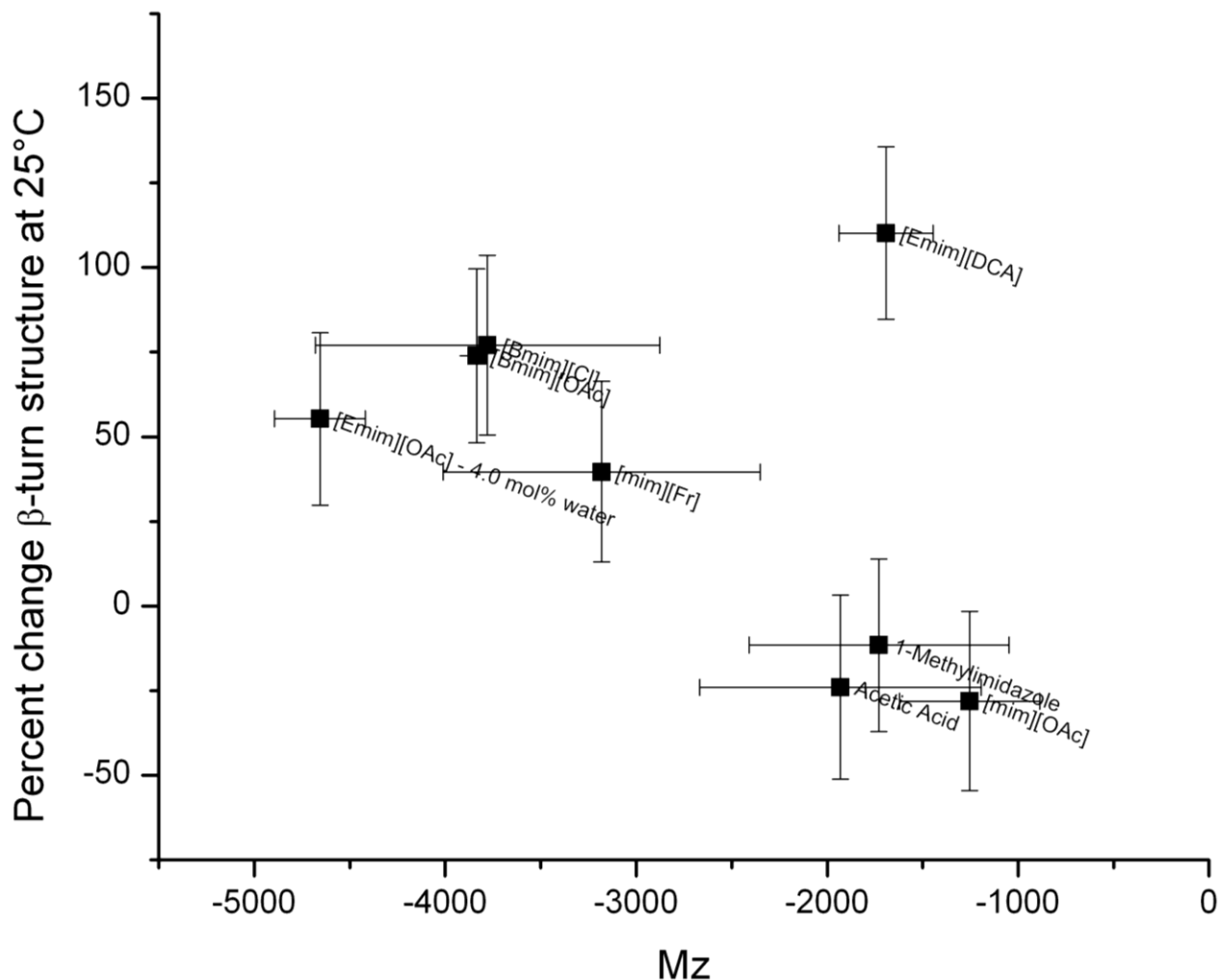
Figure 5.14 Percent change β-turn secondary structure versus Mz.

As one can see from Figure 5.14, low Mz results yields more β-turn structure. The exception to this is [Emim][DCA] which has both a high secondary structure change and a high Mz. The high Mz seen for zein in acetic acid (-1900 ± 700), 1-methylimidazole (-1700 ± 700), and [mim][OAc] (-1300 ± 400) is reflected in the minor structural disruption, compared to the zein film, seen for zein in those solvents in Figure 5.12.

By contrast, zein in [Emim][DCA] has a similarly high Mz (-1700 ± 300), but the structure is very different, with far more β-sheet than zein in any other solvent and less of the other secondary structures. This peculiar behavior is likely related to the dicyanamide ([DCA]) anion's strong protein destabilizing abilities, as well as its poor hydrogen-bonding ability compared to chloride or acetate.[21, 29] These characteristics limit [Emim][DCA]'s ability to form intra-solvent hydrogen bond networks (thus requiring less energy to overcome solvent-solvent

interactions compared to the other aprotic ionic liquids).[21, 29] This effect is discussed in Chapter 2. This chaotropic anion effect can be seen in Figure 5.12 for the strongly denatured zein in [Emim][DCA], as well as the high Mz in Table 5.1. The protein destabilizing behavior of dicyanamide ionic liquids (including [Emim][DCA]) has been reported in the literature, albeit as aqueous organic salts, not as the primarily ionic liquid solutions reported here.[19, 21, 22, 29] It has also been found that chaotropic anions, because of their weaker interactions with water, are poorly hydrated, thus allowing the chaotropic anions to interact preferentially with the protein, forming the new bonds that may help to explain [Emim][DCA]'s high Mz.[19, 30] Because the other aprotic ionic liquids have strongly interacting kosmotropic anions, the energy required to overcome their solvent-solvent bonding is higher. While above it was discussed that dicyanamide's weak interactions with water account for the high Mz of zein, it has still been found that even anions that interact poorly with water are able to deactivate water in solution.[24-27]

The other aprotic ionic liquids [Emim][OAc], [Bmim][OAc], and [Bmim][Cl], and protic [mim][Fr] all have low Mz, and increase β-turn and decrease β-sheet secondary structures in the zein compared to the zein film. The lower Mz for these solvents means that relatively more energy is required to dissolve the zein, and that energy also affects the secondary structure. Therefore, solvents to maintain zein, or another hydrophobic protein, secondary structure should be designed to have a high Mz, which corresponds to a low temperature dependence of zein solubility (as discussed in Chapter 4).

Conclusions

Zein's secondary structure in 1-methylimidazole compared to the secondary structure in the ionic liquids studied gives insight into how solvent chemical differences affect the solute. As could be seen from the temperature dependent analysis of zein's secondary structure, zein's secondary structure was less dependent on temperature in 1-methylimidazole and the ionic liquids than as a solid film or dissolved in either acetic acid or aqueous ethanol. Therefore 1-methylimidazole and its ionic liquid derivatives reduce the secondary structure dependence on temperature, meaning that, if thermal stability is desired, the ionic liquids examined here are suitable.

However the aprotic ionic liquids ([Emim][DCA], [Emim][OAc], [Bmim][OAc], and [Bmim][Cl]) affect the secondary structure of zein more than conventional solvents or

[mim][OAc] due to their protein destabilizing kosmotropic cations. Aprotic ionic liquids also tend to have lower Mz than conventional solvents or [mim][OAc]. However, [Emim][DCA] changed the secondary structure of zein even with its high Mz. The effect of [Emim][DCA] on zein secondary structure is likely related to the dicyanamide anion's strong chaotropic properties, that is, dicyanamide's ability to disrupt protein secondary structure. The difference in the secondary structure (and solubility shown in Chapter 4) of zein in [mim][OAc] compared to zein in [mim][Fr] shows the effect of anions, even of anions that may be expected to behave similarly given their similar chemical structure.

References

1. Gennadios, A.; Weller, C. L.; Testin, R. Temperature Effect on Oxygen Permeability of Edible Protein-based Films, *J. Food Sci.* **2006***, 1,* 212-214.

2. Nack, T. J.; Ludescher, R. D. Molecular mobility and oxygen permeability in amorphous bovine serum albumin films, *Food Biophysics* **2006***, 3,* 151-162.

3. Selling, G. W.; Woods, K. K. Improved isolation of zein from corn gluten meal using acetic acid and isolate characterization as solvent, *Cereal Chem.* **2008***, 2,* 202-206.

4. Lau, R. M.; Sorgedrager, M. J.; Carrea, G.; van Rantwijk, F.; Secundo, F.; Sheldon, R. A. Dissolution of Candida antarctica lipase B in ionic liquids: effects on structure and activity, *Green Chem.* **2004***, 9,* 483-487.

5. Forato, L. A.; Bicudo, T. D. C.; Colnago, L. A. Conformation of α zeins in solid state by Fourier transform IR, *Biopolymers* **2003***, 6,* 421-426.

6. Cabra, V.; Arreguin, R.; Vazquez-Duhalt, R.; Farres, A. Effect of temperature and pH on the secondary structure and processes of oligomerization of 19 kDa alpha-zein, *Biochim Biophys Acta* **2006***, 6,* 1110-1118.

7. Li, Y.; Li, J.; Xia, Q.; Zhang, B.; Wang, Q.; Huang, Q. Understanding the Dissolution of α-Zein in Aqueous Ethanol and Acetic Acid Solutions, *J. Phys. Chem. B* **2012**, 12057-12064.

8. Li, Y.; Xia, Q.; Shi, K.; Huang, Q. Scaling Behaviors of α-Zein in Acetic Acid Solutions, *J. Phys. Chem. B* **2011**, 9695-9702.

9. Biswas, A.; Shogren, R. L.; Stevenson, D. G.; Willett, J. L.; Bhowmik, P. K. Ionic liquids as solvents for biopolymers: Acylation of starch and zein protein, *Carbohydr. Polym.* **2006***, 4,* 546-550.

10. Choi, H. M.; Kwon, I. Dissolution of Zein Using Protic Ionic Liquids: N-(2-Hydroxyethyl) Ammonium Formate and N-(2-Hydroxyethyl) Ammonium Acetate, *Ind Eng Chem Res* **2011**, 2452-2454.

11. Xu, W.; Reddy, N.; Yang, Y. An acidic method of zein extraction from DDGS, *J. Agric. Food Chem.* **2007***, 15,* 6279-6284.

12. Qin, Z.; Buehler, M. J. Molecular dynamics simulation of the α-helix to β-sheet transition in coiled protein filaments: evidence for a critical filament length scale, *Phys. Rev. Lett.* **2010***, 19,* 198304-1-198304-4.

13. Fan, P.; Bracken, C.; Baum, J. Structural characterization of monellin in the alcohol-denatured state by NMR: Evidence for. beta.-sheet to. alpha.-helix conversion, *Biochemistry (N. Y.)* **1993**, *6,* 1573-1582.

14. Duodu, K. G.; Tang, H.; Grant, A.; Wellner, N.; Belton, P. S.; Taylor, J. R. N. FTIR and Solid State 13C NMR Spectroscopy of Proteins of Wet Cooked and Popped Sorghum and Maize, *J. Cereal Sci.* **2001**, *3,* 261-269.

15. Duodu, K. G.; Taylor, J. R. N.; Belton, P. S.; Hamaker, B. R. Factors affecting sorghum protein digestibility, *J. Cereal Sci.* **2003**, *2,* 117-131.

16. Huang, H.; Xie, J.; Chen, H. Adsorption behavior of human serum albumin on ATR crystal studied by in situ ATR/FTIR spectroscopy and two-dimensional correlation analysis, *Analyst* **2011**, *8,* 1747-1752.

17. Fujita, K.; MacFarlane, D. R.; Forsyth, M. Protein solubilising and stabilising ionic liquids, *Chem. Comm.* **2005**, *38,* 4804-4806.

18. Pace, C. N.; Treviño, S.; Prabhakaran, E.; Scholtz, J. M. Protein structure, stability and solubility in water and other solvents, *Phil. Trans. R. Soc. Lond. B* **2004**, *1448,* 1225-1235.

19. Zhao, H.; Campbell, S. M.; Jackson, L.; Song, Z.; Olubajo, O. Hofmeister series of ionic liquids: kosmotropic effect of ionic liquids on the enzymatic hydrolysis of enantiomeric phenylalanine methyl ester, *Tetrahedron: Asymmetry* **2006**, *3,* 377-383.

20. Zhang, Y.; Cremer, P. S. Interactions between macromolecules and ions: the Hofmeister series, *Curr. Opin. Chem. Biol.* **2006**, *6,* 658-663.

21. Constantinescu, D.; Weingärtner, H.; Herrmann, C. Protein denaturation by ionic liquids and the Hofmeister series: a case study of aqueous solutions of ribonuclease A, *Angew. Chem. , Int. Ed.* **2007**, *46,* 8887-8889.

22. Yang, Z. Hofmeister effects: an explanation for the impact of ionic liquids on biocatalysis, *J. Biotechnol.* **2009**, *1,* 12-22.

23. Pickering, K. L.; Verbeek, C. J. R.; Viljoen, C. The Effect of Aqueous Urea on the Processing, Structure and Properties of CGM, *J. Polym. Environ.* **2012**, 1-9.

24. Parnham, E. R.; Morris, R. E. Ionothermal Synthesis of Zeolites, Metal–Organic Frameworks, and Inorganic–Organic Hybrids, *Acc. Chem. Res.* **2007**, 1005.

25. Cammarata, L.; Kazarian, S. G.; Salter, P. A.; Welton, T. Molecular states of water in room temperature ionic liquids, *Physical Chemistry Chemical Physics* **2001**, 5192.

26. Hanke, C. G.; Lynden-Bell, R. M. A Simulation Study of Water− Dialkylimidazolium Ionic Liquid Mixtures, *J Phys Chem B* **2003**, *39,* 10873-10878.

27. Amigues, E.; Hardacre, C.; Keane, G.; Migaud, M.; O'Neill, M. Ionic liquids—media for unique phosphorus chemistry, *Chemical Communications* **2006**, *1,* 72-74.

28. Fu, D. Zein Properties and Alternative Recovery Methods, University of Nebraska - Lincoln, University of Nebraska, 2000.

29. Constantinescu, D.; Herrmann, C.; Weingärtner, H. Patterns of protein unfolding and protein aggregation in ionic liquids, *Phys. Chem. Chem. Phys.* **2010***, 8,* 1756-1763.

30. Zhao, H.; Olubajo, O.; Song, Z.; Sims, A. L.; Person, T. E.; Lawal, R. A.; Holley, L. D. A. Effect of kosmotropicity of ionic liquids on the enzyme stability in aqueous solutions, *Bioorg. Chem.* **2006***, 1,* 15-25.

Chapter 6 - Solvent Properties

Introduction

Ionic liquids can dissolve zein, and zein's secondary structure changes when dissolved in some but not all ionic liquids. These results raise the question of what solvent properties control the dissolution or structural changes of zein. Previous research into protein behavior in ionic liquids has been primarily concerned with proteins that have already been extensively studied in aqueous solution, such as hen egg-white lysozyme, bovine ribonuclease A, or the enzyme *Candida antarctica* lipase B (CALB).[1-7] However, it has been found that the solubility of these proteins in neat ionic liquids is usually poor (1.0 wt.% or less).[2, 5, 7-9] As the previously studied proteins dissolve well in water, it might be expected that their solubility in organic solvents or imidazolium-based ionic liquids would be poor. Research has shown that zein is soluble in [Bmim][Cl] and protic quaternary ammonium ionic liquids but without discussion as to why those ionic liquids dissolved zein or what structure changes may have occurred in the protein.[10, 11] The research into the solubility of cellulose and wood in ionic liquids, discussed in Chapter 2, found that [Emim][OAc]'s ability to disrupt the cellulose hydrogen bond network by accepting hydrogen bonds is what enables [Emim][OAc] to dissolve woody material.[12, 13] The hydrogen bonding ability of solvents is characterized by the Kamlet-Taft method, which uses solvatochromic dyes to quantify the ability of a solvent to donate hydrogen bonds (α parameter), accept hydrogen bonds (β parameter), and the solvent's polarizability/dipolarity (π^* parameter), as described in Chapter 2.[14]

This research uses single and multivariate regression for identifying and quantifying which solvent properties are important for controlling zein's solubility and secondary structure in solution. The parameters include Kamlet-Taft solvatochromic parameters, the pure solvent molar volume, and the $E_T(30)$ scale polarity from Chapter 2. This is the first work to specifically examine these effects for a protein in ionic liquid, and this is also the first report modeling a hydrophobic protein's solubility in ionic liquids.

The changes in zein secondary structure reported in this chapter are at 25°C and are relative to the percent of that secondary structure found from the solid zein film (see Chapter 5). This percent change quantifies the changes in zein secondary structure due to the solvent. The percent secondary structure change is calculated using equation 6.1.

$$\%structure\ change = \frac{y_{zein\ in\ solution} - y_{zein\ film}}{y_{zein\ film}} \times 100\% \qquad\qquad 6.1$$

In equation 6.1, y is the fraction of that secondary structure in solution or in the solid zein film. The full names and structures of all the ionic liquids are given in Appendix G.

Results and Discussion

Solubility

To examine what solvent properties are important for solubility, zein's solubility at 30°C was examined as a function of the following properties: Mz from Chapter 4, pure solvent molar volume from Chapter 2, and the Kamlet-Taft parameters of each solvent obtained from the literature (discussed in Chapter 2). Table 6.1 gives the values of the solvent parameters examined.

Table 6.1 Mz, pure solvent molar volume, and Kamlet-Taft parameters for solvents examined

Solvent	Mz (from Chapter 4)	Pure solvent molar volume at 25°C (mL/mol)	Kamlet-Taft hydrogen bond donating ability (α)	Kamlet-Taft hydrogen bond accepting ability (β)	Kamlet-Taft dipolarity/ polarizability (π^*)
Acetic Acid	-1900 ± 700	57.47 ± 0.02	1.12[15]	0.45[15]	0.64[15]
1-Methylimidazole	-1700 ± 700	79.57 ± 0.03	0.232[16]	0.712[16]	0.961[16]
[mim][OAc]	-1300 ± 400	132.8 ± 0.01	0.506[17]	0.85[17]	1.03[17]
[mim][Fr]	-3200 ± 800	113.13 ± 0.03	0.812[17]	0.81[17]	1.1[17]
[Emim][OAc] - 11.1 mol% water	-4300 ± 600		0.53[18]	1.06[18]	0.97[18]
[Emim][OAc] - 4.0 mol% water	-4700 ± 200	154.98 ± 0.03	0.53[18]	1.06[18]	0.97[18]
[Bmim][OAc]	-3800 ± 50	187.30 ± 0.14	0.57[18]	1.18[18]	0.89[18]
[Bmim][Cl]	-3800 ± 900	165.98 ± 0.03	0.47[19]	0.87[19]	1.1[19]
[Emim][DCA]	-1700 ± 300	160.93 ± 0.04	0.53[20]	0.35[20]	1.08[20]

As hydrogen bond accepting ability has been credited with [Emim][OAc]'s ability to dissolve cellulose and wood, Figure 6.1 shows the solubility (and error bars representing one standard

deviation) of zein at 30°C from Chapter 3 versus the Kamlet-Taft hydrogen bond accepting ability (β) of the solvents.
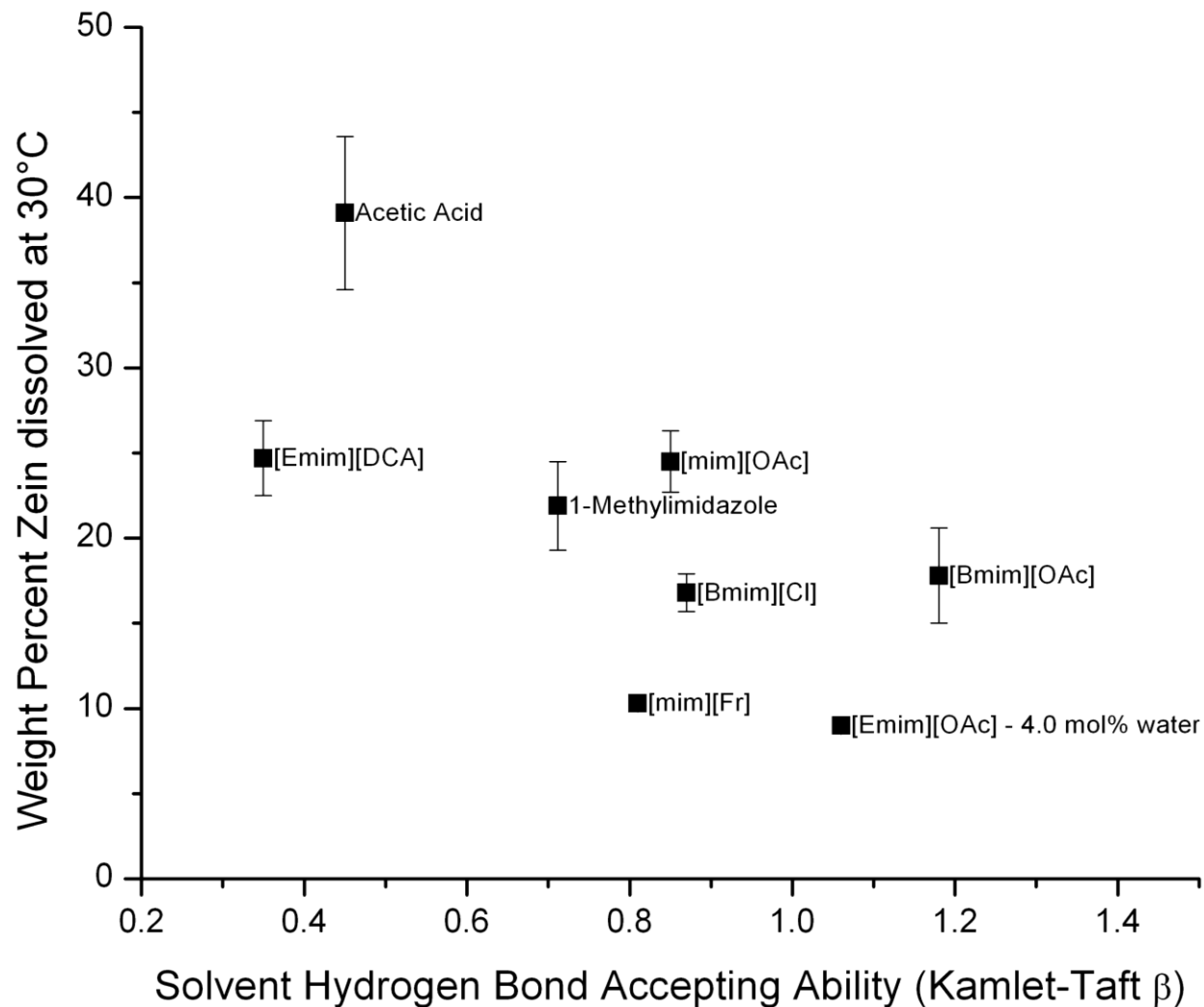
Figure 6.1 Solubility at 30°C versus solvent hydrogen bond accepting ability

Figure 6.1 shows an inverse correlation between β zein's solubility at 30°C. This indicates that strong hydrogen bond accepting ability is not desirable for a zein solvent. Single variable correlation between zein solubility at 30°C and the other Kamlet-Taft parameters shows that correlation (R^2) is largest with β at 0.49, 0.34 for the Kamlet-Taft dipolarity/polarizability (π^*), and only 0.09 for the Kamlet-Taft hydrogen-bond donating ability (α). This indicates that β is the most important solvatochromic parameter in single variable regression and that smaller values are desired to increase zein solubility.

Figure 6.2 shows the relationship between the hydrogen bond accepting ability of the solvent and Mz (Table 4.2), which is related to the enthalpy of dissolution of zein (see Chapter 2).
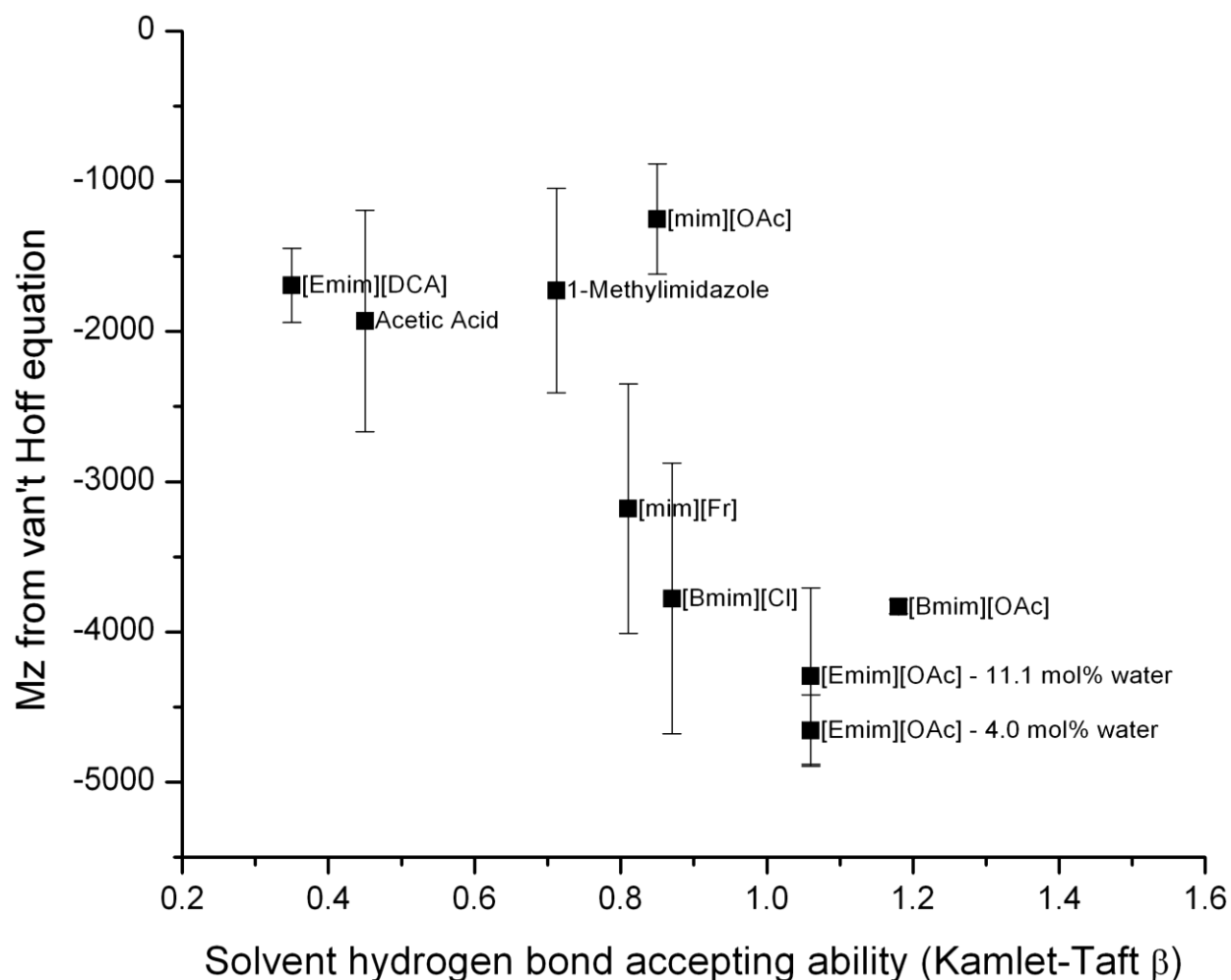
Figure 6.2 Mz versus solvent hydrogen bond accepting ability

Figure 6.2 shows a linear correlation between Mz and β. The value of Mz is related to the enthalpy of dissolution for zein. Relating Mz to β means that the better the hydrogen bond acceptor, the greater the magnitude of the enthalpy of dissolution ($R^2 = 0.517$). That is, the better the hydrogen bond acceptor, the greater the relative energy hurdle to dissolve zein. This means that more energy is required to dissolve zein in [Emim][OAc] than to dissolve zein in [mim][OAc]. It is interesting to note that the ionic liquid with the best solubility of zein, [mim][OAc], does not fit the trend. Removal of the [mim][OAc] point increases the correlation R^2 from 0.517 to 0.724, showing that [mim][OAc]'s Mz is poorly modeled by β, while the other

solvents' Mz are well modeled by β. This indicates that there is some other solvent parameter that increases the Mz of only zein in [mim][OAc], which thus facilitates zein's solubility.

In contrast, it has been found that cellulose solubility improves with stronger hydrogen bond accepting solvents. This difference in zein solubility compared to cellulose solubility in ionic liquids is likely because cellulose is a polymer of many repeating D-glucose molecules, and cellulose forms fibrils in solution.[21] Each fibril is composed of polar D-glucose molecules which give the fibril opportunities for hydrogen bonding with the solvent.[21] By contrast zein is not separated into hydrogen bonding fibrils upon dissolution, and thus it is more difficult to solvate because the zein does not create as many new solvent-solute hydrogen bonds, an exothermic process, to lower the energy of dissolution.[22]

The pure solvent molar volume is also related to the solubility of zein, as shown by Figure 6.3.
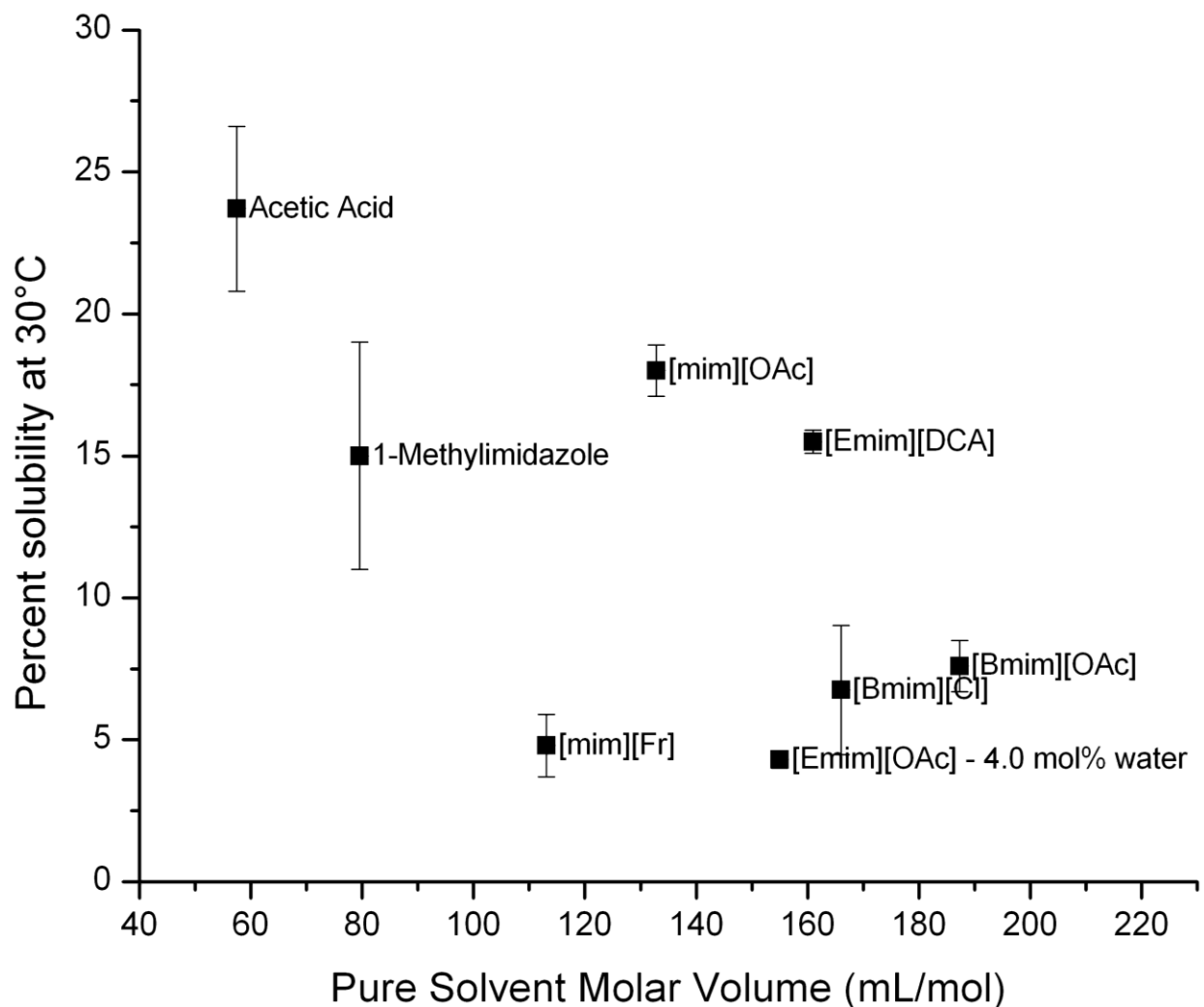
Figure 6.3 Percent solubility at 30°C versus the pure solvent molar volume (mL/mol)

Figure 6.3 shows that solvents with smaller pure solvent molar volumes are superior for dissolving zein. However, the correlation is poor (R^2 of 0.295) even between similar sized molecules compared to the correlation for β discussed above, indicating that it is the chemical nature (such as β), not the structure that is more important for protein solubility. This is similar to results for zein's solubility in aqueous alcohols, where zein was found to be more soluble in the smaller alcohols (methanol and ethanol) than in larger alcohols (propanol and t-butanol).[23]

Linear solvation energy relationship applied to solubility

Applying the LSER regression model discussed in Chapter 2 with α, β, and π* to model the solubility of zein at 30°C and 60°C results in the following Figures 6.4 and 6.5 and Table 6.2,

showing how well LSER models the solubility. The solid black line showing x = y is included

help guide the eye.
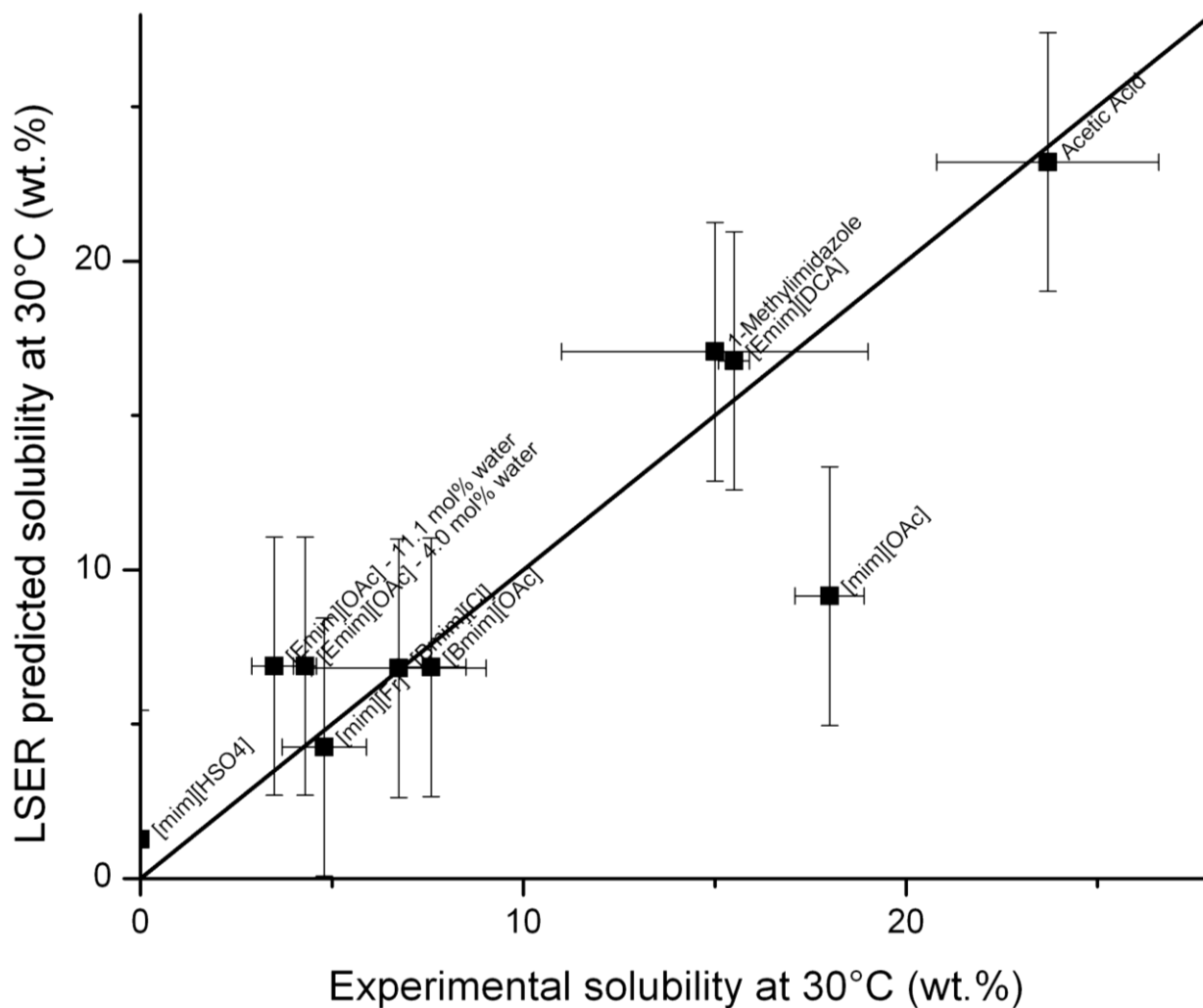
Figure 6.4 Comparison of LSER calculated and experimentally obtained zein solubilities at 30°C
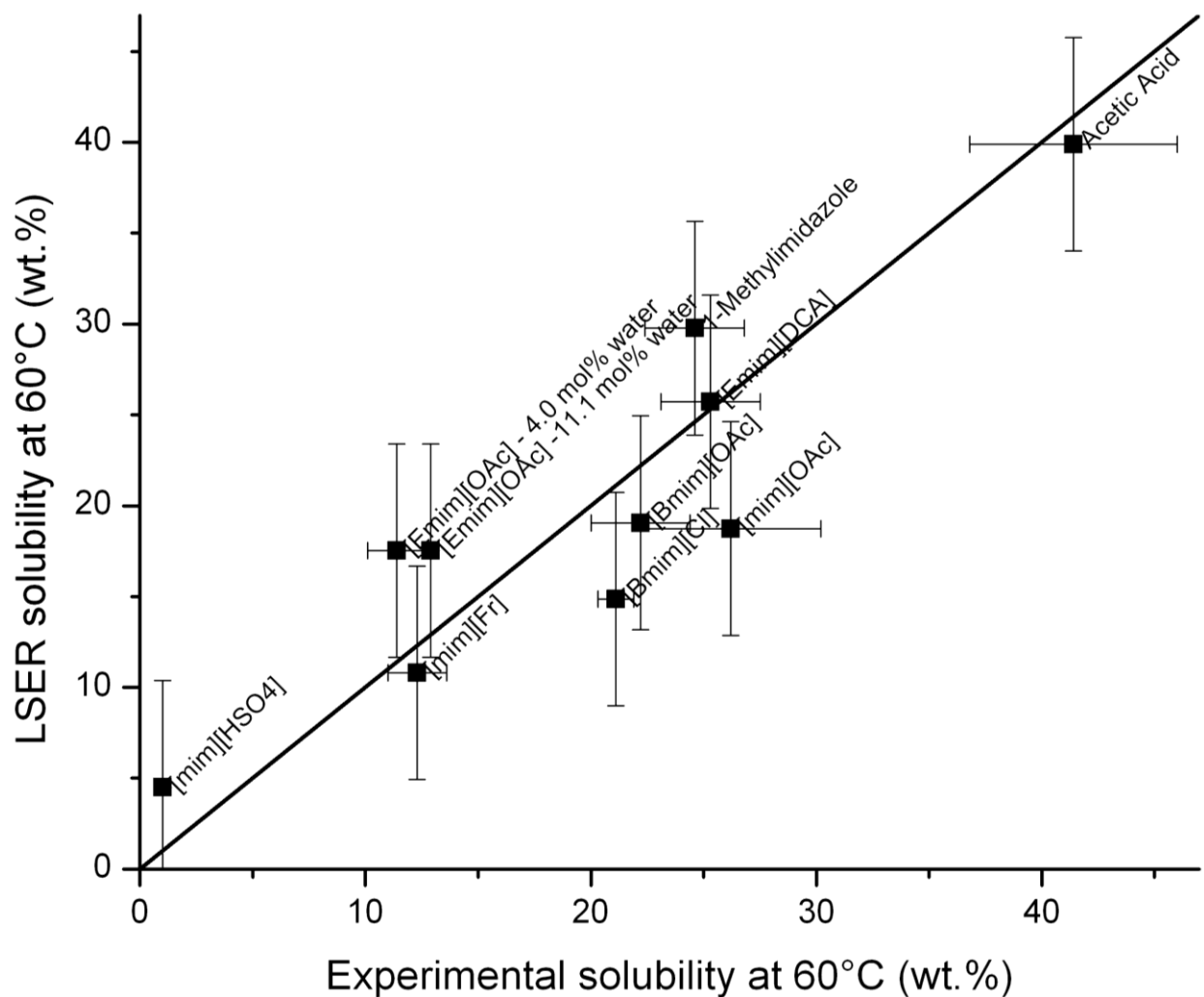
Figure 6.5 Comparison of LSER calculated and experimentally obtained zein solubilities at 60°C

Table 6.2 LSER results for zein solubility at 30°C and 60°C as a function of α, β, and π* -

$$XYZ = XYZ_0 + a\alpha + b\beta + s\pi^*$$

Parameter	Value at 30°C	Value at 60°C
XYZ_0 (intercept)	65.4	103.2
a (coefficient for α)	-10.8	-15.4
b (coefficient for β)	-19.1	-20.5
s (coefficient for π*)	-33.5	-57.5
R²	0.800	0.811
Model standard error from regression	4.2	5.9

In Table 6.2 it is seen that π^* of the solvent is the most important parameter in the multivariate analysis because of the large magnitude of its coefficient, and that π^*'s importance increases at higher temperature. The overall model fit is good with an R^2 of 0.800 at 30°C and 0.811 at 60°C, indicating that 80% of the solubility in this system can be modeled by α, β, and π^* parameters. Comparing the plots of predicted solubility at 30°C and 60°C to the experimental values in Figure 6.4 reflects the good correlation reflected by the R^2 values. The experimental solubility of zein in [mim][OAc] at 30°C (18.0 ± 0.9 wt.%) is nearly twice than the predicted solubility (9.1 wt.%), but at 60°C the difference is only 40% (experimental solubility of 26.2 ± 4.0 wt.% versus predicted solubility of 18.7 wt.%). This shows that [mim][OAc] behavior is poorly modeled at lower temperatures.

Figures 6.4 and 6.5 and Table 6.2 show that an estimation of the solubility of zein is possible using only the solvent α, β, and π^* values. The decrease in the coefficient of both α and β at 60°C compared to π^* shows the decreased importance of hydrogen bonds at higher temperatures. The LSER analysis indicates that an ionic liquid designed for zein dissolution will have low hydrogen bonding accepting ability (β) and have a low dipolarity/polarizability (π^*), but be a weak hydrogen bond donor (α).

Analyzing Mz, related to the enthalpy of dissolution, with multivariate regression as a function of α, β, and π^*, results in Figure 6.6 and Table 6.3.
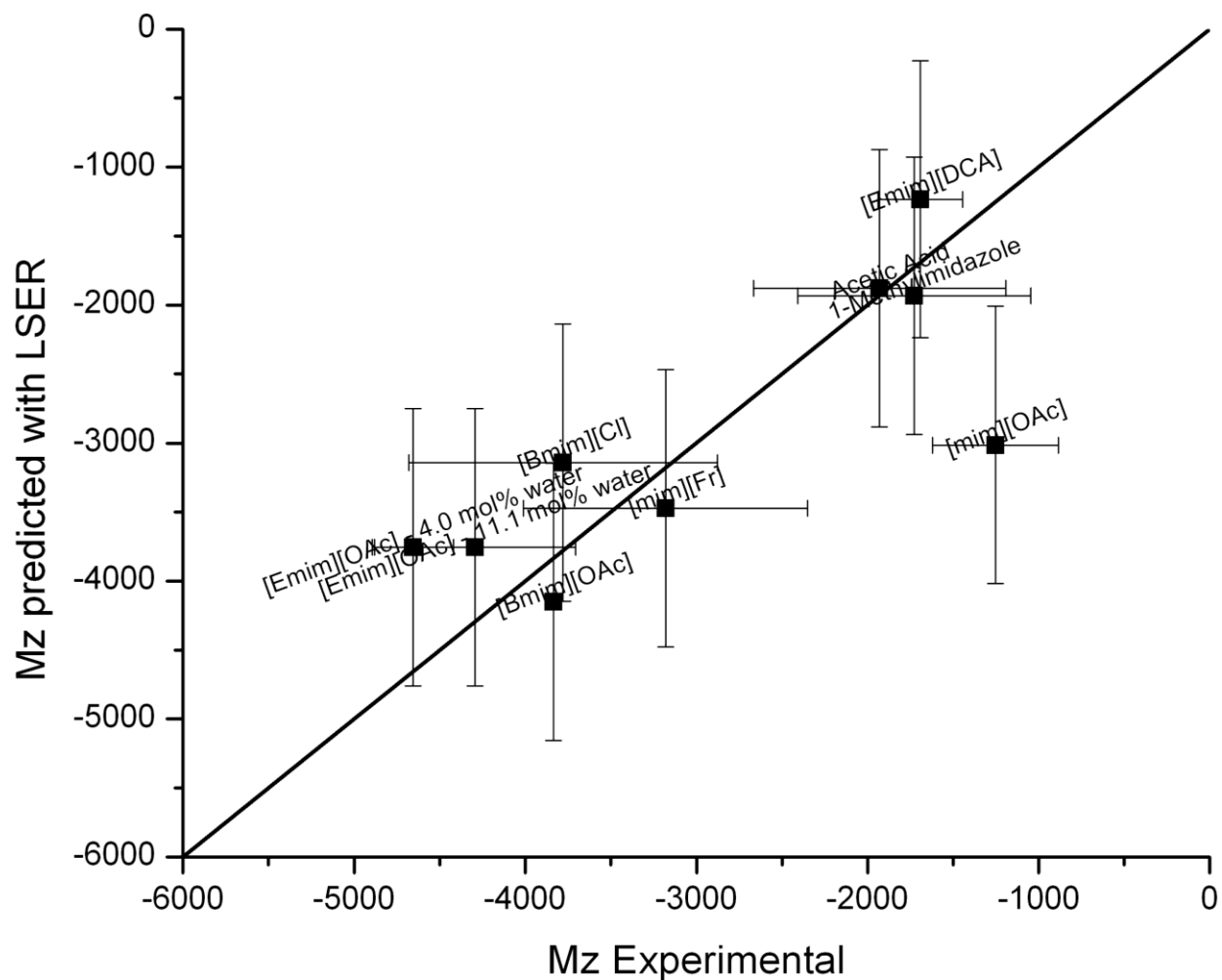
Figure 6.6 Comparison of Mz modeled by LSER versus experimental Mz.

Similar to the behavior seen for Mz as a function of β (Figure 6.2), Figure 6.6 shows that [mim][OAc] does not quite fit on the trend, with a much higher LSER-predicted Mz than the value obtained experimentally. This again shows that [mim][OAc]'s behavior is poorly modeled at low temperatures. If the [mim][OAc] point is removed, the R^2 value increases to 0.833, showing good modeling for the Mz based on the LSER coefficients from Table 6.2.

Table 6.3 LSER results for Mz as a function of α, β, and π* - XYZ = XYZ$_0$ + aα + bβ + sπ*.

Parameter	Value
XYZ$_0$ (intercept)	-2670
a (coefficient for α)	-1630
b (coefficient for β)	3800
s (coefficient for π*)	1580
R²	0.618
Model standard error from regression	1000

Table 6.3 shows that β of the solvent is more important than either α or π* of the solvent because of the higher coefficient. The R² value of 0.618 says that approximately 62% of Mz can be modeled by these parameters.

Structure

The change in zein's secondary structure at 30°C was examined using equation 6.1 as a function of pure solvent molar volume, solvent polarity, hydrogen bond donating or accepting ability, and dipolarity/polarizability.

Pure solvent molar volume (mL/mol)

As discussed in Chapter 5 the secondary structure of zein in aqueous ethanol, acetic acid, 1-methylimidazole, and [mim][OAc] was similar to that of solid zein, whereas zein in the other ionic liquid solvents had a different secondary structure, despite the larger pure solvent molar volume of the structure-changing solvents. Comparing the secondary structure change observed for zein in the solvents versus the pure solvent molar volume in Figure 6.7 and Table 6.4, one can see the effect of pure solvent molar volume on β-turn and α-helix secondary structures.
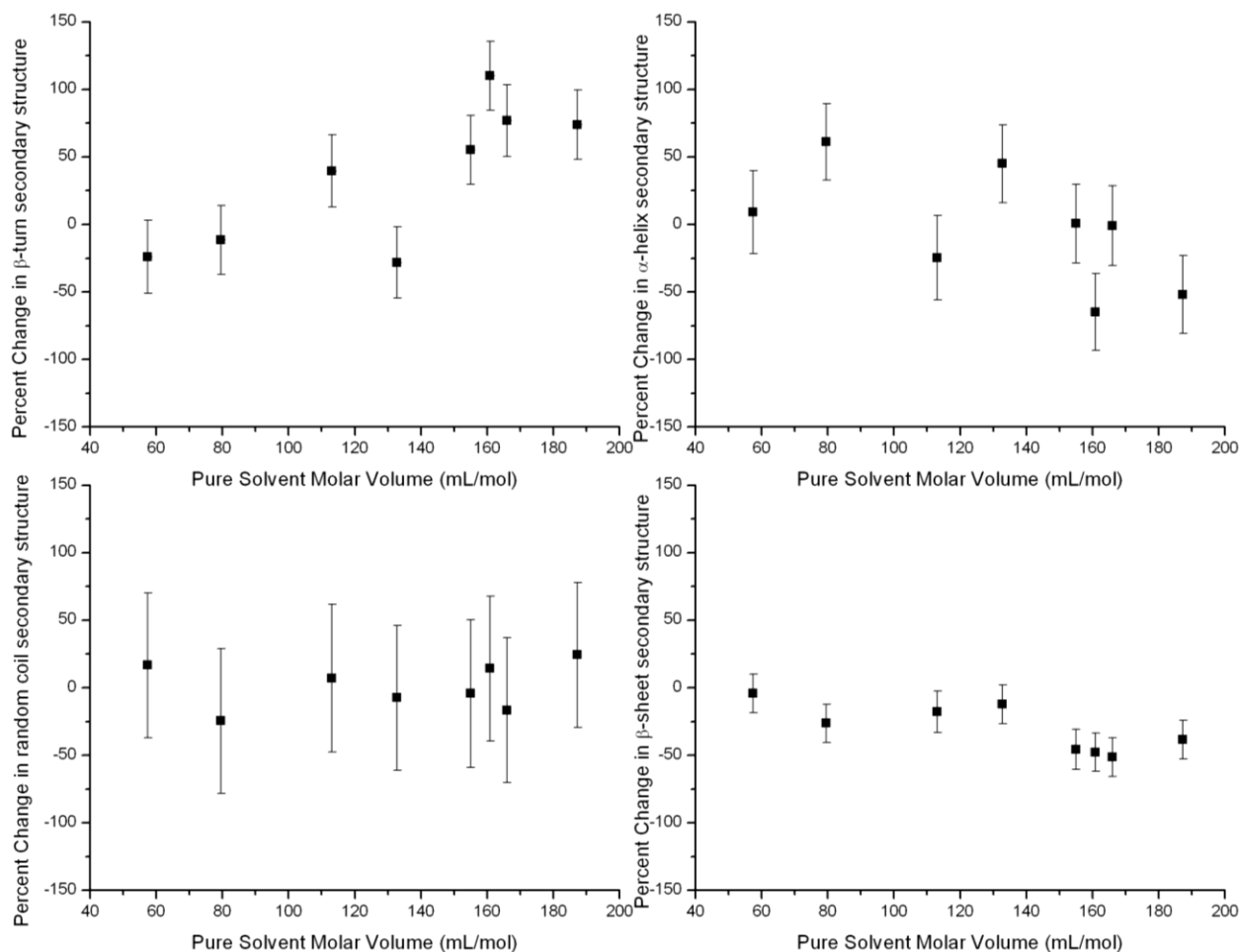
Figure 6.7 Percent change in zein secondary structures versus pure solvent molar volume.

Table 6.4 Pure solvent molar volume versus percent change in secondary structures for dissolved zein compared to solid zein at 30°C.

Solvent	Pure solvent molar volume (mL/mol)	B-turn	A-helix	Random coil	B-sheet
Acetic Acid	57.47 ± 0.02	-24 ± 27	9 ± 31	16 ± 54	-4 ± 14
1-Methylimidazole	79.57 ± 0.03	-12 ± 26	61 ± 28	-25 ± 54	-27 ± 14
[mim][OAc]	132.8 ± 0.01	-28 ± 26	45 ± 30	-8 ± 54	-12 ± 14
[mim][Fr]	113.13 ± 0.03	40 ± 27	-25 ± 31	7 ± 55	-18 ± 15
[Emim][OAc]	154.98 ± 0.03	55 ± 26	0 ± 29	-4 ± 55	-46 ± 15
[Bmim][OAc]	187.27 ± 0.14	74 ± 26	-52 ± 29	24 ± 54	-39 ± 14
[Bmim][Cl]	165.98 ± 0.03	77 ± 27	-1 ± 29	-17 ± 54	-51 ± 14
[Emim][DCA]	160.93 ± 0.04	110 ± 26	-65 ± 28	14 ± 54	-48 ± 14

100

Figure 6.7 shows that there is an influence on β-turn (increase) and α-helix (decrease) secondary structure with increased pure solvent molar volume, in contrast to the results described above where organic solvents were seen to prevent conformational changes.[24] Solvents with larger pure solvent molar volume result in more β-turn and less α-helix secondary structure in zein compared to solid zein's secondary structure. The solvents with larger molar volume are the aprotic ionic liquids, [Emim][DCA], [Emim][OAc], [Bmim][OAc], and [Bmim][Cl]. As seen in Chapter 5, these aprotic ionic liquids result in more β-turn and less α-helix secondary structure.

Previous research has shown that proteins are more denatured in aqueous-organic mixtures than in pure organic solvents (such as acetonitrile or tetrahydrofuran), even though it is known that acetonitrile and tetrahydrofuran denature proteins.[24] This behavior was described as the balancing of two simultaneous effects. The first is the tendency of the protein to denature in the organic solvent. The second is that the conformational mobility of the protein declines in organic solvents compared to aqueous solutions (that the proteins are "kinetically trapped") in the larger organic solvents which prevent the denaturing of the protein.[24] In contrast to the previous research, the zein secondary structure changes seen in Chapter 5 show that in the aprotic ionic liquids (with their larger pure solvent molar volumes) zein undergoes more secondary structure change than in the smaller conventional solvents and [mim][OAc].

Pure solvent polarity using the $E_T(30)$ (kcal/mol) scale

The polarity of solvents is a well-known descriptor for how solvents interact with solutes. Polar solvents better dissolve polar solutes, and nonpolar solvents better dissolve nonpolar solutes. In zein the amino acids proline (8.9 wt.%), tyrosine (4.3 wt.%), and phenylalanine (6.0 wt.%) all contain nonpolar structural elements such as lactam (on proline) or phenyl rings (tyrosine and phenylalanine) that can interact with the aromatic imidazolium ring or the aliphatic butyl or ethyl substitutions.[7, 25-27] Thus a change in the secondary structure might be expected as a function of the polarity of the solvent. In particular, less polar ionic liquid would be expected to increase a specific type of secondary structure that favors nonpolar interactions. To examine that hypothesis, the $E_T(30)$ polarity scale is used.[28-30] The $E_T(30)$ scale is widely used to describe the polarity of solvents (in units of kcal/mol), and the $E_T(30)$ values of the ionic liquids used in this research are presented in Table 6.5.
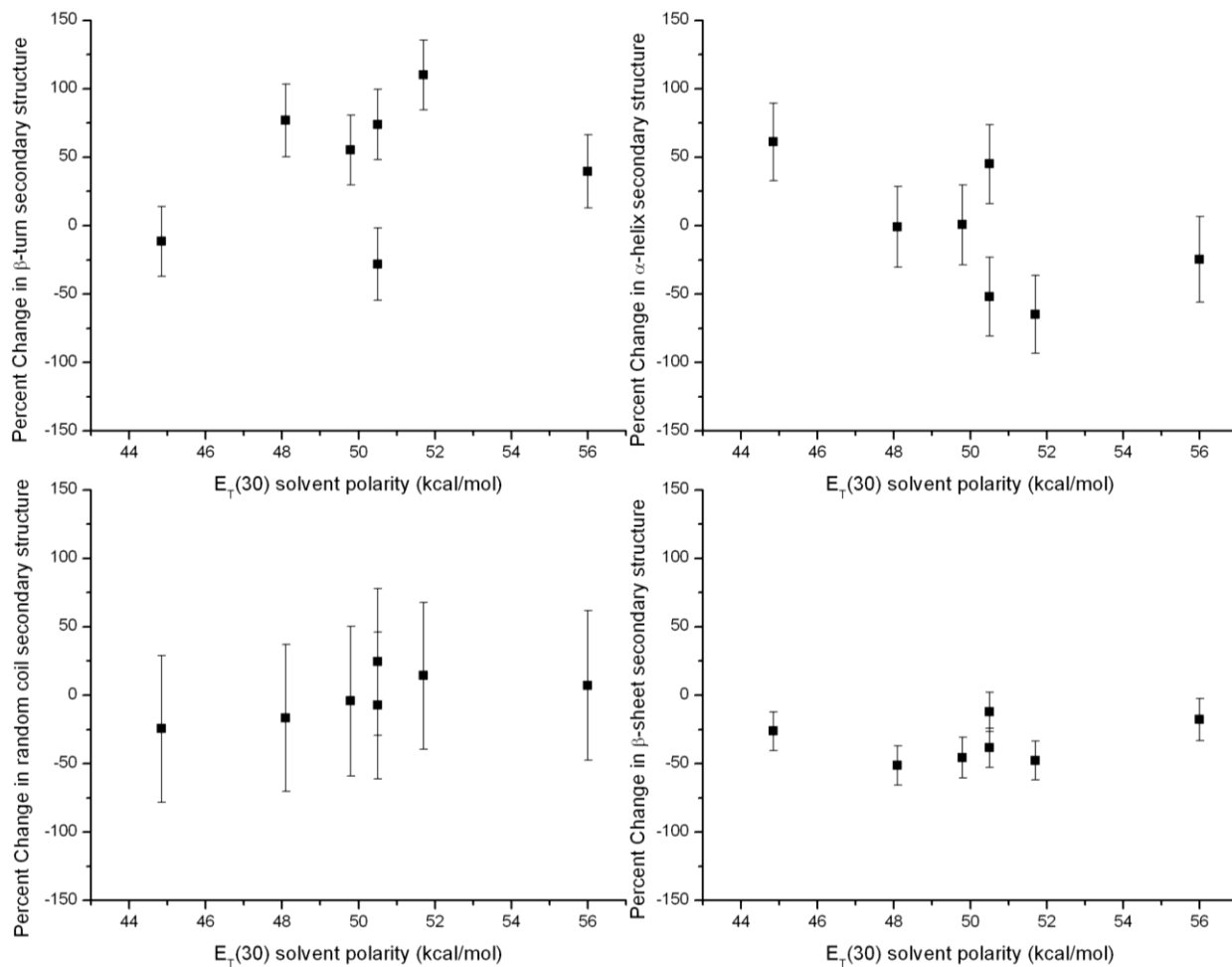
Figure 6.8 Percent change in zein secondary structure as a function of polarity, per the $E_T(30)$ scale.

Table 6.5 Polarity of solvents measured with $E_T(30)$ scale versus percent change in secondary structures for dissolved zein compared to solid zein at 30°C.

Solvent	$E_T(30)$ polarity (kcal/mol)	B-turn	A-helix	Random coil	B-sheet
Acetic Acid	N/A	-24 ± 27	9 ± 31	16 ± 54	-4 ± 14
1-Methylimidazole	44.9[16]	-12 ± 26	61 ± 28	-25 ± 54	-27 ± 14
[mim][OAc]	50.5[17]	-28 ± 26	45 ± 30	-8 ± 54	-12 ± 14
[mim][Fr]	56.0[17]	40 ± 27	-25 ± 31	7 ± 55	-18 ± 15
[Emim][OAc]	49.8[18]	55 ± 26	0 ± 29	-4 ± 55	-46 ± 15
[Bmim][OAc]	50.5[31]	74 ± 26	-52 ± 29	24 ± 54	-39 ± 14
[Bmim][Cl]	48.1[19]	77 ± 27	-1 ± 29	-17 ± 54	-51 ± 14
[Emim][DCA]	51.7[20]	110 ± 26	-65 ± 28	14 ± 54	-48 ± 14

Figure 6.8 shows how changes to each of the secondary structure elements of zein are a function of the solvent polarity. Similar to the importance of pure solvent molar volume on secondary structure, only the β-turn and α-helix portions of the secondary structure seem to be affected by the polarity of the solvent. More polar solvents result in more β-turn and less α-helix, while the amount of random coil and β-sheet secondary structures remain roughly unchanged.

Kamlet-Taft hydrogen bond accepting ability (β)

The effect of the solvent β parameter on secondary structure is similar to the effect of the pure solvent molar volume seen in Figure 6.7, except for [Emim][DCA], which is shown as a circle in each plot.
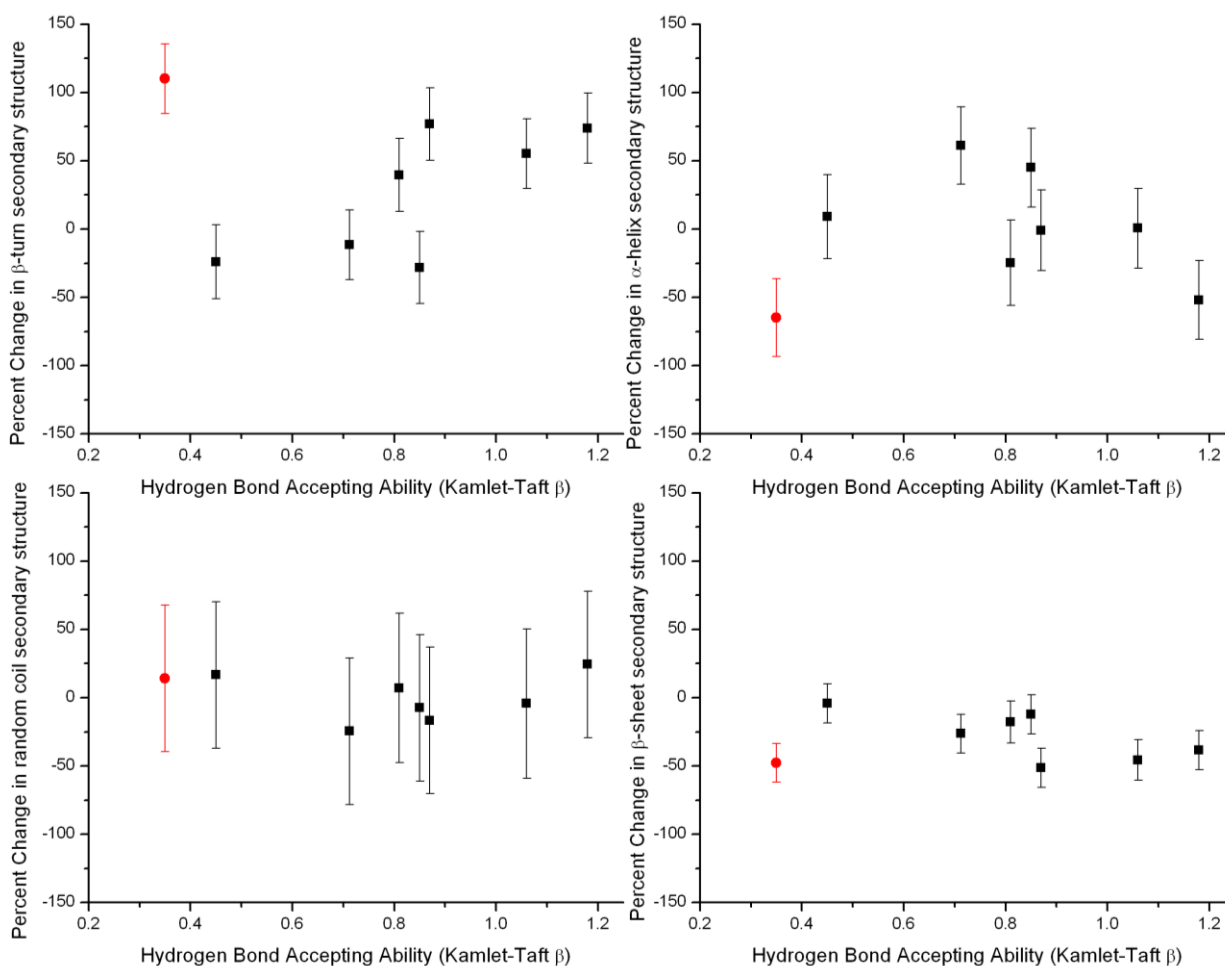
Figure 6.9 Percent change in zein secondary structure versus solvent hydrogen bond accepting ability (Kamlet-Taft β). Circles are [Emim][DCA].

Table 6.6 Solvent hydrogen bond accepting ability (Kamlet-Taft β parameter) versus percent change in secondary structures for dissolved zein compared to solid zein at 30°C.

Solvent	Kamlet-Taft hydrogen bond accepting ability (β)	B-turn	A-helix	Random coil	B-sheet
Acetic Acid	0.45[15]	-24 ± 27	9 ± 31	16 ± 54	-4 ± 14
1-Methylimidazole	0.712[16]	-12 ± 26	61 ± 28	-25 ± 54	-27 ± 14
[mim][OAc]	0.85[17]	-28 ± 26	45 ± 30	-8 ± 54	-12 ± 14
[mim][Fr]	0.81[17]	40 ± 27	-25 ± 31	7 ± 55	-18 ± 15
[Emim][OAc]	1.06[18]	55 ± 26	0 ± 29	-4 ± 55	-46 ± 15
[Bmim][OAc]	1.18[18]	74 ± 26	-52 ± 29	24 ± 54	-39 ± 14
[Bmim][Cl]	0.87[19]	77 ± 27	-1 ± 29	-17 ± 54	-51 ± 14
[Emim][DCA]	0.35[20]	110 ± 26	-65 ± 28	14 ± 54	-48 ± 14

Figure 6.9 shows that most of the solvents show similar trends with increasing β. The aprotic ionic liquid solvents show more β-turn and less α-helix, similar to Figure 6.6 showing the effect of the pure solvent molar volume. However, unlike Figure 6.7 showing the effect of solvent size, [Emim][DCA] stands apart when examined as a hydrogen bond donating solvent in its effects on β-turn and α-helix secondary structures. This may be due to the dicyanamide anion's strong protein destabilizing ability as a chaotropic anion, despite its poor hydrogen bond accepting ability.[32, 33] As discussed in Chapter 5 it has been found that aqueous solutions with the dicyanamide anion strongly destabilizes proteins.[5, 8, 32-35] By contrast the acetate, formate, and chloride are weakly stabilizing (kosmotropic anions).[7] Therefore, the unexpectedly large change in zein secondary structure from [Emim][DCA] despite the anion's weak hydrogen-bond accepting ability is due to its ability, unique among the anions examined here, to form weak solvent-solvent hydrogen bonds but strongly interact with the protein.[32, 35]

Kamlet-Taft hydrogen bond donating ability (α)

It has been found that the hydrogen attached at the C-2 position of the imidazole ring is weakly acidic, so all of the ionic liquids' cations have some hydrogen bond donating character.[36, 37] Thus differences in α for each solvent are dependent on the ionic liquids' anions. Comparing the effect of α on the secondary structure of zein, shown in Table 6.7 and Figure 6.10, one sees less correlation than is seen for secondary structure changes as a function of β.
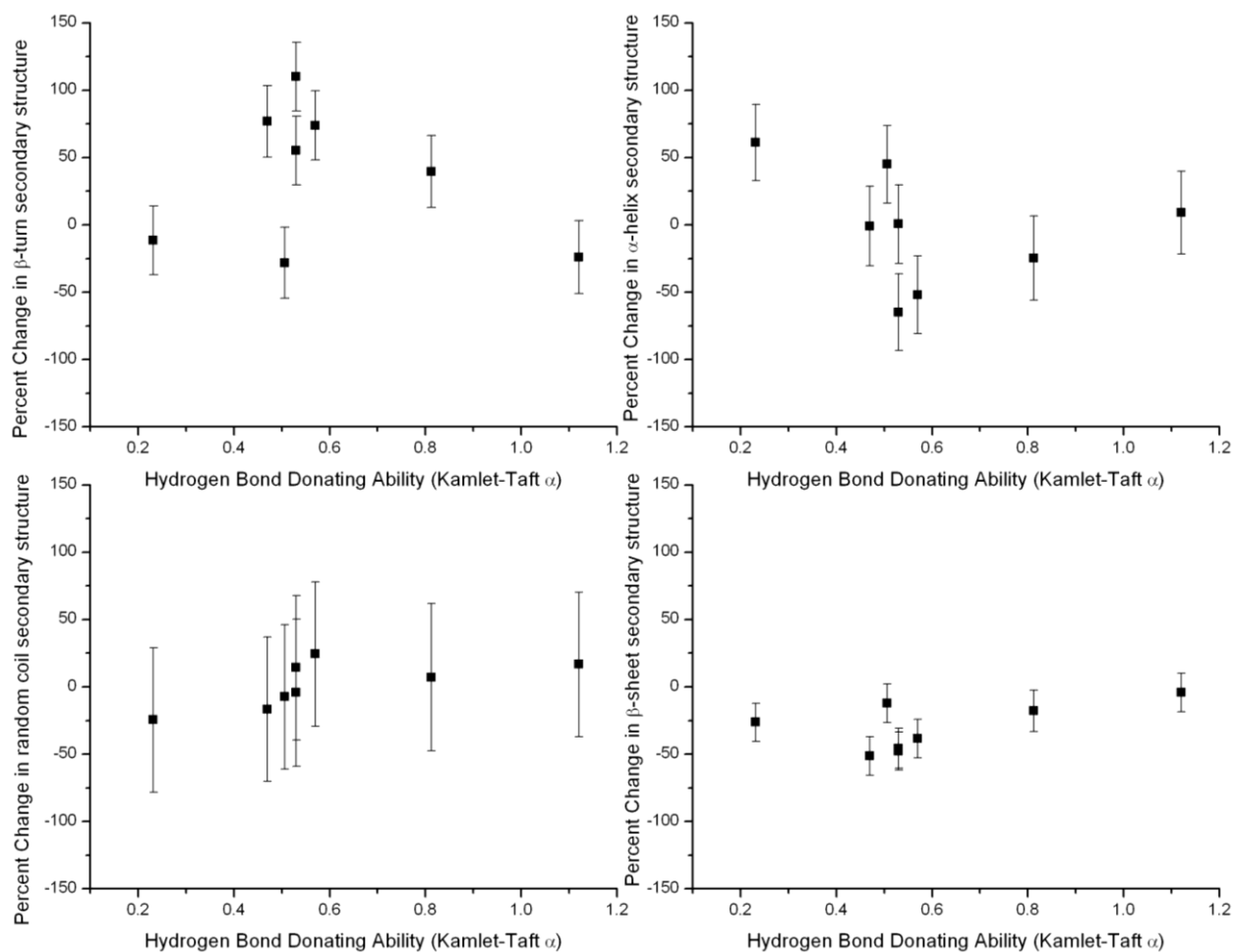
Figure 6.10 Percent change in zein secondary structure versus solvent hydrogen bond donating ability (Kamlet-Taft α).

Table 6.7 Solvent hydrogen bond donating ability (Kamlet-Taft α parameter) versus percent change in secondary structures for dissolved zein compared to solid zein at 30°C.

Solvent	Kamlet-Taft hydrogen bond donating ability (α)	B-turn	A-helix	Random coil	B-sheet
Acetic Acid	1.12[15]	-24 ± 27	9 ± 31	16 ± 54	-4 ± 14
1-Methylimidazole	0.232[16]	-12 ± 26	61 ± 28	-25 ± 54	-27 ± 14
[mim][OAc]	0.506[17]	-28 ± 26	45 ± 30	-8 ± 54	-12 ± 14
[mim][Fr]	0.812[17]	40 ± 27	-25 ± 31	7 ± 55	-18 ± 15
[Emim][OAc]	0.53[18]	55 ± 26	0 ± 29	-4 ± 55	-46 ± 15
[Bmim][OAc]	0.57[18]	74 ± 26	-52 ± 29	24 ± 54	-39 ± 14
[Bmim][Cl]	0.47[19]	77 ± 27	-1 ± 29	-17 ± 54	-51 ± 14
[Emim][DCA]	0.53[20]	110 ± 26	-65 ± 28	14 ± 54	-48 ± 14

The lack of systematic change in secondary structure over the range of hydrogen bond donating abilities shows that α has only a limited effect on the secondary structure of zein. However, Figure 6.10 shows a maximum in β-turn change and a minimum in α-helix change at an α of approximately 0.5. From Table 6.7 it can be seen that the maximum and minimum are clusters of the aprotic ionic liquids, including [Emim][DCA], which stood out in Figure 6.8. This indicates the effects of the aprotic ionic liquids on secondary structure are controlled by some other solvent property.

Kamlet-Taft dipolarity/polarizability (π)*

In addition to the affect hydrogen bonding interactions are known to have on solvent secondary structure, it has been found that dipolarity/polarizability (π*) is important to protein stability and structure in other solvents due to the non-hydrogen bonding portions of amino acids, such as the aromatic rings on tyrosine and phenylalanine.[38-40] These aromatic rings can also interact with the solvent through the "aromatic interactions" with the delocalized π electrons in the aromatic molecules.[26] As aromatic compounds are more polarizable because of their delocalized π electron networks, it reasonable to expect that π* can serve as a measure of a solvent's ability to participate in "aromatic interactions."[15, 26, 41] Table 6.8 and Figure 6.11 shows that β-turn and α-helix secondary structures of zein are related to the solvent's π*.
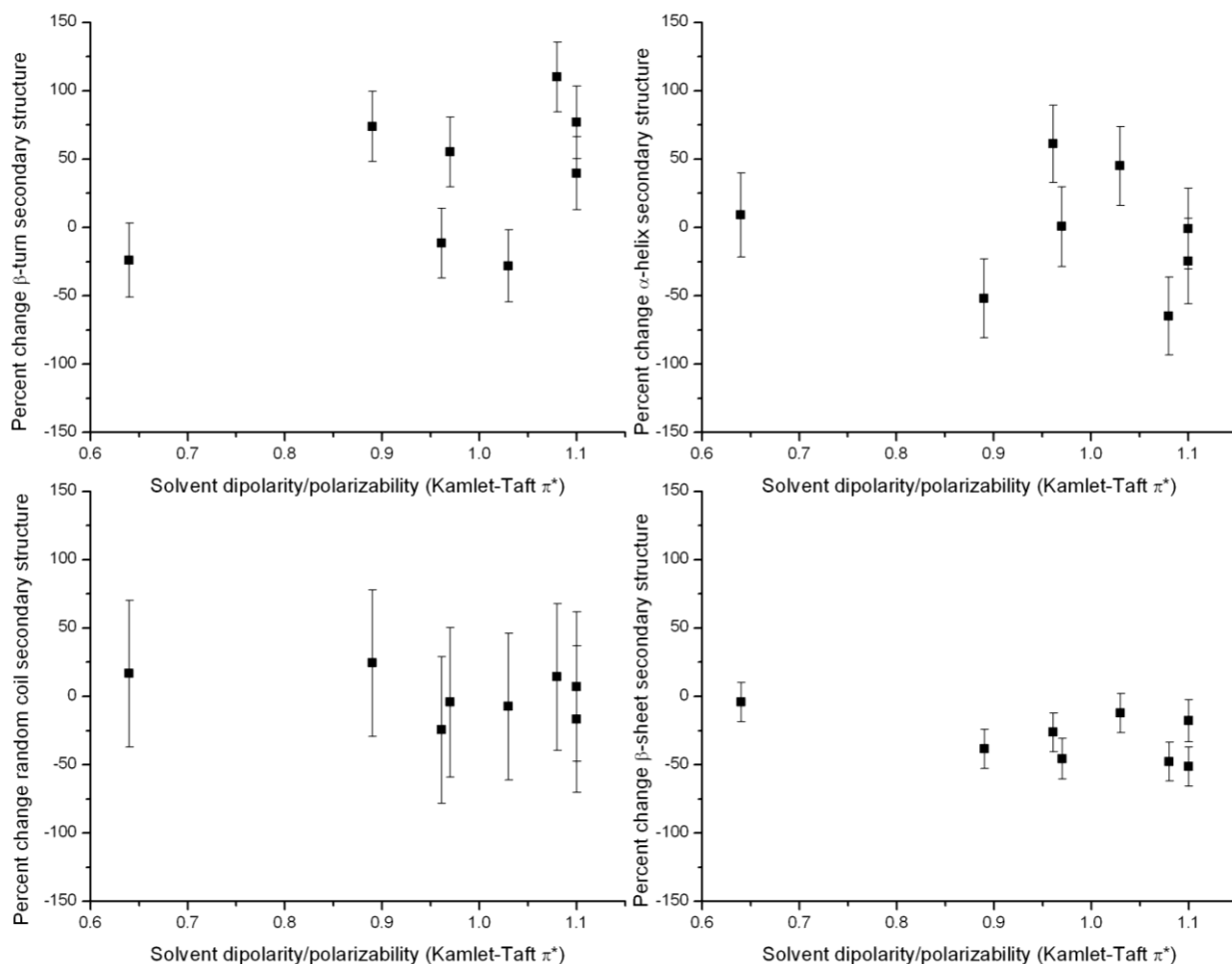
Figure 6.11 Percent change in zein secondary structure versus solvent dipolarity/polarizability (Kamlet-Taft π*).

Table 6.8 Solvent dipolarity/polarizability (Kamlet-Taft π* parameter) versus percent change in secondary structures for dissolved zein compared to solid zein at 30°C.

Solvent	Kamlet-Taft dipolarity/ polarizability (π*)	B-turn	A-helix	Random coil	B-sheet
Acetic Acid	0.64[15]	-24 ± 27	9 ± 31	16 ± 54	-4 ± 14
1-Methylimidazole	0.961[16]	-12 ± 26	61 ± 28	-25 ± 54	-27 ± 14
[mim][OAc]	1.03[17]	-28 ± 26	45 ± 30	-8 ± 54	-12 ± 14
[mim][Fr]	1.1[17]	40 ± 27	-25 ± 31	7 ± 55	-18 ± 15
[Emim][OAc]	0.97[18]	55 ± 26	0 ± 29	-4 ± 55	-46 ± 15
[Bmim][OAc]	0.89[18]	74 ± 26	-52 ± 29	24 ± 54	-39 ± 14
[Bmim][Cl]	1.1[19]	77 ± 27	-1 ± 29	-17 ± 54	-51 ± 14
[Emim][DCA]	1.08[20]	110 ± 26	-65 ± 28	14 ± 54	-48 ± 14

Figure 6.11 shows that, in general, greater π* solvents have more β-turn and less α-helix secondary structure, similar to the impact of hydrogen bond accepting ability shown in Figure 6.8. However, [Emim][DCA] does not stand out from the rest of the solvents because the dicyanamide anion has poor dipolar or polarizable character.

Conclusions

It is intuitive that the properties of solvents are important for controlling protein solubility and secondary structure. This chapter has examined what properties and combination of properties are important in the solubility and thermodynamics of zein dissolution. In particular it has been shown that the hydrogen bond accepting character of the solvent (β) is important, as has been seen in previous cellulose and ionic liquid research, but in the reverse of that previous research. The superior solvents for zein are weaker hydrogen bond acceptors. It was also shown that the magnitude of Mz (related to the enthalpy of dissolution) is related to β. Using multivariate correlation, it was found that the π* of the solvent is more important than single variable regression establishes. The dipolarity/polarizability (π*) becomes more important and hydrogen bond accepting strength becomes less important at higher temperatures. It also showed that hydrogen bond donating strength (α) has only a small effect on zein solubility. It can be concluded from this work that better imidazolium-based solvents for zein will have lower β and π* character but some weak α character.

The analysis of the secondary structure effects of the solvents on zein is more complicated. From Figures 6.7, 6.9, 6.10, and 6.11, it appears that the aprotic ionic liquids promote the formation of β-turn at the expense of α-helix conformations. This may be due to the "hydrophobic interactions" that are commonly discussed in aqueous protein literature. [40, 42-45] The "hydrophobic" interactions are important in ionic liquids-protein interactions because nonpolar groups no longer need to aggregate to limit their interactions with water. Instead these nonpolar portions of the protein can associate with the nonpolar portions of the ionic liquids, or in the case of [Emim][DCA], the dicyanamide which is known to strongly interact with proteins.[5, 8, 34] This may result in the greater amount of β-turn and less α-helix seen in the aprotic ionic liquids because of the greater surface area afforded by the β-turn compared to the α-helix. The larger surface area allows more non-polar interactions between the aromatic and aliphatic portions of the ionic liquid with the similarly aromatic or aliphatic portions of the protein.[40, 42, 45]

The changes in the secondary structure of zein in the aprotic ionic liquids differs from previous research into the denaturing of zein using aqueous urea, which showed that urea decreases β-turn and increases α-helix and random coil secondary structures.[46] Thermal denaturing of zein has been shown to result in more β-sheet at the expense of α-helix, so the denaturing of zein caused by the protic ionic liquids results in unusual new denatured secondary structure.[47, 48] These results indicate a different set of interactions than has previously been reported for the denaturing of process of zein.

It has been shown that to retain the secondary structure of zein, a solvent should be smaller (contrary to previous research which showed that larger solvents better stabilize protein structure) and have intermediate values for α, β, and π*. However, it was seen that the strong protein destabilizer dicyanamide affects zein structure more than its hydrogen bond accepting ability would indicate. It is also likely that the ability of the larger aprotic ionic liquids to interact with the nonpolar parts of zein that are most exposed in the β-turn conformation explain why zein shows more β-turn secondary structure in the aprotic ionic liquids than in the less conformation-change-hindering smaller solvents.

References

1. Suzuki, Y.; Konda, E.; Hondoh, H.; Tamura, K. Effects of temperature, pressure, and pH on the solubility of triclinic lysozyme crystals, *J. Cryst. Growth* **2011**, *1,* 1085-1088.

2. Byrne, N.; Angell, C. A. The Solubility of Hen Lysozyme in Ethylammonium Nitrate/H2O Mixtures and a Novel Approach to Protein Crystallization, *Molecules* **2010**, *2,* 793-803.

3. Aldabaibeh, N.; Jones, M. J.; Myerson, A. S.; Ulrich, J. The solubility of orthorhombic lysozyme crystals obtained at high pH, *Crystal Growth and Design* **2009**, *7,* 3313-3317.

4. Sazaki, G.; Nagatoshi, Y.; Suzuki, Y.; Durbin, S. D.; Miyashita, S.; Nakada, T.; Komatsu, H. Solubility of tetragonal and orthorhombic lysozyme crystals under high pressure, *J. Cryst. Growth* **1999**, *2,* 204-209.

5. Constantinescu, D.; Weingärtner, H.; Herrmann, C. Protein denaturation by ionic liquids and the Hofmeister series: a case study of aqueous solutions of ribonuclease A, *Angew. Chem. , Int. Ed.* **2007**, *46,* 8887-8889.

6. Lau, R. M.; Sorgedrager, M. J.; Carrea, G.; van Rantwijk, F.; Secundo, F.; Sheldon, R. A. Dissolution of Candida antarctica lipase B in ionic liquids: effects on structure and activity, *Green Chem.* **2004**, *9,* 483-487.

7. Weingärtner, H.; Cabrele, C.; Herrmann, C. How ionic liquids can help to stabilize native proteins, *Phys. Chem. Chem. Phys.* **2012**, *2,* 415-426.

8. Constantinescu, D.; Herrmann, C.; Weingärtner, H. In *In Protein Denaturation by Ionic Liquids and the Hofmeister Series;* ACS symposium series; ACS Publications: 2009; Vol. 1030, pp 107-117.

9. Constantinescu, D.; Herrmann, C.; Weingärtner, H. Patterns of protein unfolding and protein aggregation in ionic liquids, *Phys. Chem. Chem. Phys.* **2010**, *8,* 1756-1763.

10. Biswas, A.; Shogren, R. L.; Stevenson, D. G.; Willett, J. L.; Bhowmik, P. K. Ionic liquids as solvents for biopolymers: Acylation of starch and zein protein, *Carbohydr. Polym.* **2006**, *4,* 546-550.

11. Choi, H. M.; Kwon, I. Dissolution of Zein Using Protic Ionic Liquids: N-(2-Hydroxyethyl) Ammonium Formate and N-(2-Hydroxyethyl) Ammonium Acetate, *Ind Eng Chem Res* **2011**, 2452-2454.

12. Kilpeläinen, I.; Xie, H.; King, A.; Granstrom, M.; Heikkinen, S.; Argyropoulos, D. S. Dissolution of wood in ionic liquids, *J. Agric. Food Chem.* **2007**, *22,* 9142-9148.

13. Sun, N.; Rahman, M.; Qin, Y.; Maxim, M. L.; Rodríguez, H.; Rogers, R. D. Complete dissolution and partial delignification of wood in the ionic liquid 1-ethyl-3-methylimidazolium acetate, *Green Chem.* **2009**, *5,* 646-655.

14. Kamlet, M. J.; Abboud, J. L. M.; Abraham, M. H.; Taft, R. Linear solvation energy relationships. 23. A comprehensive collection of the solvatochromic parameters,. pi.*,. alpha., and. beta., and some methods for simplifying the generalized solvatochromic equation, *J. Org. Chem.* **1983**, *17,* 2877-2887.

15. AnonymousKamlet-Taft solvent parameters. *http://www.stenutz.eu/chem/solv26.php* (accessed January 30, 2013).

16. Schleicher, J. C.; Scurto, A. M. Kinetics and solvent effects in the synthesis of ionic liquids: imidazolium, *Green Chem.* **2009**, *5,* 694-703.

17. Shukla, S. K.; Khupse, N. D.; Kumar, A. Do anions influence the polarity of protic ionic liquids? *Phys.Chem.Chem.Phys.* **2011**, 2761.

18. Doherty, T. V.; Mora-Pale, M.; Foley, S. E.; Linhardt, R. J.; Dordick, J. S. Ionic liquid solvent properties as predictors of lignocellulose pretreatment efficacy, *Green Chem.* **2010**, *11,* 1967-1975.

19. Gericke, M.; Liebert, T.; Seoud, O. A. E.; Heinze, T. Tailored Media for Homogeneous Cellulose Chemistry: Ionic Liquid/Co-Solvent Mixtures, *Macromolecular Materials and Engineering* **2011**, *6,* 483-493.

20. Zhang, S.; Qi, X.; Ma, X.; Lu, L.; Deng, Y. Hydroxyl Ionic Liquids: The Differentiating Effect of Hydroxyl on Polarity due to Ionic Hydrogen Bonds between Hydroxyl and Anions, *J. Phys. Chem. B* **2010**, *11,* 3912-3920.

21. Zhu, S.; Wu, Y.; Chen, Q.; Yu, Z.; Wang, C.; Jin, S.; Ding, Y.; Wu, G. Dissolution of cellulose with ionic liquids and its application: a mini-review, *Green Chem.* **2006**, *4,* 325-327.

22. Li, Y.; Xia, Q.; Shi, K.; Huang, Q. Scaling Behaviors of α-Zein in Acetic Acid Solutions, *J. Phys. Chem. B* **2011**, 9695-9702.

23. Mossé, J. Monographie sur une protéine du mais: La zéine, *Ann. Physiol. Veg* **1961**, 105-139.

24. Griebenow, K.; Klibanov, A. M. On protein denaturation in aqueous-organic mixtures but not in pure organic solvents, *J. Am. Chem. Soc.* **1996**, *47,* 11695-11700.

25. Paulis, J. W. Disulfide structures of zein proteins from corn endosperm, *Cereal Chem.* **1981**, 542-546.

26. Burley, S.; Petsko, G. Aromatic-aromatic interaction: a mechanism of protein structure stabilization, *Science* **1985**, *4708,* 23-28.

27. Fujita, K.; MacFarlane, D. R.; Forsyth, M. Protein solubilising and stabilising ionic liquids, *Chem. Comm.* **2005**, *38,* 4804-4806.

28. Reichardt, C. Solvatochromism, thermochromism, piezochromism, halochromism, and chiro-solvatochromism of pyridinium N-phenoxide betaine dyes, *Chem. Soc. Rev.* **1992**, *3,* 147-153.

29. Reichardt, C. Polarity of ionic liquids determined empirically by means of solvatochromic pyridinium N-phenolate betaine dyes, *Green Chem.* **2005**, *5,* 339-351.

30. Matyushov, D. V.; Schmid, R.; Ladanyi, B. M. A Thermodynamic Analysis of the π* and ET (30) Polarity Scales, *J. Phys. Chem. B* **1997**, *6,* 1035-1050.

31. Wu, Y.; Sasaki, T.; Kazushi, K.; Seo, T.; Sakurai, K. Interactions between spiropyrans and room-temperature ionic liquids: Photochromism and solvatochromism, *J. Phys. Chem. B* **2008**, *25,* 7530-7536.

32. Zhang, Y.; Cremer, P. S. Interactions between macromolecules and ions: the Hofmeister series, *Curr. Opin. Chem. Biol.* **2006**, *6,* 658-663.

33. Cacace, M.; Landau, E.; Ramsden, J. The Hofmeister series: salt and solvent effects on interfacial phenomena, *Q. Rev. Biophys.* **1997**, *03,* 241-277.

34. Zhao, H.; Campbell, S. M.; Jackson, L.; Song, Z.; Olubajo, O. Hofmeister series of ionic liquids: kosmotropic effect of ionic liquids on the enzymatic hydrolysis of enantiomeric phenylalanine methyl ester, *Tetrahedron: Asymmetry* **2006**, *3,* 377-383.

35. Yang, Z. Hofmeister effects: an explanation for the impact of ionic liquids on biocatalysis, *J. Biotechnol.* **2009**, *1,* 12-22.

36. Takamuku, T.; Kyoshoin, Y.; Shimomura, T.; Kittaka, S.; Yamaguchi, T. Effect of Water on Structure of Hydrophilic Imidazolium-Based Ionic Liquid, *The Journal of Physical Chemistry B* **2009**, *31,* 10817-10824.

37. Wu, B.; Liu, Y.; Zhang, Y.; Wang, H. Probing Interomolecular Interactions in Ionic Liquid-Water Mixtures by Near-Infrared Spectroscopy, *Chemistry - A European Journal* **2009**, 6889.

38. Ross, P. D.; Subramanian, S. Thermodynamics of protein association reactions: forces contributing to stability, *Biochemistry (N. Y.)* **1981**, *11,* 3096-3102.

39. Bowie, J. U. Membrane protein folding: how important are hydrogen bonds? *Curr. Opin. Struct. Biol.* **2011**, *1,* 42-49.

40. Pace, C. N.; Fu, H.; Fryar, K. L.; Landua, J.; Trevino, S. R.; Shirley, B. A.; Hendricks, M. M. N.; Iimura, S.; Gajiwala, K.; Scholtz, J. M. Contribution of hydrophobic interactions to protein stability, *J. Mol. Biol.* **2011**, *3,* 514-528.

41. Reichardt, C. Solvatochromic dyes as solvent polarity indicators, *Chem. Rev.* **1994**, *8,* 2319-2358.

42. Zou, Q.; Habermann-Rottinghaus, S. M.; Murphy, K. P. Urea effects on protein stability: hydrogen bonding and the hydrophobic effect, *Proteins* **1998**, *2,* 107-115.

43. Horton, H. R.; Moran, L. A.; Ochs, R. S.; Rawn, J. D.; Scrimgeour, K. G. *Principles of Biochemistry;* Prentice Hall: Upper Saddle River, NJ, 1996; , pp 862.

44. Jones, S.; Thornton, J. M. Principles of protein-protein interactions, *Pro. Nat. Acad. Sci.* **1996**, *1,* 13-20.

45. Pace, C. N.; Treviño, S.; Prabhakaran, E.; Scholtz, J. M. Protein structure, stability and solubility in water and other solvents, *Phil. Trans. R. Soc. Lond. B* **2004**, *1448,* 1225-1235.

46. Pickering, K. L.; Verbeek, C. J. R.; Viljoen, C. The Effect of Aqueous Urea on the Processing, Structure and Properties of CGM, *J. Polym. Environ.* **2012**, 1-9.

47. Duodu, K. G.; Tang, H.; Grant, A.; Wellner, N.; Belton, P. S.; Taylor, J. R. N. FTIR and Solid State 13C NMR Spectroscopy of Proteins of Wet Cooked and Popped Sorghum and Maize, *J. Cereal Sci.* **2001**, *3,* 261-269.

48. Duodu, K. G.; Taylor, J. R. N.; Belton, P. S.; Hamaker, B. R. Factors affecting sorghum protein digestibility, *J. Cereal Sci.* **2003**, *2,* 117-131.

Chapter 7 - Conclusions and recommendations

Conclusions

Zein solubility

The solubility and secondary structure of zein in seven imidazolium-based ionic liquids and the conventional solvents acetic acid and 1-methylimidazole have been reported as a function of temperature. This is the first work to systematically report the solubility of zein (a hydrophobic protein) in ionic liquids. Zein is most soluble in acetic acid, the ionic liquids [mim][OAc] and [Emim][DCA], and 1-methylimidazole. Both cation and anion were found to be important in zein solubility. Larger cations can interact more effectively through non-polar interactions with the non-polar portions of the protein, shown in the comparison of [Emim] versus [Bmim] cations. Anions were also found to be important, particularly for protic ionic liquids, because of the anion contribution to the ionic liquid's polarity. Highly polar ionic liquids were found to be poor solvents for zein, as expected, because zein is insoluble in highly polar water. Pure solvent molar volume was also found to play a role, because smaller solvents had generally superior zein solubility.

Gelation, a common problem for zein dissolved in aqueous alcohols, was found only for zein dissolved in [mim][Fr] and [mim][OAc], and then only after weeks had elapsed. Gelation never occurred for zein dissolved in the aprotic ionic liquids, indicating that the aprotic ionic liquids are superior long-term solvents for zein.

The water concentration in the ionic liquid solvents was not found to be an important component in controlling zein solubility. This lack of sensitivity to water concentration is likely due to the water deactivating effect of ionic liquids described in previous literature. This is important because all ionic liquids adsorb some water (even hydrophobic ionic liquids are hygroscopic). The ability to use ionic liquids with a wide range of water concentration without a loss of zein solubility or an effect on zein secondary structure is an important attribute for commercial applications as drying ionic liquids is an time and cost intensive process.

Zein structure

The secondary structure as a function of temperature of the protein zein as a solid film and dissolved in seven imidazolium-based ionic liquids and the conventional solvents acetic

114

acid, 1-methylimidazole, and 70 vol% aqueous ethanol have been reported. Infrared spectroscopy and curve-fitting were used to quantify the secondary structure. Aprotic ionic liquids affect the secondary structure of zein more than the conventional solvents or [mim][OAc]. As protein properties such as tensile strength and gas permeability are related to secondary structure, this research has implications for the commercial application of ionic liquids as zein solvents because of the need to balance solubility with changes to secondary structure. Temperature was found to have only a small effect on the secondary structure of the protein due to the apparent thermal stabilization by the ionic liquids. Most secondary structures were changed during zein dissolution at room temperature. Water concentration was not found to affect the secondary structure of zein dissolved in [Emim][DCA], even up to 25 mol%. Similar to the results for the effect of water on the solubility of zein, this is beneficial as it means secondary structure is insensitive to water content, at least below 25 mol%.

While aprotic ionic liquids strongly affect protein secondary structure, primarily by increasing the fraction of β-turn, the two protic ionic liquids affect secondary structure differently. It was found that zein in [mim][OAc] has a broadly similar secondary structure of zein in 70 vol% aqueous ethanol or acetic acid, but zein in [mim][Fr] has a secondary structure much more similar to zein in the aprotic ionic liquids.

Infrared spectroscopy has been a valuable tool for protein analysis, and this research has shown that quantitative IR spectroscopy is just as useful for ionic liquid solutions. The lack of ionic liquid absorbance in the Amide I region means solvent subtraction (a key issue in aqueous protein IR spectroscopy) is less critical. The promising *in situ* techniques used here can be applied for other materials in ionic liquids as well, such as examining inorganic zeolite synthesis for information regarding precursor formation and the effects of water on product formation.

Solvent properties

One of the principal goals for this project was to identify what solvent properties are important for dissolving zein. It was found that the pure solvent molar volume and hydrogen bond accepting ability (Kamlet-Taft β parameter) are important parameters for the solubility of zein. Smaller solvents dissolve more zein. Solvents with lower β also dissolve more zein, in contrast to previous research which showed that higher β solvents are better for dissolving cellulose. It was also shown that the dipolarity/polarizability (π*) of the solvent becomes

important at higher temperatures. Thus better solvents for zein will be smaller and have lower β and π^* but some weak α character. The modeling of zein solubility was performed and it was found that an adequate model (with $R^2 => 0.75$) could be prepared using the α, β, and π^* solvent parameters.

The solvent's size, hydrogen bond accepting and donating abilities (Kamlet-Taft β and α), and the solvent's dipolarity/polarizability (Kamlet-Taft π^*) were all found to affect the secondary structure of zein. Smaller and lower β and α solvents all had less effect on the secondary structure of zein, which makes those properties useful when designing a solvent as changes in the secondary structure affect protein properties.

This direct comparison of protic and aprotic ionic liquids (with [mim][OAc], [Emim][OAc], and [Bmim][OAc]) is also unusual, and it highlights the advantages and disadvantages of both types of ionic liquids. The protic [mim][OAc]'s lower viscosity promoted the solubility of zein at low temperatures, and the smaller cation has less effect on zein's secondary structure, which can be beneficial in some applications. By contrast, the larger [Bmim][OAc] had a large increase in solubility at higher temperature and the denaturing effect could also be helpful depending on the application.

Examination of the anion effect on protein solubility and structure was also insightful, as the polarity of the protic ionic liquids was controlled by the anion (as the cations were the same). The more polar the ionic liquid, the worse the solubility and the greater the secondary structure change.

Recommendations

Further research into using ionic liquids with hydrophobic proteins is recommended. The proteins primarily studied are hydrophilic and have poor solubility in ionic liquids, requiring ionic liquid and protein interactions to be studied in aqueous solution. The research examined in this work will promote the study of proteins in ionic liquids because it has been identified that hydrophobic proteins are soluble in primarily ionic liquid solvents.

While it was found that a change in concentration from 4.0 mol% to 11.1 mol% had no effect on solubility, and from 2.1 mol% to 25.0 mol% had no effect on secondary structure, the impact of water should be further investigated. Water caused the precipitation of zein from ionic liquid solutions, forming an opaque film, but the concentration required is unknown.

Infrared spectroscopy again proved its worth as a tool to examine protein secondary structure *in situ* and as a function of temperature. Further research should continue to use IR spectroscopy as a tool for the characterization of proteins, particularly as ionic liquid solutions are capable of avoiding the solvent-subtraction issues that plague aqueous protein analysis.

This research used well-characterized imidazolium-based ionic liquids, but it is recommended that research into using more environmentally benign ionic liquids be conducted. For example, it is possible to prepare ionic liquids using choline, guanidine, or amino acids, which can have less harmful environmental impacts than imidazole. The thermal stability of proteins has been increased by dissolving them in ionic liquids. However, hydrophilic protein solubility has been poor in previous research. As proteins are composed of amino acids, it may be possible to improve the solubility of proteins by using an ionic liquid composed of amino acids present in that protein, and yet maintain the improved thermal stability.

More broadly this work into using ionic liquids for hydrophobic protein solubility continues the expansion of knowledge as to where these versatile solvents can be applied. For example, a hydrophobic protein dissolved in a benign ionic liquid could be applied to a wound and then the ionic liquid could be washed off with water, precipitating a film of protein to protect the wound.

A worthy goal is to create a bio-refinery that uses biological materials to make chemical products. Using ionic liquids is a promising step because of their proven ability to dissolve a wide variety of biological products (such as wood). This research into the solubility and secondary structure effects of hydrophobic proteins in ionic liquids opens up other cereal products for use. For example, zein is closely related to gliadin in wheat and kafirin in sorghum, but those have not yet been studied for their applications with ionic liquids.

Appendix A - Infrared Spectroscopic Examination of CIT-6, and a Family of *BEA Zeolites

Sean R. Tomlinson, Tyler McGown, John R. Schlup, and Jennifer L. Anthony

Abstract

Infrared spectroscopy is a useful complimentary tool for identifying local structure changes in zeolites that occur from chemical treatment, which are difficult to see using X-ray diffraction alone. Structural changes in zeolite CIT-6 and its zeolite beta (*BEA) analogs upon chemical treatment have been identified with mid- and far-infrared spectroscopy. Changes resulting from calcination, altering the framework composition, and ion-exchange are examined and discussed. Differences in the local structure of the sample were observed in the mid- and far-infrared spectra, including changes in the intratetrahedral asymmetric stretch, the double ring mode, and the intratetrahedral bending mode regions. The far-infrared spectra indicated that calcination or acetic acid extraction changed the structure of the CIT-6 to the structure of zeolite beta (*BEA) while ion exchange with Zn or substitution of aluminum into the framework structure of acetic acid extracted samples retained the CIT-6 structure.

Introduction

Microporous molecular sieves are of great scientific and commercial interest.[1-3] Zeolites are a category of microporous molecular sieves and are often used in catalysis, ion exchange, and adsorption/separation processes.[4] The term zeolite refers specifically to aluminosilicate microporous molecular sieves. However, the term is often applied to all compounds having similar crystalline structures. Zeolites are of interest because of their small uniform pores (less than 2 nm), their channel configuration, and their void space organization.

Because of the many potential applications of zeolites, the characterization of their chemical composition, their structure, and the bonding of zeolites is important, and various analytical techniques have been employed to obtain such data. The chemical composition of zeolites can be obtained with atomic absorption spectroscopy (AAS), atomic emission spectrometry (ICP-AES) and X-ray fluorescence spectrometry (XRF).[5] Both ^{29}Si and ^{27}Al NMR have proven to be valuable tools in understanding the local environments around the atoms in the lattice. When NMR data are coupled with density functional theory (DFT) calculations, these data have resulted in valuable insight into the crystalline structure of zeolites.[6] From XRD data it is possible to determine the crystalline structure of zeolitic materials using Rietveld refinement. These XRD data permit identification of samples by comparison with XRD results of known samples.[7-9]

Vibrational spectroscopy, including both Raman and infrared (IR), is often employed to investigate short-range order in zeolites. The structures of zeolites, examination of zeolite functional groups, and examinations of zeolite chemistry with probe molecules have been examined with Fourier transform infrared spectroscopy (FTIR).[10-18] In the 1970s Flanigen et al. proposed functional group assignments for the absorption bands between 1250 and 300 cm^{-1}.[17, 18] The assignments divide the spectra into regions which are classified with respect to intra- or intertetrahedral vibrations. Intratetrahedral vibrations are the stretches associated with movements within the TO$_4$ tetrahedra. These movements can be the O-T-O bending, or the symmetric or asymmetric stretches of the O-T-O bonds. The intertetrahedral (between adjacent tetrahedra) vibrations include pore-opening (also known as breathing) modes. These guidelines have become the primary tool for assignment of the absorptions in the infrared spectra of zeolites.[16, 19] Far-infrared spectroscopy (FIR), less than 400 cm^{-1}, has been used to examine the local environment of zeolites with cation probes.[20-25] In addition to being able to probe the local

cation environment,[24] FIR also provides structural information on the zeolite network, such as the pore-breathing and intra-tetrahedral bending modes.[17]

The present study of experimental work performed by a previous graduate student examines the infrared peaks of the zincosilicate molecular sieve CIT-6 and modified versions of CIT-6.[26] CIT-6 was first synthesized and characterized in 1999.[27] CIT-6 has since been examined for its chemical properties,[9] the mechanism of its crystallization,[28] and its ability to catalyze propane dehydrogenation.[7] CIT-6 is of interest in this study as it can be changed from the original zincosilicate to a pure silicate without changing the XRD spectra of the sample.[9] This pure silicate can subsequently be modified, without changing the XRD spectra, to an aluminosilicate with the insertion of aluminum into the T-atom locations formerly occupied by zinc.[9]

CIT-6 has the framework structure of zeolite Beta (International Zeolite Association designation *BEA),[9] which is of particular interest because it is an in-growth of two polymorphs.[29] It is also useful in industrial applications such as gas separation and the reforming of industrial naphtha.[30, 31] Zeolite *BEA has been analyzed for long-range order in the development of its polymorphs;[32] short-range order with NMR ^{29}Si chemical shifts to identify its structure;[6] the effects of partial replacement of silicon with tin or titanium atoms;[33] and the development of connectivity-defect-free zeolite *BEA.[34] The structural[10, 35, 36] and chemical properties [37, 38] of pure silica zeolite *BEA have been investigated using infrared spectroscopy. However, there have been no reported attempts to analyze the structure or chemical properties of CIT-6 and the modified versions listed above with infrared spectroscopy. Of particular interest is to demonstrate that IR, and especially FIR, can be used to view short-range changes made to the structure that are otherwise difficult to see using XRD alone.

In this work, the vibrational spectra of CIT-6 and its derivatives are reported over the spectral range from 4000 cm^{-1} to 200 cm^{-1}. Seven samples are included in this report: 1. the as-synthesized sample, prior to any treatments (As-made CIT-6); 2. the as-synthesized sample after calcination at 550°C (Calcined); 3. a low temperature (60°C) acetic acid structural-zinc-extracted (Low-T Si *BEA); 4. a high temperature (135°C) acetic acid structural-zinc-extracted sample (High-T Si *BEA); 5. the low temperature acetic acid sample with aluminum inserted into the T-atoms structural locations where the zinc was extracted (Aluminum); 6. the as-synthesized

sample that has been ion-exchanged to substitute zinc for the original lithium cation (Zn CIT-6); and 7. a pure silica *BEA sample (Pure Si *BEA).[7, 9, 34]

Experimental

CIT-6 was synthesized following the procedure from Takewaki et al.[9] The reactants were mixed at a molar composition of 0.05 moles LiOH: 0.03 moles $Zn(OAc)_2$ (zinc acetate): 0.65 moles TEAOH (tetraethylammonium hydroxide): 1 mole SiO_2: 30 moles H_2O and heated for four days at 150°C in a Teflon-lined autoclave. The product was recovered via filtration, washed with water, and dried at 100°C overnight in air. This "As-made CIT-6" is a zincosilicate zeolite with lithium cations present to balance the framework charge. It also contains residual TEAOH in the pores that served as the structure-directing agent (SDA).
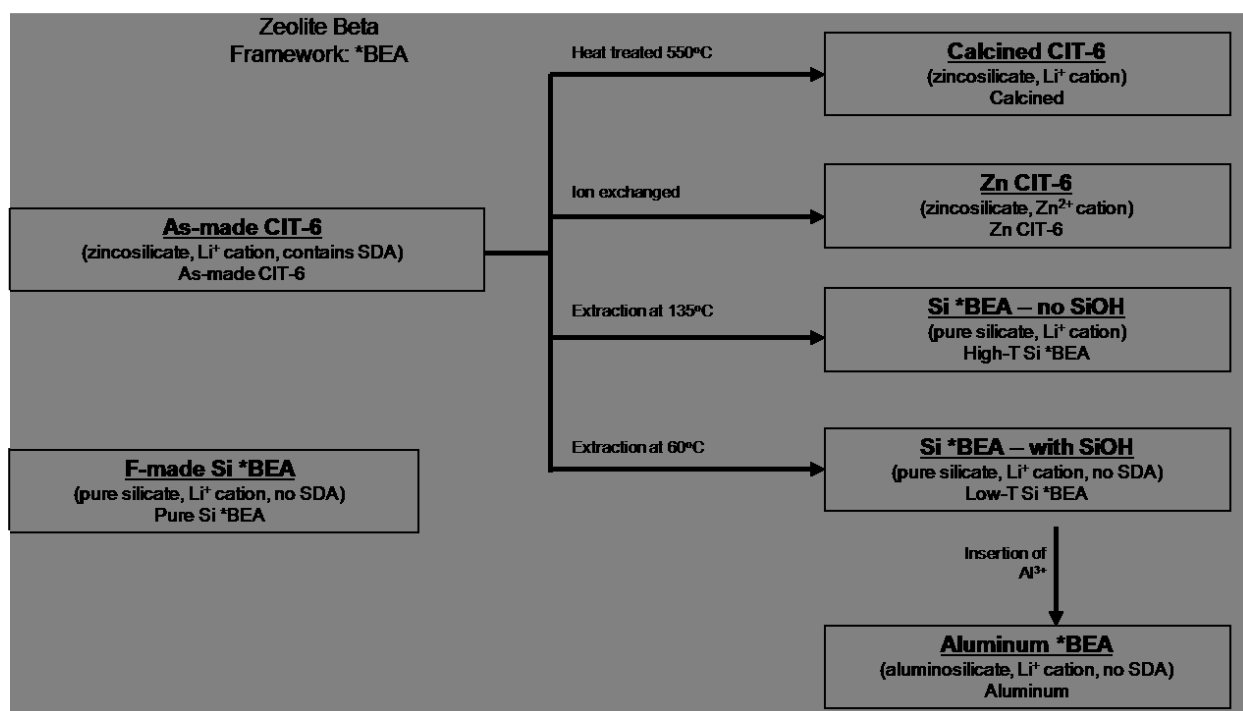
Figure A.1 Flowchart of synthesis procedures

The As-made CIT-6 was then exposed to five treatments to modify the framework composition while maintaining the bulk *BEA structure.[9] Figure A.1 shows the treatments and the resulting samples. The "Calcined" sample was obtained by heating the As-made CIT-6 at 550°C for ten hours to remove the remaining SDA.[9] The "Zn CIT-6" was prepared by ion-exchanging the lithium cations in the As-made CIT-6 with zinc cations through exposure to a 1 molar $Zn(NO_3)_2$ solution for ten hours at 80°C.[9] In both the "High-T Si *BEA" and the "Low-T

121

Si *BEA," the intra-tetrahedral zinc atoms were extracted from the As-made CIT-6 zincosilicate framework with acetic acid, leaving behind a pure silica zeolite with the *BEA framework.[9] The High-T Si *BEA resulted from exposing the As-made CIT-6 to acetic acid at 135°C for two days, where the higher temperature is expected to anneal the extracted zinc sites.[9] The Low-T Si *BEA was made by exposing As-made CIT-6 to acetic acid at 60°C for three days, which is reported to result in exposed silanol groups at the sites of the extracted zinc.[9] Contacting the Low-T Si *BEA with aluminum nitrate nonahydrate at a 1:2.50 weight ratio of zeolite to $Al(NO_3)_3 \cdot 9H_2O$ at 80°C for 1 day inserted an aluminum atom into the tetrahedral framework.[9] This treatment results in the aluminosilicate form of zeolite *BEA is referred to here as "Aluminum".

The "Pure Si *BEA", a pure silica zeolite *BEA, was synthesized following the procedure from Camblor et al.[34] This is the only sample studied in this work that did not originate from post-synthesis treatments of As-made CIT-6. The Pure Si *BEA was synthesized using hydrofluoric acid and resulted in the formation of zeolite *BEA without connectivity defects and with enhanced crystallinity.[34] This is an excellent model of the *BEA structure for comparison with the other samples in this study.[34]

After synthesis the samples were analyzed by x-ray diffraction, either a Bruker AXS D8 Advance or Rigaku MiniFlex II X-ray diffractometer, using copper Kα radiation to confirm their crystal structures.

The infrared spectroscopic data were obtained with a Mattson Instruments Cygnus 100 FTIR spectrometer (Madison Instruments, Madison, WI). All the data were obtained via diffuse reflection utilizing a SpectraTech "COLLECTOR" diffuse reflection accessory.

In the mid-infrared (MIR) region, a high temperature ceramic source and a germanium-coated potassium bromide (KBr) beam splitter were employed. The detector was a deuterated triglyceride sulfate (DTGS) detector with a KBr window, and the mirror velocity was 0.6 cm/sec. The iris setting was 50%. Resolution was set at two cm^{-1}. 1,024 scans were co-added for each spectrum.

In the far-infrared (FIR) region, a high temperature ceramic source was employed. The beam splitter was a three-micron Mylar film. The detector was a DTGS detector with a polyethylene window. The mirror velocity was 0.3 cm/sec, and the iris was 50% open. The resolution was two cm^{-1}. Each spectrum was the result of co-adding 1,024 scans.

Due to the requirements of the diffuse reflection technique, all samples were mixed with cesium iodide powder at an approximate ratio of 1:5 (zeolite:CsI). A mortar and pestle was used to reduce the particle size of the solids and to mix the cesium iodide powder and the sample. CsI was used for the background spectra.

Results and Discussion

XRD Patterns

As reported in the literature,[7] the XRD patterns of the samples did not change significantly upon treatment. Figure A.2 shows the similarities between As-made CIT-6, Calcined, and Aluminum samples with the defect-free Pure Si *BEA as a representative pattern for comparison.[7] All patterns exhibit strong similarities, the only difference between the spectra is the appearance of peaks at 13.4° and 14.4° 2θ in the Calcined sample versus the aluminum and As-made samples. These differences are consistent with the results reported in the literature and are similar to peaks seen in the XRD of the Pure Si *BEA sample.[9]
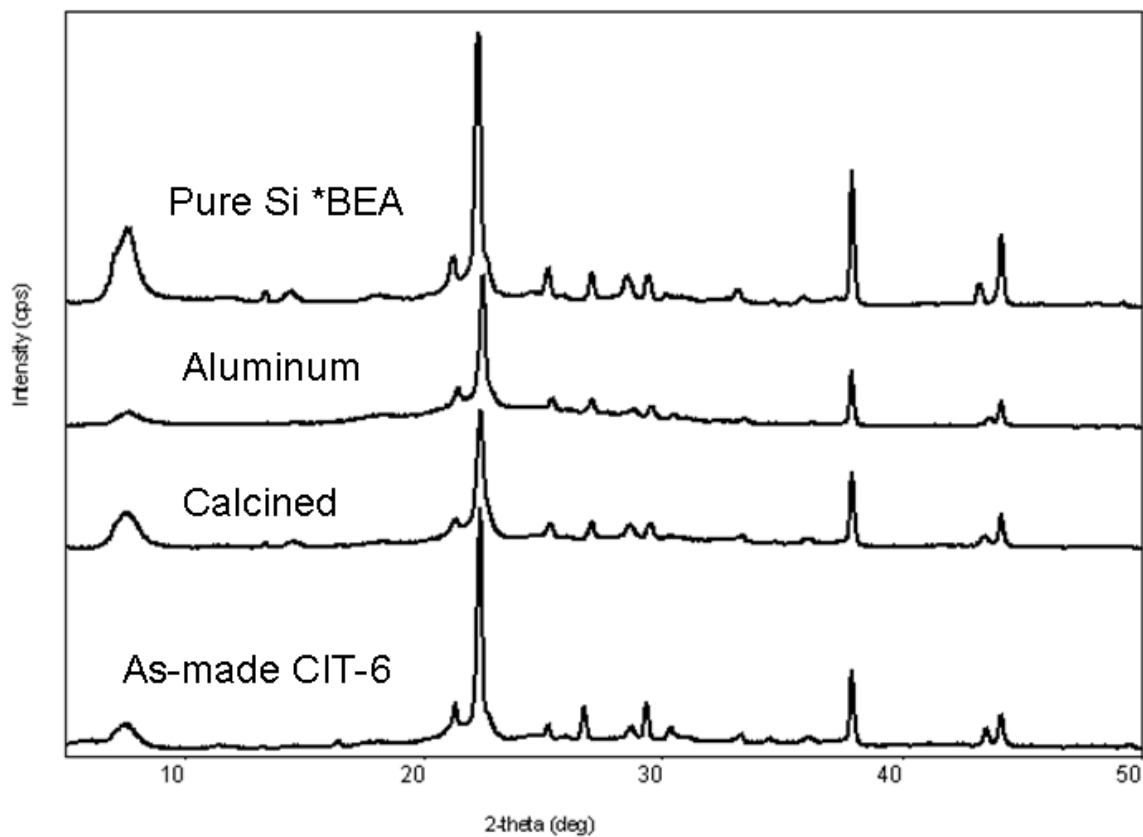
**Figure A.2 XRD results of Pure Si *BEA, Aluminum, Calcined, and As-made CIT-6
samples**

MIR Analysis

The mid-infrared peak assignments are given in Table A.1; the MIR spectra for all seven
samples can be seen in Figures A.3 and A.4.

Table A.1 Mid-IR peaks for CIT-6 and its derivatives

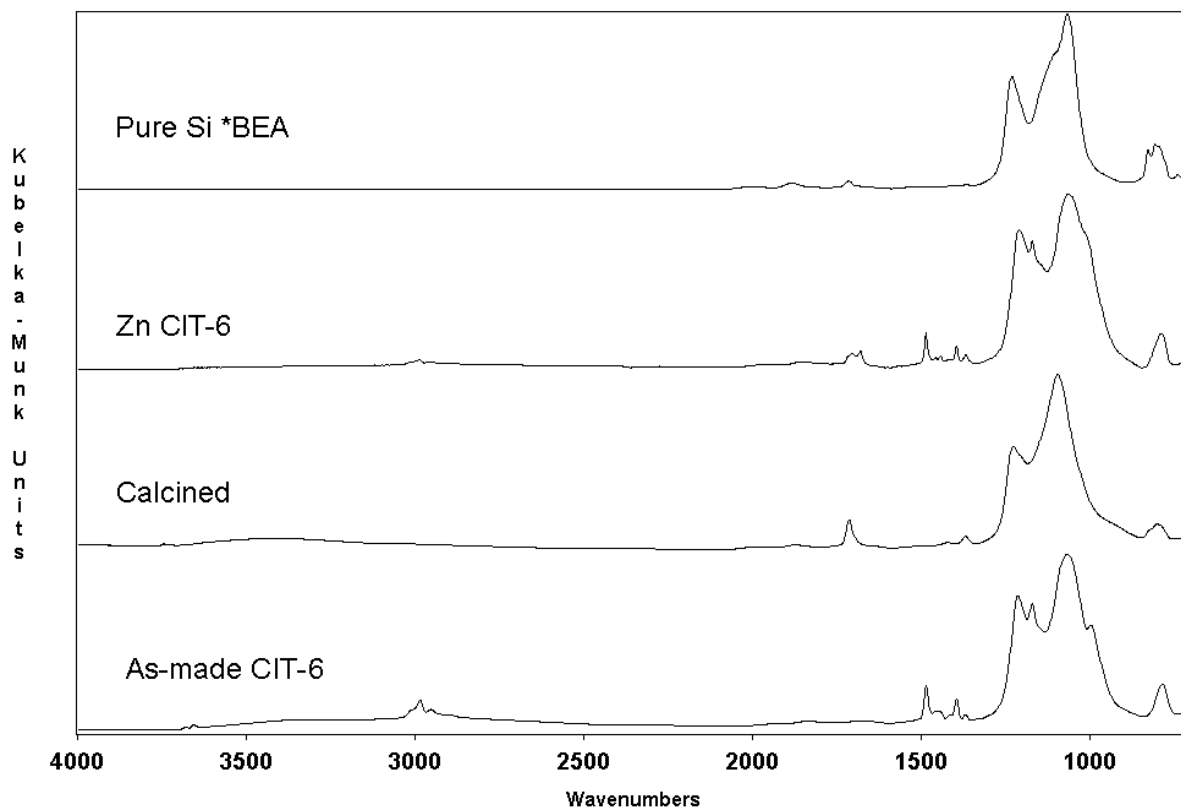| As-made CIT-6	Calcined	Zn CIT-6	Pure Si *BEA	High-T Si *BEA	Low-T Si *BEA	Aluminum	Assignment
3655 w	3742 w			3739 vw	3734 w	3743 w	ν_s OH[39]
3270 br, w	3407 br, w	3362 br, vw		3360 br, vw	3336 w, br	3336 br, st	ν_s OH --- H[39]
2983 m		2986 w				2991 w	ν_s C-H[39]
2952 w						2958 w	
			2002 vw	1995 vw		1971 w	Si-O vibration overtones[40, 41]
1836 w	1874 w	1853 br, w	1881 w	1878 w	1874 w	1865 w	
	1712 m	1706 w	1714 w	1710 w	1708 m	1702 w	δ water[42-44]
1669 w		1679 w				1643 w	
1484 m		1484 m		1484 w	1484 w		δ C-H[39, 45] and NO_3^- (for Aluminum sample only)
1454 w		1455 w				1459 m	
		1441 w				1438 m	
1393 m		1394 w		1394 w		1394 m	
1367 w	1369 w	1366 w		1366 w	1367 w	1366 m	
						1352 m	
	1225 s		1230 s	1231 s	1220 s		ν_a (O-T-O)[17, 18]
1212 s		1198 s				1202 s	
1171 s	1168 sh, s	1166 s	1103 sh, s	1165 sh, s	1169 sh, s	1167 s	
	1093 vs			1092 vs	1086 vs	1086 vs	
1065 vs			1065 vs			1078 vs	
	1036 s						
997 s		1010 sh, s					
				961 sh, m	952 m	949 m	acetic acid from extraction process[45]
	825 sh, m		826 m	824 m	823 sh, m		ν_s (O-T-O)[17, 18]
783 m	799 m	788 m	805 m	804 m	799 m	795 m	
725 w	728	729 w	738 w	737 m	738 m		

Figure A.3 Mid-infrared spectra of Pure Si *BEA, Zn CIT-6, Calcined, and As-made CIT-6
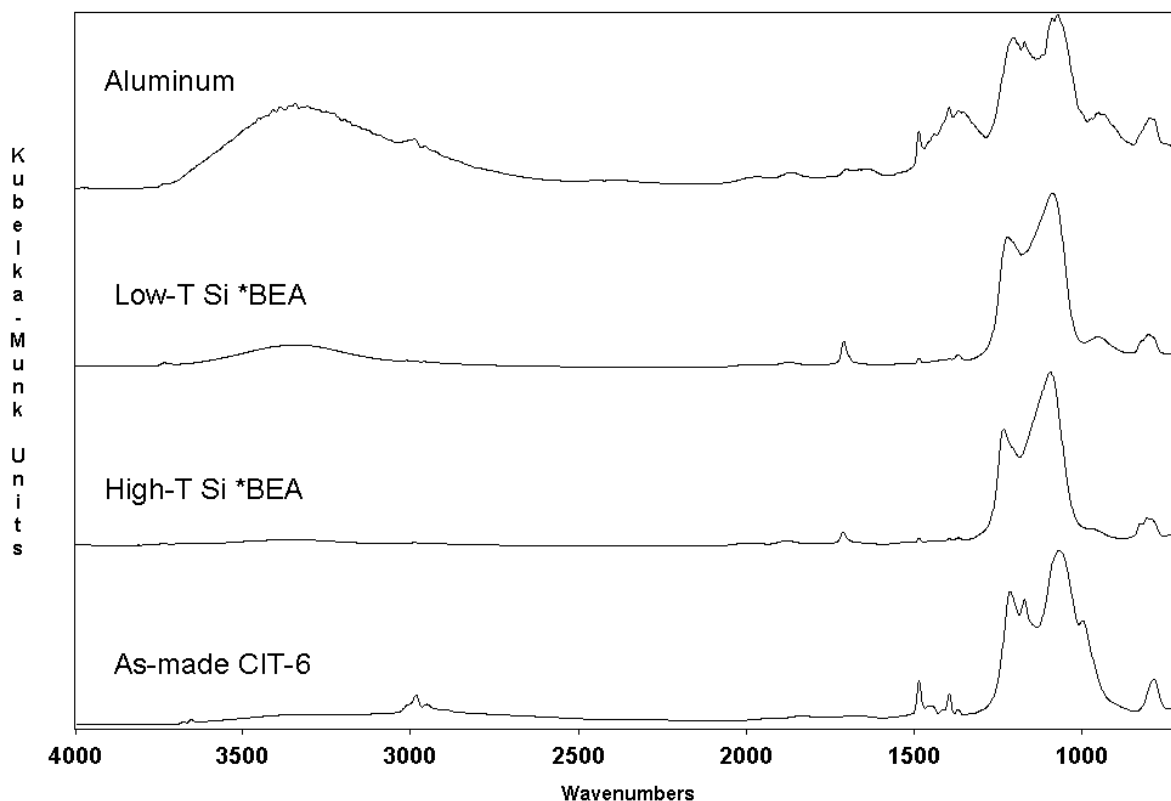
Figure A.4 Mid-infrared of Aluminum, Low-T Si *BEA, High-T Si *BEA, and As-made CIT-6

It can be seen in Table A.1 that most of the samples have absorptions characteristic of isolated and hydrogen-bonded hydroxide stretches, with the exception of the hydrophobic Pure Si *BEA.[34, 39] In Figure A.4 it can be seen in the region from ~3600 to 3000 cm^{-1} that the Low-T and High-T Si *BEA samples have different concentrations of retained hydroxide, even though both are hydrophobic due to their pure silica nature.[9] This is consistent with previous literature which states that the vacancies in the crystal structure from the extraction of the zinc T-atoms are expected to anneal at high temperatures, but at lower temperatures the terminal hydroxide groups remain, resulting in the hydroxides observed with IR.[9] All of the samples have weak absorptions between 2000 and 1800 cm^{-1} indicative of Si-O vibration overtones.[40, 41] The peak present in the spectra between 1712 and 1644 cm^{-1} is indicative of water bending modes, and this shift from its normal position around 1650 cm^{-1} is consistent with other reported examples of adsorbed water on zeolites.[42-44] The slightly greater intensity of the hydroxide bending mode at 1710 cm^{-1} in the Low-T Si *BEA when compared with the High-T Si *BEA is expected based on the discussion above of the different amounts of hydroxide.[9]

Carbon-hydrogen bonds are seen in the absorptions between 3000 to 2900 cm^{-1} and 1500 to 1350 cm^{-1} (Figures A.3 and A.4). These figures show that the As-made CIT-6, Zn CIT-6 and Aluminum samples have absorptions between 3000 and 2900 cm^{-1} that indicate residual SDA.[39] In the aliphatic C-H bending mode region from 1500 to 1350 cm^{-1}, all samples (except for the Pure Si *BEA sample that is prepared without SDA) show some absorptions characteristic of leftover SDA, even after calcination or acetic acid extraction.[7, 39, 45] The presence of leftover SDA is consistent with the report that 24% of the SDA remains after acetic acid extraction in CIT-6.[7]

The Aluminum sample is unique with its much greater absorbances in the region from 1500 to 1250 cm^{-1}. The greater absorbances are due to retained acetic acid and nitrate from the aluminum insertion process, which combine absorptions in this region to give the medium intensity, broad peak from 1500 to 1250 cm^{-1}.[39, 45] Additionally, the High-T and Low-T Si *BEA, and the Aluminum samples have small peaks at approximately 950 cm^{-1}, which indicates some remaining adsorbed acetic acid.[45]

Differences between the spectra in the region from 1230 cm^{-1} to 725 cm^{-1} indicate short-range structural changes due to chemical treatments (Figures A.3 and A.4).[17, 18] The zinc present as T-atoms in the crystal structure of the As-made CIT-6, Calcined, and Zn CIT-6 samples does not yield different absorbances when compared to the pure silica (Pure Si *BEA, Low-T and High-T Si *BEA) or aluminosilicate (Aluminum) samples. This is because zinc is only 3% of the T-atom sites in the structure.[9] The As-made CIT-6 has four distinct peaks between 1210 and 997 cm^{-1}, the region previously identified in the literature as intratetrahedral asymmetric O-T-O stretches.[16-19] The As-made CIT-6 sample spectrum matches other CIT-6 mid-infrared spectra reported in the literature,[28] and the Pure Si *BEA sample also matches the spectrum reported in the literature.[46] The other spectra maintain similar shape and features, including the weaker peak or shoulder at approximately 1168 cm^{-1}, except for the Pure Si *BEA sample.[28] A notable difference is the change in the strongest of the absorbances from approximately 1065 cm^{-1} for the As-made CIT-6 and the Pure Si *BEA samples to 1036 cm^{-1} for the Zn CIT-6 and approximately 1090 cm^{-1} for the rest of the samples. The Pure Si *BEA sample has a shoulder at 1103 cm^{-1}, which has been reported in the literature.[46] The shoulder appears to be absent from the other spectra, but may be hidden by the broader absorbance in those spectra. The Zn CIT-6 sample has a shoulder at 1010 cm^{-1} which is absent from the other samples and is likely due to ion-exchange

modifying the intratetrahedral structure slightly. The As-made CIT-6 has a smaller peak at 997 cm^{-1} which is not seen on any other spectra.

As can be seen in Figure A.4, the High-T and Low-T Si *BEA and the Calcined samples are very similar in the region from 1250 to 720 cm^{-1}. However, the Aluminum sample has a distinct peak at 1167 cm^{-1}, which is similar to the As-made CIT-6, rather than the shoulders present in the High-T and Low-T samples. This indicates an intratetrahedral environment similar to the original As-made CIT-6, rather than its predecessor the Low-T Si *BEA.

All the samples have a peak at approximately 800 cm^{-1} and a smaller peak or shoulder at approximately 735 cm^{-1} identified by Flanigen et al. as symmetric intertetrahedral O-T-O stretches.[17, 18] The Calcined, High-T and Low-T Si *BEA samples again have absorption that are more similar to the Pure Si *BEA sample than to the original As-made CIT-6. These changes further demonstrate the intratetrahedral structural modifications upon thermal or chemical treatment studied herein.

FIR Analysis

Far-infrared peak assignments are given in Table A.2, and the FIR spectra can be seen in Figures A.5 and A.6.

Table A.2 Far-IR peaks for CIT-6 and its derivatives

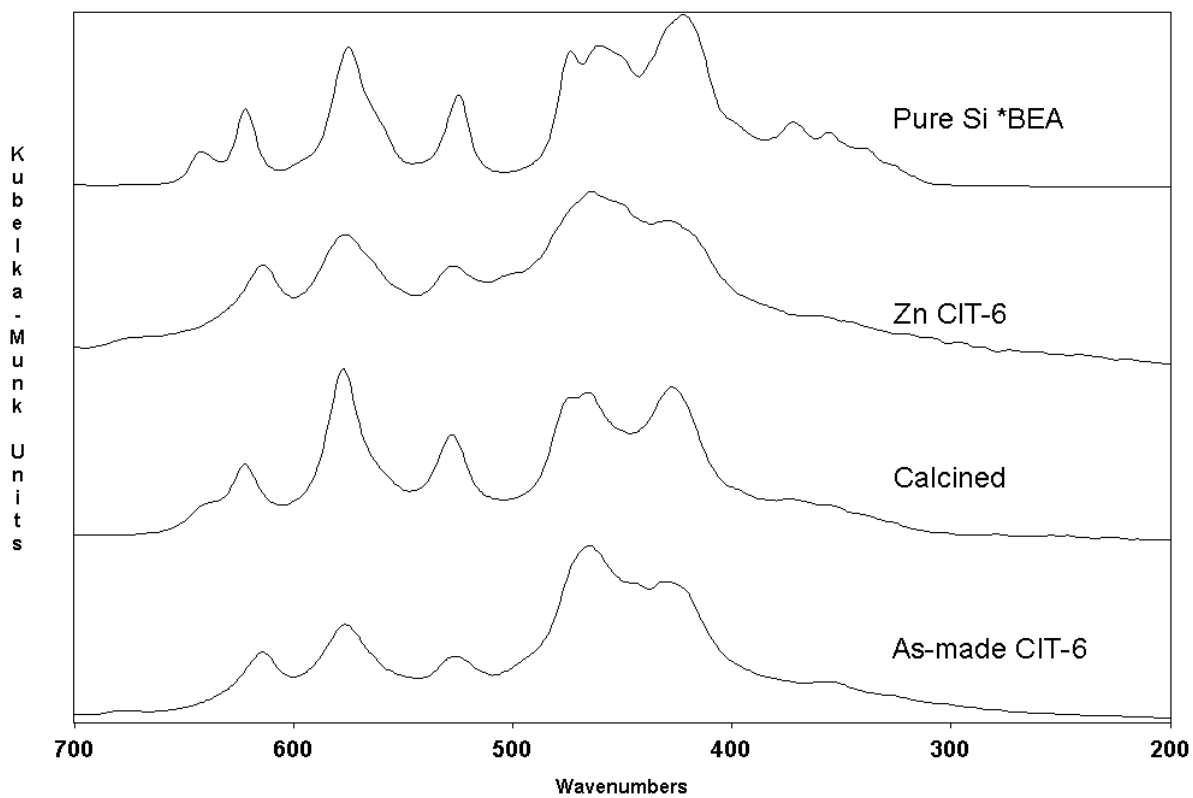| As-made CIT-6	Calcined	Zn CIT-6	Pure Si *BEA	High-T Si *BEA	Low-T Si *BEA	Aluminum	Assignment
	640 sh, m		642 w	640 w	638 sh, w	635 sh, vw	double ring modes[17, 18]
614 m	622 m	614 m	622 m	622 m	624 w	622 w	
577 m	577 s	576 s	575 s	576 s	574 m	569 m	
			561 sh, w				
526 m	528 m	527 m	524 w	527 w	526 m	521 w	
	474 s	473 sh, w	474 s	475 s	473 sh, s	472 sh, s	δ (T-O)[17, 18]
466 s	465 s	463 s	461 s	466 s	463 s	463 s	
431 s	427 s	429 s	423 vs	426 s	429 s		
	374 w		373 w	373 sh, w	373 sh, w		Pore-opening modes[17, 18]
360 w	357 sh, w	362 w	355 w	357 sh, w			
			340 w	342 sh, w	347 sh, w	350 sh, m	

Figure A.5 FIR of Pure Si *BEA, Zn CIT-6, Calcined, and As-made CIT-6
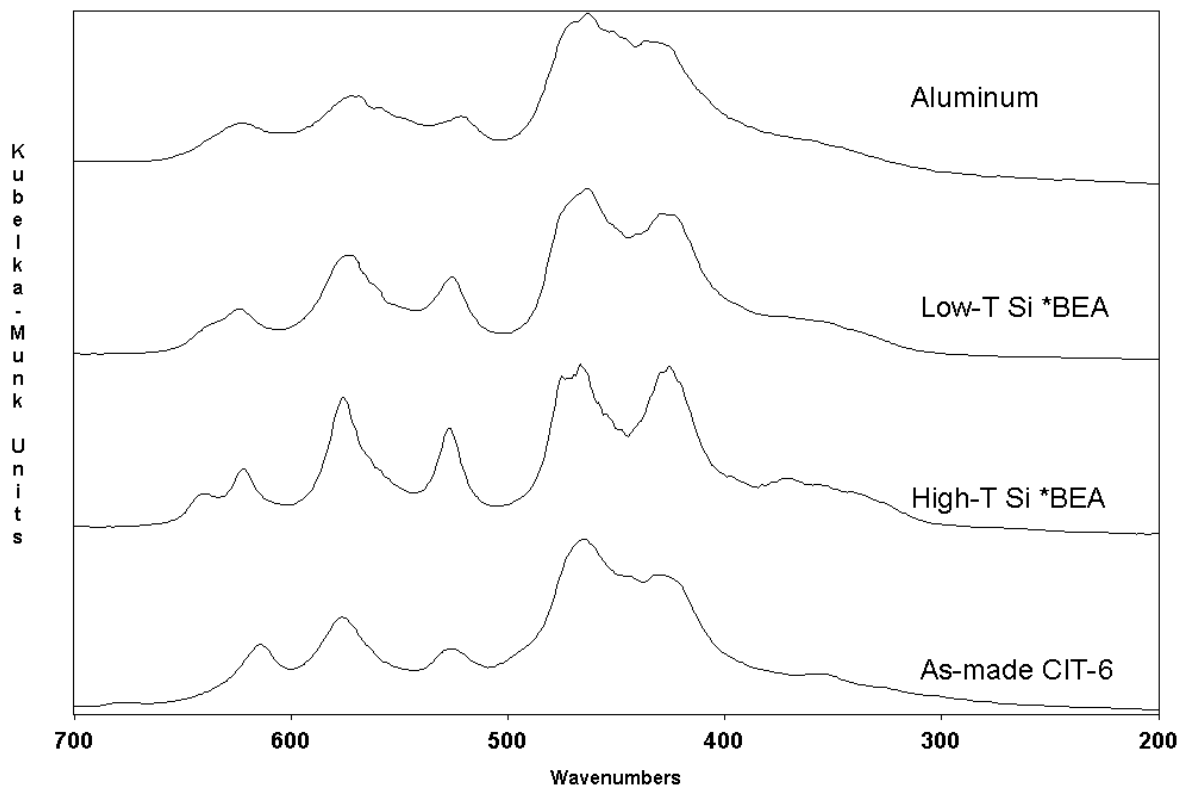
130

Figure A.6 FIR of Aluminum, Low-T Si *BEA, High-T Si *BEA, and As-made CIT-6

The Pure Si *BEA and Calcined samples in Figure A.5, and the Low-T and High-T Si *BEA samples in Figure A.6 have an additional peak when compared to the As-made CIT-6 at approximately 640 cm^{-1}, in the double ring mode region.[17, 18] The Pure Si *BEA sample has an FIR spectrum consistent with what has been reported in the literature.[46] The synthesis method for the Pure Si *BEA results in defect-free material,[34] and a lack of defects contributes to improved resolution of the absorption bands in this spectrum. The heat- and acid-treated samples (Calcined, Low-T and High-T Si *BEA, and Aluminum) all exhibit features more similar to the Pure Si *BEA than their starting material, As-made CIT-6. The difference between the Calcined, Low-T and High-T Si *BEA, and Aluminum samples, and the As-made CIT-6 indicates an additional environment in the intertetrahedral double ring vibrations versus what is seen in the As-made CIT-6 and Zn CIT-6 samples.

In the region from 500 to 420 cm^{-1}, which was identified by Flanigen et al. as the intratetrahedral T-O bending region,[17, 18] the High-T and Low-T Si *BEA, Calcined, and Aluminum samples show an additional peak or shoulder at approximately 473 cm^{-1} compared to the As-made CIT-6. The presence of a peak or shoulder at 473 cm^{-1} in the T-O bending region is

always matched by the presence of a peak or shoulder at 640 cm^{-1} in the double ring mode region. Therefore it can be seen that chemical or thermal treatments affect the structure of the sample by modifying both intratetrahedral T-O bending modes and intertetrahedral double ring modes. These changes can then be seen in the FIR of the sample. The changes in both the double-ring region and in the intratetrahedral region verify that through chemical or thermal treatment the As-made CIT-6 was converted to the *BEA structure, while the ion-exchanged Zn CIT-6 does not exhibit a structural change.[9] The progression of As-made CIT-6 to *BEA is consistent with what is seen in Figure A.2 and with the results in the literature where there are no discernible changes in the XRD of the samples.[9]

The 420 to 300 cm^{-1} region of the spectra shows the pore-opening modes of the zeolites.[17, 18] The Pure Si *BEA sample has three clear peaks, and the High-T Si *BEA has three weak peaks at the same wavenumbers. The other samples show little difference from the As-made CIT-6. The similarity of the As-made CIT-6 and its derivatives in the pore-opening region shows that the long-range order of the sample remains unaffected by chemical or thermal treatment. The lack of change in the pore-opening region corroborates what is seen in the XRD results where the samples maintain similar patterns even after treatment.[9]

Both the Aluminum and Zn CIT-6 samples exhibit peak broadening in the FIR. The Aluminum sample's broader absorbances in the FIR are indicative of distortions of the tetrahedral bond angles due to the extraction and insertion process. The Zn CIT-6 samples show the limited effect ion exchange has in the modification of the FIR of the samples, where the ion-exchange broadened the peaks in the O-T-O bending modes (between 500 and 420 cm^{-1}).

Conclusions

The mid- and far- infrared spectra of CIT-6 and related structures have been reported and band assignments have been made. In the MIR, the Pure Si *BEA, the Calcined, and the Low-T and High-T Si *BEA samples all have two peaks in the intratetrahedral asymmetric stretch region compared to the four peaks seen in the As-made CIT-6, Aluminum, and Zn CIT-6 samples. The FIR in particular gives information regarding how the short- and long-range structures of the samples are modified by thermal or chemical treatment. The significant changes in the FIR of the samples are easier to identify than small changes seen in the XRD. In particular, the development of a new intratetrahedral bending mode and a new double ring mode upon

chemical or thermal treatment of As-made CIT-6 shows its structure changes to the *BEA framework. The ion-exchange process did not change the As-made CIT-6 structure to *BEA. The broadening of the Aluminum and Zn CIT-6 samples in the FIR shows that chemical treatments and ion exchange disrupt the order of the structure, which is difficult to see in XRD. This work demonstrates the utility of IR, and particularly FIR, for the qualitative analysis of chemical effects on zeolite structures as a compliment to XRD.

References

1. Lin, C. C. H.; Dambrowitz, K. A.; Kuznicki, S. M. Evolving applications of zeolite molecular sieves, *The Canadian Journal of Chemical Engineering* **2011**.

2. Davis, M. E.; Lobo, R. F. Zeolite and Molecular Sieve Synthesis, *Chemistry of Materials* **1992**, 756-768.

3. van Bekkum, H.; Cejka, J.; Corma, A.; Schueth, F. *Introduction to Zeolite Molecular Sieves;* Elsevier Science: 2007; .

4. Davis, M. E. Ordered porous materials for emerging applications, *Nature* **2002**, 813-821.

5. Kosslick, H.; Fricke, R. Chemical Analysis of Aluminosilicates, Aluminophosphates, and Related Molecular Sieves. In *Molecular Sieves;* Kosslick, H., Fricke, R., Eds.; Springer: Berlin/Heidelberg, 2007; Vol. 5, pp 1-66.

6. Valerio, G.; Goursot, A.; Vetrivel, R.; Malkina, O.; Malkin, V.; Salahub, D. R. Calculation of ^{29}Si and ^{27}Al MAS NMR Chemical Shifts in Zeolite-A Using Density Functional Theory: Correlation with Lattice Structure, *J. Am. Chem. Soc.* **1998**, 11426-11431.

7. Andy, P.; Davis, M. E. Dehydrogenation of Propane over Platinum Containing CIT-6, *Ind. Eng. Chem. Res.* **2004**, *12,* 2922-2928.

8. Baerlocher, C.; Olson, D. H.; Meier, W. M. *Atlas of Zeolite Framework Types;* Elsevier: Amsterdam, 2001; , pp 308.

9. Takewaki, T.; Beck, L. W.; Davis, M. E. Zincosilicate CIT-6: A Precursor to a Family of BEA-Type Molecular Sieves, *J. Phys. Chem. B* **1999**, *14,* 2674-2679.

10. Hajjar, R.; Millot, Y.; Man, P. P.; Che, M.; Dzwigaj, S. Two Kinds of Framework Al Sites Studied in BEA Zeolite by X-ray Diffraction, Fourier Transform Infrared Spectroscopy, NMR Techniques, and V Probe, *J. Phys. Chem. C* **2008**, *51,* 20167-20175.

11. Stevens, R. W.; Siriwardane, R. V.; Logan, J. In Situ Fourier Transform Infrared (FTIR) Investigation of CO2 Adsorption onto Zeolite Materials, *Energy & Fuels* **2008**, 3070-3079.

12. Chowdhury, A.; Thompson, P. R.; Milne, S. J. TGA-FTIR study of a lead zirconate titante gel made from a triol-based sol-gel system, *Thermochimica Acta* **2008**, 59-64.

13. Baltrusaitis, J.; Schuttlefield, J.; Jensen, J. J.; Grassian, V. H. FTIR spectroscopy combined with quantum chemical calculations to investiage adsorbed nitrate on aluminum oxide surfaces in the presence and absence of co-adsorbed water, *Physical Chemistry Chemical Physics* **2007**, 4970-4980.

14. May, M.; Asomoza, M.; Lopez, T.; Gomez, R. Precursor Aluminum Effect in the Synthesis of Sol− Gel Si− Al Catalysts: FTIR and NMR Characterization, *Chem. Mater.* **1997**, *11,* 2395-2399.

15. Endregard, M.; Nicholson, D. G.; Stoecker, M.; Beagley, B. Cobalticenium ions adsorbed on large-pore aluminophosphate VPI-5 studied by x-ray absorption, 13C solid-state NMR and FTIR spectroscopy, *J. Mater. Chem.* **1995**, *3,* 485-491.

16. Lercher, J. A.; Jentys, A. Infrared and Raman spectroscopy for characterizing zeolites, *Stud. Surf. Sci. Catal.* **2007**, 435-476.

17. Flanigen, E. M.; Khatami, H.; Szymanski, H. A. Infrared structural studies of zeolite frameworks, *Adv. Chem. Ser.* **1971**, 201-229.

18. Flanigen, E. M. Structural analysis by infrared spectroscopy, *ACS Monograph* **1976**, 80-117.

19. Mestl, G.; Knozinger, H. Vibrational Spectroscopies. In *Handbook of Heterogeneous Catalysis;* Ertl, G., Knozinger, H., Schuth, F. and Weitkamp, J., Eds.; Wiley-VCH: Weinheim, 2008; Vol. 2, pp 932-971.

20. Ozin, G. A.; Gil, C. Intrazeolite organometallics and coordination complexes: internal versus external confinement of metal guests, *Chemical Reviews* **1989**, *8,* 1749-1764.

21. Godber, J., mark D. Baker,Geoffrey A.Ozin Far-IR Spectroscopy of Alkali-Metal and Alkaline-Earth Cations in Faujasite Zeolites, *J. Phys. Chem.* **1989**, 1409-1421.

22. Ozin, G. A.; Baker, M. D.; Godber, J.; Wu, S. Crystal-field effects on the far-infrared cation vibrations of transition metal (2+) ion exchanged faujasite zeolites, *J. Am. Chem. Soc.* **1985**, *7,* 1995-2000.

23. Baker, M. D.; Ozin, G. A.; Godber, J. Direct probe Fourier transform far-infrared spectroscopy of metal atoms, metal ions, and metal clusters in zeolites, *Catal. Rev.* **1985**, *4,* 591-651.

24. Baker, M. D.; Godber, J.; Ozin, G. A. Frequency and intensity considerations in the far-IR spectroscopy of faujasite zeolites: experiment and theory. Metal cation vibrational assignments, site locations, and populations, *J. Am. Chem. Soc.* **1985**, *11,* 3033-3043.

25. Baker, M. D.; Godber, J.; Helwig, K.; Ozin, G. A. Probing extra-framework cations in alkali- and alkaline-earth-metal Linde type A zeolites by Fourier transform far-infrared spectroscopy, *J. Phys. Chem.* **1988**, *21,* 6017-6024.

26. McGown, T. Infrared Spectroscopy For The Characterization of Porous Zincosilicate Materials and Their Use in Lead Capture**2006**, 1.

27. Takewaki, T.; Beck, L. W.; Davis, M. E. Synthesis of CIT-6, a Zincosilicate With the BEA Topology, *Top. Catal.* **1999**, 35-42.

28. Serrano, D. P.; Van Grieken, R.; Davis, M. E.; Melero, J. A.; Garcia, A.; Morales, G. Mechanism of CIT-6 and VPI-8 crystallization from zincosilicate gels, *Chem. --Eur. J.* **2002**, *22,* 5153-5160.

29. Treacy, M. M. J.; Newsam, J. M. Two new three-dimensional twelve-ring zeolite frameworks of which zeolite beta is a disordered intergrowth, *Nature* **1988**, 249-251.

30. Huang, Z.; Su, J.; Guo, Y.; Su, X.; Teng, L. Synthesis of Well-Crystallized Zeolite Beta at Large Scale and Its Incorporation into Polysulfone Matrix for Gas Separation , *Chem. Eng. Commun.* **2009**, *9 September 2009,* 969-986.

31. Zhang, W.; Smirniotis, P. G. Dealuminated zeolite-based composite catalysts for reforming of an industrial naphthene-rich feedstock, *Appl. Catal. , A* **1998**, *1,* 113-130.

32. Cantin, A.; Corma, A.; Diaz-Cabanas, M. J.; Jorda, J. L.; Moliner, M.; Rey, F. Synthesis and characterization of the all-silica pure polymorph C and an enriched polymorph B intergrowth of zeolite beta, *Angew. Chem. , Int. Ed.* **2006**, *47,* 8013-8015.

33. Shetty, S.; Kanhere, D. G.; Goursot, A.; Pal, S. A Comparative Study of Structural, Acidic and Hydrophobic properties of Sn-BEA with Ti–BEA using Periodic Density Functional Theory, *J. Phys. Chem. B* **2008**, *9,* 2573-2579.

34. Camblor, M. A.; Corma, A.; Valencia, S. Spontaneous nucleation and growth of pure silica zeolite-P free of connectivity defects, *Chem. Comm.* **1996**, 2365.

35. Busca, G.; Vevilacqua, M.; Armaroli, T.; Trombetta, M. FT-IR studies of internal, external and extraframework sites of FER, MFI, BEA and MOR type protonic zeolite materials, *Stud. Surf. Sci. Catal.* **2002**, 975-982.

36. Yuvaraj, S.; Palanichamy, M. P. Characterization of Chromium-Substituted Zeolite BEA, *Bull. Chem. Soc. Jpn.* **2002**, *1,* 155.

37. Bisio, C.; Martra, G.; Coluccia, S.; Massiani, P. FT-IR Evidence of Two Distinct Protonic Sites in BEA Zeolite: Consequence on Cationic Exchange and on Acido-Basic Properties in the Presence of Cesium, *J. Phys. Chem. C* **2008**, *10520,.*

38. Marques, J. P.; Gener, I.; Ayrault, P.; Bordado, J. C.; Lopes, J. M.; Ramoa Ribeiro, F.; Guisnet, M. Infrared spectroscopic study of the acid properties of dealuminated BEA zeolites, *Micro. Meso. Mater.* **2003**, 251.

39. Socrates, G. *Infrared Characteristic Group Frequencies;* John Wiley & Sons: Chichester, 1994; , pp 249.

40. Cejka, J.; van Bekkum, H.; Corma, A.; Schueth, F. *Introduction to Zeolite Science and Practice, Volume 168, Third Edition (Studies in Surface Science and Catalysis;* Elsevier Science: Amsterdam, The Netherlands, 2007; Vol. 168, pp 1094.

41. Zhang, M.; Salje, E., K. H.; Ewing, R., C. Infrared spectra of Si-O overtones, hydrous species, and U ions in metamict zircon: radiation damage and recrystallization, *J. Phys. : Condens. Matter* **2002**, 3333.

42. Jentys, A.; Warecka, G.; Derewinski, M.; Lercher, J., A. Adsorption of Water on ZSM-5 Zeolites, *J. Phys. Chem.* **1989**, 4837-4843.

43. Szymanski, H. A.; Stamires, D. N.; Lynch, G. R. Infrared spectra of water sorbed on synthetic zeolites, *JOSA* **1960**, *12,* 1323-1328.

44. Frohnsdorff, G. J. C.; Kington, G. L. A note on the thermodynamic properties and infra-red spectra of sorbed water, *Proceedings of the Royal Society of London.Series A, Mathematical and Physical Sciences* **1958**, *1251,* 469-472.

45. Kinugasa, S.; Tanabe, K.; Tamura, T. Spectral Database for Organic Compounds. *http://riodb01.ibase.aist.go.jp/sdbs/cgi-bin/direct_frame_top.cgi* (accessed July 29, 2010, July, 2010).

46. Newsam, J. M.; Treacy, M. M. J.; Koetsier, W. T.; De Gruyter, C. B. Structural characterization of zeolite beta, *Proceedings of the Royal Society of London.Series A, Mathematical and Physical Sciences* **1988**, *1859,* 375-405.

Appendix B - Infrared Spectroscopic Examination of VPI-7 and VPI-9

Sean R. Tomlinson, Tyler McGown, John R. Schlup, and Jennifer L. Anthony

Introduction

Microporous molecular sieves are of great scientific and commercial interest.[1-3] Zeolites are a category of microporous molecular sieves and are often used in catalysis, ion exchange, and adsorption/separation processes.[4] The term zeolite refers specifically to aluminosilicate microporous molecular sieves. However, the term is often applied to all compounds having similar crystalline structures. Zeolites are of interest because of their small uniform pores (less than 2 nm), channel configuration, and void space organization.

Because of the many potential applications of zeolites, the characterization of their chemical composition, structure, and bonding is important, and various analytical techniques have been employed to obtain such data. The chemical composition of zeolites can be obtained with atomic absorption spectroscopy (AAS), atomic emission spectrometry (ICP-AES) and X-ray fluorescence spectrometry (XRF).[5] Both ^{29}Si and ^{27}Al NMR have proven to be valuable tools in understanding the local environments around the atoms in the lattice. When NMR data are coupled with density functional theory (DFT) calculations, these data have resulted in valuable insight into the crystalline structure of zeolites.[6] From X-ray diffraction (XRD) data it is possible to determine the crystalline structure of zeolitic materials using Rietveld refinement. These XRD data also permit identification of samples by comparison with XRD results of known samples.[7-9]

Vibrational spectroscopy, including both Raman and infrared (IR), is often employed to investigate short-range order in zeolites. The structures of zeolites, examination of zeolite functional groups, and examinations of zeolite chemistry with probe molecules have been studied with Fourier transform infrared spectroscopy (FTIR).[10-18] In the 1970s Flanigen et al. proposed functional group assignments for the absorption bands between 1250 and 300 cm^{-1}.[17, 18] The assignments divide the spectra into regions which are classified with respect to intra- or intertetrahedral vibrations. Intratetrahedral vibrations are the stretches associated with movements within the TO$_4$ tetrahedra. These movements can be the O-T-O bending or the symmetric or asymmetric stretches of the O-T-O bonds. The intertetrahedral (between adjacent

138

tetrahedra) vibrations include pore-opening (also known as breathing) modes. These guidelines have become the primary tool for assignment of the absorptions in the infrared spectra of zeolites.[16, 19] Far-infrared spectroscopy (FIR), less than 400 cm^{-1}, has been used to examine the local environment of zeolites with cation probes.[20-25] In addition to being able to probe the local cation environment,[24] FIR also provides structural information on the zeolite network, such as the pore-breathing and intra-tetrahedral bending modes.[17]

This study of experimental work performed by a previous graduate student identifies the infrared peaks of the zincosilicate molecular sieves VPI-7 and VPI-9, both before and after lead ion exchange, using Flanigen's assignments.[17, 18, 26] VPI-7 was first synthesized and characterized in 1991 by Annen et al.[27] Since then VPI-7 has been examined for its physiochemical properties,[28] its stability and vibrational spectra,[29] with Raman and ^{29}Si MAS NMR,[30] its use lead capture,[26] and it has undergone Rietveld refinement to confirm the proposed topology.[31] VPI-9 was first synthesized and characterized by McCusker et al. in 1996.[32] The conductivity of mono- and divalent cations in VPI-9 has also been examined.[33] Both zincosilicates have been examined for their heavy metal (lead and mercury) capture ability in aqueous solution, as well as their possible uses in a chemical warfare sensing array.[34]

VPI-7 and 9 were chosen because of their similar chemical compositions, but different structures. VPI-7 was the first microporous zincosilicate synthesized with three-member rings.[27] VPI-9 was synthesized by the replacement of the sodium with rubidium in the VPI-7 synthesis mixture.[32] The recipes are otherwise similar but yield different structures and unit cells. This research identifies what structural differences can be seen using MIR and FIR spectroscopy. Additionally, samples of VPI-7 and VPI-9 were ion-exchanged with lead to examine what changes are visible upon ion-exchange. However, some of the samples became X-ray amorphous upon ion exchange, and their IR spectra are also examined below.

Experimental

VPI-7 used in this research was synthesized as follows. The synthesis was performed in water with a molar composition of: 1.0 SiO_2: 0.88 NaOH: 0.3 KOH: 0.032 TEAOH (tetraethylammonium hydroxide): 0.039 ZnO: 26 H_2O.[35] The mixture was then heated for four days at 200°C in a Teflon-lined autoclave. After heating, the product was washed with water and

recovered via filtration. According to literature the final formula for the VPI-7 unit cell is $Na_{28.5}H_{3.5}[Si_{56}Zn_{16}O_{144}]$ • 40 H_2O for a total of 72 T-sites (22% zinc) per unit cell.[31]

VPI-9 was synthesized according to the procedure from McCusker et al.[32] with molar ratios of: 1.0 SiO_2: 0.6 RbOH: 0.3 KOH: 0.08 TEAOH (tetraethylammonium hydroxide): 0.039 ZnO: 26 H_2O. As in the VPI-7 method, the solution was heated for four days at 200°C in a Teflon-lined autoclave. Then the product was washed with water, recovered via filtration and dried for 24 hours in a 50°C oven. The Rietveld refinement of the unit cell of VPI-9 gives a formula of: $Rb_{38-43}K_{5-10}[Si_{96}Zn_{24}O_{240}]$ • 48 H_2O for a total of 120 T-sites (20% zinc) per unit cell.[32]

The VPI-7 and VPI-9 samples prepared above were submerged in a 1000 ppm lead nitrate aqueous solution for 10 hours at room temperature to exchange the sodium and potassium cations (VPI-7) or rubidium and potassium cations (VPI-9) for lead. Ion-exchange was quantified with an atomic absorption spectrometer (AAS). The AAS is a Varian model AA240 which uses a Varian graphite tube atomizer model GTA 120 or a slot-type flame burner and a Varian programmable sample dispenser model PSD 120. Water circulation was performed by a Lytron circulator. Prior to analysis in the AAS, samples were diluted with distilled water 50, 1,000 or 10,000 times depending on their initial concentration. After ion-exchange, the samples were examined using XRD with either a Bruker AXS D8 Advance or Rigaku MiniFlex II X-ray diffractometer, using copper Kα radiation. It was found that while some of the samples maintained their long-range crystallinity, some of the samples did not and became XRD amorphous. It was decided to use infrared (IR) spectroscopy to examine both XRD amorphous and crystalline samples to see what changes could be identified using IR that were not visible using XRD. However there was no consistency in which samples maintained their XRD crystallinity and which became amorphous.

The infrared spectroscopic data were obtained with a Mattson Instruments Cygnus 100 FTIR spectrometer (Madison Instruments, Madison, WI). All the data were obtained via diffuse reflection utilizing a SpectraTech "COLLECTOR" diffuse reflection accessory. In the mid-infrared (MIR) region, a high temperature ceramic source and a germanium-coated potassium bromide (KBr) beam splitter were employed. The detector was a deuterated triglyceride sulfate (DTGS) detector with a KBr window, and the mirror velocity was 0.6 cm/sec. The iris setting was 50%. Resolution was set at two cm^{-1}. 1,024 scans were co-added for each spectrum. In the

far-infrared (FIR) region, a high temperature ceramic source was employed. The beam splitter was a three-micron Mylar film. The detector was a DTGS detector with a polyethylene window. The mirror velocity was 0.3 cm/sec, and the iris was 50% open. The resolution was two cm^{-1}. Each spectrum was the result of co-adding 1,024 scans.

Due to the requirements of the diffuse reflection technique, all samples were mixed with cesium iodide powder at an approximate ratio of 1:5 (zeolite:CsI). A mortar and pestle was used to reduce the particle size of the solids and to mix the cesium iodide powder and the sample. CsI was used for the background spectra.

Results and Discussion

MIR VPI-7

The zincosilicate molecular sieve VPI-7 ion exchanged significantly more lead than did VPI-9. The mean percent exchanged for VPI-7 was 86%, while for VPI-9, it was 62%.[26] This higher amount of lead exchanged could explain the greater effects from ion exchange seen on VPI-7 (see below). The mid-infrared (MIR) peaks and assignments for the VPI-7 samples are shown in Table B.1 and Figures B.1 and B.2.

Table B.1 Table of Mid-IR peaks of VPI-7 samples.

| As-made VPI-7	VPI-7 A1	VPI-7 A2	VPI-7 C1	VPI-7 C2	Assignment
3557 m	3509 sh	3509 sh	3558 m	3556 m	ν_s OH[36]
3099 m, br	3355 st, br	3335 st, br	3124 m, br	3180 m, br	ν_s OH --- H[36]
	2387 w, br	2363 w, br			ν_s CO$_2$[36]
	1751 w	1751 w			N-O or C=O bonds[36]
1666 m	1640 m	1646 m	1652 m	1651 m	δ water[37, 38]
1470 vw			1401 w	1407 w	δ C-H[36]
	1382 s	1392 s			
	1330 s	1326 m			
		1201 sh	1210 sh	1210 sh	ν_a (O-T-O)[17]
1094 s	1074 sh	1112 sh	1098 s	1096 s	
1005 vs	1037 st, br	1043 st, br	1007 vs	1006 vs	
977 sh		953 s	970 sh	973 sh	
935 s	915 sh	912 sh	932 s	928 s	Skeletal T-O-T vibrations[39]
796 m	807 m	808 m	796 m	797 m	intertetrahedral vs (O-T-O)[17]
736 w			729 w	728 w	
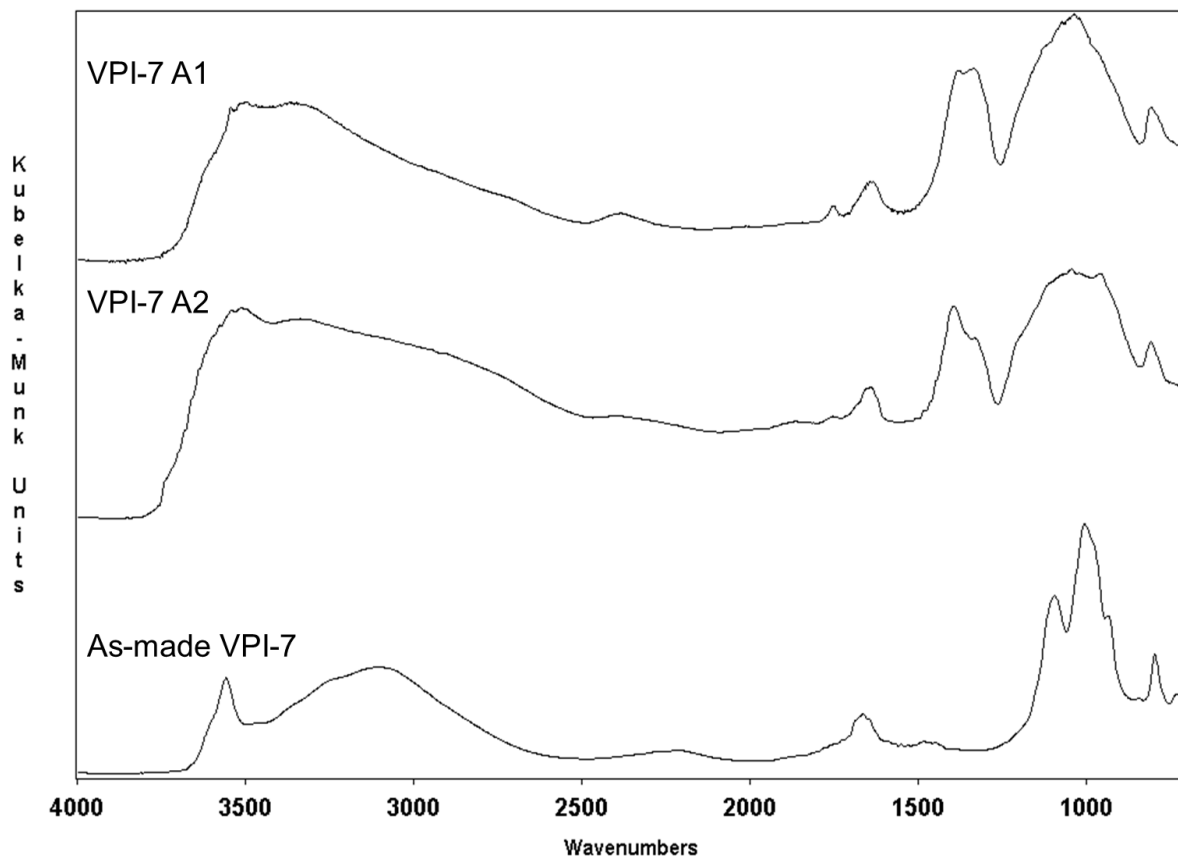
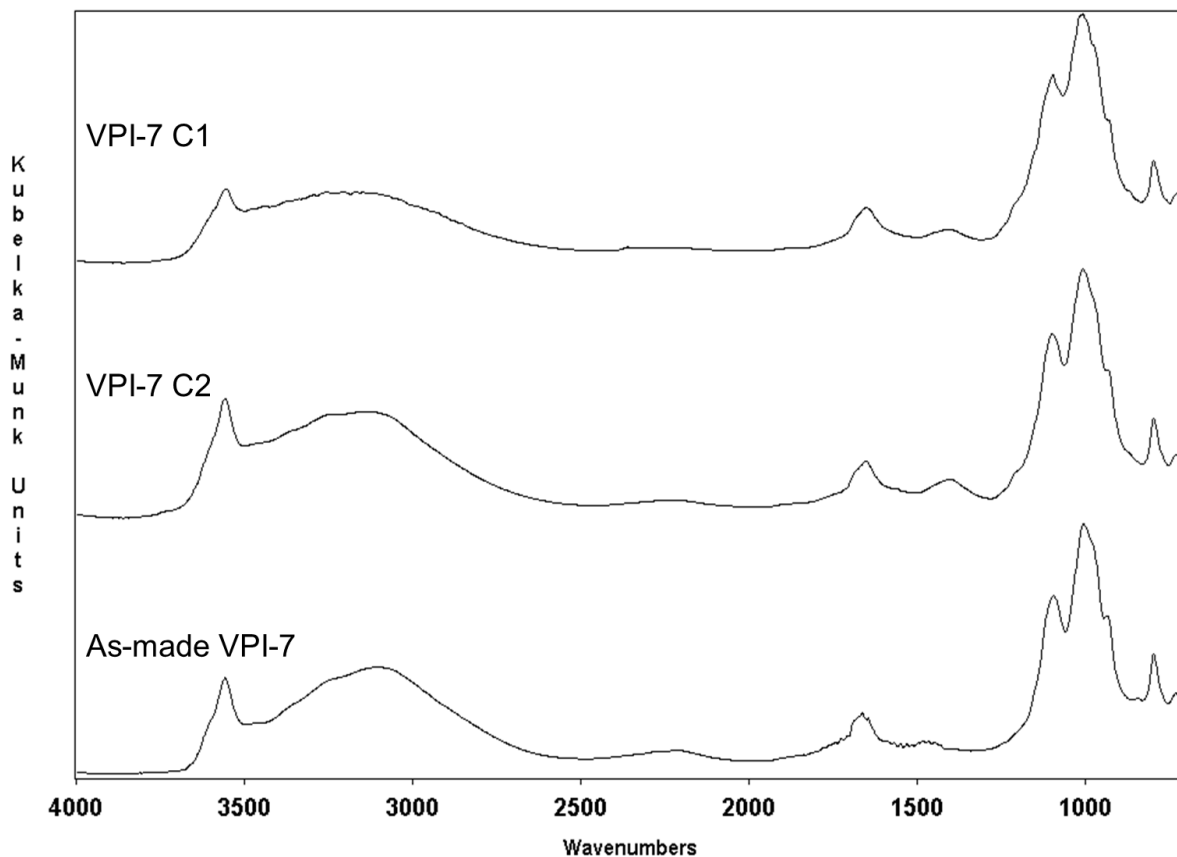**Figure B.1 Mid-IR of XRD-amorphous VPI-7 samples.**

Figure B.2 Mid-IR of crystalline VPI-7 samples.

The ion-exchanged samples are named with A (amorphous) or C (crystalline) and then either 1 or 2 to differentiate the samples. All of the samples have absorptions between 3600 and 3000 cm^{-1} characteristic of isolated and hydrogen-bonded hydroxides, as expected from the hydrophilic nature of the molecular sieves.[36] The weak and broad peaks on the two XRD amorphous samples, VPI-7 A1 and A2, at ~2370 cm^{-1} and 1751 cm^{-1} may be from lead nitrate that was not washed out of the samples.[40] There is a small peak at ~2211 cm^{-1} that may be adsorbed carbon dioxide.[36] All of the samples show absorptions in the water bending-mode region from 1666 to 1640 cm^{-1}.[41-43]

The as-made VPI-7 sample has weak peaks at 1470 cm^{-1} from structure-directing agent that was not completely removed during washing. The two crystalline samples have weak absorptions slightly lower, in the lead nitrate region, show that not all of the lead nitrate was washed out. By contrast, the two amorphous samples have strong absorptions in the lead nitrate region, after the same washing procedures for the crystalline samples, showing that the amorphous structure retained more lead nitrate than the crystalline samples. The peak between

143

1470 and 1401 cm^{-1} on each spectra is probably C-H bending modes from leftover structure directing agent.[36] In the case of the XRD crystalline samples, those peaks could be nitrate from the ion exchange, but that does not explain the presence of a similar peak in the as-made VPI-7. The large peaks at 1094, 1005 and 997 cm^{-1} are indicative of intratetrahedral asymmetric O-T-O stretches within the microporous molecular sieves framework.[17, 18] The peak between 935 and 912 cm^{-1} is at a slightly lower wavenumber than Flanigen's guidelines pertaining to the intratetrahedral asymmetric O-T-O stretches. That may be due to the impact of the zinc in the tetrahedral sites (approximately 22%, as stated above) that could draw the microporous molecular sieves peaks lower because of the higher weight of the neighboring zinc slowing the oscillations. The peaks at 796 and 736 cm^{-1} can be assigned to be intertetrahedral symmetric stretches, between adjacent tetrahedral units.[17, 18]

The comparison of the as-made VPI-7 sample with the two ion-exchanged but XRD amorphous samples in Table B.1 and Figure B.1 shows many differences. The peak at ~2375 cm^{-1} is within the expected range of the adsorbed CO_2.[36] There are also the much larger peaks at ~1378 and 1330 cm^{-1} compared to the rest of the spectra, and these may be due to leftover nitrates from the ion-exchange process.[36] This indicates that the two amorphous samples retained more nitrate after washing than the other samples. There is also the distinctly broader peak from ~1250 cm^{-1} to ~900 cm^{-1} for both spectra that cover the area usually assigned to the intratetrahedral asymmetric O-T-O stretches, and which in the other sample is seen as a trio of independent peaks.[17, 18] This broadening is probably an indication of the disruption of the structure from the ion-exchange of lead into the framework pores. The single peak at ~807 cm^{-1} (in the symmetric intertetrahedral stretch region) indicates the continued presence of the O-T-O bond between tetrahedral units, even if much of the order has been destroyed during ion exchange.

The large peaks in Figure B.2 for the as-made VPI-7 and the two crystalline samples from 1210 to 970 cm^{-1} are similar, showing only small changes between the as-made and the ion-exchanged samples. This is the short-range intratetrahedral asymmetric stretch region, and the similarities indicate that ion-exchange did not affect the short-range structure of the samples, so long as the samples remained crystalline.[17, 18] By contrast the differences between the as-made VPI-7 and the two amorphous samples shows different intratetrahedral environments (1210 to 970 cm^{-1}) when the crystalline structure was destroyed. Instead of three relatively distinct

144

intratetrahedral environments, after ion-exchange there are many intratetrahedral environments, indicating the destruction of the tetrahedra. However, the two amorphous samples have shoulders in the skeletal T-O-T region from 935 to 912 cm^{-1} which indicate the presence of some similar tetrahedral environments within the samples compared to the XRD crystalline samples.[39] Additionally all of the samples have similar peaks in the symmetric intertetrahedral region from 820 to 750 cm^{-1}.

FIR VPI-7

The far infrared (FIR) of the VPI-7 samples is given in Table B.2 and Figures B.3 and B.4.

Table B.2 Table of Far-IR peaks of VPI-7 samples.

| As-made VPI-7	VPI-7 A1	VPI-7 A2	VPI-7 C1	VPI-7 C2	Assignment
653 w	669 w	683	665 w	665 w	intratetrahedral vs (O-T-O)[17]
626 w			642 w	641 w	
			592 w		
552 m			552 m	551 m	double ring mode[17]
	527 m, sh	530 w, sh	526 s, sh		
513 s			515 s	510 s	
	473 s	480 s	480 s, sh		
475 s			445 s		
442 s	442 s		440 s	440 s	δ (O-T-O)[17]
433 s					
405 s		402 s	406 s	406 s	
	365 s		355 w	356 w	Pore opening modes[17]
324 w	329 m, sh		324 w	326 w	
257 s	258 w	254 s	256 m	256 w	Unknown peak
230 s					
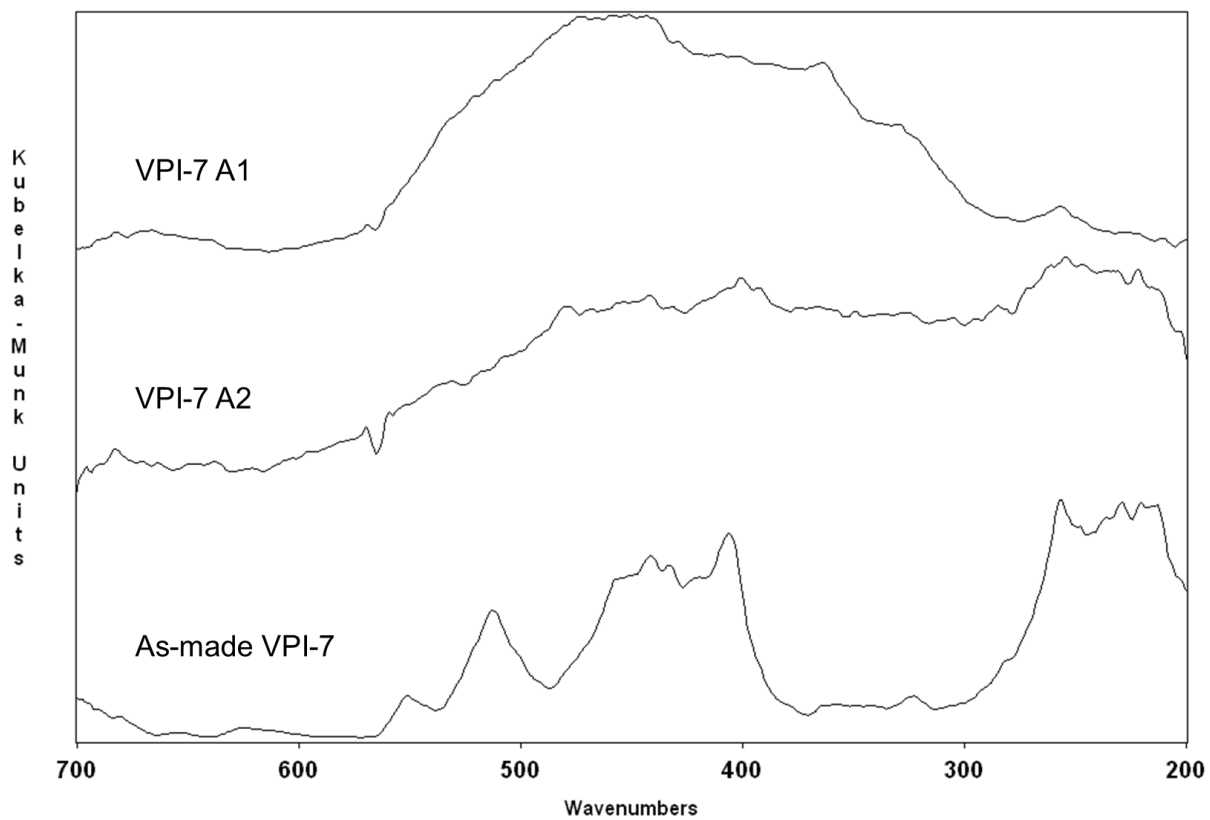
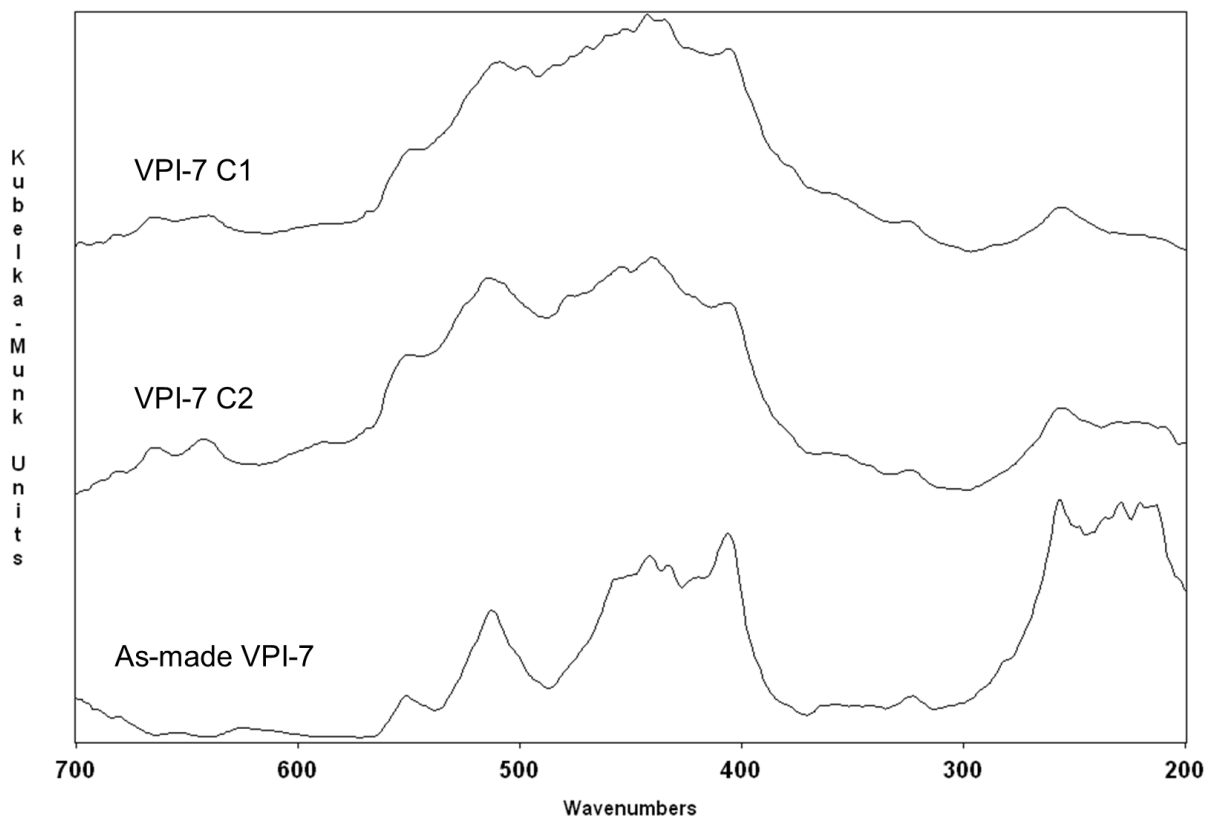**Figure B.3 Far-IR of amorphous VPI-7 samples.**

Figure B.4 Far-IR of crystalline VPI-7 samples.

As in the MIR, the as-made and crystalline samples are similar, but the amorphous samples are very different. All of the samples have weak absorptions in the symmetric intratetrahedral O-T-O region, showing similar intratetrahedral environments. The crystalline samples absorptions in the double-ring mode region (from 650 to 500 cm^{-1}), the intratetrahedral O-T-O bending mode region (from 500 to 420 cm^{-1}), and the pore opening mode region (420 to 300 cm^{-1}) are similar to the as-made sample, indicating very similar long- and short-range structure. However, the crystalline samples show broader absorptions in this longer-range mode region, indicating some effects from the ion-exchange of the larger lead ions for the smaller sodium and potassium ions. The breadth of the amorphous sample's absorptions indicates a multitude of tetrahedral absorption regions, indicating the destruction of the crystalline structure.

Figure 3 gives an indication of the changes caused by ion exchange when the structure becomes X-ray amorphous. The distinct order of the as-made VPI-7 sample disappears with the amorphous Figure B.3 gives strong evidence of the destruction of the microporous molecular sieves crystalline framework upon ion exchange.

147

The comparison of peaks in the far infrared (FIR) for the as-made VPI-7 and the two XRD crystalline samples can be seen in Table B.2 and Figures B.4. Figure B.4 shows significant shape differences in peak shape between the as-made VPI-7 sample and the two XRD crystalline ion-exchange samples. This region can be broken up according to Flanigen's work into five regions: intratetrahedral symmetric stretches ($720 - 650$ cm^{-1}), intertetrahedral double-ring vibrations ($650 - 500$ cm^{-1}), intratetrahedral T-O bends ($500 - 420$ cm^{-1}), intertetrahedral pore-opening ($420 - 300$ cm^{-1}), and below 300 cm^{-1} the interactions between the charge balancing cation with the microporous molecular sieves structure dominate.[17, 18, 20, 25] There is a weak peak at 665 cm^{-1} for the two XRD crystalline samples at 665 cm^{-1} in the intratetrahedral symmetric stretch region but there is no equivalent peak in the as-made VPI-7 sample, likely due to the lead ion exchange process. This may indicate a small change in the intratetrahedral stretches of the sample from the ion exchange. At 653 cm^{-1} the As-made VPI-7 sample has a peak, but it is not seen in the other spectra. The two XRD crystalline samples have a peak at 641 cm^{-1} in the inter-tetrahedral double ring vibration region, but the most similar peak in the as-made sample is at 626 cm^{-1}. It can be seen that all three samples have two peaks, at $\sim$552 cm^{-1} and $\sim$515 cm^{-1}, in the double-ring vibration region. However the differentiation between the two peaks has decreased compared to as-made VPI-7 sample. There is similarly less clarity between the peaks in the T-O band region between 500 and 420 cm^{-1}. These decreases in delineation between the peak regions may be indicative of a decline in the short-range order of the sample. This change in the short-range order may not be visible in the XRD pattern, which examines the long-range order of the sample.

MIR VPI-9

Table B.3 and Figure B.5 show the MIR spectra of the as-made VPI-9 and both the XRD crystalline and amorphous VPI-9 samples.

Table B.3 Table of Mid-IR peaks of VPI-9 samples.

As-made VPI-9	VPI-9 A	VPI-9 C	Assignment
3567 w		3535 w, sh	v_s OH[36]
3245 m, br			
	2836 m, br	2864 m, br	Pb-NO3 peaks[40]
2248 w, br	2248 w	2238 w	v_s CO_2[36]
2035 w	2039 w	2033 w	
1708 w	1734 w	1722 w	N-O or C=O bonds[36]
	1444 w		δ C-H[36]
	1411 w	1418 w	
1108 s	1110 s	1106 s	v_a (O-T-O)[17]
1027 vs	1026 vs	1025 vs	
1003 vs	995 sh	998 vs	
972 vs	976 vs	973 vs	Skeletal T-O-T vibrations[39]
892 s	890 s	890 s	
771 m	768 m	767 m	v_s (O-T-O)[17]
	713 w	713 w	
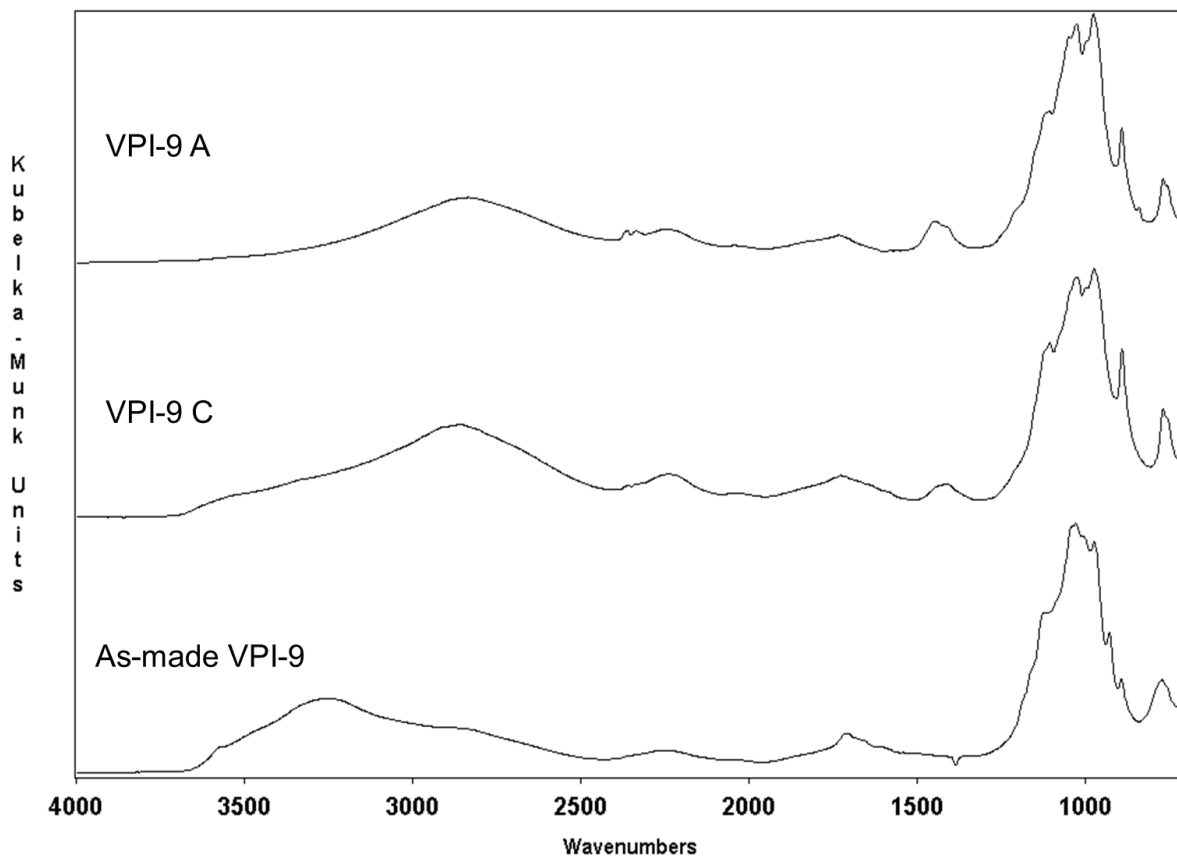
Figure B.5 Mid-IR of VPI-9 samples.

The as-made VPI-9 sample has both isolated and hydrogen bonded hydroxide stretches, similar to the VPI-7 samples. VPI-9 C has small absorptions for both hydroxide stretches, but VPI-9 A does not. VPI-9 A and C have a large absorption at 2864 or 2836 cm^{-1} due to lead nitrate.[40] All of the samples show similar absorptions between for adsorbed CO_2 from 2200 to 2000 cm^{-1}.[36] The ion-exchanged samples show C-H bending modes, but the as-made VPI-9 does not.[36] This is unusual as none of the samples would be expected to show signs of hydrocarbons. The cause of this is unknown. The intratetrahedral asymmetric stretch region from 1110 to 972 cm^{-1} is very similar for all the samples, except that the ion-exchanged samples have reversed intensities for their strongest peaks, compared to the as-made sample. This may be due to the ion-exchanged lead affecting the short-range (intratetrahedral) structure of the samples.[17] The peak at 890 cm^{-1} only appears for the ion-exchanged samples, but its identity is unknown. All of the samples have medium absorptions in the intertetrahedral symmetric O-T-O stretch region at ~770 cm^{-1}, indicating little disruption of the intertetrahedral stretches.[17, 18] The ion-exchanged samples each have a peak at 713 cm^{-1} from lead nitrate.[40]

Retention of both of the ion-exchanged samples exhibit peaks in the nitrate absorbance region, which indicates some of the nitrate from the ion exchange remained after washing.[40] In the intratetrahedral region it can be seen that the intensities of the large peaks at ~1025 and ~973 cm^{-1} change their relative intensities from the as-made to the ion-exchanged samples. This may indicate a change in intratetrahedral structure upon ion exchange. The as-made sample also has a peak at 928 cm^{-1}, which is not apparent in the other samples. The reason for this peak is unknown, but it fits in the skeletal T-O-T vibrations. In the region from 770 cm^{-1} to 620 cm^{-1} the spectra are similar, but with slightly different peak intensities, which again indicates some changes in the structure upon ion exchange.

FIR VPI-9

The FIR spectra can be seen in Table B.4 and Figure B.6.

Table B.4 Table of Far-IR peaks of VPI-9 samples.

As-made VPI-9	VPI-9 C	VPI-9 A	Assignment
680 m	679 m	679 m	vs (O-T-O)[17]
631 m	630 m	629 m	double ring modes[17]
614 w	616 w	616 w	
540 m	542 m	540 m	
526 s, sh	525 s, sh	525 s, sh	
515 s	514 s	513 s	
495 sh	499 sh	496 sh	δ (O-T-O)[17]
489 sh	490 sh	490 sh	
453 s	453 s	455 s	
430 sh	431 sh	429 sh	
406 m	407 m	408 m	Pore opening modes[17]
373 m	373 m	372 m	
343 m	343 m	345 m	
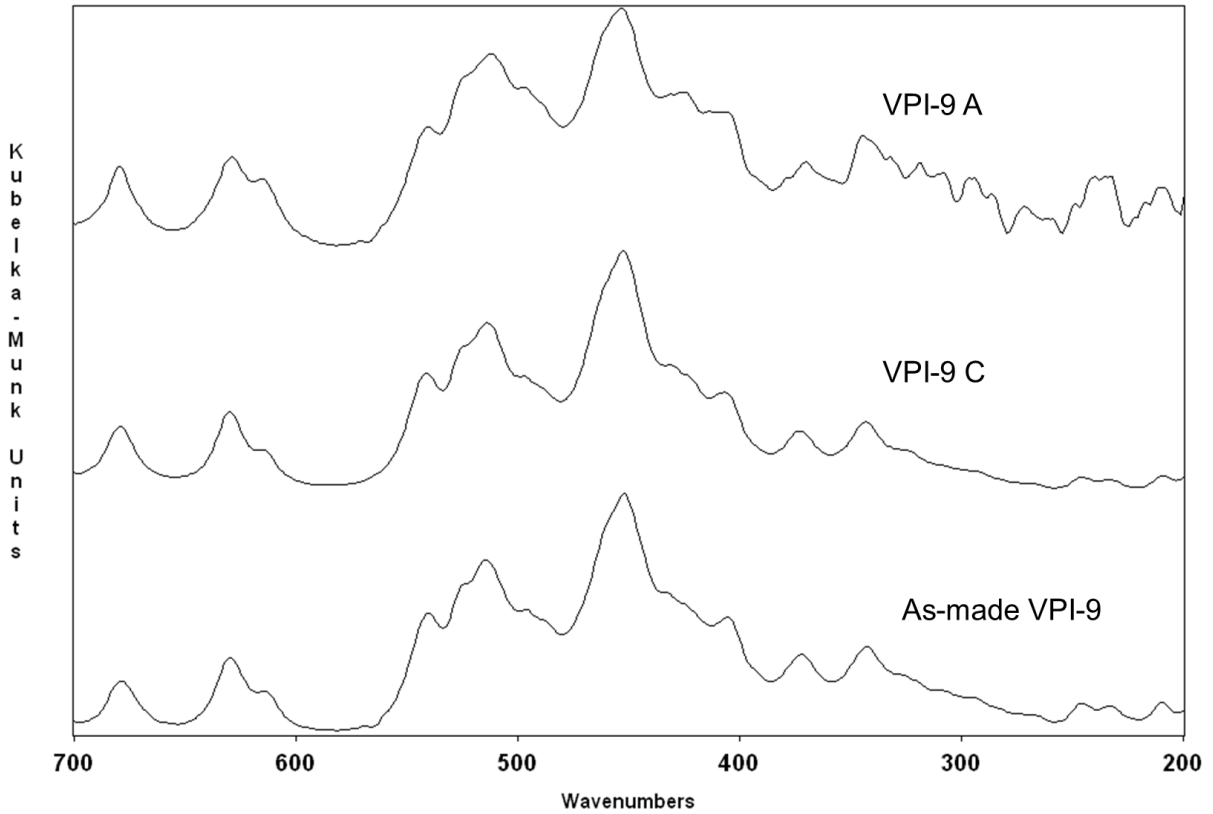
Figure B.6 Far-IR of VPI-9 samples.

The similarities between the spectra in this region, which primarily examines the long-range structure of the samples, is apparent. This indicates that despite the VPI-9 A sample becoming XRD amorphous, the there was no apparent change in the structure visible using FIR.

Comparing the IR visible structural effects of lead-ion exchange for VPI-7 and VPI-9, it is clear that the VPI-7 structure was changed more dramatically than VPI-9. This is likely due to the greater amount of lead ion-exchanged. This spectra is very similar between ion-exchanged and as-made VPI-9 sample, indicating that the ion exchange did not affect the inter- and intratetrahedral structure of the microporous molecular sieves as much as in VPI-7.

Conclusions

The mid- and far- infrared spectra of VPI-7 and VPI-9, and lead ion-exchanged molecular sieves have been reported and band assignments have been made. Inter- and intratetrahedral structure changes caused by lead ion-exchange can be clearly seen in the differences in the MIR and FIR of VPI-7 (Figures B.1, B.2, B.3, and B.4), while structure changes caused by lead ion-exchange in VPI-9 are more difficult to identify. This may be due to the smaller amount of lead that was ion-exchanged by VPI-9. This work demonstrates the utility of MIR and FIR for the qualitative analysis of chemical effects on zeolite structures as a compliment to XRD.

References

1. Lin, C. C. H.; Dambrowitz, K. A.; Kuznicki, S. M. Evolving applications of zeolite molecular sieves, *The Canadian Journal of Chemical Engineering* **2011**.

2. Davis, M. E.; Lobo, R. F. Zeolite and Molecular Sieve Synthesis, *Chemistry of Materials* **1992**, 756-768.

3. van Bekkum, H.; Cejka, J.; Corma, A.; Schueth, F. *Introduction to Zeolite Molecular Sieves;* Elsevier Science: 2007; .

4. Davis, M. E. Ordered porous materials for emerging applications, *Nature* **2002**, 813-821.

5. Kosslick, H.; Fricke, R. Chemical Analysis of Aluminosilicates, Aluminophosphates, and Related Molecular Sieves. In *Molecular Sieves;* Kosslick, H., Fricke, R., Eds.; Springer: Berlin/Heidelberg, 2007; Vol. 5, pp 1-66.

6. Valerio, G.; Goursot, A.; Vetrivel, R.; Malkina, O.; Malkin, V.; Salahub, D. R. Calculation of ^{29}Si and ^{27}Al MAS NMR Chemical Shifts in Zeolite-A Using Density Functional Theory: Correlation with Lattice Structure, *J. Am. Chem. Soc.* **1998**, 11426-11431.

7. Andy, P.; Davis, M. E. Dehydrogenation of Propane over Platinum Containing CIT-6, *Ind. Eng. Chem. Res.* **2004**, *12*, 2922-2928.

8. Baerlocher, C.; Olson, D. H.; Meier, W. M. *Atlas of Zeolite Framework Types;* Elsevier: Amsterdam, 2001; , pp 308.

9. Takewaki, T.; Beck, L. W.; Davis, M. E. Zincosilicate CIT-6: A Precursor to a Family of BEA-Type Molecular Sieves, *J. Phys. Chem. B* **1999**, *14*, 2674-2679.

10. Hajjar, R.; Millot, Y.; Man, P. P.; Che, M.; Dzwigaj, S. Two Kinds of Framework Al Sites Studied in BEA Zeolite by X-ray Diffraction, Fourier Transform Infrared Spectroscopy, NMR Techniques, and V Probe, *J. Phys. Chem. C* **2008**, *51*, 20167-20175.

11. Stevens, R. W.; Siriwardane, R. V.; Logan, J. In Situ Fourier Transform Infrared (FTIR) Investigation of CO2 Adsorption onto Zeolite Materials, *Energy & Fuels* **2008**, 3070-3079.

12. Chowdhury, A.; Thompson, P. R.; Milne, S. J. TGA-FTIR study of a lead zirconate titante gel made from a triol-based sol-gel system, *Thermochimica Acta* **2008**, 59-64.

13. Baltrusaitis, J.; Schuttlefield, J.; Jensen, J. J.; Grassian, V. H. FTIR spectroscopy combined with quantum chemical calculations to investiage adsorbed nitrate on aluminum oxide surfaces in the presence and absence of co-adsorbed water, *Physical Chemistry Chemical Physics* **2007**, 4970-4980.

14. May, M.; Asomoza, M.; Lopez, T.; Gomez, R. Precursor Aluminum Effect in the Synthesis of Sol− Gel Si− Al Catalysts: FTIR and NMR Characterization, *Chem. Mater.* **1997**, *11,* 2395-2399.

15. Endregard, M.; Nicholson, D. G.; Stoecker, M.; Beagley, B. Cobalticenium ions adsorbed on large-pore aluminophosphate VPI-5 studied by x-ray absorption, 13C solid-state NMR and FTIR spectroscopy, *J. Mater. Chem.* **1995**, *3,* 485-491.

16. Lercher, J. A.; Jentys, A. Infrared and Raman spectroscopy for characterizing zeolites, *Stud. Surf. Sci. Catal.* **2007**, 435-476.

17. Flanigen, E. M.; Khatami, H.; Szymanski, H. A. Infrared structural studies of zeolite frameworks, *Adv. Chem. Ser.* **1971**, 201-229.

18. Flanigen, E. M. Structural analysis by infrared spectroscopy, *ACS Monograph* **1976**, 80-117.

19. Mestl, G.; Knozinger, H. Vibrational Spectroscopies. In *Handbook of Heterogeneous Catalysis;* Ertl, G., Knozinger, H., Schuth, F. and Weitkamp, J., Eds.; Wiley-VCH: Weinheim, 2008; Vol. 2, pp 932-971.

20. Ozin, G. A.; Gil, C. Intrazeolite organometallics and coordination complexes: internal versus external confinement of metal guests, *Chemical Reviews* **1989**, *8,* 1749-1764.

21. Godber, J., mark D. Baker,Geoffrey A.Ozin Far-IR Spectroscopy of Alkali-Metal and Alkaline-Earth Cations in Faujasite Zeolites, *J. Phys. Chem.* **1989**, 1409-1421.

22. Ozin, G. A.; Baker, M. D.; Godber, J.; Wu, S. Crystal-field effects on the far-infrared cation vibrations of transition metal (2+) ion exchanged faujasite zeolites, *J. Am. Chem. Soc.* **1985**, *7,* 1995-2000.

23. Baker, M. D.; Ozin, G. A.; Godber, J. Direct probe Fourier transform far-infrared spectroscopy of metal atoms, metal ions, and metal clusters in zeolites, *Catal. Rev.* **1985**, *4,* 591-651.

24. Baker, M. D.; Godber, J.; Ozin, G. A. Frequency and intensity considerations in the far-IR spectroscopy of faujasite zeolites: experiment and theory. Metal cation vibrational assignments, site locations, and populations, *J. Am. Chem. Soc.* **1985**, *11,* 3033-3043.

25. Baker, M. D.; Godber, J.; Helwig, K.; Ozin, G. A. Probing extra-framework cations in alkali- and alkaline-earth-metal Linde type A zeolites by Fourier transform far-infrared spectroscopy, *J. Phys. Chem.* **1988**, *21,* 6017-6024.

26. McGown, T. Infrared Spectroscopy For The Characterization of Porous Zincosilicate Materials and Their Use in Lead Capture**2006**, 1.

27. Annen, M. J.; Davis, M. E.; Higgins, J. B.; Schlenker, J. L. VPI-7: the first zincosilicate molecular sieve containing three-membered T-atom rings, 1991.

28. Annen, M. J.; Davis, M. E.; Higgins, J. B.; Schlenker, J. L. In *In The physicochemical properties of VPI-7: a microporous zinco-silicate with three membered rings;* Materials Research Society Symposium Proceedings; 1991; Vol. 233, pp 245-253.

29. De Man, A. J. M.; Ueda, S.; Annen, M. J.; Davis, M. E.; Van Santen, R. A. The stability and vibrational spectra of three-ring containing zeolitic silica polymorphs, *Zeolites* **1992**, *September/October,* 789.

30. Annen, M. J.; Davis, M. E. Raman and ^{29}Si MAS NMR spectroscopy of framework materials containing three-membered rings, *Microporous Materials* **1993**, *1,* 57-65.

31. Rohrig, C.; Gies, H.; Marler, B. Rietveld refinement of the crystal structure of the synthetic porous zincosilicate VPI-7, *Zeolites* **1994**, 498-503.

32. McCusker, L. B.; Grosse-Kunstleve, R. W.; Baerlocher, C.; Yoshikaway, M.; Davis, M. E. Synthesis optimization and structure analysis of the zincosilicate molecular sieve VPI-9, *Microporous and Mesoporous Materials* **1996**, 295-309.

33. McKeen, J. C.; Davis, M. E. Conductivity of Mono- and Divalent Cations in the Microporous Zincosilicate VPI-9, *Journal of Physical Chemistry C* **2009**, *22,* 9870-9877.

34. Selbe, T. Applications of aluminosilicate and zincosilicate materials: aqueous phase ion exchange and gas phase adsorption, Kansas State University, Manhattan, Kansas, 2010.

35. Annen, M. J. Synthesis and Characterization of Novel Molecular Sieves Containing Three-Membered Rings, Virginia Polytechnic Institute and State University, Chemical Engineering, Blacksburg, VA, 1992.

36. Socrates, G. *Infrared Characteristic Group Frequencies;* John Wiley & Sons: Chichester, 1994; , pp 249.

37. Beta, I. A.; Böhlig, H.; Hunger, B. Structure of adsorption complexes of water in zeolites of different types studied by infrared spectroscopy and inelastic neutron scattering, *Physical Chemistry Chemical Physics* **2004**, *8,* 1975-1981.

38. Hunger, J.; Beta, I. A.; Bohlig, H.; Ling, C.; Jobic, H.; Hungers, B. Adsorption structures of water in NaX studied by DRIFT spectroscopy and neutron powder diffraction, *J Phys Chem B* **2006**, *1,* 342-353.

39. Sobalik, Z.; Tvaruazkova, Z.; Wichterlova, B. Skeletal T-O-T Vibrations As a Tool for Characterization of Divalent Cation Complexation in Ferrierite, *Journal of Physical Chemistry B* **1998**, *7,* 1077-1085.

40. Kinugasa, S.; Tanabe, K.; Tamura, T. Spectral Database for Organic Compounds. *http://riodb01.ibase.aist.go.jp/sdbs/cgi-bin/direct_frame_top.cgi* (accessed July 29, 2010, July, 2010).

41. Jentys, A.; Warecka, G.; Derewinski, M.; Lercher, J., A. Adsorption of Water on ZSM-5 Zeolites, *J. Phys. Chem.* **1989**, 4837-4843.

42. Szymanski, H. A.; Stamires, D. N.; Lynch, G. R. Infrared spectra of water sorbed on synthetic zeolites, *JOSA* **1960***, 12,* 1323-1328.

43. Frohnsdorff, G. J. C.; Kington, G. L. A note on the thermodynamic properties and infra-red spectra of sorbed water, *Proceedings of the Royal Society of London.Series A, Mathematical and Physical Sciences* **1958***, 1251,* 469-472.

Appendix C - The Effects of Aluminum Isopropoxide Sublimation on Aluminophosphate Molecular Sieve Particle Size

Sean R. Tomlinson, Xin Sun, John R. Schlup, Jennifer L. Anthony*

Abstract

The effect of the polymeric state of the aluminum isopropoxide reagent on the particle size of $AlPO_4$-5 and $AlPO_4$-11 aluminophosphate molecular sieves (AlPOs) is examined. AlPOs were synthesized in both water and ionic liquid solutions with sublimated and unsublimated aluminum isopropoxide, and the AlPO particle sizes are compared. The systems are also examined for the effect of solvent on the syntheses, as well as the effect of differences in temperature and duration of heating. It is found that sublimation of aluminum isopropoxide produces significantly larger particles in all syntheses. Solvent is found to play an important role in $AlPO_4$-5 particle sizes, but a less significant role in $AlPO_4$-11 particle sizes. The duration of heating and temperature have a small effect the product formed in $AlPO_4$-5 syntheses. Aluminum isopropoxide's role is discussed and causes of the larger particles produced are identified.

Introduction

Microporous materials, including aluminosilicate zeolites and aluminophosphate molecular sieves (AlPOs), are widely used in a variety of applications such as catalysis, ion exchange, soaps, and membranes.[1-4] Because of their wide variety of applications, much attention has been devoted to the formation of both aluminosilicates and aluminophosphates in the effort to direct their synthesis, with particular emphasis on controlling particle size.[5-9] Solution chemistry effects on aluminosilicate formation have been examined in a variety of papers wherein the authors have analyzed the effects of alkalinity,[10-12] the effects of cation-to-aluminum ratio,[13] silica-to-alumina ratio,[14] and the effects of sodium ions and ageing.[15] The effects of both the silica[16] and aluminum source[17-20] have been examined. Additionally, the impact of agitation on the solution have been investigated.[21, 22]

Aluminophosphate molecular sieves have received less attention,[23] but work has been done to examine the effects of temperature control,[24] water content,[25] and seeded growth.[26] A novel method of AlPO synthesis uses ionic liquids (IL), low-melting point organic salts, as the solvent to replace water in a method called ionothermal synthesis.[27-29] Because of the IL's polarity they can dissolve the precursors of AlPOs and behave as both solvent and structure directing agent.[30] In particular, the vanishingly low vapor pressure of many ionic liquids is beneficial for safety.[31] Finally, new framework structures have been synthesized in ionic liquids that have not been synthesized in water,[32-34] as well as modified versions of previously known structures.[35]

Aluminum isopropoxide is a common reagent for both zeolite and AlPO synthesis.[36-40] Aluminum isopropoxide exists in three polymeric forms, a dimer in the vapor phase[41, 42] and as a trimer upon distillation that ages to a tetramer in the solid phase.[41, 43-45] Duda et al. have reported that the trimer and tetramer form have been found to behave differently as initiators for organic polymerization reactions, wherein the trimer form reacts more rapidly than the tetramer form.[46-48] However, how the different polymeric states affect microporous molecular sieve syntheses has not been reported.

In this work we examine how the trimer and tetramer forms of aluminum isopropoxide affect AlPO particle size. Two AlPOs, AlPO$_4$-5 (AFI) and AlPO$_4$-11 (AEL) are synthesized using both hydrothermal (water as solvent) and ionothermal synthesis with sublimated (trimeric) and unsublimated (tetrameric) aluminum isopropoxide. The crystal structures are confirmed with

X-ray diffraction (XRD), and their particle sizes were measured via scanning-electron microscope (SEM).

Experimental Section

Aluminum isopropoxide (99%, Aldrich) was sublimated in a glass vessel in an oil bath at 140°C, under vacuum, with a tap water condenser. Syntheses were performed immediately with the freshly sublimated aluminum isopropoxide to minimize aging effects. The unsublimated aluminum isopropoxide was used directly from the container with no further purification.

Hydrothermal synthesis of AlPO$_4$-11 (AEL) was performed as follows. A gel with the mole ratio composition of 1 Al$_2$O$_3$: 1 P$_2$O$_5$: 1 dipropylamine: 70 H$_2$O was prepared. Orthophosphoric acid (85%, Fisher) and aluminum isopropoxide (99%, Aldrich) were added to water and stirred at room temperature for 90 minutes. Then dipropylamine (DPA; 99%, Acros) was added before stirring another 90 minutes. The mixture was then transferred to a Teflon liner in a stainless steel autoclave. The mixture was heated at 185°C for 30 hours. The autoclave was quenched in water, allowed to cool, and then the product was recovered with a Fisher Scientific Centrific Model 228 centrifuge operating at 3,300 rpm for 5 minutes. The clear solution was decanted. The solid product was washed and centrifuged again for 5 minutes. This solution was decanted, and the product dried.

Ionothermal synthesis of AEL used the ionic liquid 1-ethyl-3-methylimidazolium bromide (emimBr) as the solvent. The molar composition of the gel was 1 Al$_2$O$_3$: 2.6 P$_2$O$_5$: 0.6 HF: 20 emimBr: 1.5 DPA. Aluminum isopropoxide, phosphoric acid, hydrofluoric acid, and DPA were added to the previously melted ionic liquid and then stirred vigorously at 100°C for 30 minutes. The mixture was then transferred to a Teflon liner in a stainless steel autoclave, heated at 190°C for 4 hours, quenched, and allowed to cool. The solid product was recovered via centrifuge for 5 minutes, and the clear solution was decanted. The product was washed, centrifuged again for 5 minutes, the solution was decanted, and the product dried.

Hydrothermal synthesis of AlPO$_4$-5 (AFI) was performed with a gel have a composition with mole ratios of 1 Al$_2$O$_3$: 1.3 P$_2$O$_5$: 1 tripropylamine: 40 H$_2$O. Orthophosphoric acid (85%, Fisher) and aluminum isopropoxide (99%, Aldrich) were added to the water and stirred at room temperature for 30 minutes. Tripropylamine (TPA; 99%, Acros) was added before stirring another 30 minutes. The mixture was then transferred to a Teflon liner in a stainless steel

159

autoclave. The mixture was heated at 150°C for 48 hours. The autoclave was quenched in water and allowed to cool. The product was centrifuged for 5 minutes, and the clear solution was decanted. The solid product was washed, centrifuged again for 5 minutes. The supernatant solution was decanted, and the product dried. To compare effects of heating time and temperature on the synthesis, this synthesis was repeated with sublimated aluminum isopropoxide for 4 hours at 190°C, but yielded no crystalline product.

Ionothermal synthesis of AFI used the ionic liquid 1-butyl-3-methylimidazolium bromide (bmimBr) as the solvent. The gel molar composition was 1 Al_2O_3: 2 P_2O_5: 0.6 HF: 20 bmimBr: 1.5 DPA. Aluminum isopropoxide, phosphoric acid, hydrofluoric acid, and DPA were added to the previously melted ionic liquid and then stirred at 100°C for 30 minutes. Then the mixture was transferred to a Teflon liner in a stainless steel autoclave, heated at 190°C for 4 hours, quenched, and allowed to cool. The product was recovered via centrifugation for 5 minutes, and the clear solution was decanted. The solid product was washed, centrifuged again for 5 minutes. That solution was decanted, and the product dried. To compare effects of heating time and temperature on the synthesis, this synthesis was repeated with sublimated aluminum isopropoxide for 48 hours at 150°C.

The framework structures of the materials were identified by powder X-ray diffraction, obtained on a Rigaku Miniflex II diffractometer with a graphite monochromator and CuKα radiation (λ = 1.5406 Å). The particle sizes were measured with scanning electron micrographs (SEM) performed on a Hitachi S-3400N scanning electron microscope. Particle sizes for each synthesis were measured using Martin's diameter.[49] At least 300 particles per sample were examined from multiple images.

Results and Discussion

Figures C.1 and C.2 show the powder XRD of the AEL and AFI samples. All of the results match with the powder patterns from the International Zeolite Association database.[50] These figures confirm the synthesis of the AEL and AFI type AlPOs using the novel ionothermal synthesis methods described above.[50]
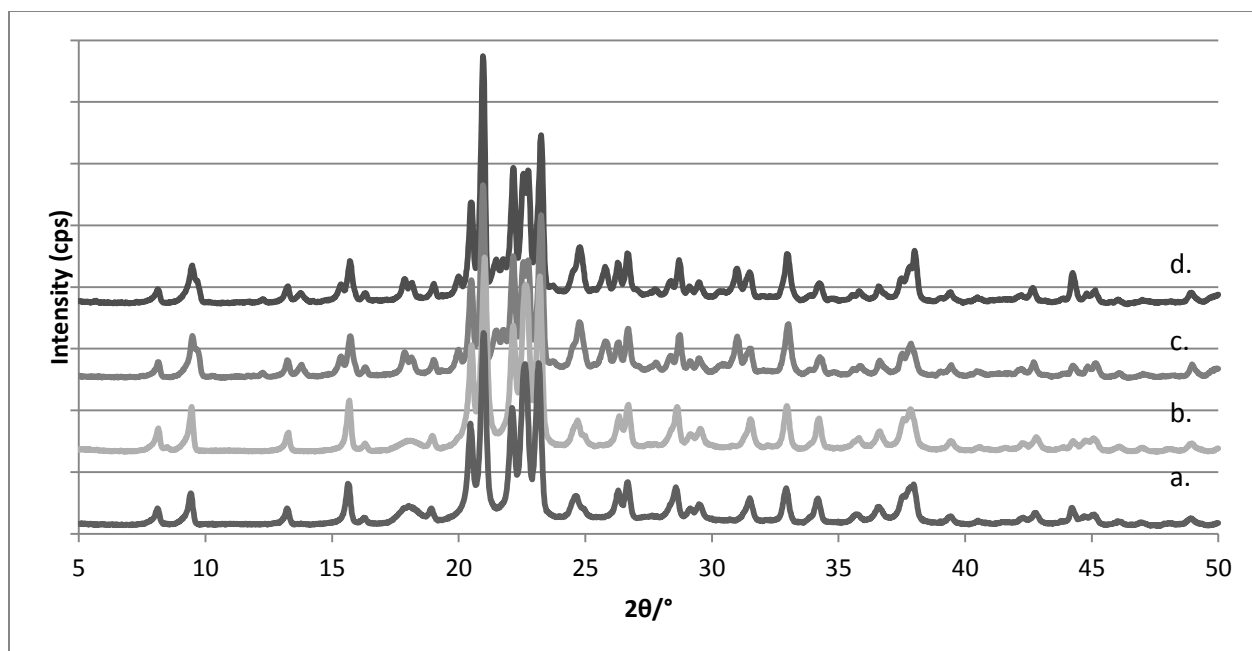
Figure C.1 XRD patterns of (a) hydrothermal AEL with sublimated aluminum isopropoxide, (b) hydrothermal AEL with unsublimated aluminum isopropoxide, (c) ionothermal AEL with sublimated aluminum isopropoxide, and (d) ionothermal AEL with unsublimated aluminum isopropoxide.
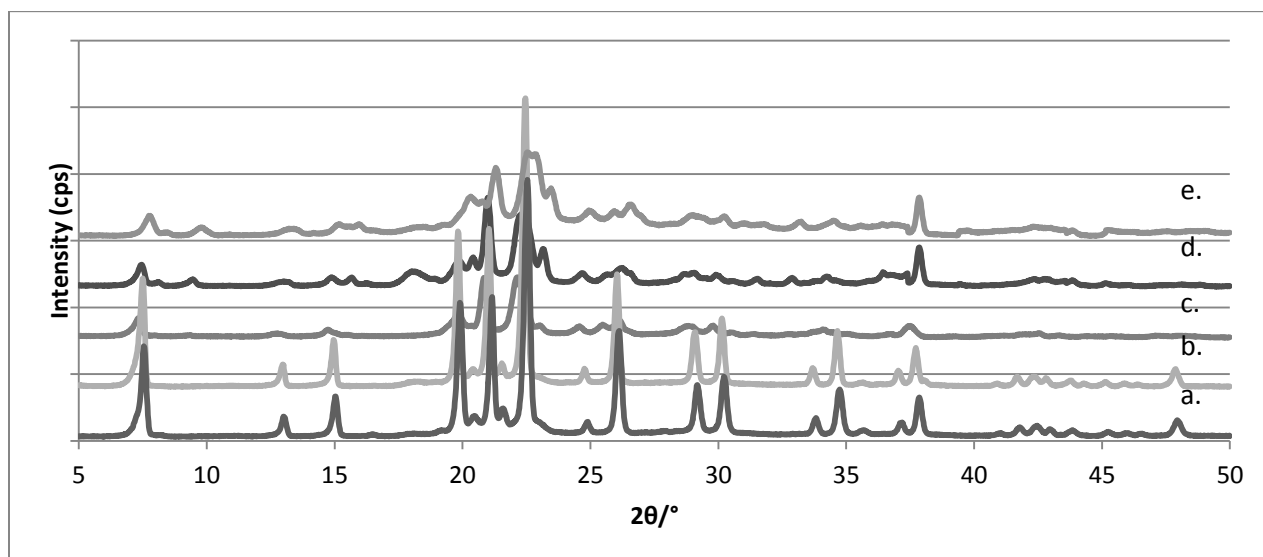
Figure C.2. XRD patterns of (a) hydrothermal AFI with sublimated aluminum isopropoxide, (b) hydrothermal AFI with unsublimated aluminum isopropoxide, (c) ionothermal AFI with sublimated aluminum isopropoxide, (d) ionothermal AFI with unsublimated aluminum isopropoxide, and (e) ionothermal AFI with sublimated aluminum isopropoxide 48 hour syntheses.

Table C.1 gives the mean and median particle size, the standard deviation of the particle size distribution, and the largest particle found for each sample. The smallest particles observed in all syntheses were approximately 0.5 μm. Figure C.3 compares the mean particle size for all of the syntheses with a 99% confidence interval for each sample mean.

Table C.1 Aluminophosphate particle size information (in µm) including mean (with experimental error), standard deviation, median, and largest particle obtained.

	Hydrothermal AEL	Ionothermal AEL	Hydrothermal AFI	Ionothermal AFI
Sublimated aluminum isopropoxide – Mean (µm)	5.0 ± 0.6	5.4 ± 1	19.8 ± 1.5	3.4 ± 0.6
Standard deviation (µm)	4.2	7.2	18.8	2.3
Median (µm)	3.5	2.8	11.6	2.9
Unsublimated aluminum isopropoxide – Mean (µm)	3.3 ± 0.6	3.6 ± 0.8	7.5 ± 0.9	1.6 ± 0.4
Standard deviation (µm)	3.6	3.7	5.9	1.6
Median (µm)	2.1	2.4	6.1	1.0
48 hour, 150°C synthesis of ionothermal AFI – Mean (µm)				2.0 ± 0.5
Standard deviation (µm)				1.8
Median (µm)				1.4
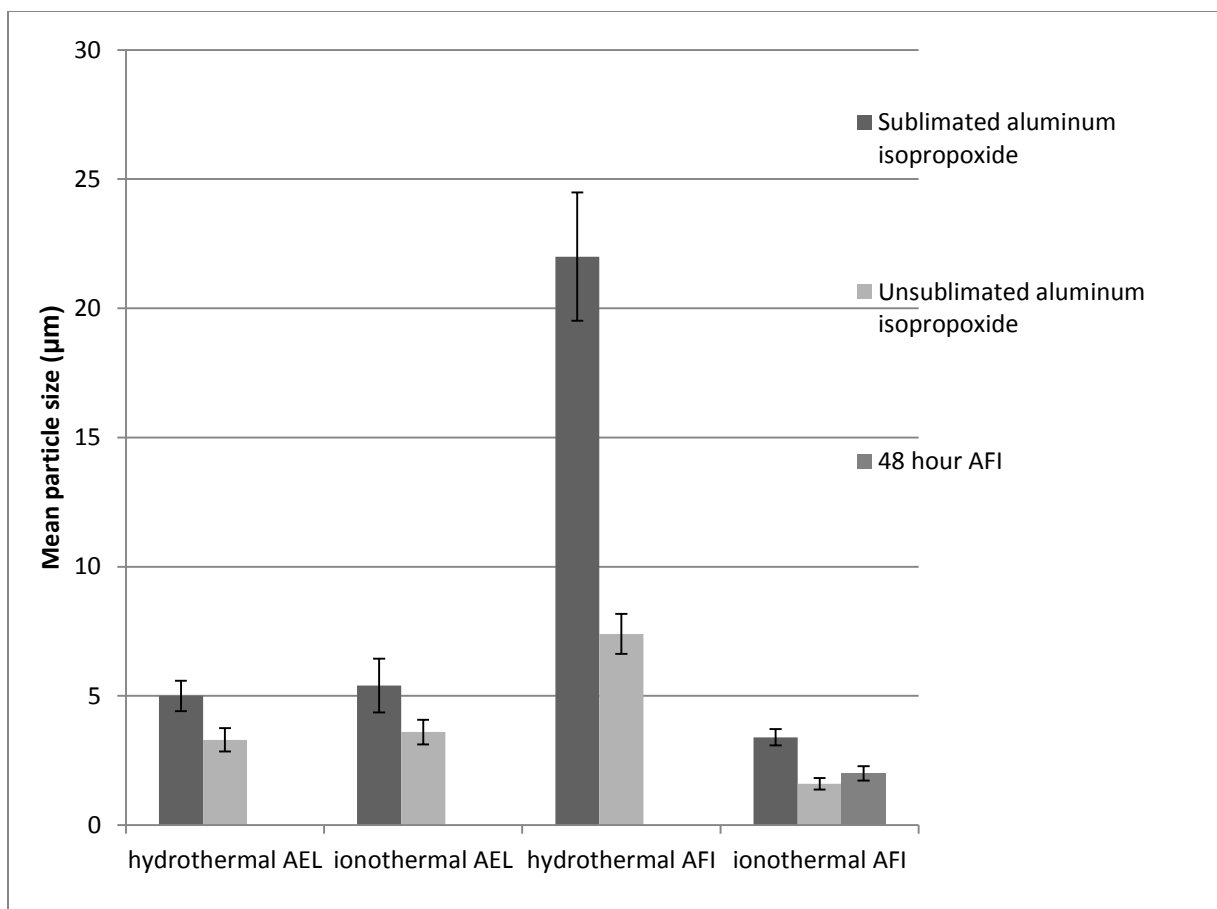
Figure C.3 Sample mean particle size of AEL and AFI, synthesized both hydrothermally and ionothermally with bars showing 99% confidence interval ($\alpha = 1\%$) for the mean. In every sample the mean particle size for the sublimated sample is statistically greater than the unsublimated sample.

As seen in Table C.1, a broad range of particle sizes were obtained for each sample, which contributes to the differences between the mean and median particle sizes. The smallest particles observed from all the syntheses were approximately 0.5 μm, and the largest particles obtained from each synthesis are noted in Table C.1. The sample mean with a 99% confidence interval ($\alpha = 1\%$) is used to compare the particle size distributions in Figure C.3. The confidence interval indicates the reproducibility of the mean and the region in which 99% of the measurements of the mean will fall. The mean particle size of each sample prepared with sublimated aluminum isopropoxide is statistically greater than the mean particle size of samples prepared with unsublimated aluminum isopropoxide (as shown by the 99% confidence interval). The particle size distributions for each sample are available in the supporting information.[51]

The synthesis of AEL yields similar particle sizes for hydro- (5.0 and 3.3 μm) and ionothermal (5.4 and 3.6 μm) syntheses, showing that they are insensitive to water versus ionic liquid as the solvent. However, the mean of the hydrothermal AFI samples is much larger (19.8 and 7.5 μm) than the mean of the ionothermal AFI (3.4 and 1.6 μm), showing a strong solvent sensitivity.

The effect on particle size of water concentration for similar synthesis methods can be seen in the differences between hydrothermal AEL and AFI. Hydrothermal AEL (Figures C.4(a) and C.4(b),) was synthesized with a water to alumina mole ratio of 70, while hydrothermal AFI (Figures C.5(a) and C.5(b),) was synthesized with a water to alumina mole ratio of 40. The lower water mole ratio resulted in larger particles when using either sublimated or unsublimated aluminum isopropoxide. In 2000 Wan et al. reported that an increase in solution concentration yields larger and more rapid particle formation for AFI.[25] The lower amount of water in the AFI synthesis (therefore higher concentration of reactants) compared to the AEL synthesis may explain the larger particle size for the hydrothermal AFI compared to hydrothermal AEL.[25]

The effect of different ionic liquids used at the same alumina-to-solvent mole ratio can be seen in the differences between ionothermal AEL and AFI. Ionothermal AEL was synthesized with emimBr, while ionothermal AFI was synthesized with the larger bmimBr. The different ionic liquid may explain the different particle sizes obtained. In 2002, Seddon et al. demonstrated that smaller cations have a lower viscosity, given the same temperature and anion, than larger cations.[52] Thus, the smaller particles in AEL may be due to the lower viscosity of the larger bmimBr ionic liquid slowing mass transfer because of its higher viscosity, thus promoting larger crystals.

In addition to solvent effects, the effect of heating duration and temperature were examined. Originally hydrothermal AFI was heated for 48 hours at 150°C, and ionothermal AFI was heated for 4 hours at 190°C. To examine the effect of synthesis conditions on the product particle size, the synthesis conditions were reversed. Hydrothermal AFI with sublimated aluminum isopropoxide was heated for 4 hours at 190°C, and ionothermal AFI with sublimated aluminum isopropoxide was heated for 48 hours at 150°C. These syntheses were chosen because they produced the same material with a large difference in particle sizes from very different synthesis times and temperatures. The goal was to see what particle sizes would result from a shorter time with higher temperature for the hydrothermal synthesis and from a longer time with

lower temperature for the ionothermal synthesis. The hydrothermal synthesis at shorter time and higher temperature produced no crystalline product, but the ionothermal synthesis at longer time and lower temperature did produce AFI. The crystals, however, were significantly smaller than those produced by heating the sample for 4 hours at 190°C. This indicates that while time and temperature do play a role in the synthesis, the composition of the solution is more influential.
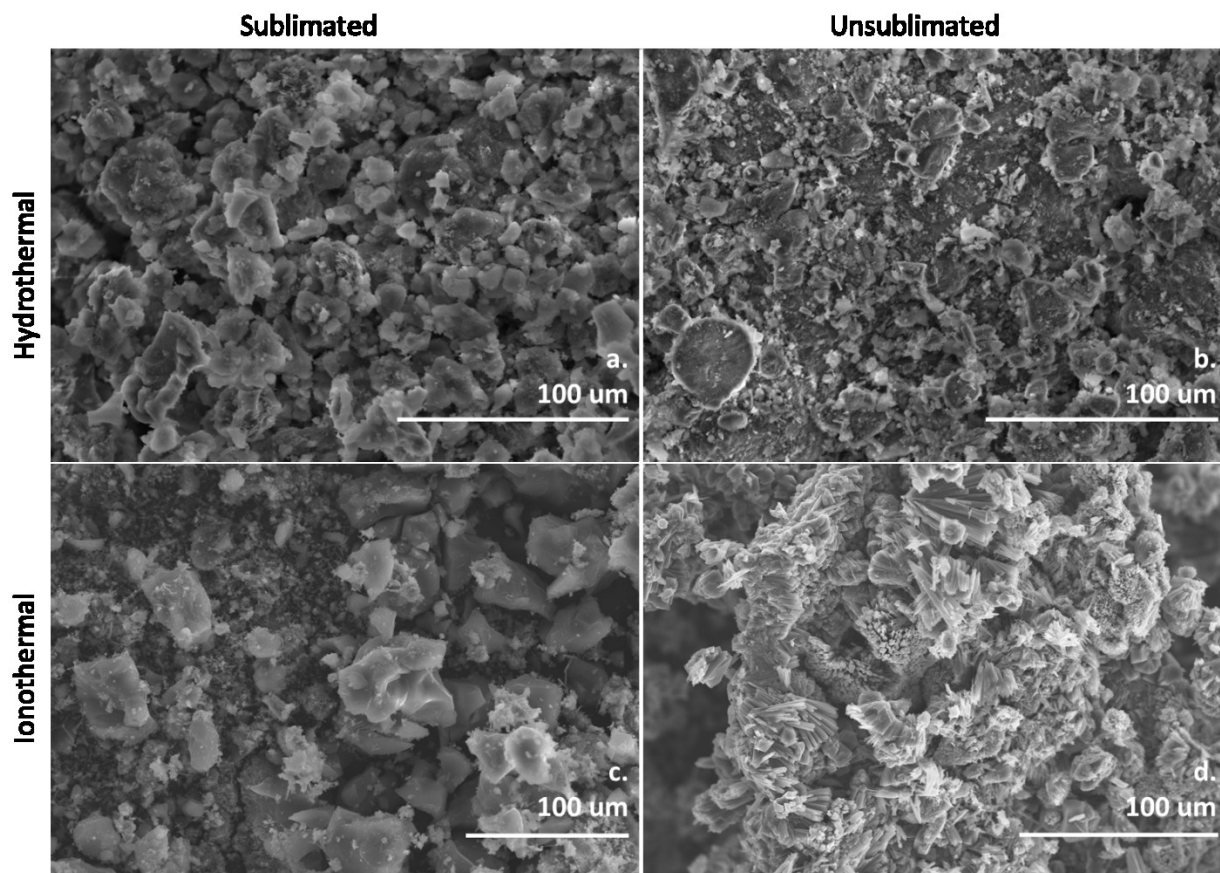

Figure C.4 SEM images of AEL AlPO products. Hydrothermal syntheses images a and b, ionothermal syntheses images c and d. Syntheses with sublimated aluminum isopropoxide a and c, with unsublimated aluminum isopropoxide b and d. Larger particles resulting from the use of sublimated aluminum isopropoxide are visible in the images.

As seen in Figure C.4, the AEL samples prepared with sublimated aluminum isopropoxide are larger than the samples prepared with unsublimated aluminum isopropoxide for both hydrothermal and ionothermal syntheses. However the particle sizes (as measured with Martin's diameter for all particles)[49] for both sublimated (4(a) and 4(c)) and both unsublimated (4(b) and 4(d)) syntheses are statistically similar, showing that the particle sizes from the AEL

syntheses were not dependent upon solvent. Images 4(a), 4(b), and 4(c) all show primarily single particles of irregular shapes over a broad range of sizes. By contrast, ionothermal AEL synthesized with unsublimated aluminum isopropoxide, seen in 4d, shows irregular aggregates of large rod-like particles, which were not seen in any other synthesis.
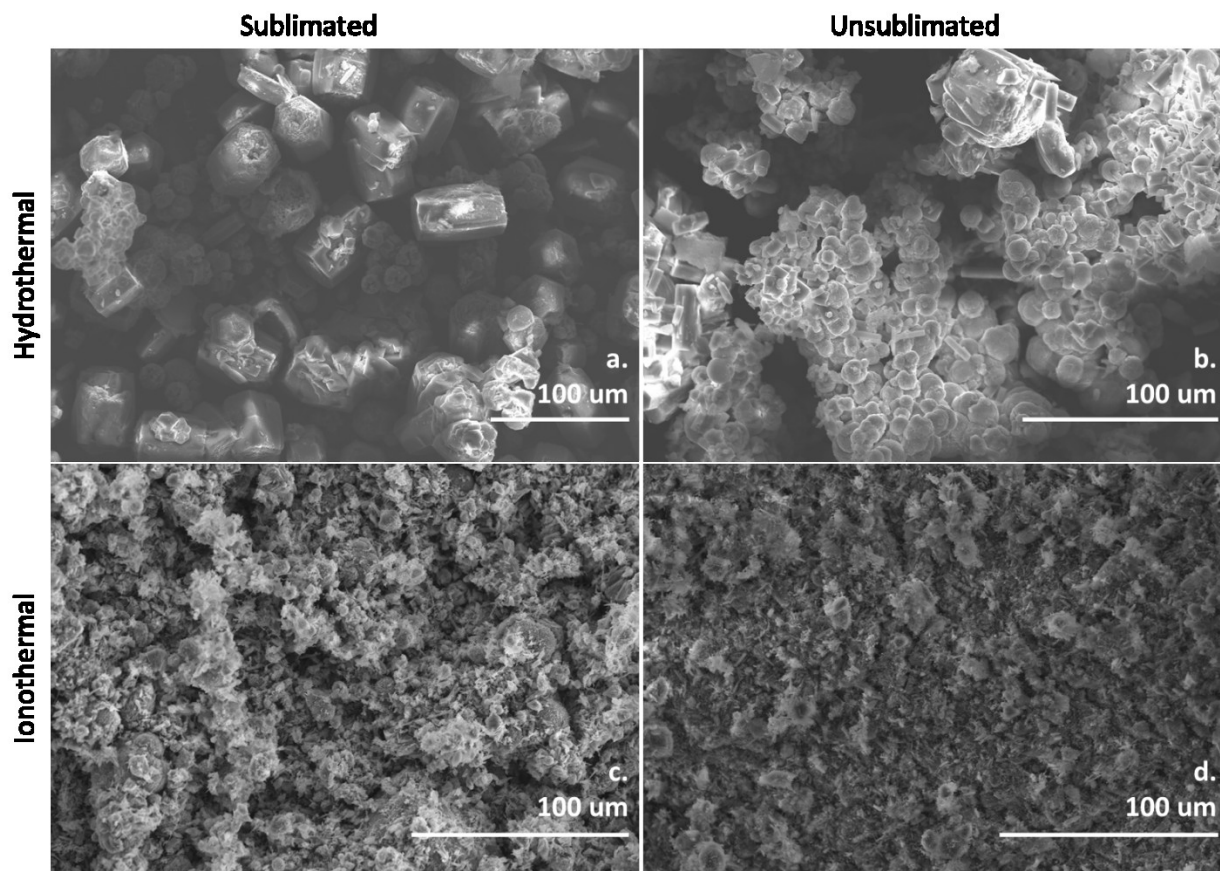
Figure C.5 SEM images of AFI AlPO products. Hydrothermal syntheses images a and b, ionothermal syntheses images c and d. Syntheses with sublimated aluminum isopropoxide a and c, with unsublimated aluminum isopropoxide b and d. Much larger particles are present in the hydrothermal syntheses (a and b) than in the ionothermal syntheses (c and d), showing the importance of the solvent in theses syntheses.

In contrast to Figure C.4, the AFI particles seen in Figure C.5 show a strong particle size dependence on solvent. The hydrothermal AFI syntheses yield the largest particles of the systems examined (with a mean particle size of 19.8 μm and 7.5 μm, for the samples prepared with sublimated and unsublimated aluminum isopropoxide, respectively), while the ionothermal AFI syntheses produced the smallest particles (with a mean particle size of 3.4 μm and 1.6 μm for the

samples prepared with sublimated and unsublimated aluminum isopropoxide, respectively). Image 5(a) shows large hexagonal prisms with some spherical particles, while 5(b) shows spherical agglomerates with some small prisms. The particles seen in images 5(a) and 5(b) are similar to those that have been seen in the literature, but these particles are much larger.[25] In 2000, Wan et al. showed the particle shape difference was due to different water concentrations in the original solutions; here the difference is due to the different aluminum isopropoxide used.[25] Images 5(c) and 5(d) are very similar, with more larger individual particles present in 5c, but the particles are very different from those obtained by hydrothermal synthesis.

Unlike the AFI syntheses where the solvent plays a large role in the particle size, the aluminum isopropoxide state affects all the systems. Aluminum isopropoxide has been found to exist in three polymer forms: a gas-phase dimer, and a trimer that slowly ages to a tetramer in the solid phase upon distillation.[41, 43-45, 53] As the sample ages after distillation, becoming less trimeric and more tetrameric, the melting point increases.[43] It has been found in our laboratory that aluminum isopropoxide samples with higher concentrations of trimeric form have a higher solubility.[54, 55] Therefore it is likely that as aluminum isopropoxide ages from trimer to tetramer, its solubility will decrease. In addition, the trimer is very soluble in pyridine while the tetramer is nearly insoluble.[56] Thus it is expected that the lower solubility of the tetramer will result in less mass transfer to the growing AlPO particles, resulting in smaller particles than the AlPO prepared with the aluminum isopropoxide trimer from sublimation. The trimer form of aluminum isopropoxide has been seen to react faster than the tetramer form in other reactions.[46-48] Therefore, different results from the syntheses when using sublimated (trimer) aluminum isopropoxide and unsublimated (tetramer) aluminum isopropoxide are expected. Figure C.6 shows SEM images of sublimated and unsublimated aluminum isopropoxide. Figure C.6(a) shows smaller, regular particle sizes for the sublimated aluminum isopropoxide, while Figure C.6(b) shows a very large particle with a range of particle sizes for the unsublimated aluminum isopropoxide.
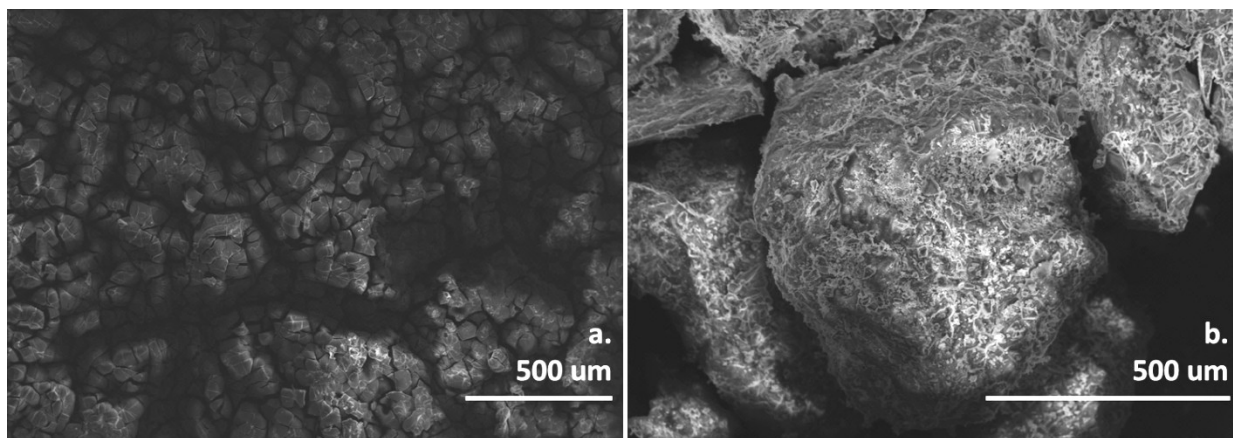
Figure C.6 SEM images of sublimated (a) and unsublimated (b) aluminum isopropoxide. (a) shows consistent particle size, while (b) shows a few very large particles with many smaller particles on the surface of the larger particles.

Sublimated aluminum isopropoxide yielding larger AlPO particles than unsublimated aluminum isopropoxide is likely due to several phenomena combining to increase mean particle size. It has been seen that sublimated (trimer) aluminum isopropoxide has greater solubility than unsublimated (tetramer) aluminum isopropoxide in pyridine.[56] Other work in our lab has shown that trimeric aluminum isopropoxide has greater solubility in ionic liquids than tetrameric aluminum isopropoxide.[54, 55] This higher solubility of the trimeric sublimated aluminum isopropoxide enables greater mass transfer to the growing AlPO particles, increasing AlPO particle size. Additionally, Ostwald ripening consumption of small AlPO precursors contributes as well. The increased solubility of sublimated aluminum isopropoxide leads to the rapid formation of many nascent AlPO particles, which are consumed by Ostwald ripening, yielding larger particles. This is in contrast to what occurs for the unsublimated aluminum isopropoxide which dissolves more slowly, resulting in fewer precursor units available to be consumed by Ostwald ripening and therefore a smaller mean particle size.

Conclusions

In the present work, we have examined the effects of sublimation of aluminum isopropoxide on aluminophosphate particle size. The results show that sublimation of the aluminum isopropoxide yields significantly larger particles. Sublimated aluminum isopropoxide dissolves more easily; and Ostwald ripening consumes the nascent AlPO particles formed in solution, increasing particle size. The AEL particle size was not influenced by using water versus

ionic liquid, but the AFI particle size depends on the solvent. The concentration of the solvent is important for the hydrothermal syntheses; less solvent (therefore a higher concentration of reactants) produced much larger particles for AFI compared to the larger amount of solvent present in the AEL syntheses. The duration and temperature of heating affect the product, but not sufficiently to explain the very large AFI particles produced.

Acknowledgments

References

1. Lin, C. C. H.; Dambrowitz, K. A.; Kuznicki, S. M. Evolving applications of zeolite molecular sieves, *The Canadian Journal of Chemical Engineering* **2011**.

2. van Bekkum, H.; Cejka, J.; Corma, A.; Schueth, F. *Introduction to Zeolite Molecular Sieves;* Elsevier Science: 2007; .

3. Cejka, J.; van Bekkum, H.; Corma, A.; Schueth, F. *Introduction to Zeolite Science and Practice, Volume 168, Third Edition (Studies in Surface Science and Catalysis;* Elsevier Science: Amsterdam, The Netherlands, 2007; Vol. 168, pp 1094.

4. Cundy, C. S.; Cox, P. A. The Hydrothermal Synthesis of Zeolites: History and Development from the Earliest Days to the Present Time, *Chem. Rev.* **2003**, 663-701.

5. Anthony, J. L.; Davis, M. E. Assembly of Zeolites and Crystalline Molecular Sieves. In *Self-Organized Nanoscale Materials;* Lockwood, D. J., Adachi, M., Eds.; Springer Science & Business Media, Inc.: New York, NY, 2006; pp 159-185.

6. Francis, R. J.; O'Hare, D. The kinetics and mechanisms of the crystallisation of microporous materials, *J. Chem. Soc. Dalt. Trans.* **1998***, 19,* 3133-3148.

7. Cundy, C. S.; Cox, P. A. The hydrothermal synthesis of zeolites: Precursors, intermediates and reaction mechanism, *Micro. Meso. Mater.* **2005**, 1-78.

8. Davis, M. E. Ordered porous materials for emerging applications, *Nature* **2002**, 813-821.

9. Beale, A. M.; Weckhuysen, B. M. Understanding the crystallisation processes leading to the formation of micropourous aluminophosphates, *From Zeolites to Porous MOF Materials - the 40th Anniversary of International Zeolite Conference* **2007**, 748.

10. Zaiku, X.; Qingling, C.; Bo, C.; Chengfang, Z. Influence of alkalinity on particle size distribution and crystalline structure in synthesis of zeolite beta, *Cryst. Eng.* **2001***, 4,* 359-372.

11. Ren, N.; Bronic, J.; Subotic, B.; Lv, X. C.; Yang, Z. J.; Tang, Y. Controllable and SDA-free synthesis of sub-micrometer sized zeolite ZSM-5. Part 1: Influence of alkalinity on the structural, particulate and chemical properties of the products, *Micro. Meso. Mater.* **2010**.

12. Bosnar, S.; Bronic, J.; Brlek, D.; Subotic, B. Chemically controlled particulate properties of zeolites: towards the face-less particles of zeolite A. 2. Influence of aluminosilicate batch concentration and alkalinity of the reaction mixture (hydrogel) on the size and shape of zeolite A crystals, *Micro. Meso. Mater.* **2010**.

13. Itani, L.; Bozhilov, K. N.; Clet, G.; Delmotte, L.; Valtchev, V. Factors That Control Zeolite L Crystal Size, *Chem-A Eur. J.* **2011***, 7,* 2199-2210.

14. Kosanovic, C.; Jelic, T. A.; Bronic, J.; Kralj, D.; Subotic, B. Chemically controlled particulate properties of zeolites: Towards the face-less particles of zeolite A. Part 1. Influence of the batch molar ratio [SiO2/Al2O3] b on the size and shape of zeolite A crystals, *Micro. Meso. Mater.* **2011**, *1-3,* 72-82.

15. Ren, N.; Bronic, J.; Subotic, B.; Song, Y. M.; Lv, X. C.; Tang, Y. Controllable and SDA-free synthesis of sub-micrometer sized zeolite ZSM-5. Part 2: Influence of sodium ions and ageing of the reaction mixture on the chemical composition, crystallinity and particulate properties of the products, *Micro. Meso. Mater.* **2011**.

16. Zhan, B. Z.; White, M. A.; Lumsden, M.; Mueller-Neuhaus, J.; Robertson, K. N.; Cameron, T. S.; Gharghouri, M. Control of particle size and surface properties of crystals of NaX zeolite, *Chem. Mater.* **2002**, *9,* 3636-3642.

17. Occelli, M. L.; Biz, S.; Auroux, A.; Ray, G. J. Effects of the nature of the aluminum source on the acidic properties of some mesostructured materials, *Micro. Meso. Mater.* **1998**, *1,* 193-213.

18. Lu, B.; Tsuda, T.; Sasaki, H.; Oumi, Y.; Itabashi, K.; Teranishi, T.; Sano, T. Effect of aluminum source on hydrothermal synthesis of high-silica mordenite in fluoride medium, and it's thermal stability, *Chem. Mater.* **2004**, *2,* 286-291.

19. Reddy, K. M.; Song, C. Synthesis of mesoporous molecular sieves: influence of aluminum source on Al incorporation in MCM-41, *Cat. Let.* **1996**, *1,* 103-109.

20. Salou, M.; Kooli, F.; Kiyozumi, Y.; Mikamizu, F. Effect of aluminium source and content on the synthesis of zeolite ZSM-5 from kanemite via solid-state transformation, *J. Mater. Chem.* **2001**, *5,* 1476-1481.

21. Brar, T.; France, P.; Smirniotis, P. G. Control of crystal size and distribution of zeolite A, *Ind. Eng. Chem. Res.* **2001**, *4,* 1133-1139.

22. Ding, L.; Zheng, Y.; Zhang, Z.; Ring, Z.; Chen, J. Effect of agitation on the synthesis of zeolite beta and its synthesis mechanism in absence of alkali cations, *J. Mater. Chem.* **2006**, *1-3,* 1-8.

23. Pastore, H. O.; Coluccia, S.; Marchese, L. Porous aluminophosphates: from molecular sieves to designed acid catalysts, *Annu. Rev. Mater. Res.* **2005**, 351-395.

24. Jhung, S. H.; Lee, J. H.; Chang, J. S. Crystal size control of transition metal ion-incorporated aluminophosphate molecular sieves: Effect of ramping rate in the syntheses, *Micro. Meso. Mater.* **2008**, *1-3,* 178-186.

25. Wan, Y.; Williams, C. D.; Duke, C. V. A.; Cox, J. J. Systematic studies on the effect of water content on the synthesis, crystallisation, conversion and morphology of AlPO4-5 molecular sieve, *J. Mater. Chem.* **2000**, *12,* 2857-2862.

26. Karanikolos, G., N; Garcia, H.; Corma, A.; Tsapatsis, M. Growth of $AlPO_4$-5 and CoAPO-5 films from amorphous seeds, *Micro. Meso. Mater.* **2008**, 11.

27. Cooper, E. R.; Andrews, C. D.; Wheatley, P. S.; Webb, P. B.; Wormald, P.; Morris, R. E. Ionic Liquids and Eutectic Mixtures as Solvent and Template in Synthesis of Zeolite Analogues, *Nature* **2004**, 1012-1016.

28. Parnham, E. R.; Morris, R. E. The Ionothermal Synthesis of Cobalt Aluminophosphate Zeolite Frameworks, *J. Amer. Chem. Soc.* **2006**, 2204.

29. Parnham, E. R.; Morris, R. E. 1-Alkyl-3-methyl Imidazolium Bromide Ionic Liquids in the Ionothermal Synthesis of Aluminum Phosphate Molecular Sieves, *Chem. Mater.* **2006**, 4882.

30. Morris, R. E. Ionothermal synthesis-ionic liquids as functional solvents in the preparation of crystalline materials, *Chem. Comm.* **2009**, 2990-2998.

31. Parnham, E. R.; Morris, R. E. Ionothermal Synthesis of Zeolites, Metal–Organic Frameworks, and Inorganic–Organic Hybrids, *Acc. Chem. Res.* **2007**, 1005.

32. Byrne, P. J.; Wragg, D. S.; Warren, J. E.; Morris, R. E. Ionothermal synthesis of two novel metal organophosphonates, *Dalton Trans.* **2009**, 795.

33. Parnham, E. R.; Wheatley, P. S.; Morris, R. E. The ionothermal synthesis of SIZ-6—a layered aluminophosphate, *Chem. Comm.* **2006***, 4,* 380-382.

34. Parnham, E. R.; Morris, R. E. Ionothermal synthesis using a hydrophobic ionic liquid as solvent in the preparation of a novel aluminophosphate chain structure, *J. Mater. Chem.* **2006**, 3682-3684.

35. Liu, L.; Wragg, D. S.; Zhang, H.; Kong, Y.; Byrne, P. J.; Prior, T. J.; Warren, J. E.; Lin, Z.; Dong, J.; Morris, R. E. Ionothermal synthesis, structure and characterization of three-dimensional zinc phosphates, *Dalton Trans.* **2009***, 34,* 6715-6718.

36. Dufau, N.; Luciani, L.; Rouquerol, F.; Llewellyn, P. Use of sample controlled thermal analysis toliberate the micropores of aluminophosphate AlPO4-11: evidenceof template evaporation, *J. Mater. Chem.* **2001***, 4,* 1300-1304.

37. Wang, J.; Song, J.; Yin, C.; Ji, Y.; Zou, Y.; Xiao, F. S. Tetramethylguanidine-templated synthesis of aluminophosphate-based microporous crystals with AFI-type structure, *Micro. Meso. Mater.* **2009***, 3,* 561-569.

38. Wragg, D. S.; Byrne, P. J.; Giriat, G.; Ouay, B. L.; Gyepes, R.; Harrison, A.; Whittaker, A. G.; Morris, R. E. In Situ Comparison of Ionothermal Kinetics Under Microwave And Conventional Heating, *J. Phys. Chem. C* **2009***, 48,* 296-319.

39. Ma, H.; Tian, Z.; Xu, R.; Wang, B.; Wei, Y.; Wang, L.; Xu, Y.; Zhang, W.; Lin, L. Effect of Water on the Ionothermal Synthesis of Molecular Sieves, *J. Amer. Chem. Soc.* **2008**, 8120.

40. Wang, L.; Xu, Y.; Wei, Y.; Duan, J.; Chen, A.; Wang, B.; Ma, H.; Tian, Z.; Lin, L. Structure-directing role of amines in the ionothermal synthesis, *J. Am. Chem. Soc.* **2006**, *23,* 7432-7433.

41. Bradley, D. C.; Mehrotra, R. C.; Rothwell, I. P.; Singh, A. *Alkoxo and Aryloxo Derivatives of Metals;* Academic Pr: 2001; .

42. Bradley, D. C.; Mehrotra, R. C.; Gaur, D. P. *Metal Alkoxides;* Academic Press: London, 1978; , pp 411.

43. Turova, N. Y.; Kozunov, V. A.; Yanovskii, A. I.; Bokii, N. G.; Struchkov, Y. T.; Tarnopol'skii, B. L. Physico-chemical and structural investigation of aluminium isopropoxide, *J. Inorg. Nucl. Chem.* **1979**, *1,* 5-11.

44. Turova, N. Y.; Turevskaya, E. P.; Kessler, V. G.; Yanovskaya, M. I. *The Chemistry of Metal Alkoxides;* Kluwer Academic Publishers: Boston, 2002; , pp 568.

45. Kleinschmidt, D. C.; Shiner Jr., V. J.; Whittaker, D. Interconversion Reactions of Aluminum Isopropoxide Polymers, *J. Org. Chem.* **1973**, *19,* 3334.

46. Duda, A.; Penczek, S. Polymerization of. epsilon.-Caprolactone Initiated by Aluminum Isopropoxide Trimer and/or Tetramer, *Macromolecules* **1995**, *18,* 5981-5992.

47. Duda, A. Polymerization of ε-caprolactone initiated by aluminum isopropoxide carried out in the presence of alcohols and diols. Kinetics and mechanism, *Macromolecules* **1996**, *5,* 1399-1406.

48. Kowalski, A.; Duda, A.; Penczek, S. Polymerization of L, L-lactide initiated by aluminum isopropoxide trimer or tetramer, *Macromolecules* **1998**, *7,* 2114-2122.

49. Allen, T. *Particle size measurement: Powder sampling and particle size measurement;* Springer: 1997; Vol. 1.

50. Baerlocher, C.; McCusker, L. B. Database of zeolite structures. *http://www.iza-structure.org/databases/*.

51. Sommer, K. 40 Years of Presentation Particle Size Distributions–Yet Still Incorrect? *Part. Part. Syst. Charact.* **2001**, *1,* 22-25.

52. Seddon, K. R.; Stark, A.; Torres, M. J. In *In Viscosity and density of 1-alkyl-3-methylimidazolium ionic liquids;* ACS Symposium series; ACS Publications: 2002; Vol. 819, pp 34-49.

53. Wilson, J. W. Heat of formation of tri-isopropoxyaluminium, *J. Chem. Soc. A* **1971***, 0,* 981-984.

54. Sun, X. Fundamental Research on the Solvent Role in the Ionothermal Synthesis of Microporous Materials, Kansas State University, .

55. Sun, X.; Anthony, J. L. Effect of structure of ionic liquids and phosphoric acid on the structure of aluminium isopropoxide, **2012**, Manuscript in preparation.

56. Shiner, V.; Whittaker, D.; Fernandez, V. The structures of some aluminum alkoxides, *J. Am. Chem. Soc.* **1963***, 15,* 2318-2322.

Appendix D - GRAMS/AI Peak-Fitting of Infrared Spectroscopic Information

Peak-Fitting Background

Infrared spectroscopy is a powerful qualitative tool for molecular analysis. It is possible to quantitatively analyze the spectra obtained, but the data must be curve-fit to obtain that quantitative information.[1-8] The infrared spectrometer control software WINFIRST version 3.61, June 17, 1999, was used for this research.

GRAMS/AI Software

The software used for this peak-fitting analysis is part of the GRAMS (Graphic Relational Array Management System) Spectroscopy Software Suite, Thermo Fisher Scientific Inc. This work was conducted on software version 9.00 R2. GRAMS/AI is capable of peak-fitting, data smoothing, quantitative analysis, peak picking, and integration. GRAMS/AI can be applied to data from FT-IR, NMR, diode-array UV-VIS, NIR, Raman, GC-MS, and chromatography. GRAMS/AI software has been widely used for FT-IR, Raman, NMR, and UV-VIS spectroscopy.[9-13]

Application of GRAMS Software to Peak-Fitting ATR Data

This section assumes that the user already has two spectra, a solvent spectrum and a solution spectrum using the same solvent. The solution spectrum is the spectrum of the solvent with solute.

To open GRAMS/AI, double click on the icon on the desktop or find it in the start menu. After opening the program, the user will see Figure D.1, the blank graphic user interface of the program.
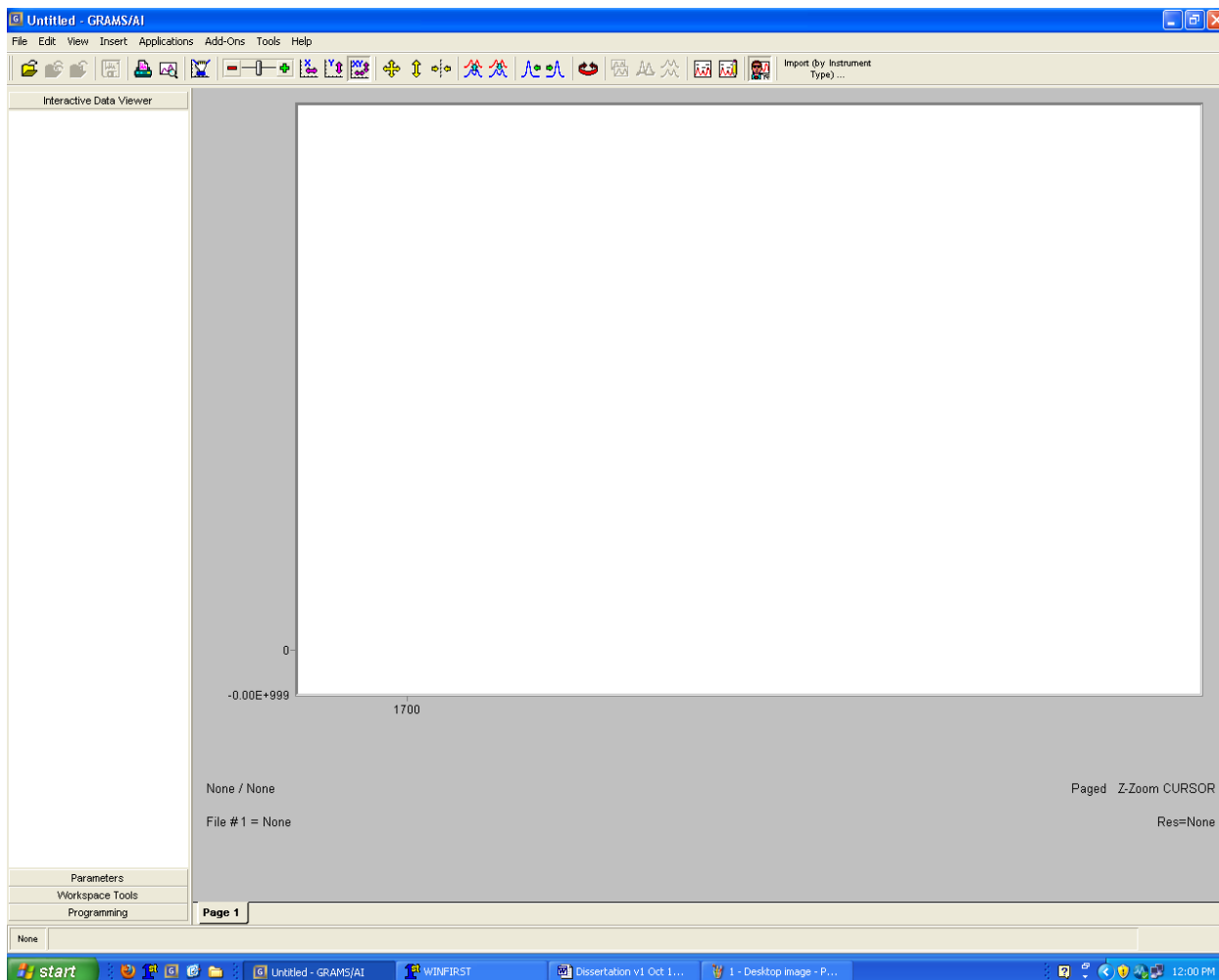
Figure D.1 GRAMS graphic user interface.

Since the WinFIRST software used to obtain the spectrum for this research uses a different file format than GRAMS/AI, the first step is to change the format of the file. To do that, click on the "Import (by Instrument Type)…" button in the top center of the image (see Figure D.2).
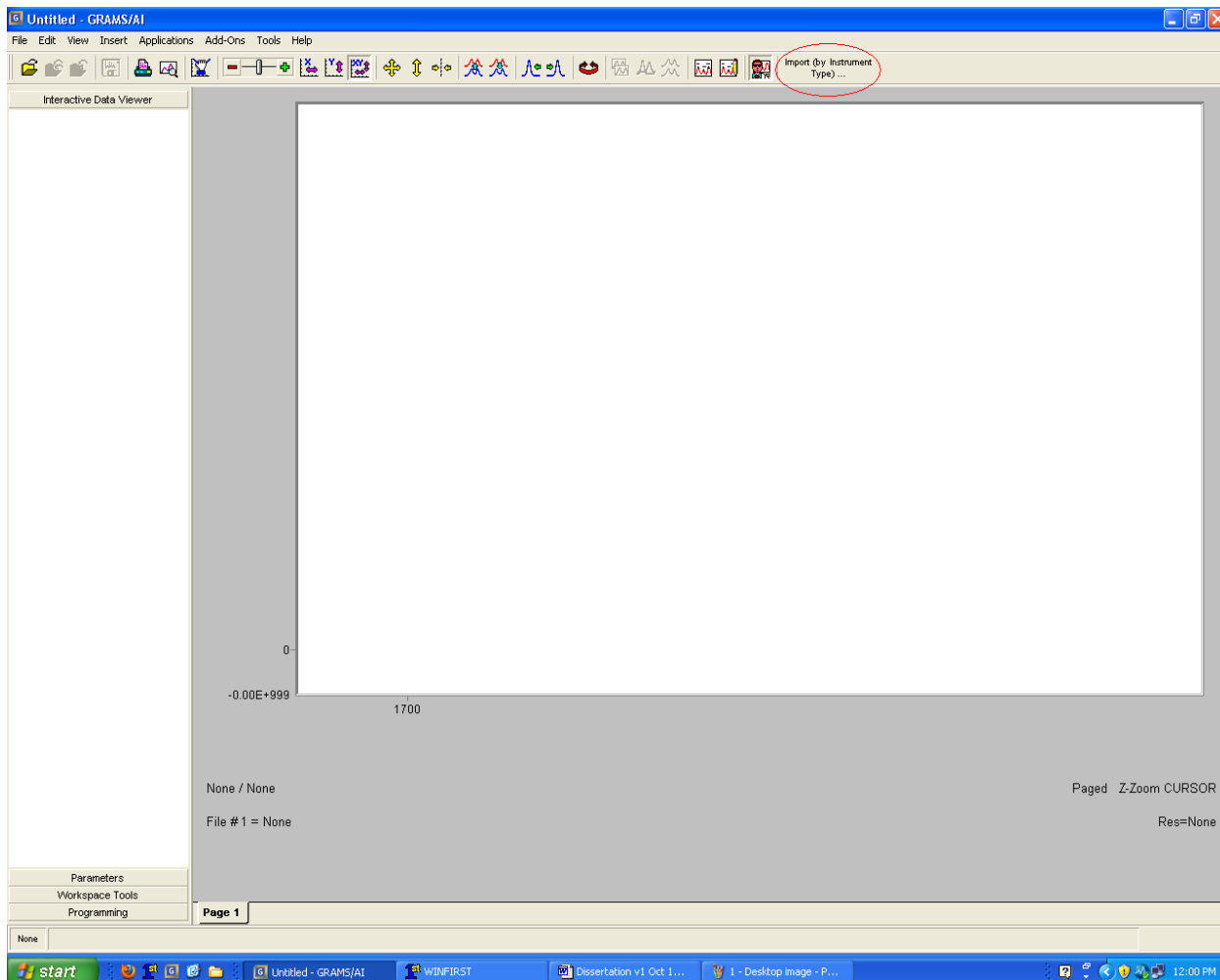
Figure D.2 Import (by Instrument Type)... button.

Then scroll through the "GRAMS/AI – Import File" list to find the type of instrument that was used. In this case, use the "Mattson FIRST/WinFIRST FT-IR". Then click Next (Figure D.3).
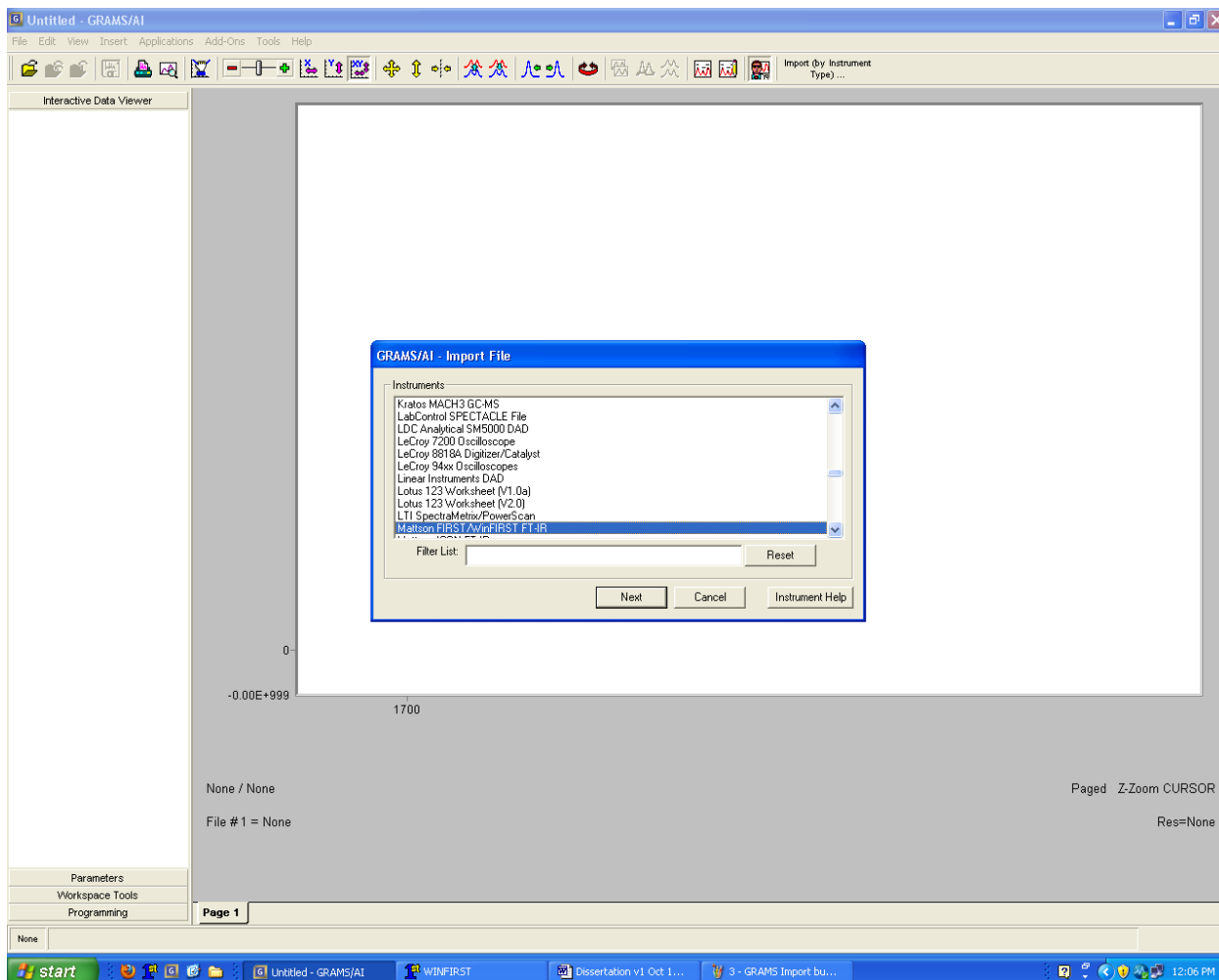
Figure D.3 Selecting file type to import.

The user will have to be aware of what file type they are using. In this case, it is the .abs (absorbance) file type, and the particular file of interest is OC1112S1.abs (the October 11th, 2012, pure solvent absorbance spectrum). Select the solvent file that needs to be saved as a new file type (Figure D.4).
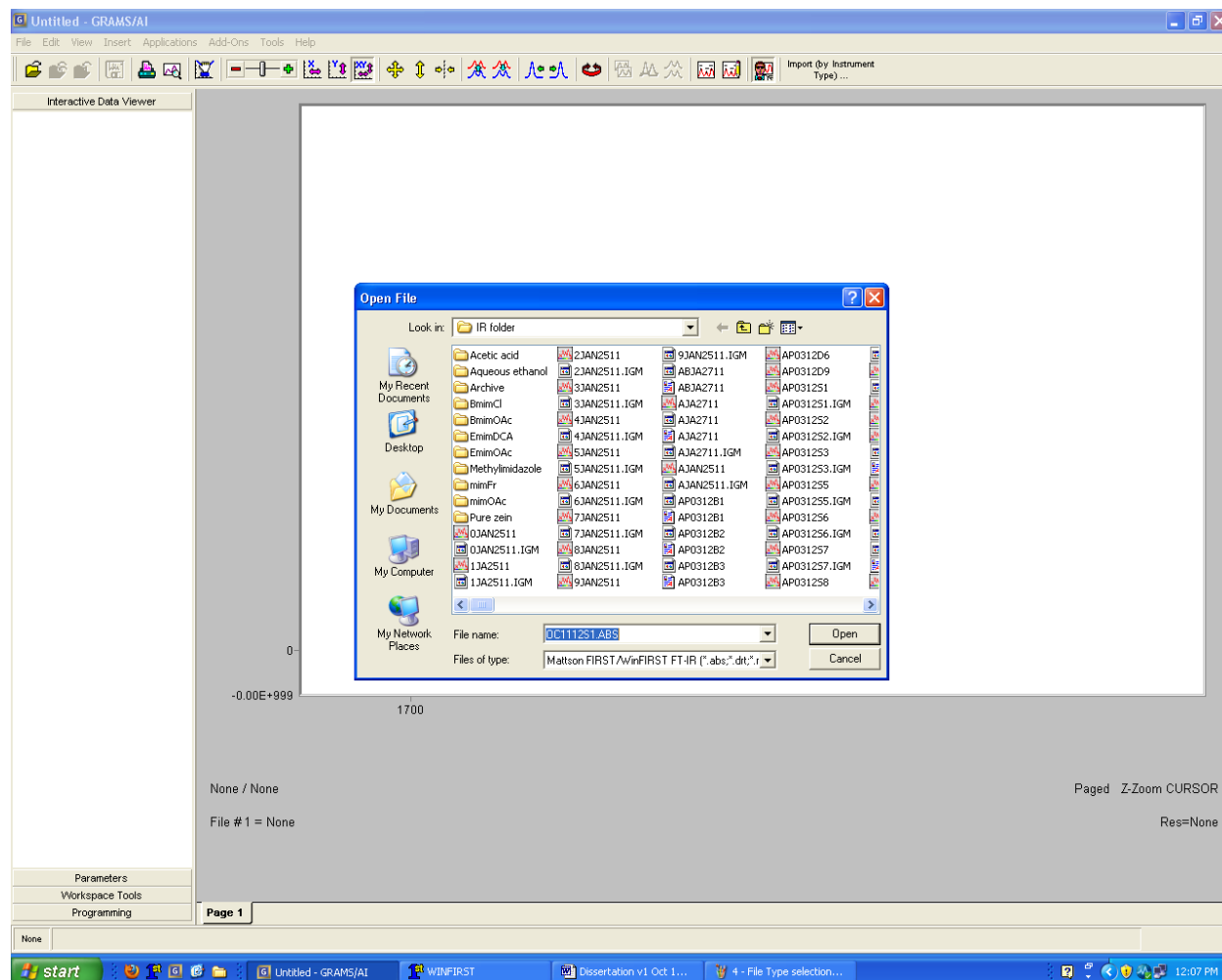
Figure D.4 Opening solvent spectrum file.

With the solvent spectrum on the main screen, now go to File > Save Trace As, then find where to save the file and save it as a .spc file type (Figure D.5).
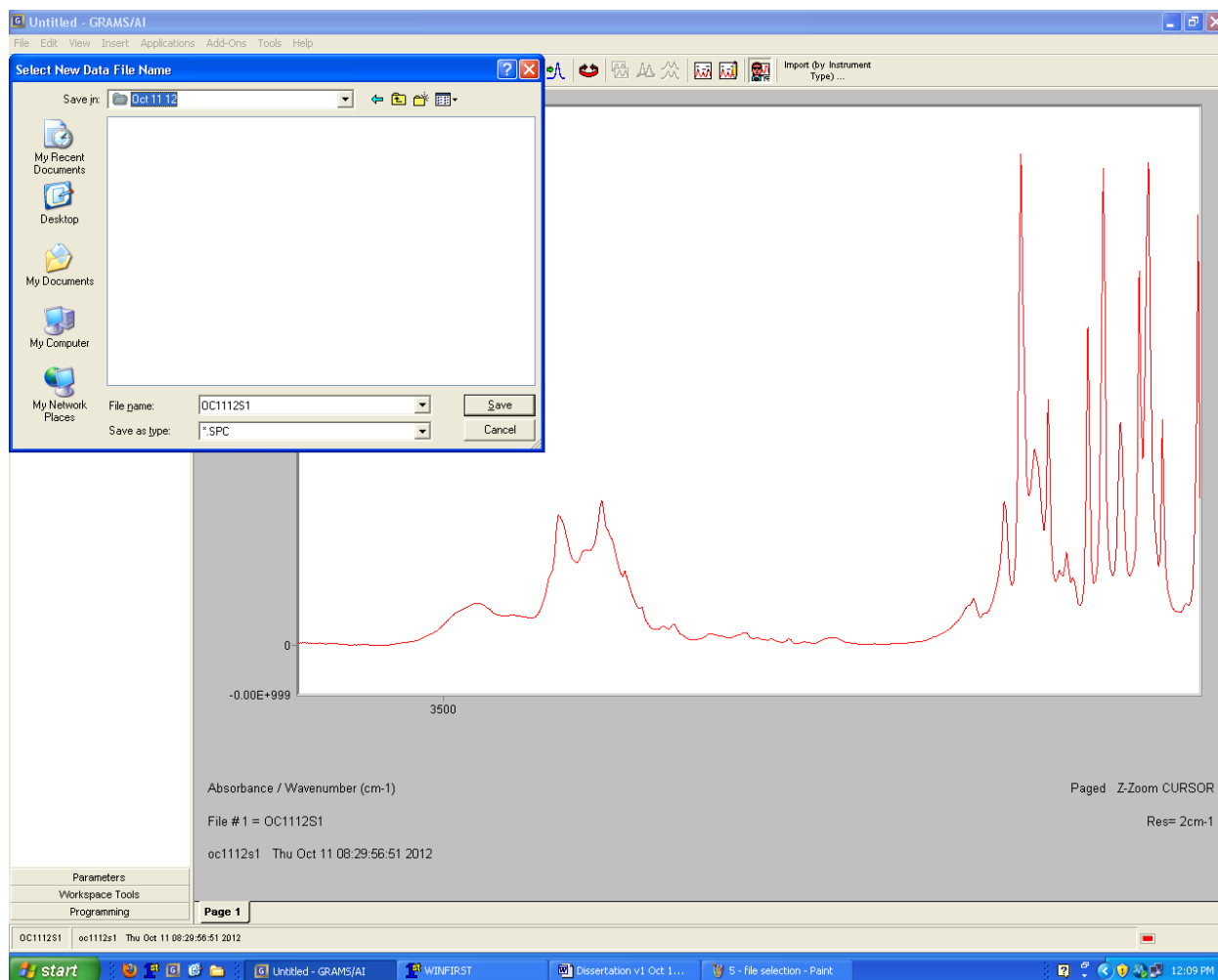
Figure D.5 Saving solvent spectrum as .spc file.

Now that the solvent is saved in the GRAMS/AI file type (.spc), it is possible to begin finding the difference spectrum to examine only the solute without the solvent.

To begin this process, find and open the solution file following the same "Import (by Instrument Type)…" process described above (Figures D.2 through D.5), in this case file OC1112S2.abs. When the solution file is open, go to Applications > Spectral Subtract (Figure D.6).
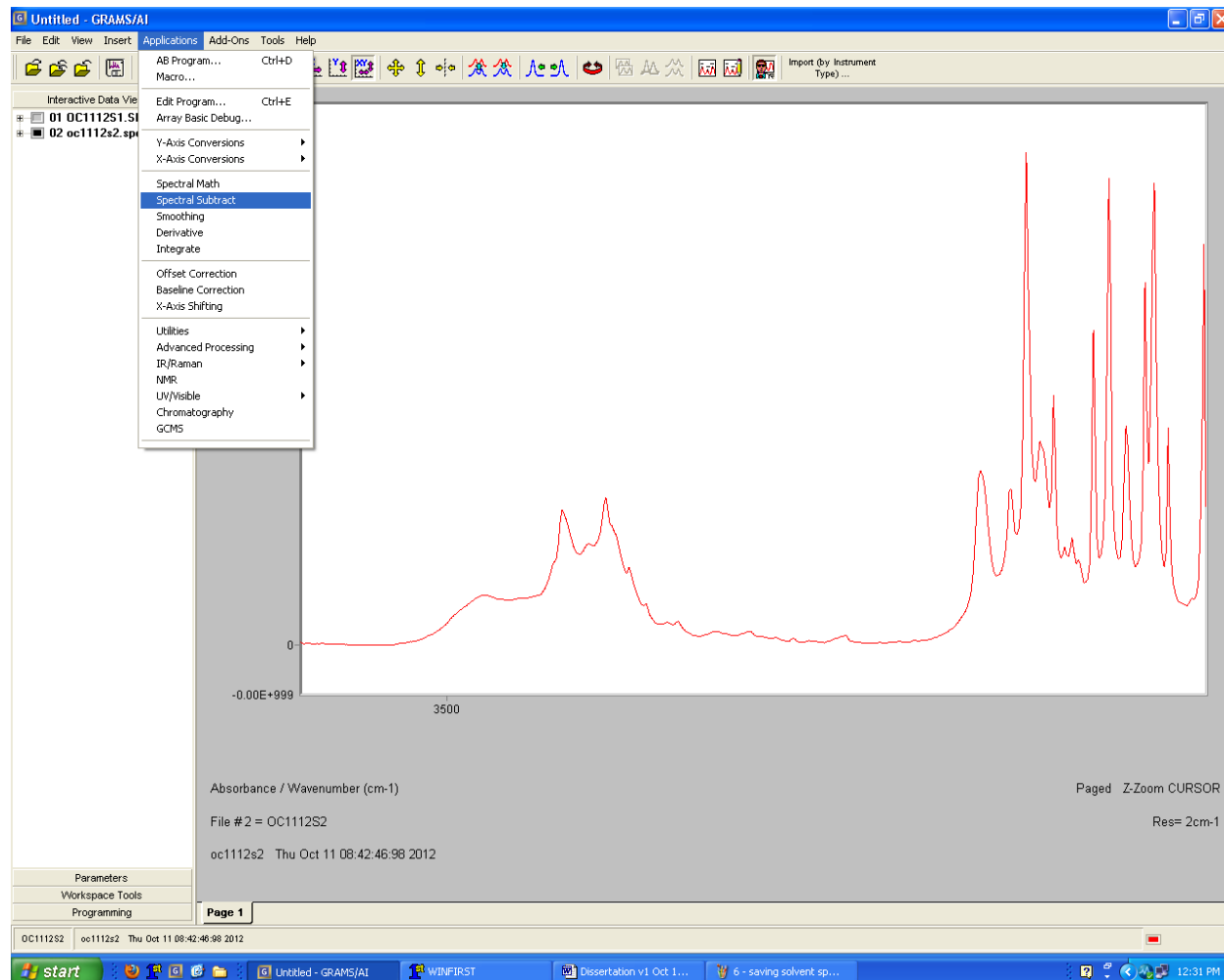
Figure D.6 Spectral Subtract

When spectral subtract is open, the first thing to do is change the "Subtrahend". Click on the Select button (Figure D.7).
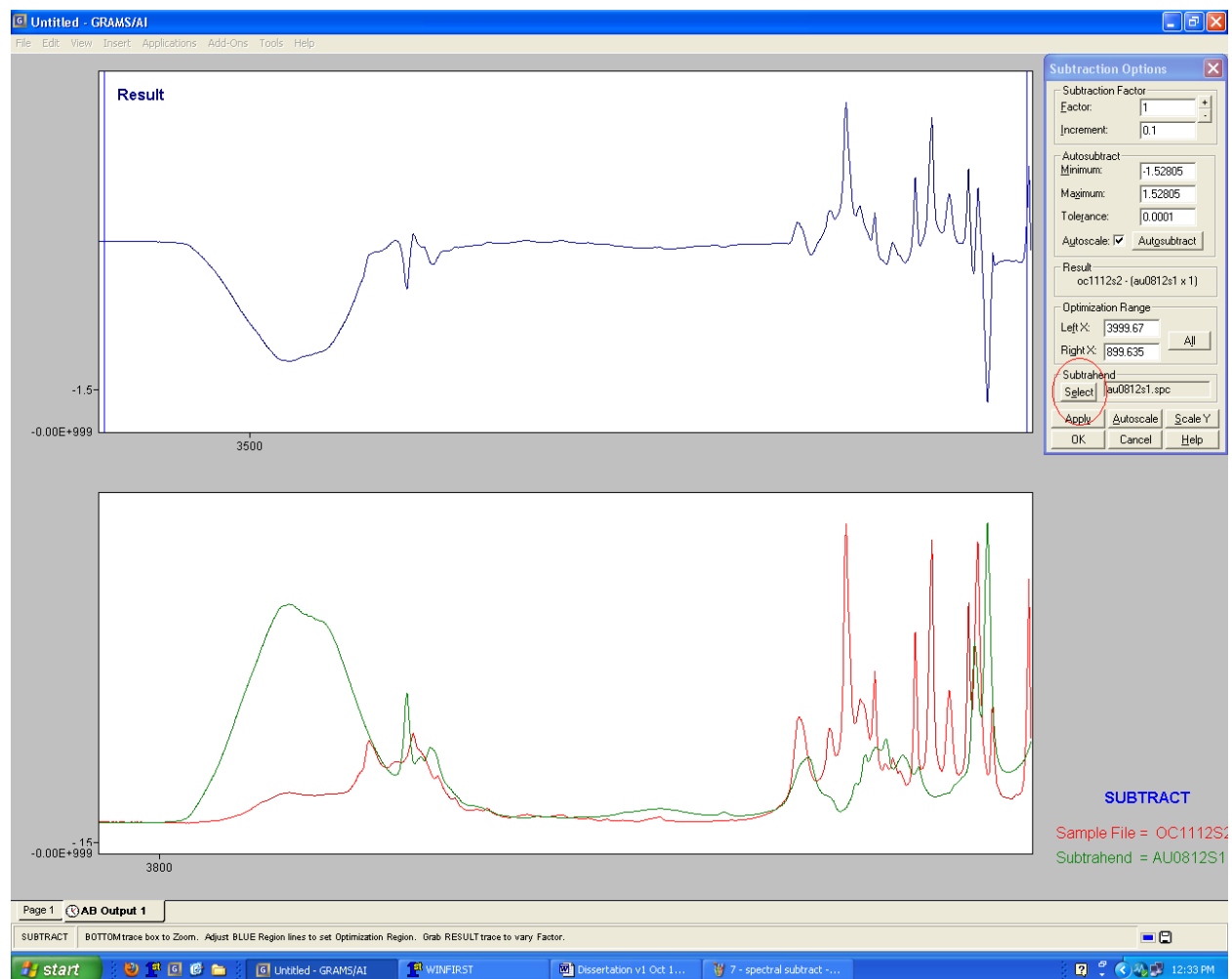
Figure D.7 Select new subtrahend.

Click on Select, and then click on Replace. Navigate to find the solution file that was saved above (Figure D.5), and then click on "Open".

Figure D.8 shows the resulting image, with the difference spectra in blue at the top, the subtrahend (the solvent spectrum) in green at the bottom, and the solution spectrum in red overlaid atop the subtrahend.
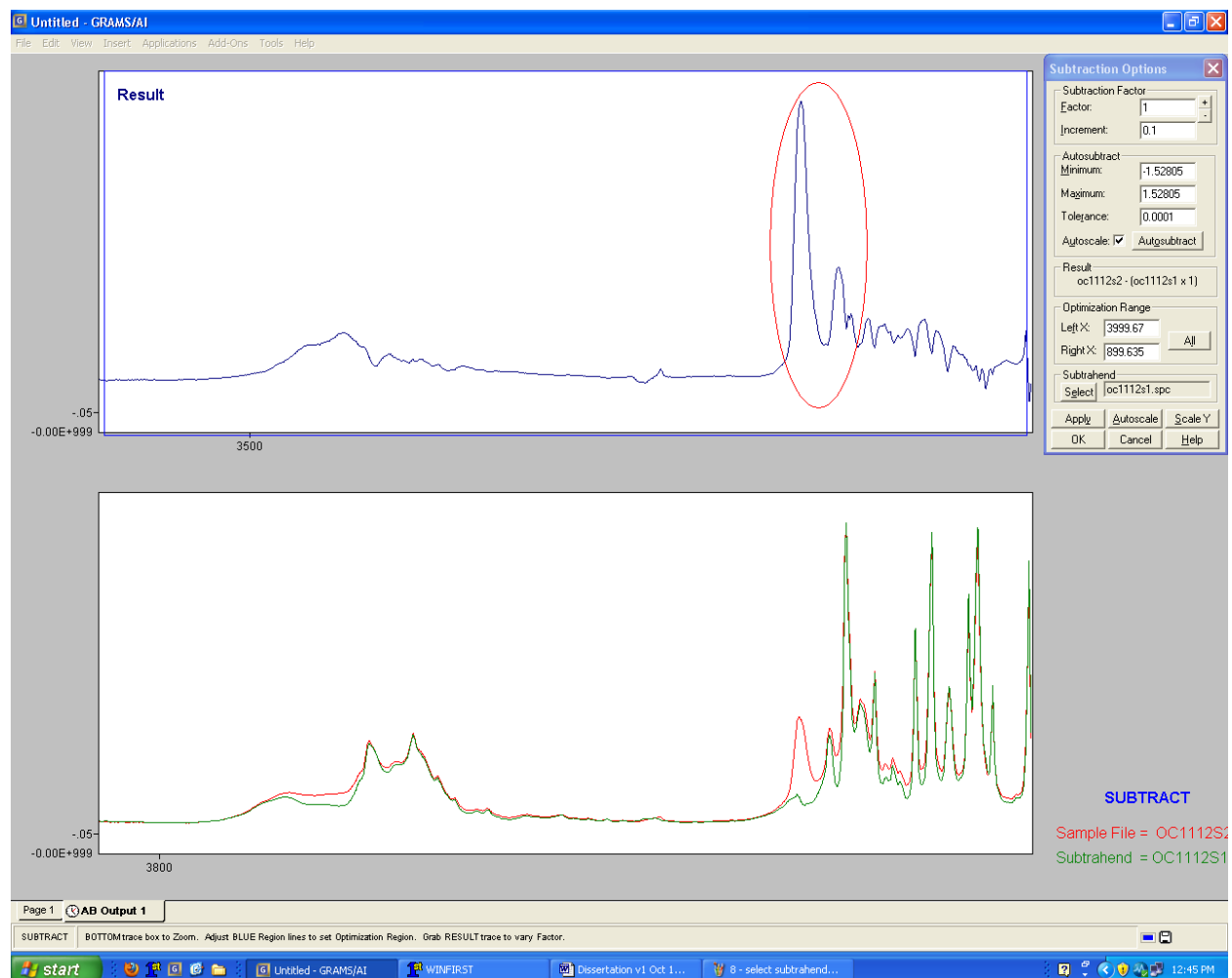
Figure D.8 Initial difference spectrum. The circle indicates the Amide I and II regions of interest.

Now the subjectivity of spectral subtraction comes into effect. In order to successfully subtract a solvent, certain requirements of the resulting difference spectrum must be met. Spectra can be subtracted by either clicking-and-holding on the difference spectrum above and then rolling the mouse forward and back to subtract the subtrahend, or the "Subtraction Factor" can be manually input in the top right of the screen. First, one must know what region is of interest. In this case, it is the Amide I and II region from ~1700 to ~1500 cm^{-1} (area encircled by the circle in Figure D.8). It is important that the region of interest be examined carefully, so all the rest of

the difference spectrum must be minimized, but without overly subtracting any part. Figure D.9 shows the effects of under-subtraction (the region of interest is not clearly visible).
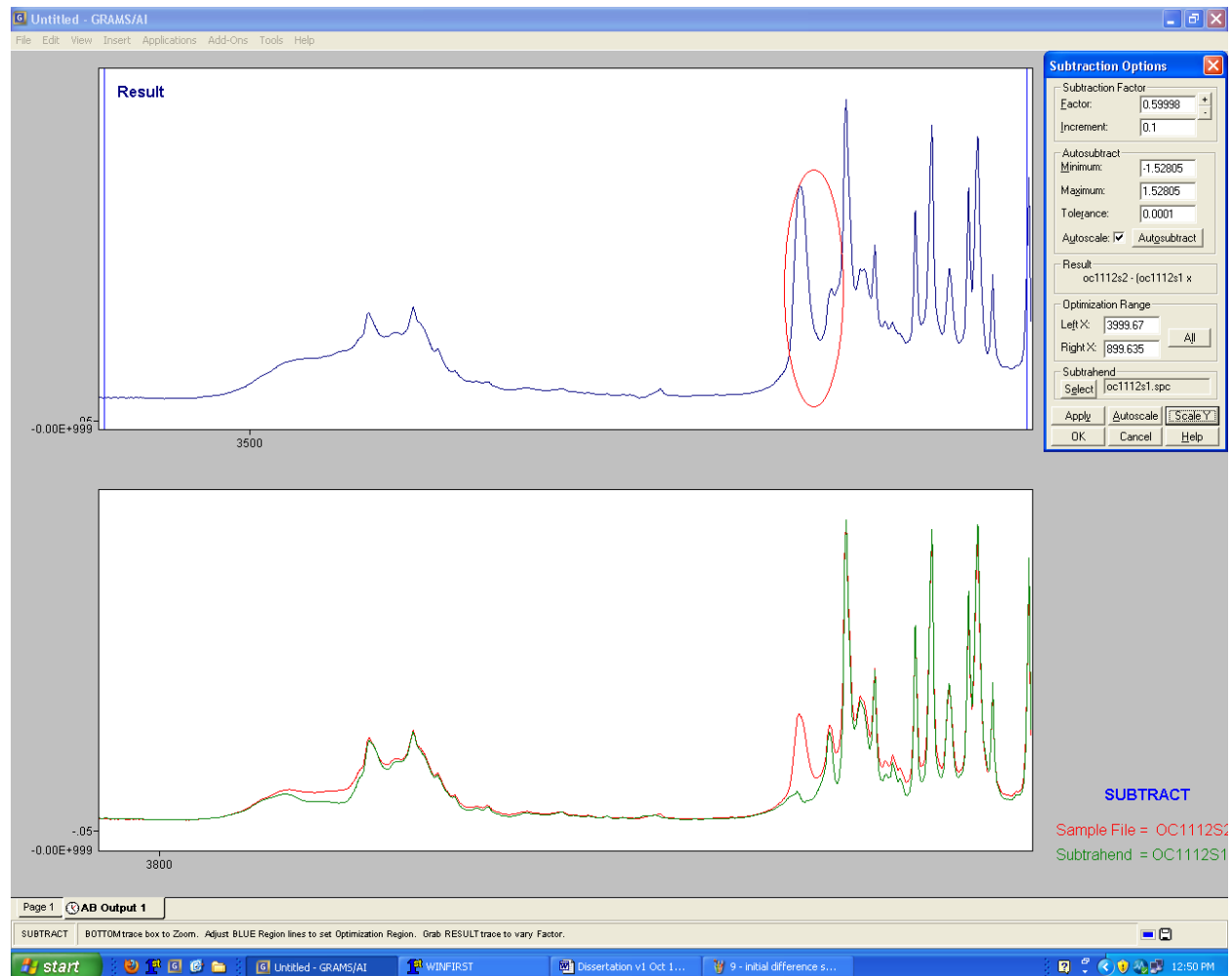
Figure D.9 Effects of undersubtraction.

Note how in Figure D.9 the smaller peak clearly visible in Figure D.8 is obscured by the larger peak that has not been effectively removed by subtraction. This will lead to poor peak-fitting.

Figure D.10 shows the effects of over-subraction.

Figure D.10 Effects of over subtraction.

In Figure D.10 the region of interest is again harmed by the subtraction, this time resulting in a smaller Amide I peak than it ought to be. Preparing a difference spectrum is a balancing act between removing too much and too little solvent. It is also important to note that the baseline of the spectrum (in Figures D.8 through D.10) ought to be flat in the difference spectrum, no matter the baseline in the solvent and solution spectra.

Good subtraction can be seen in Figure D.11
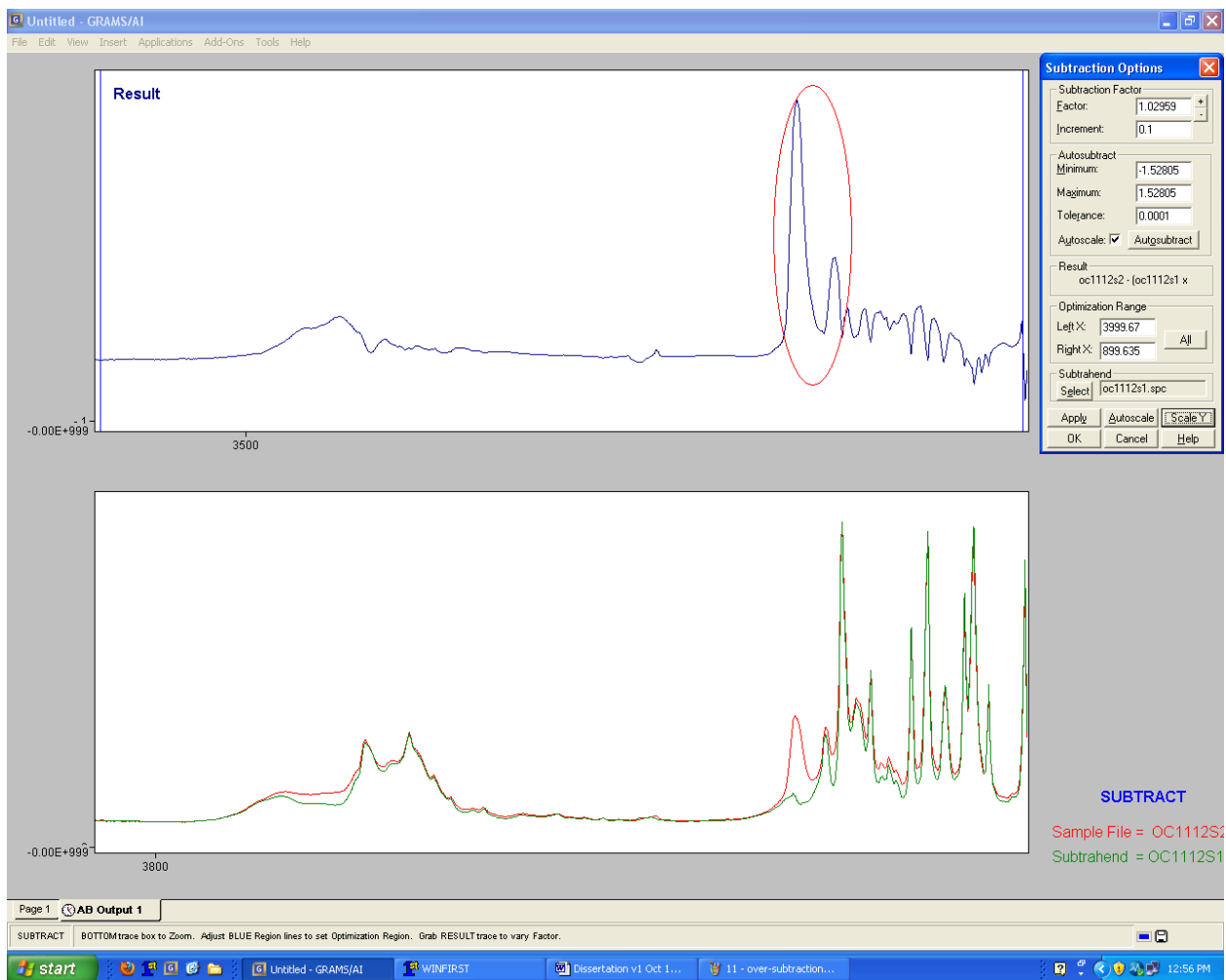
Figure D.11 Good subtraction with the region of interest noted.

Figure D.11 has good subtraction, with a flat baseline and minimized solvent contributions to the spectrum. Now click "OK", and then "Replace". Next, click File > Save Trace As… and save the file. It is possible to save this with the same file name used for the original WinFIRST solution spectrum as the file type is now different (GRAMS/AI uses the .spc file type).

The next step is to select the region of interest by clicking and dragging a box (see Figure D.12). The box size can be edited by clicking and holding on each of the 8 solid black boxes around the outside. This enables the user to alter the size after creating the box initially.
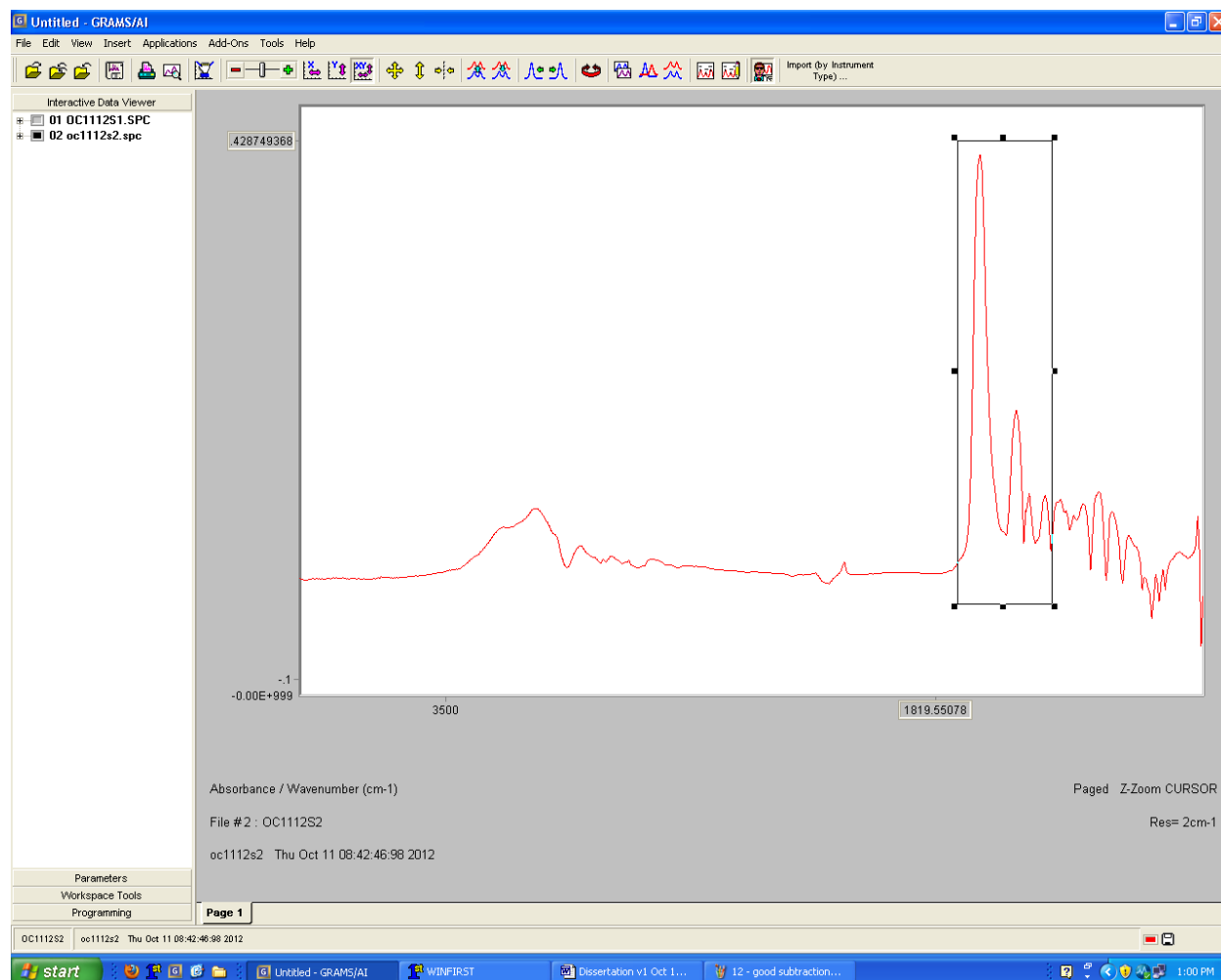
Figure D.12 Selecting the region of interest.

In this case, the region of interest is the two peaks at approximately 1650 and 1550 cm^{-1}.

Then place the cursor into the box selected (the cursor will turn into a box with a + sign inside, and then click. This will zoom into the selected area (see Figure D.12).
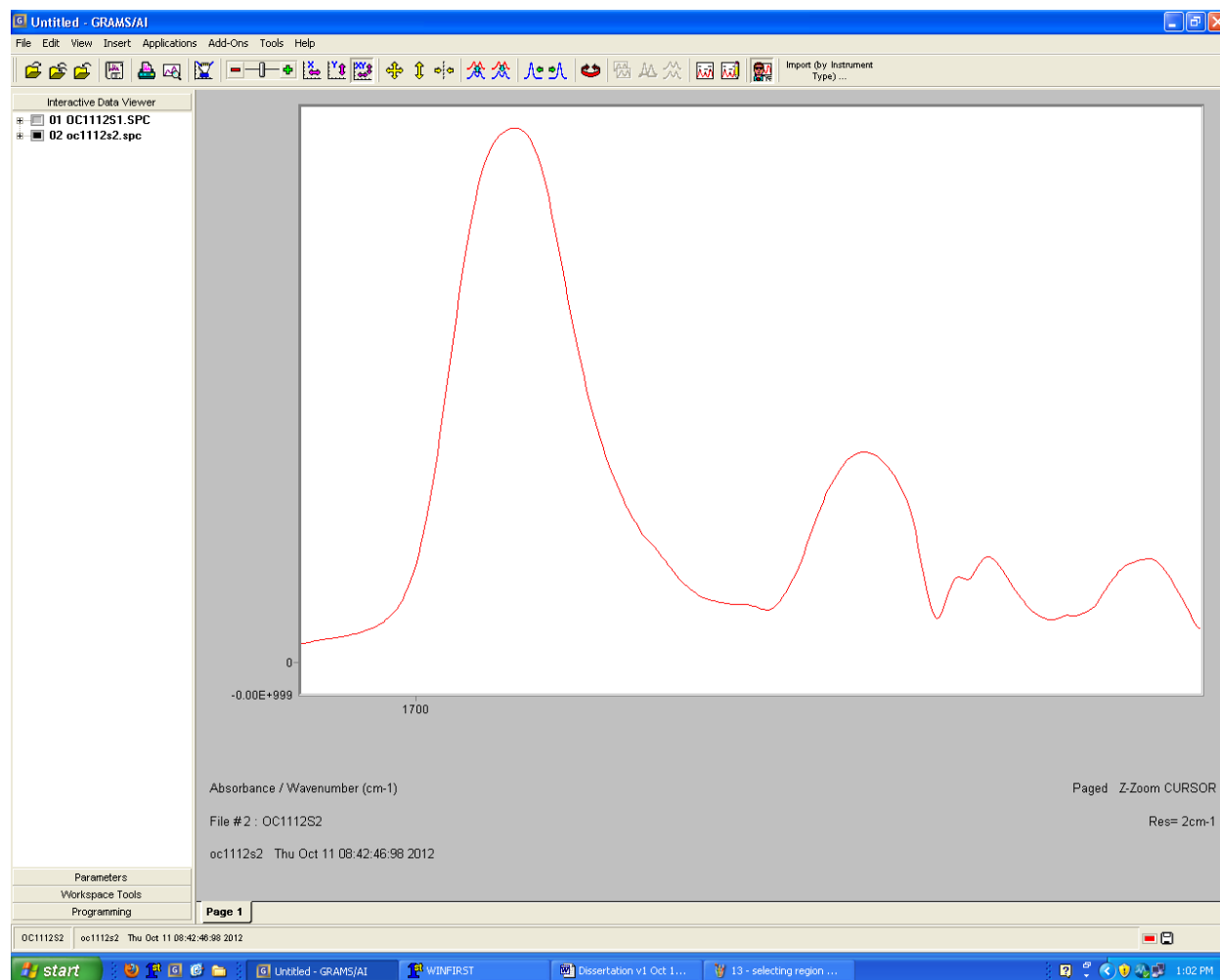
Figure D.13 Zoomed area of interest.

Now that the area of interest is selected, go to Applications > Advanced Processing > Peak Fitting, and click on Peak Fitting (see Figure D.14).
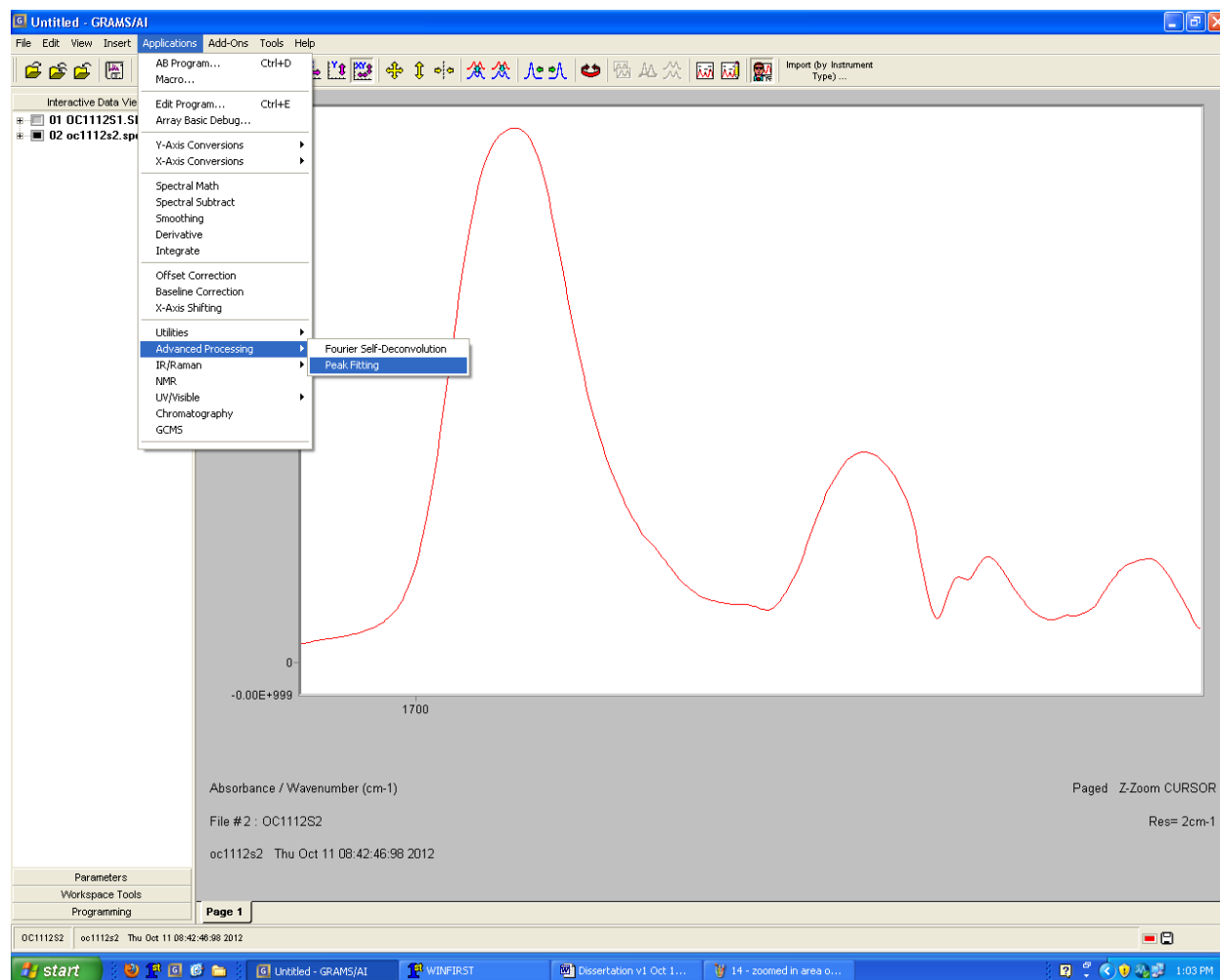
Figure D.14 Selecting peak fitting.

That will lead to Figure D.15, the Peak Fitting screen. Note the menu right side of the image that says "Peak Fitting Options" with the tabs Peaks, Find, Iterate (currently greyed out because there are no peaks to iterate) and Options.
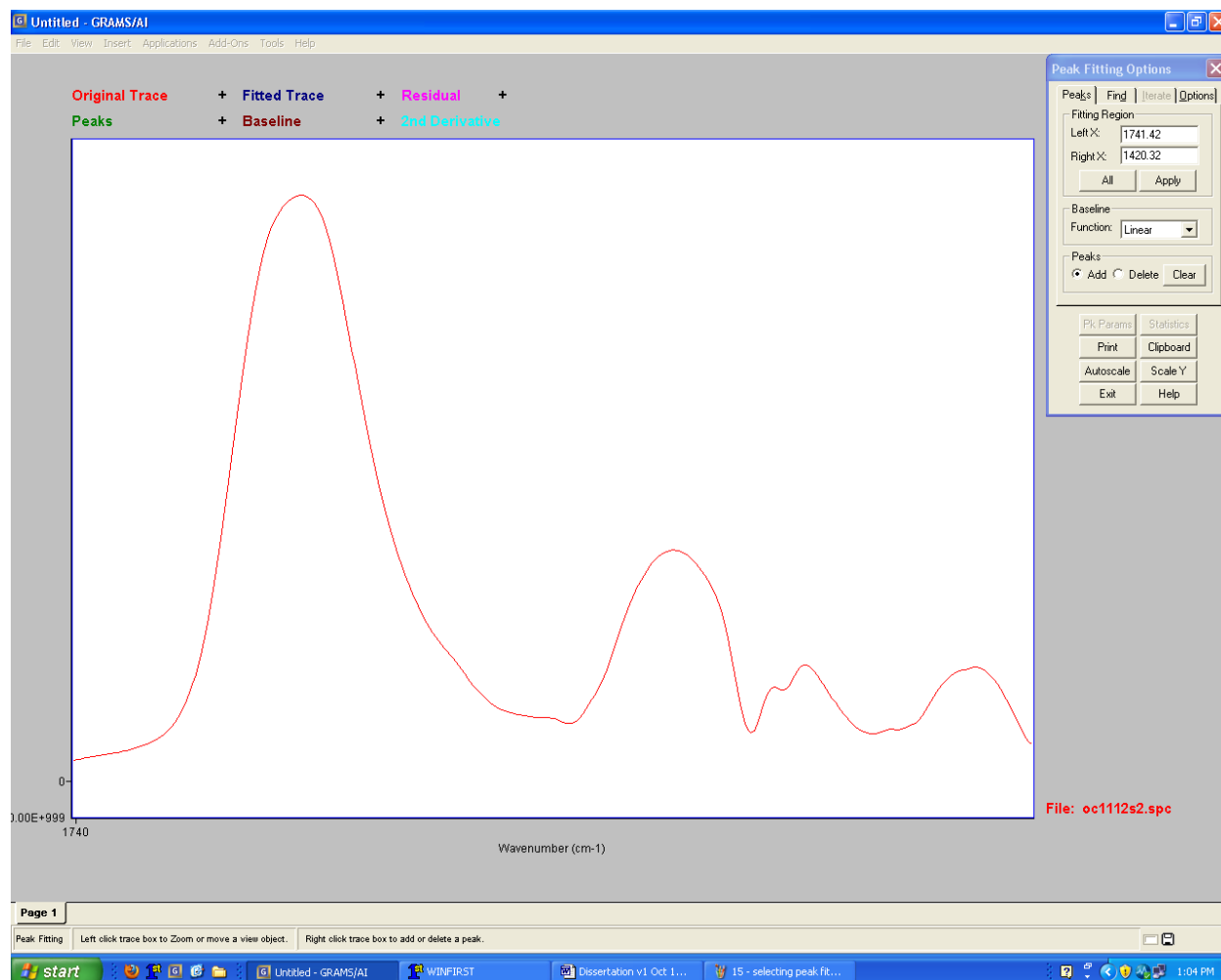
Figure D.15 Peak fitting screen.

In the peak fitting screen it is possible to change the region of interest by entering numbers into the Fitting Region Left X:, and Right X:, boxes. It is also possible to give the difference spectrum a specified type of baseline (Baseline Function:). The second tab, Find, is the command to have GRAMS/AI identify peaks on its own. First, change the Baseline Function to None. This assumes that the baseline obtained for the difference spectrum is adequate, but it also prevents GRAMS/AI from giving an erroneous baseline. Next, select the Find tab.

In the Find tab it is possible to change the type of Function the GRAMS/AI software uses. Infrared spectroscopy often results in either a Gaussian or Lorentzian function, so select Mixed G+L from the dropdown menu. The Sensitivity alters how many peaks the program will

190

find. GRAMS/AI will find its own Full Width Half Height (FWHH). So now click on the "Find Now" button. A notice box with the number of peaks found will pop up (in this case 14), and then click "OK". This will give Figure D.16.
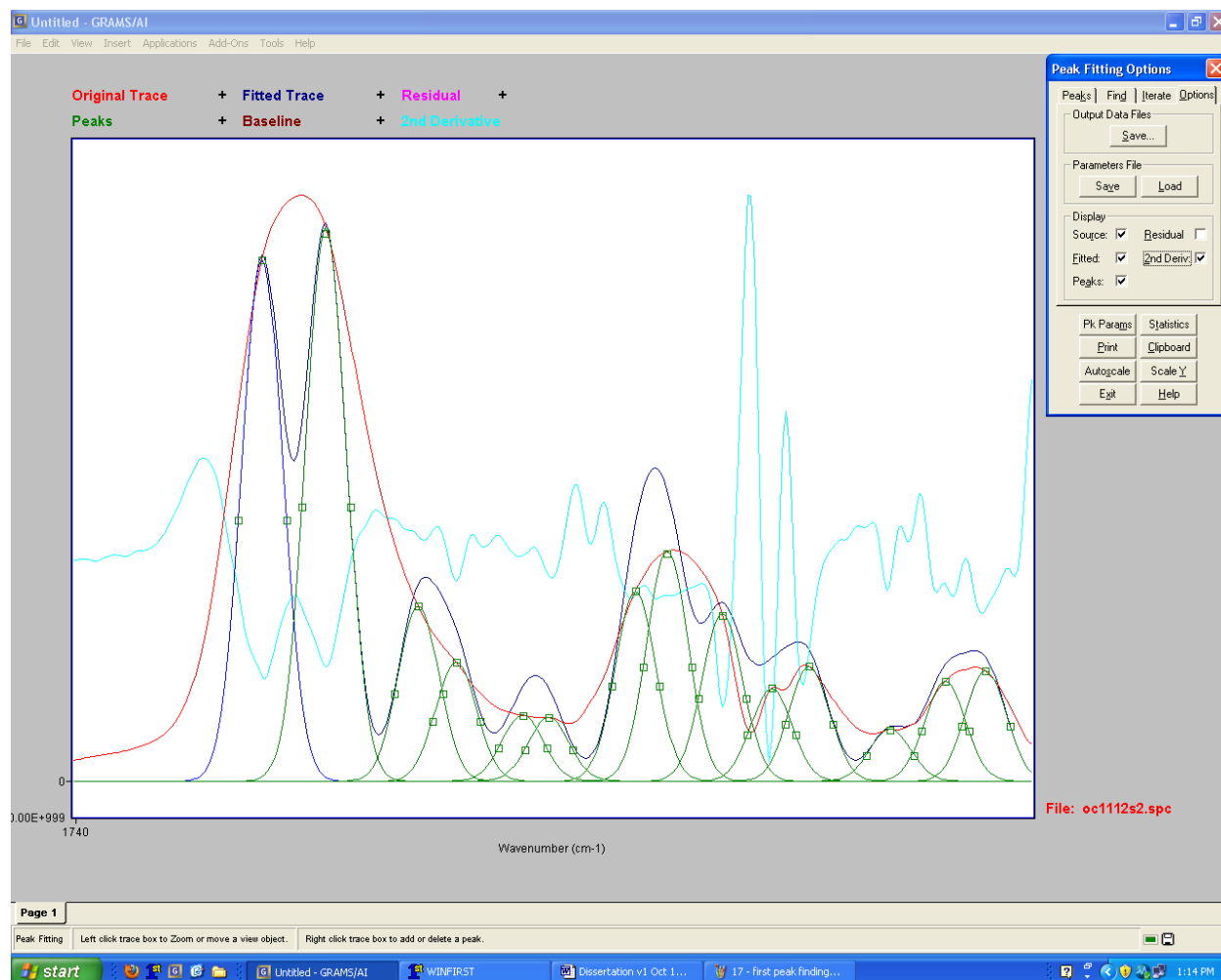
Figure D.16 Initial result of peak finding.

As one can see from the key above the image, the coloration of the lines are important. Red is the difference spectra to be analyzed. Dark blue is the sum of the peaks (in green). Pale blue is the second derivative of the red spectrum (the spectrum that is being fit), selected from the Options tab. It is recommended to turn on the second derivative. The second derivative of the difference spectrum is important because it can give strong indication of where the peaks are in the difference spectrum. The second derivative is used to identify where to insert missing curves, or delete extraneous curves from the peak fitting performed by GRAMS/AI. Click on the "Pk Params" button will give a list of the information for all the peaks found (see Figure D.17).
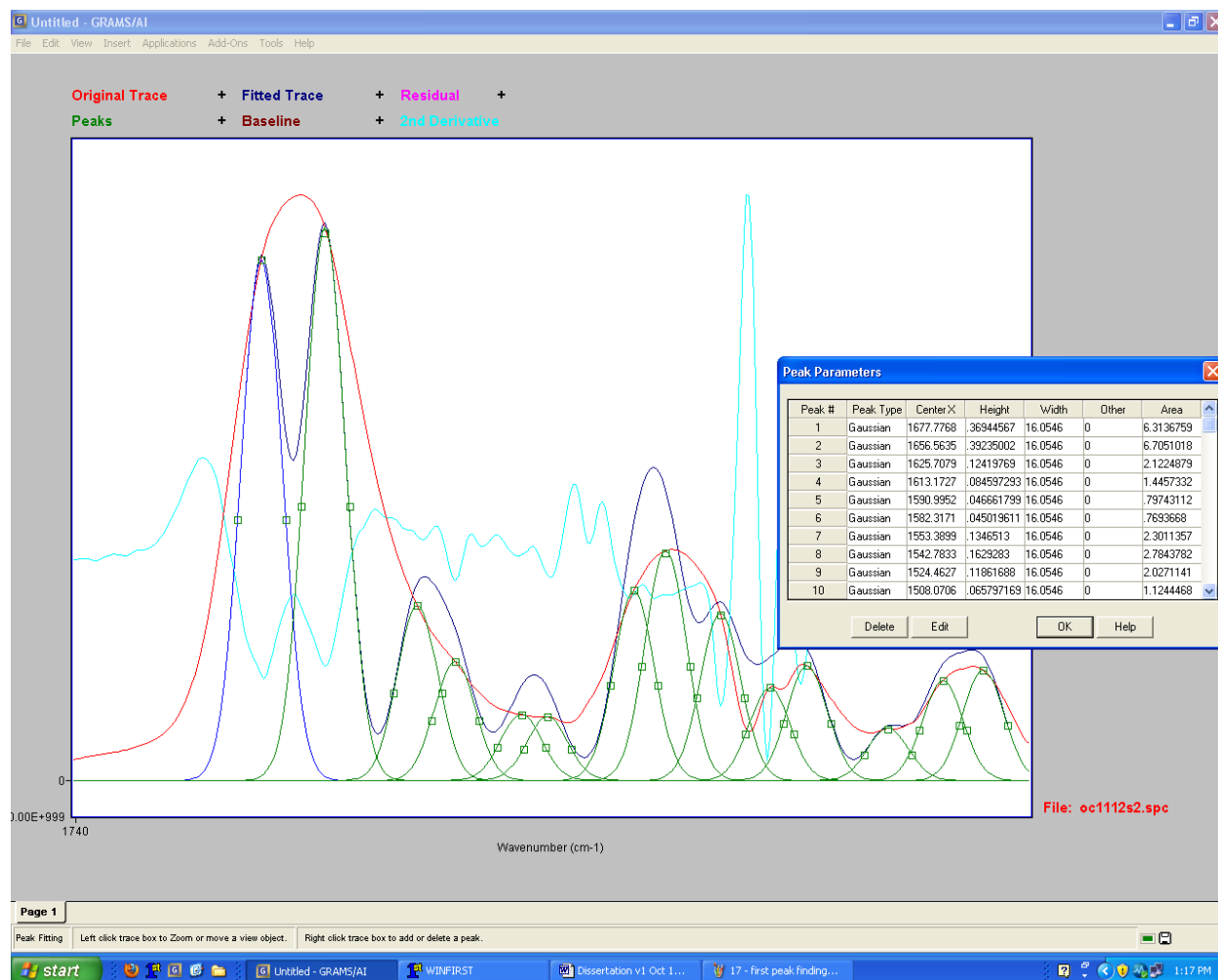
Figure D.17 Peak parameters list.

In Figure D.17 a list of peaks is given. If there are peaks that are not wanted (for example the peak at 1590.9952 cm^{-1}), it is possible to click on the peak number and then click delete to remove it. If there are peaks missing from the list, by comparison with the pale-blue second derivative line, it is possible to add them to the spectrum by right clicking where the maximum of the missing peak is expected to be. It is also possible to change the peak parameters by clicking on the "Edit" button. In there it is possible to change peak value (the location of the peak maximum), height, and width, as well as fix any or all of those three parameters. However in this case the peaks found match the second derivative of the difference spectrum (the pale blue line), therefore click "OK".

The locations of Amide I secondary structure peaks from the literature are as shown in Table D.1.[7, 8]

Table D.1 Amide I regions.

Peak name	Location (cm^{-1})
β-turn	1680 – 1665
α-helix	1665 – 1655
Random coil	1655 – 1645
β-sheet	1640 – 1615

There may be two β-sheet peaks present, depending on the protein. For example, the zein used here has two β-sheet peaks, but those peaks are visible from the second derivative analysis referred to earlier.

Click on the Iterate tab of the Peak Fittings Option section of the screen, which will give Figure D.18.
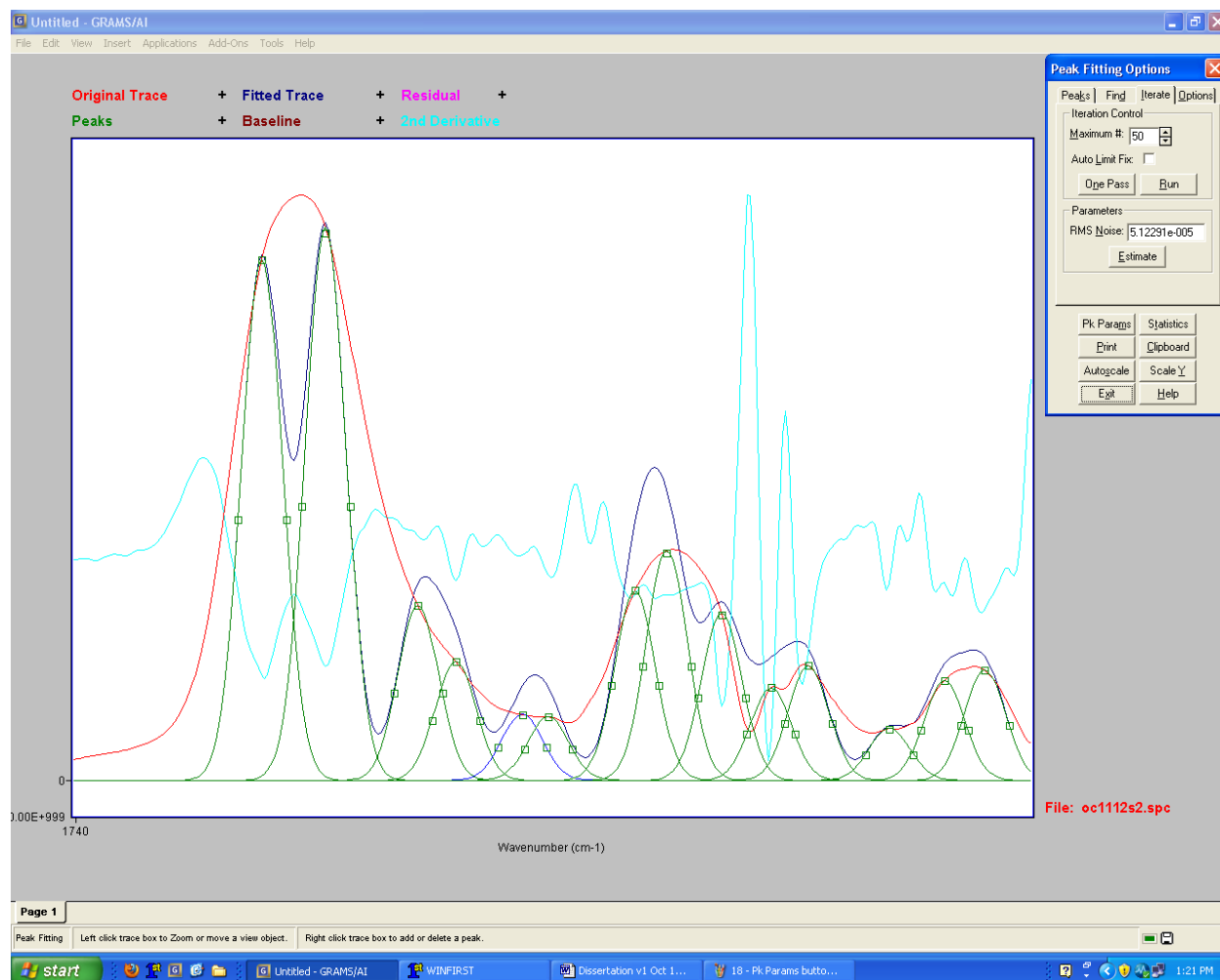
Figure D.18 Iterate tab.

In the Iterate tab it is possible to change the number of iterations performed, and to "Run", that is, to use the Levenberg-Marquardt algorithm to adjust the peak parameters.{{{}}}[14, 15] Clicking on "Run" once results in the following image (Figure D.19).
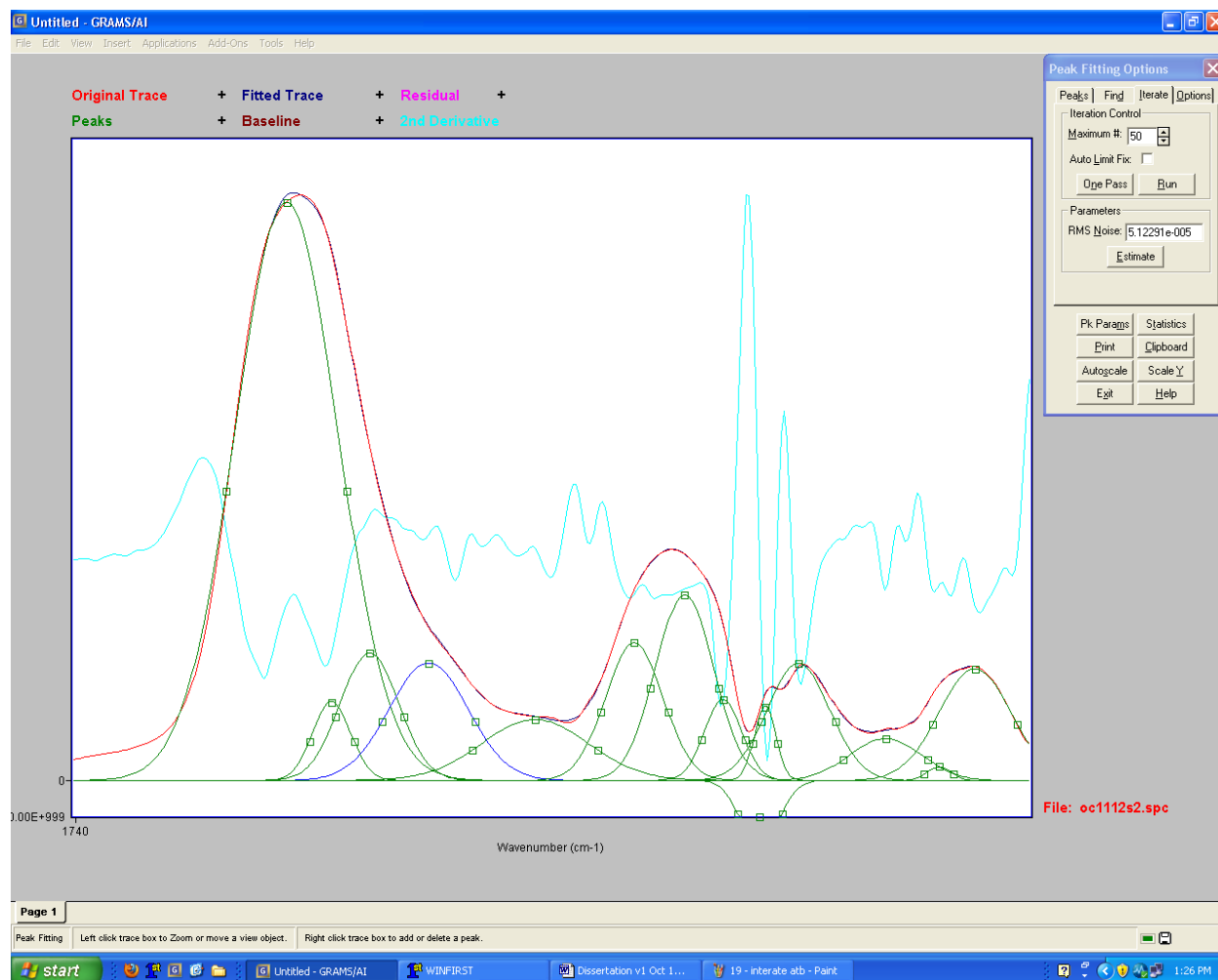
Figure D.19 Initial results of run.

Figure D.19 gives the initial results of the "Run" command. Occasionally a dialog box will appear that will inform the user of errors that have occurred. Click "Cancel" on the dialog box. In the case of Figure D.19 a reasonable fit has been obtained because the red (original data) is overlaid by the dark blue (summation of fit curves) line. The statistics of the fit (RMS Noise, Correlation (R^2), and Standard Error can all be obtained by clicking on the "Statistics" button on the right side.

In this case there is a negative peak at approximately 1510 cm^{-1} that can be removed by clicking on the "Pk Params" button and then selecting the peak and then deleting it (see Figure D.20).
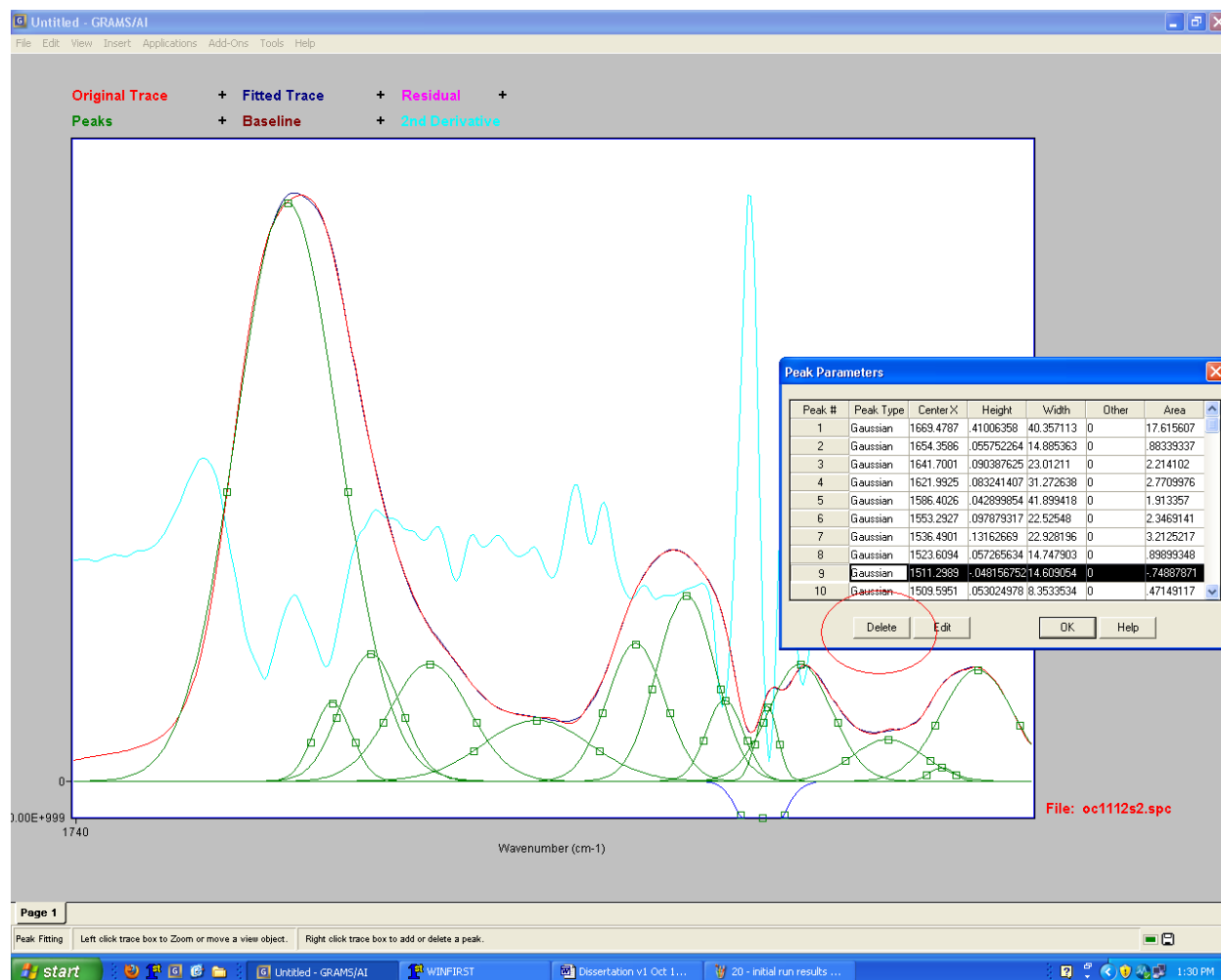
Figure D.20 How to delete a peak.

After deleting the peak, hit "Run" again in the Iterate tab. This will result in the following image (Figure D.21).
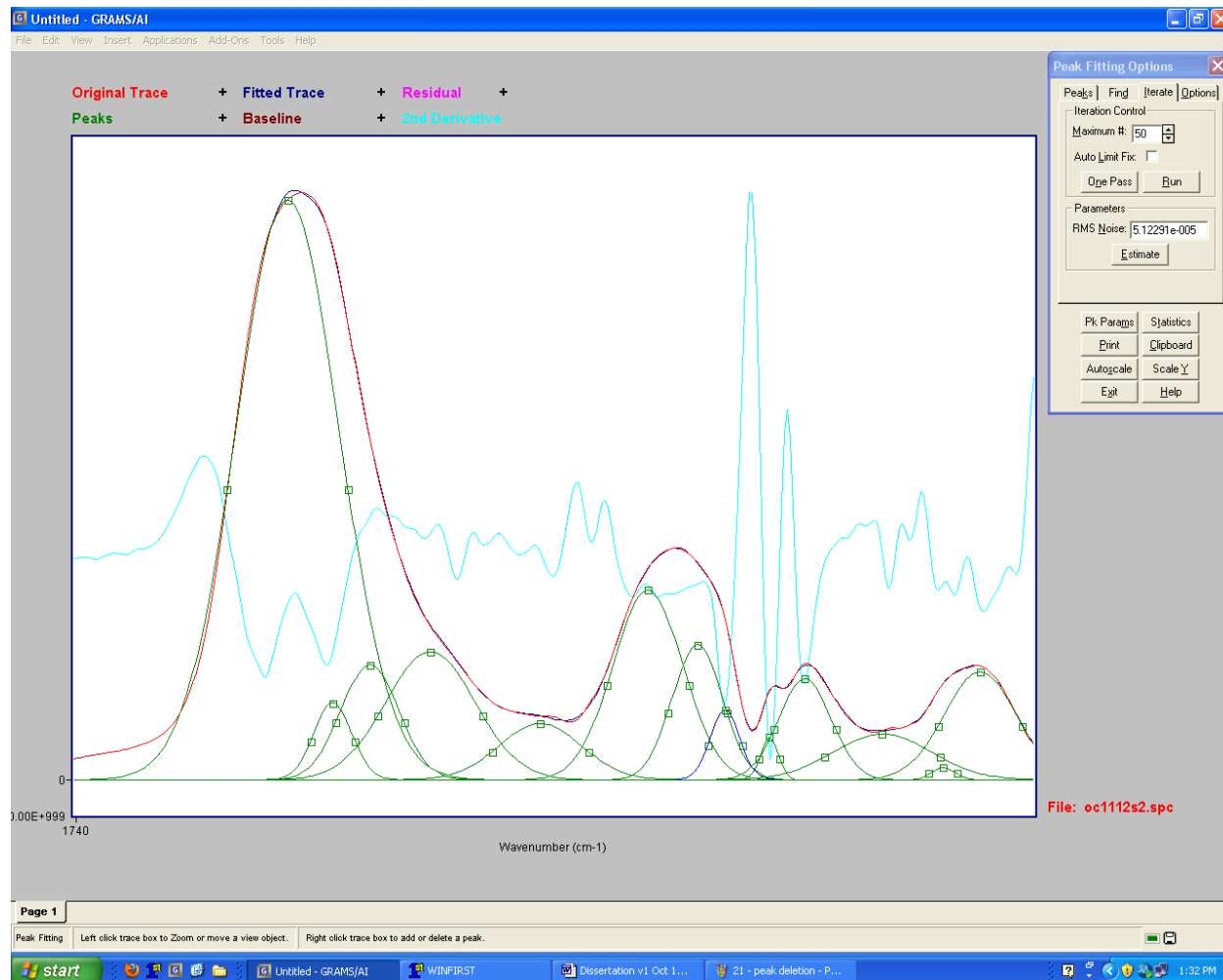
Figure D.21 Iterated peak-fitting.

Now that the peak-fitting is completed, click on the Options tab and then click Output Data Files Save. In the box that appears it is possible to save the results trace, peaks to metafile, peaks to a .csv (comma-separated values), and a peaks report (which saves as a .txt file information regarding the location, integrated area, and more of each peak) from the Options tab, see Figure D.22.
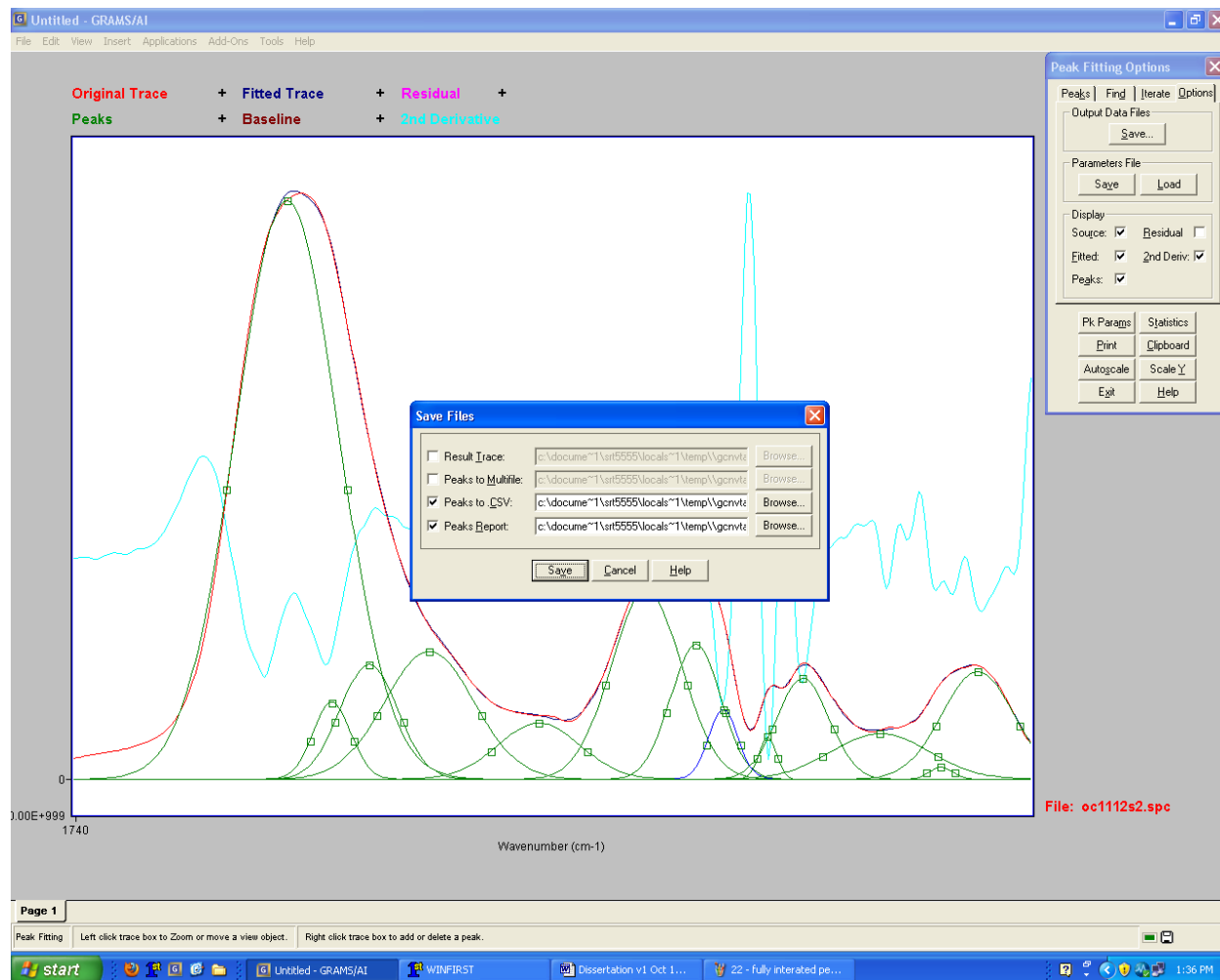
Figure D.22 Peak fitting save options.

In this case save the peaks to a .csv file and peaks report. It is possible to alter where the files are saved by clicking the "Browse" button. The .csv file is used to recreate the plot seen in Figure D.22 in a spreadsheet, while the Peaks Report is used to extract the necessary information for the quantitative analysis of the results described in Chapters 5 and 6.

References

1. Susi, H.; Michael Byler, D. Protein structure by Fourier transform infrared spectroscopy: second derivative spectra, *Biochem. Biophys. Res. Commun.* **1983**, *1,* 391-397.

2. Byler, D. M.; Susi, H. Examination of the secondary structure of proteins by deconvolved FTIR spectra, *Biopolymers* **1986**, *3,* 469-487.

3. Jackson, M.; Mantsch, H. H. The use and misuse of FTIR spectroscopy in the determination of protein structure, *Crit. Rev. Biochem. Mol. Biol.* **1995**, *2,* 95-120.

4. Surewicz, W. K.; Mantsch, H. H.; Chapman, D. Determination of protein secondary structure by Fourier transform infrared spectroscopy: a critical assessment, *Biochemistry (N. Y.)* **1993**, *2,* 389-394.

5. Kauppinen, J. K.; Moffatt, D. J.; Mantsch, H. H.; Cameron, D. G. Fourier self-deconvolution: a method for resolving intrinsically overlapped bands, *Appl. Spectrosc.* **1981**, *3,* 271-276.

6. Kauppinen, J. K.; Moffatt, D. J.; Mantsch, H. H.; Cameron, D. G. Fourier transforms in the computation of self-deconvoluted and first-order derivative spectra of overlapped band contours, *Anal. Chem.* **1981**, *9,* 1454-1457.

7. Barth, A. Infrared spectroscopy of proteins, *Biochim Biophys Acta* **2007**, *9,* 1073-1101.

8. Barth, A.; Zscherp, C. What vibrations tell us about proteins, *Q. Rev. Biophys.* **2002**, *4,* 369-430.

9. Dehring, K. A.; Smukler, A. R.; Roessler, B. J.; Morris, M. D. Correlating changes in collagen secondary structure with aging and defective type II collagen by Raman spectroscopy, *Appl. Spectrosc.* **2006**, *4,* 366-372.

10. Dehring, K. A.; Crane, N. J.; Smukler, A. R.; McHugh, J. B.; Roessler, B. J.; Morris, M. D. Identifying chemical changes in subchondral bone taken from murine knee joints using Raman spectroscopy, *Appl. Spectrosc.* **2006**, *10,* 1134-1141.

11. Nowak, A. M.; McCreery, R. L. Characterization of carbon/nitroazobenzene/titanium molecular electronic junctions with photoelectron and Raman spectroscopy, *Anal. Chem.* **2004**, *4,* 1089-1097.

12. Hearns, N. G. R.; Korčok, J. L.; Paquette, M. M.; Preuss, K. E. Dinuclear cobalt bis (dioxolene) complex exhibiting two sequential thermally induced valence tautomeric transitions, *Inorg. Chem.* **2006**, *22,* 8817-8819.

13. Vu, V. V.; Emerson, J. P.; Martinho, M.; Kim, Y. S.; Münck, E.; Park, M. H.; Que, L. Human deoxyhypusine hydroxylase, an enzyme involved in regulating cell growth,

activates O2 with a nonheme diiron center, *Proceedings of the National Academy of Sciences* **2009**, *35,* 14814-14819.

14. More, J. The Levenberg-Marquardt algorithm: implementation and theory, *Numerical analysis* **1978**, 105-116.

15. Gillette, P. C.; Lando, J. B.; Koenig, J. L. Band shape analysis of Fourier transform infrared spectra, *Appl. Spectrosc.* **1982**, *4,* 401-404.

Appendix E - Two-Dimensional Correlation Spectroscopy

This appendix provides some background and a step-by-step procedure for two-dimensional correlation maps using 2Dshige© freeware, from Shigeaki Morita of Kwansei-Gakuin University, 2004-2005. The 2Dshige© software is available for free from:

http://sci-tech.ksc.kwansei.ac.jp/~ozaki/2D-shige.htm

The author is grateful to Michael Hollock for his instructions how to use 2Dshige© and guidance for 2-D correlation spectroscopy analysis.[1]

Background on Two-Dimensional Correlation Spectroscopy

Two-dimensional (2-D) correlation spectroscopy arose from the desire to improve the visualization of complex nuclear magnetic resonance (NMR) spectra by spreading the peaks over a second dimension, thereby enabling the examination of many overlapped peaks.[2] The application of 2-D correlation spectroscopy to IR spectroscopy was first proposed by Noda in 1986.[3-5] When a perturbation is applied to a system various constituents of the system are selectively excited or transformed. The changes caused by the perturbation can be monitored by techniques such as NMR, IR, or Raman. The monitored changes are then transformed in to two dimensions mathematically.[2] This monitoring of changes and mathematical transformation process is the essence of 2-D correlation spectroscopy. One of Noda's important contributions is that 2-D correlation spectra consist of two orthogonal components, the synchronous and asynchronous correlation spectra, which carry distinct and useful information for subsequent analysis. Some of the advantages of 2-D correlation spectroscopy, as discussed in Two-dimensional Correlation Spectroscopy, Noda and Ozaki, 2004, include the simplification of complex spectra of many overlapped peaks, probing the sequential order of spectral changes, the heterospectral correlations arising from the correlation of two different types of spectroscopy, and finally the universal applicability of the technique which is not limited to any type of spectroscopy or analytical technique.[2]

Data Analysis

The original data were obtained in the course of the research for this dissertation, monitoring secondary structure changes of the protein zein as a function of temperature. Infrared spectroscopy (IR) was performed with a Mattson Cygnus IR spectrometer, using a Harrick

Scientific Horizon attenuated-total reflectance (ATR) accessory with a zinc selenide crystal and a temperature controlled top plate. The IR spectrometer control software is WinFIRST, version 3.61, from Mattson Instruments of Madison, Wisconsin. Each sample and background spectrum was collected with 256 co-added scans at 2 cm^{-1} resolution. Spectra were obtained from 25°C to 95°C every 10°C, with each temperature being held for 20 minutes prior to obtaining the spectra. Thus the perturbation applied to the system was systematically increasing temperature.

The 2Dshige© program states it can use raw data; however, no useable results were obtained. Thus a dynamic spectrum was prepared. A dynamic spectrum is the difference between the perturbed data and some reference spectrum. The reference spectrum can be the original (pre-perturbation) spectrum, or the final (post-perturbation) spectrum. However, Noda and Ozaki recommend the following equation to calculate the reference spectrum:[2]

$$y_{ref} = \frac{1}{T_{max} - T_{min}} \int_{T_{min}}^{T_{max}} y(T) dT \hspace{3cm} 1$$

In equation 1 y_{ref} is the reference data, y(T) is the original data, T is temperature (in degrees Celsius in this work), T_{max} was 95°C, and T_{min} was 25°C. Equation 1 was evaluated numerically, using Simpson's rule. As there were eight columns of data as a function of temperature, from 25 to 95°C, it was found that h = 10 ([95-25]/[8-1] = 10). Equation 2 is an example Microsoft Excel formula for the Simpson's rule numerical integral:

$$=10/3*(B2+4*C2+2*D2+4*E2+2*F2+4*G2+2*H2+I2) \hspace{2cm} 2$$

Multiplying the results from equation 2 by the coefficient 1/(95-25) results in the reference spectrum for the data, equation 1.

Using the reference spectrum, the dynamic spectrum was calculated using equation 3:

$$y_{dynamic} = y(T) - y_{ref} \hspace{4cm} 3$$

Subtracting the equation 2 reference spectrum from the raw data yields the dynamic spectrum.

The 2Dshige© software requires comma-separated value (CSV) files for input. Microsoft Excel can save workbook pages as CSV files (listed as .csv) by selecting File > Save As and then selecting CSV (comma delimited) from the drop down menu. However, 2Dshige© cannot use files that have any formulas, formatting, or heading titles (that is, no letters). The A1 cell must also be left blank otherwise the program cannot use the .csv file. The independent or abscissa value (in this case wavenumber) must be placed in the A column starting at A2. The dependence or ordinate value (in this case temperature) must be placed in the B row starting at B1. The corresponding dynamic data will populate the rest of the spreadsheet.

While 2Dshige© is Windows based (in this work it was run on with Windows XP operating system) it is possible to run 2Dshige© on Apple operating systems using a Windows emulator (see Hollock, 2012, for more information).

Figure E.1 shows 2Dshige© graphical user interface (GUI) with a data set loaded and a 2-D correlation map.
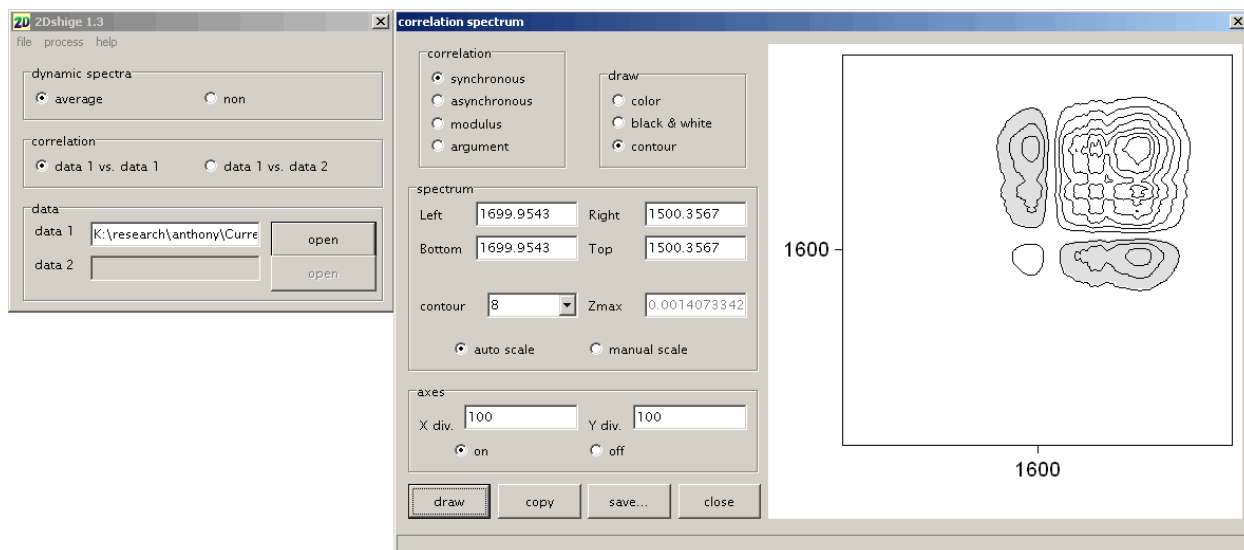
Figure E.1 2Dshige© graphical user interface.

To use the program, load the .csv file of interest with open, and then click process > 2D spectrum. The program will seem to freeze but shortly (depending on the RAM load of and CPU speed of the computer) the correlation spectrum window will open. After any changes are made to the options in the correlation spectrum window (such as correlation type between synchronous or asynchronous), drawing type, spectrum limits, or axes, clicking the draw button will run the program to prepare the new map. Peaks can be found by placing the mouse cursor over them. 2Dshige© displays the coordinates of the mouse cursor on the bottom edge of the program.

Results

These following figures show the Amide I and II 2-D correlation of one of the dissolved zein samples prepared (each zein in solvent mixture was repeated at least three times). The Amide I (1700 to 1600 cm^{-1}) and Amide II (1580 to 1510 cm^{-1}) regions are used for 2-D analysis protein changes in solution.[2, 6-8]
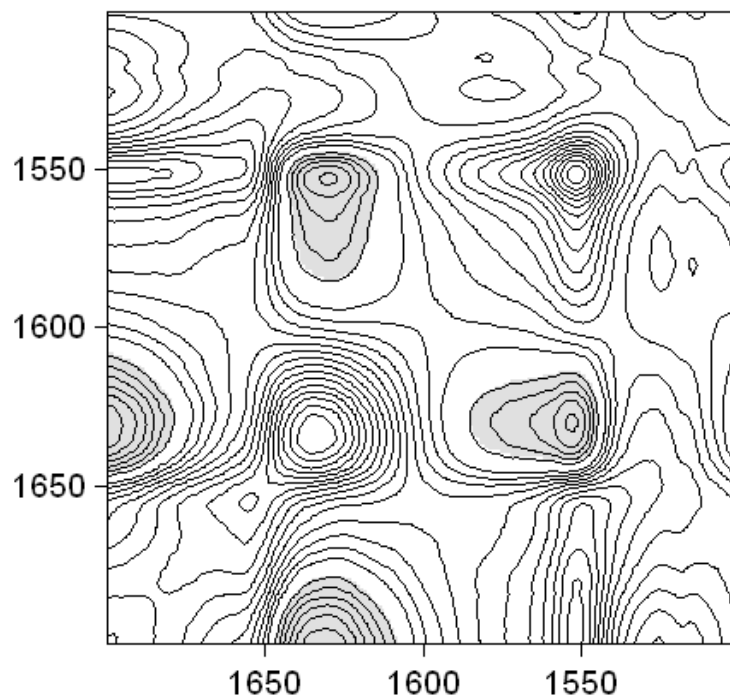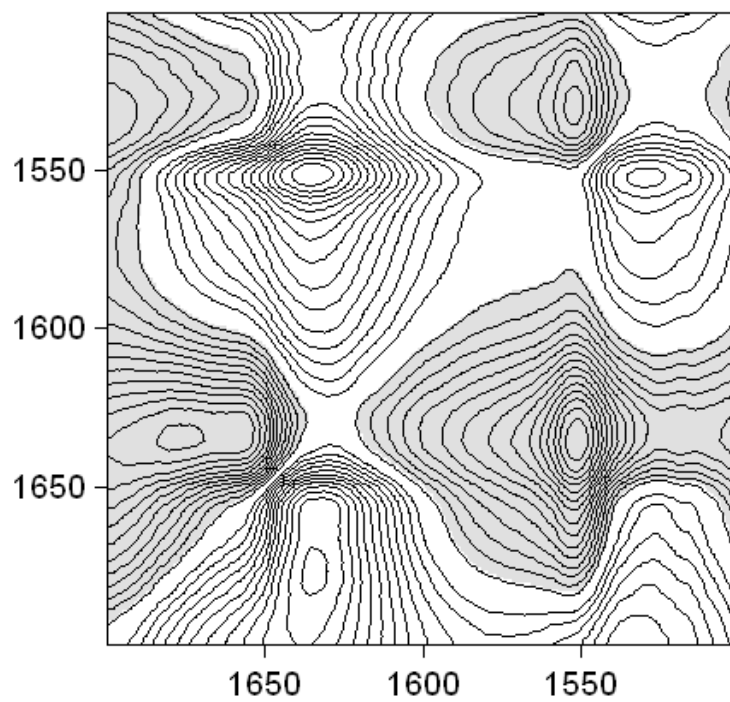
Figure E.2 Zein in 70 vol% aqueous ethanol synchronous.

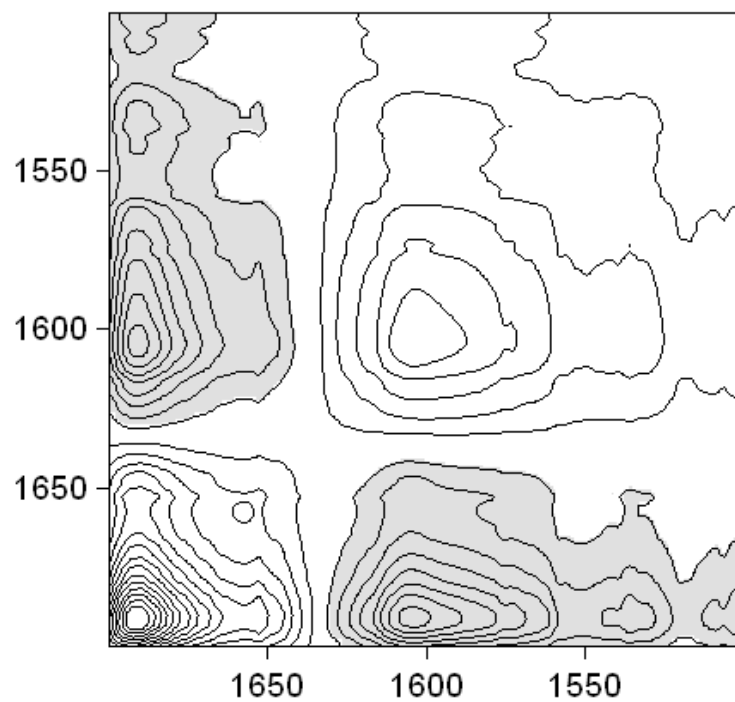
Figure E.3 Zein in 70 vol% aqueous ethanol asynchronous.
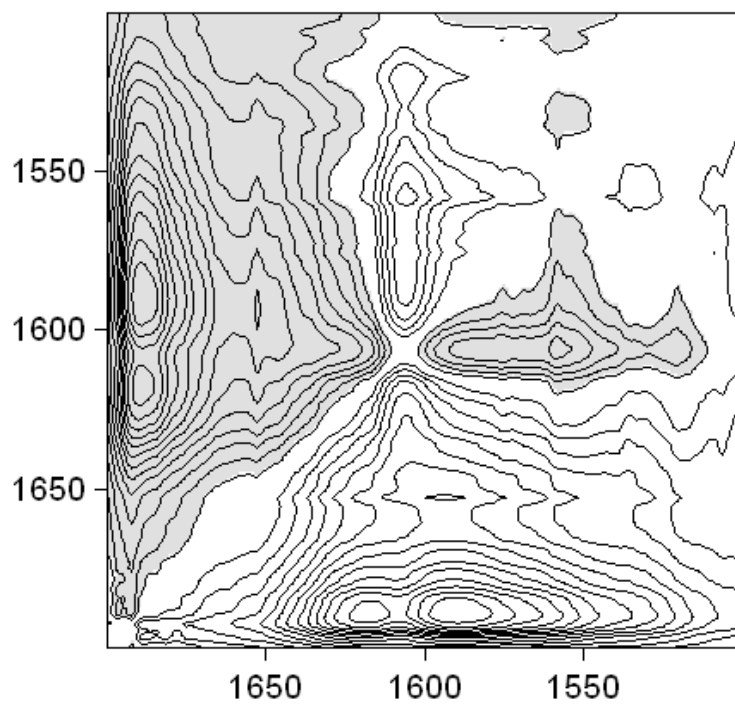
Figure E.4 Zein in acetic acid synchronous.

Figure E.5 Zein in acetic acid asynchronous.
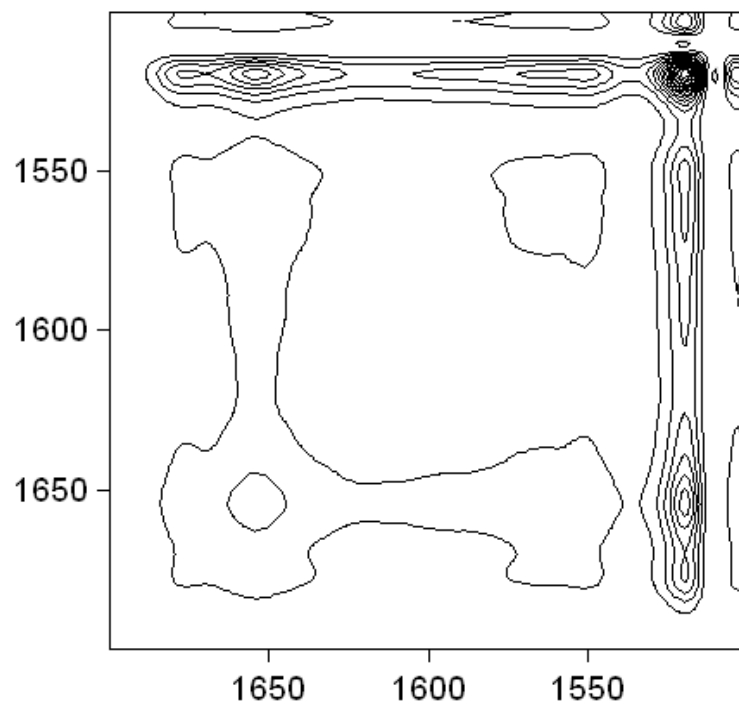
Figure E.6 Zein in 1-methylimidazole synchronous.
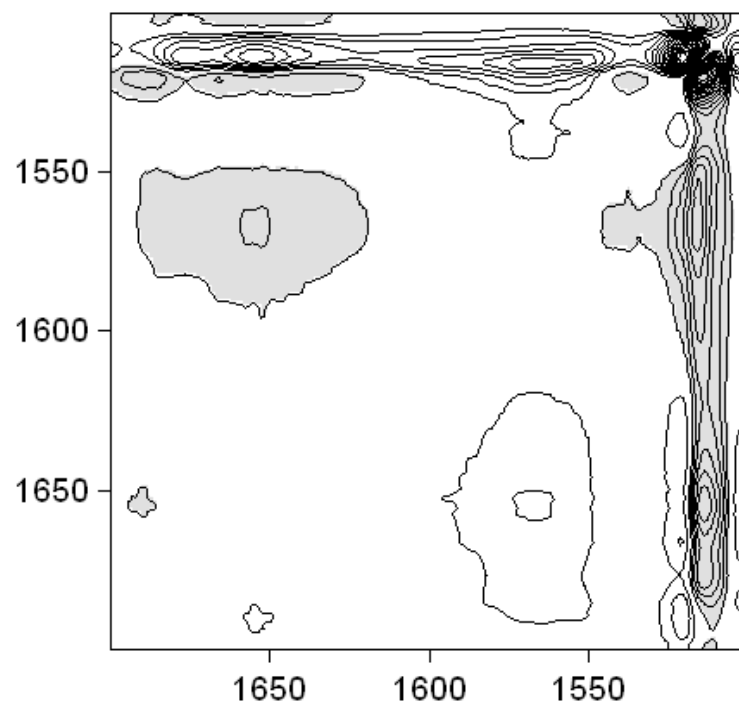
Figure E.7 Zein in 1-methylimdiazole asynchronous.
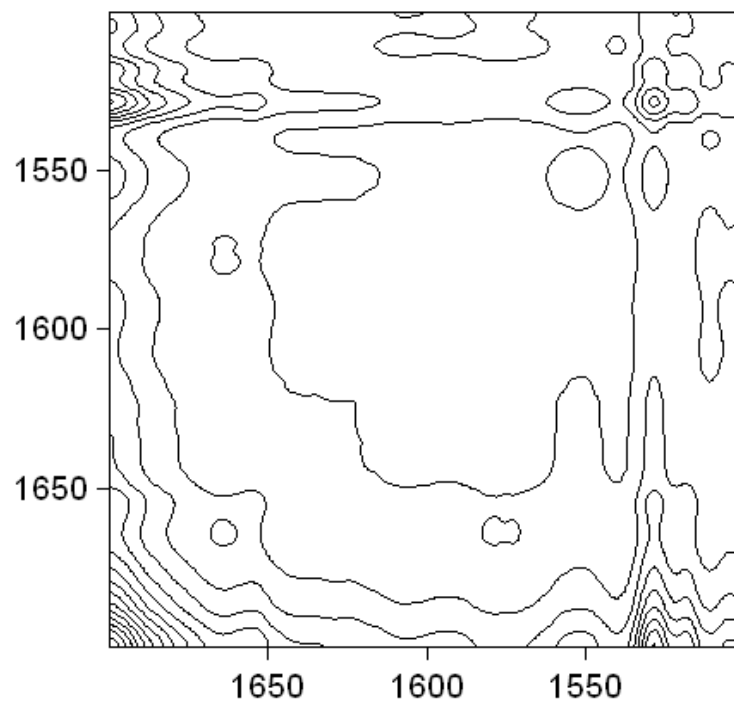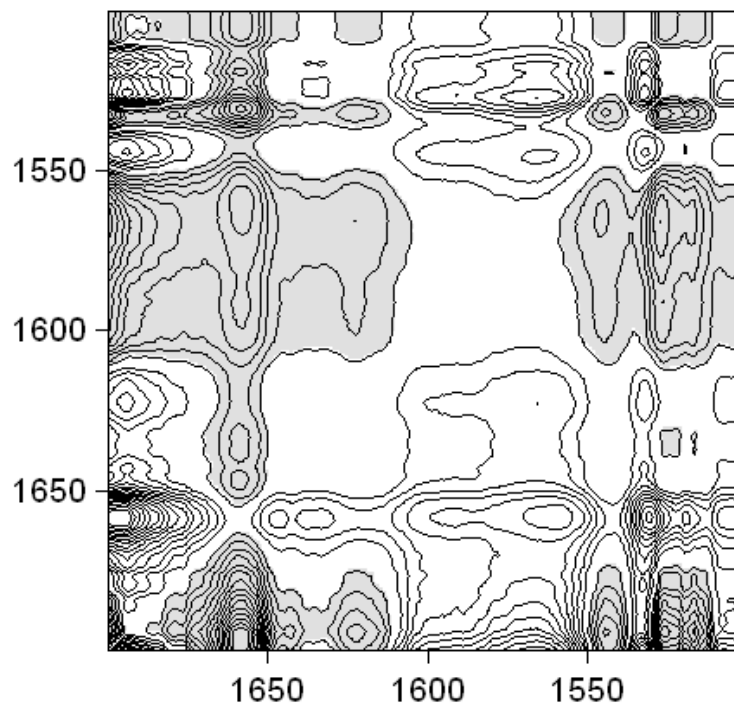
Figure E.8 Zein in [mim][OAc] synchronous.
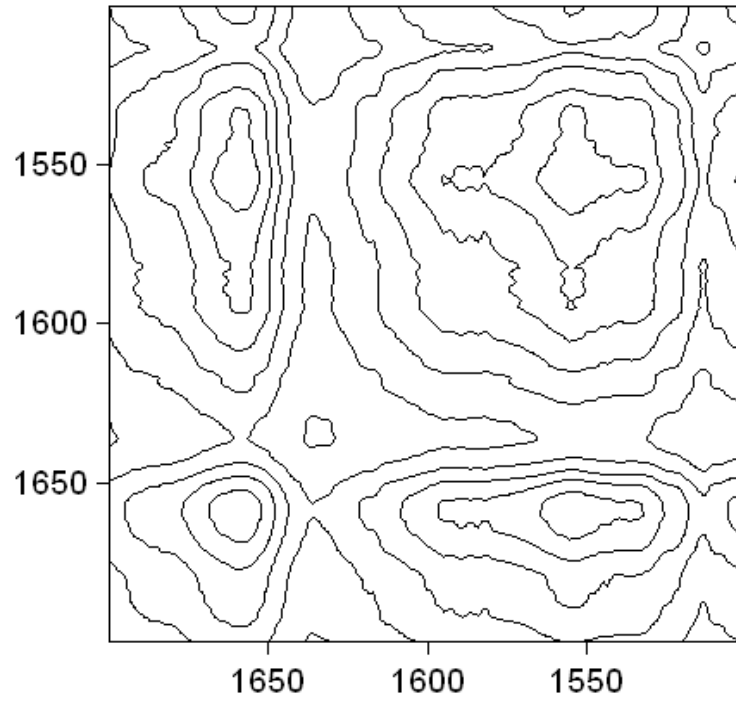

Figure E.9 Zein in [mim][OAc] asynchronous.
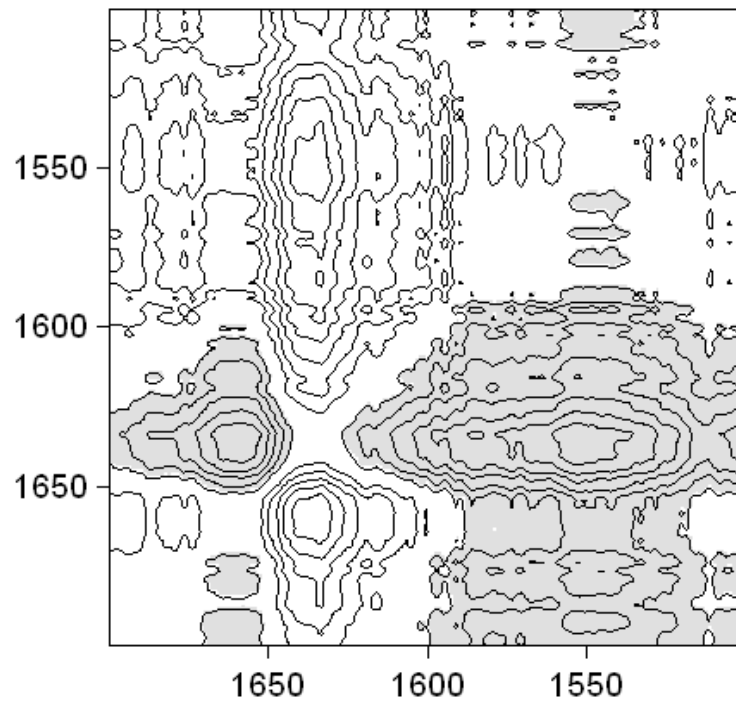
Figure E.10 Zein in [mim][Fr] synchronous.

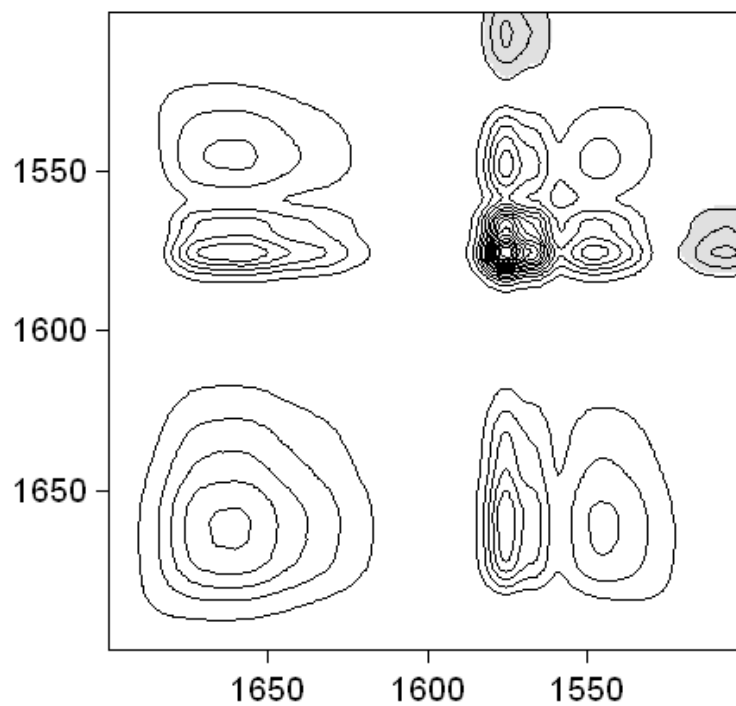
Figure E.11 Zein in [mim][Fr] asynchronous.

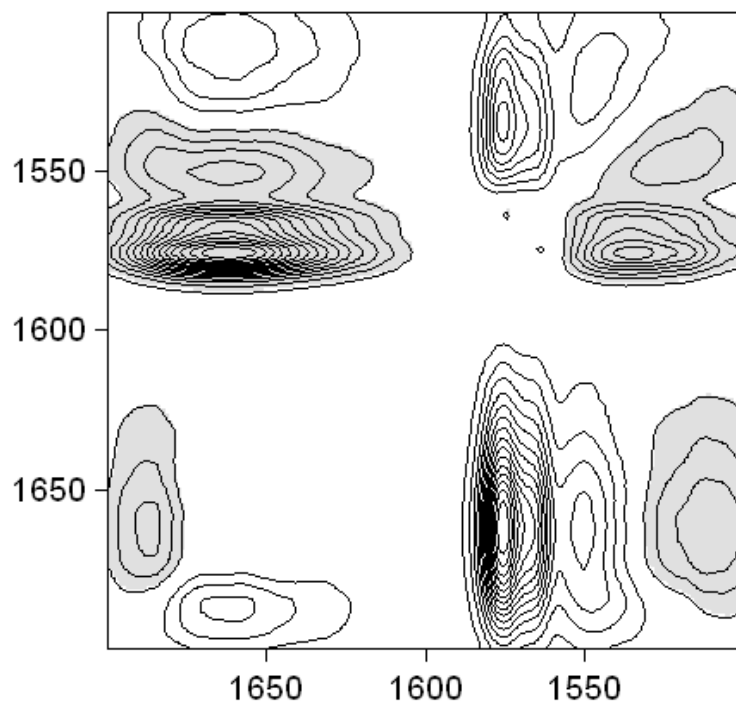**Figure E.12 Zein in [Emim][DCA] synchronous.**

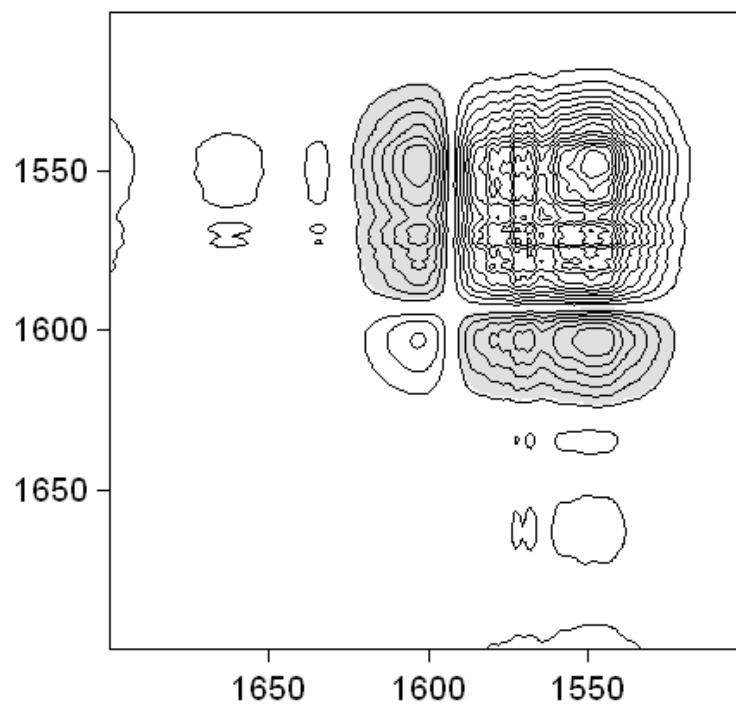**Figure E.13 Zein in [Emim][DCA] asynchronous.**

Figure E.14 Zein in [Emim][OAc] synchronous.

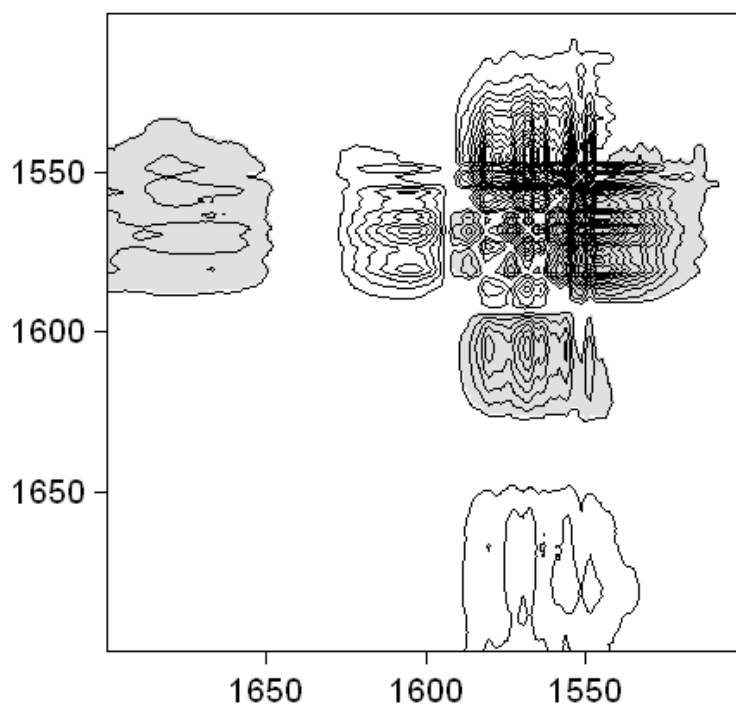

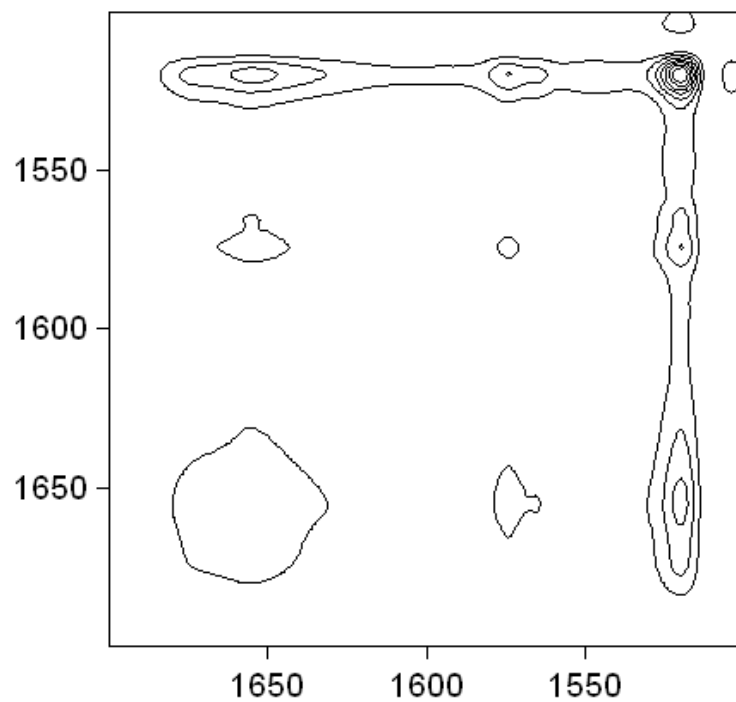**Figure E.15 Zein in [Emim][OAc] asynchronous.**
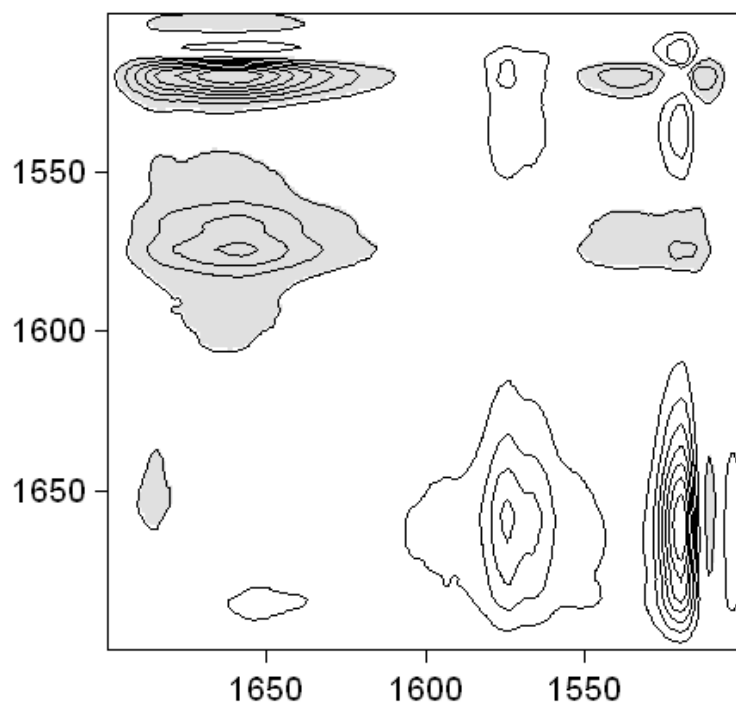
211

Figure E.16 Zein in [Bmim][Cl] synchronous.

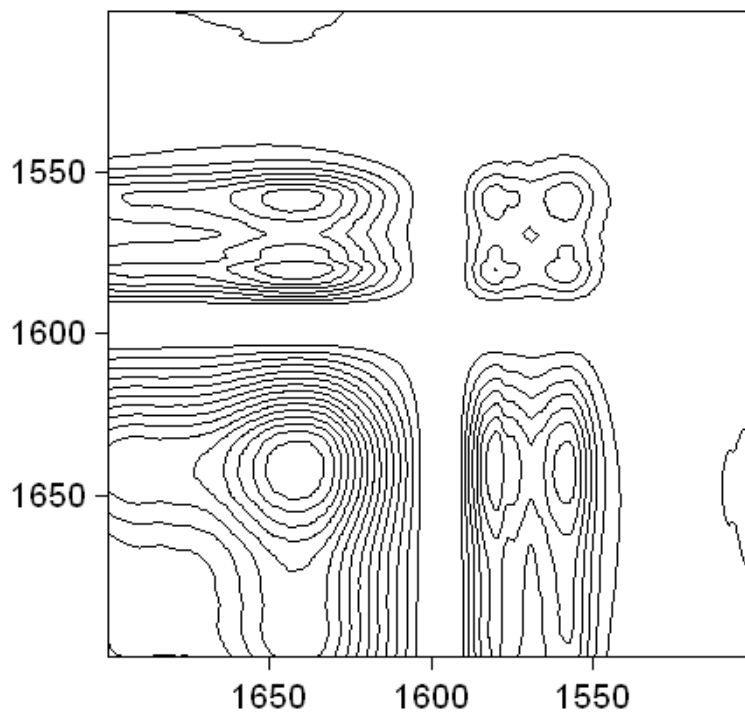
Figure E.17 Zein in [Bmim][Cl] asynchronous.
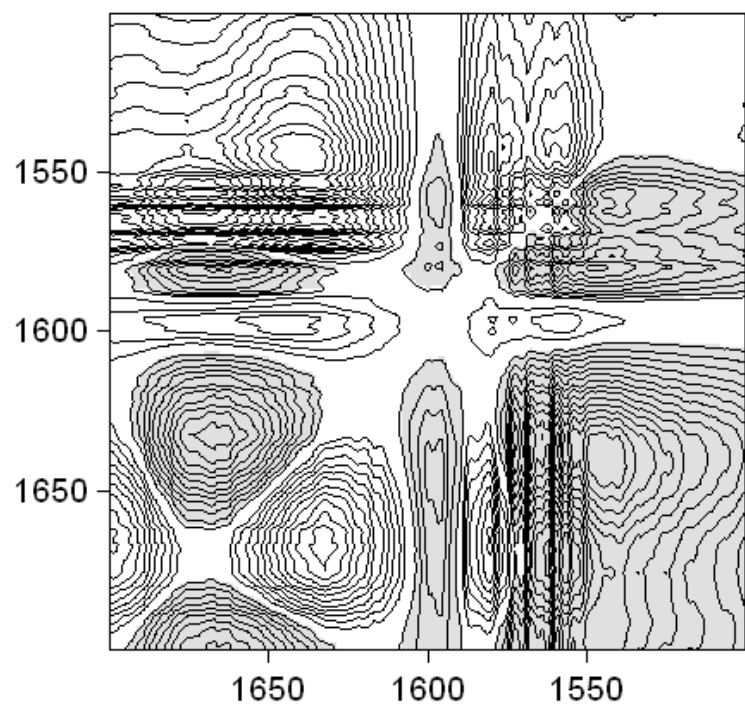
Figure E.18 Zein in [Bmim][OAc] synchronous.

Figure E.19 Zein in [Bmim][OAc] asynchronous.

213

Common Errors Encountered

Adapted from Hollock, 2012.[1]

Floating point error:

According to Hollock, Microsoft Excel 2011 for Mac seemed to add metadata to the worksheet when it is saved as a CSV file, which caused 2Dshige© to crash due to floating point errors. Hollock solved this issue by creating the .csv data files in Google Documents. After calculating all values in Excel, the values (not the formulas) were copied into Google Documents online and the document saved as a CSV file. This process eliminated the frustrating floating point errors. Microsoft Excel for Windows did not have this problem.[1]

I/O Error 32:

Having the .csv file open while attempting to run 2Dshige© will cause this error. Simply close the program with the .csv file open and try again.

Blank or Blot error:

If no data appears in the window, or too much data appears, it is advised to alter the range of the spectrum axes or adjust the contour scale manually.

References

1. Hollock, M. Application of Two-Dimensional Correlation Spectroscopy for Monitoring the Mechanism of Reaction Between Phenyl Glycidyl Ether (PGE) and Metaphenylene Diamine (MPDA), Kansas State University, 2012.

2. Noda, I.; Ozaki, Y.; Wiley, J. *Two-dimensional correlation spectroscopy: Applications in vibrational and optical spectroscopy;* Wiley Online Library: 2004; .

3. Noda, I. Two-dimensional infrared (2D IR) spectroscopy of synthetic and biopolymers, *Bull. Am. Phys. Soc.* **1986***, 3,* 520.

4. Noda, I. Two-dimensional infrared spectroscopy, *J. Am. Chem. Soc.* **1989***, 21,* 8116-8118.

5. Noda, I. Generalized two-dimensional correlation method applicable to infrared, Raman, and other types of spectroscopy, *Appl. Spectrosc.* **1993***, 9,* 1329-1336.

6. Noda, I. Generalized two-dimensional correlation method applicable to infrared, Raman, and other types of spectroscopy, *Appl. Spectrosc.* **1993***, 9,* 1329-1336.

7. Wu, Y.; Jiang, J. H.; Ozaki, Y. A new possibility of generalized two-dimensional correlation spectroscopy: Hybrid two-dimensional correlation spectroscopy, *J. Phys. Chem. A* **2002***, 11,* 2422-2429.

8. Huang, H.; Xie, J.; Chen, H. Adsorption behavior of human serum albumin on ATR crystal studied by in situ ATR/FTIR spectroscopy and two-dimensional correlation analysis, *Analyst* **2011***, 8,* 1747-1752.

Appendix F - Van't Hoff Equation Derivation

The van't Hoff equation can be used to find the enthalpy of interaction of a solute in a solvent, given in formation on equilibrium conditions.[1-3] What follows is a derivation of the van't Hoff equation beginning from the thermodynamic description of equilibrium. At equilibrium the chemical potential between the solute and solution are equal.

$$\mu_i^{solute} = \mu_i^{solution} = \mu_i^{liquid} + RT ln \frac{f_i^L}{f_i^S} \qquad \text{F.1}$$

In equation F.1, μ is the chemical potential of species i, f is the fugacity of i in states L (liquid) and S (solid), R is the gas constant, and T is the absolute temperature. The change in Gibbs free energy of fusion is the difference between the chemical potential of i in the solid state and i in the liquid state, see equation F.2.

$$\mu_i^{solute} - \mu_i^{liquid} = \Delta G_{fusion}^o \qquad \text{F.2}$$

Therefore, change in Gibbs free energy of fusion is –

$$\Delta G_{fusion}^o = RT ln \frac{f_i^L}{f_i^S} \qquad \text{F.3}$$

Using the Gibbs-Helmholtz equation –

$$\frac{-\Delta H_{fusion}^o}{T^2} = \left(\frac{\partial \left(\frac{\Delta G^o}{T} \right)}{\partial T} \right)_P \qquad \text{F.4}$$

Assuming constant pressure and substituting equation F.3 into equation F.4 yields –

$$\frac{-\Delta H^o_{fusion}}{T^2} = \frac{\partial\left(\frac{RT ln\frac{f_i^L}{f_i^S}}{T}\right)}{\partial T} \qquad \text{F.5}$$

Simplification of equation F.5 yields

$$\frac{-\Delta H_{i_{fusion}}}{RT^2} = \frac{\partial\left(ln\frac{f_i^L}{f_i^S}\right)}{\partial T} \qquad \text{F.6}$$

Dropping the i species identifiers and then multiplying both sides by ∂T and integrating from the temperature of fusion to the solution temperature, and to thermodynamic equilibrium results in –

$$ln\frac{f^L}{f^S} = \frac{\Delta H_{fusion}}{R}\left(\frac{1}{T_{solution}} - \frac{1}{T_{fusion}}\right) \qquad \text{F.7}$$

The entropy of fusion is –

$$\Delta S_{fusion} = \frac{\Delta H_{fusion}}{T_{fusion}} \qquad \text{F.8}$$

Substituting equation F.8 into equation F.7 yields

$$ln\frac{f^L}{f^S} = \frac{\Delta H_{fusion}}{RT_{solution}} - \frac{\Delta S_{fusion}}{R} \qquad \text{F.9}$$

In solution the fugacity of the liquid is 1, and the fugacity of the solid is the mole fraction of the species of interest (x) at equilibrium times the activity coefficient (γ), giving –

$$ln\frac{1}{\gamma x} = \frac{\Delta H_{fusion}}{RT_{solution}} - \frac{\Delta S_{fusion}}{R} \qquad \text{F.10}$$

Inverting the natural log, and assuming the activity coefficient to be near 1 yields the van't Hoff equation –

$$lnx = \frac{-\Delta H_{fusion}}{RT_{solution}} + \frac{\Delta S_{fusion}}{R} \qquad\qquad\qquad \text{F.11}$$

It is also possible to use the equilibrium coefficient K, or a dimensionless mass fraction, C_z, in place of x for the analysis.[4-6]

References

1. Prausnitz, J. M.; Lichtenthaler, R. N.; de Azevedo, E. G. *Molecular Thermodynamics of Fluid-Phase Equilibria;* Prentice-Hall PTR: Upper Saddle River, New Jersey, 1998; , pp 860.

2. Krug, R.; Hunter, W.; Grieger, R. Enthalpy-entropy compensation. 1. Some fundamental statistical problems associated with the analysis of van't Hoff and Arrhenius data, *J. Phys. Chem.* **1976**, *21,* 2335-2341.

3. Krug, R.; Hunter, W.; Grieger, R. Enthalpy-entropy compensation. 2. Separation of the chemical from the statistical effect, *J. Phys. Chem.* **1976**, *21,* 2341-2351.

4. Eghrary, S. H.; Zarghami, R.; Martinez, F.; Jouyban, A. Solubility of 2-Butyl-3-benzofuranyl 4-(2-(Diethylamino) ethoxy)-3, 5-diiodophenyl Ketone Hydrochloride (Amiodarone HCl) in Ethanol Water and N-Methyl-2-pyrrolidone Water Mixtures at Various Temperatures, *J. Chem. Eng. Data* **2012**, 1544-1550.

5. Delgado, D. R.; Vargas, E. F.; Martínez, F. Thermodynamic Study of the Solubility of Procaine HCl in Some Ethanol Water Cosolvent Mixtures, *J. Chem. Eng. Data* **2010***, 8,* 2900-2904.

6. Suzuki, Y.; Konda, E.; Hondoh, H.; Tamura, K. Effects of temperature, pressure, and pH on the solubility of triclinic lysozyme crystals, *J. Cryst. Growth* **2011***, 1,* 1085-1088.

Appendix G - Table of Nomenclature

This appendix explains all the nomenclature used in this dissertation, such as ionic liquid cation and anion abbreviations, and defines the symbols used

Ionic liquids

Abbreviation	Name	Structure
[mim][Fr]	1-methylimidazolium formate	
[mim][HSO₄]	1-methylimidazolium hydrogensulfate	
[mim][OAc]	1-methylimidazolium acetate	
[Bmim][Cl]	1-butyl-3-methylimidazolium chloride	
[Bmim][OAc]	1-butyl-3-methylimidazolium acetate	
[Emim][DCA]	1-ethyl-3-methylimidazolium dicyanamide	
[Emim][OAc]	1-ethyl-3-methylimdiazolium acetate	

Other terms

α   Solvent hydrogen bond donating ability, as measured by the Kamlet-Taft method[1]

β   Solvent hydrogen bond accepting ability, as measured by the Kamlet-Taft method[1]

π*   Solvent dipolarity/polarizability, as measured by the Kamlet-Taft method[1]

$E_T(30)$ Solvent polarity, as measured by the Reichardt method[2]

V_m Pure solvent molar volume obtained with a calibrated pycnometer

LSER   Linear solvation energy relationship[3]

Mz   Coefficient of 1/T term from van't Hoff equation, related to enthalpy of dissolution[4]

IR spectroscopy   Infrared spectroscopy

Attenuated Total Reflectance   A type of infrared spectroscopy[5]

Primary structure (of proteins)   Sequence of amino acids in a protein[6]

Secondary structure (of proteins)   Arrangement of amino acids into 3-dimensional segments[6]

Tertiary structure (of proteins)   Three dimensional location of atoms in a protein[6]

β-turn   Characteristic protein secondary structure[6]

α-helix   Characteristic protein secondary structure[6]

Random coil   Characteristic protein secondary structure[6]

β-sheet   Characteristic protein secondary structure[6]

References

1. Kamlet, M. J.; Abboud, J. L. M.; Abraham, M. H.; Taft, R. Linear solvation energy relationships. 23. A comprehensive collection of the solvatochromic parameters,. pi.*,. alpha., and. beta., and some methods for simplifying the generalized solvatochromic equation, *J. Org. Chem.* **1983***, 17,* 2877-2887.

2. Reichardt, C. Polarity of ionic liquids determined empirically by means of solvatochromic pyridinium N-phenolate betaine dyes, *Green Chem.* **2005***, 5,* 339-351.

3. Kamlet, M.; Abboud, J.; Taft, R. An examination of linear solvation energy relationships, *Progress in Physical Organic Chemistry, Volume 13* **2007**, 485-630.

4. Haynie, D. T. *Biological thermodynamics;* Cambridge University Press: University Press, Cambridge, 2008; , pp 422.

5. Harrick, N. J. *Internal Reflection Spectroscopy;* John Wiley & Sons: New York, 1967; , pp 327.

6. Horton, H. R.; Moran, L. A.; Ochs, R. S.; Rawn, J. D.; Scrimgeour, K. G. *Principles of Biochemistry;* Prentice Hall: Upper Saddle River, NJ, 1996; , pp 862.